
THE UNIVERSITY *of* EDINBURGH

# Analysis of OFDM-based Intensity Modulation Techniques for Optical Wireless Communications

*Svilen Dimitrov*


A thesis submitted for the degree of Doctor of Philosophy.
**The University of Edinburgh**.
August 2012

# Abstract

Optical wireless communication (OWC) is a promising alternative to radio frequency (RF) communication with a significantly larger and unregulated spectrum. Impairments in the physical layer, such as the non-linear transfer characteristic of the transmitter, the dispersive optical wireless channel and the additive white Gaussian noise (AWGN) at the receiver, reduce the capacity of the OWC system. Single-carrier multi-level pulse position modulation ($M$-PPM) and multi-level pulse amplitude modulation ($M$-PAM) suffer from inter-symbol interference (ISI) in the dispersive channel which reduces their capacity even after channel equalization. Multi-carrier modulation such as optical orthogonal frequency division multiplexing (O-OFDM) with multi-level quadrature amplitude modulation ($M$-QAM) is known to maximize the channel capacity through bit and power loading. There are two general signal structures: bipolar Gaussian signal with a direct current (DC) bias, *i.e.* DC-biased O-OFDM (DCO-OFDM), or unipolar half-Gaussian signal, employing only the odd subcarriers, *i.e.* asymmetrically clipped O-OFDM (ACO-OFDM). In this thesis, the signal distortion from the transmitter nonlinearity is minimized through pre-distortion, optimum signal scaling and DC-biasing.

The optical front-ends impose minimum, average and maximum optical power constraints, as well as an average electrical power constraint, on the information-carrying signals. In this thesis, the optical signals are conditioned within these constraints through optimum signal scaling and DC-biasing. The presented analysis of the optical-to-electrical (O/E) conversion enables the derivation of the electrical signal-to-noise ratio (SNR) at the receiver, including or excluding the additional DC bias power, which is translated into bit-error rate (BER) performance.

In addition, a generalized piecewise polynomial model for the non-linear transfer characteristic of the transmitter is proposed. The non-linear distortion in O-OFDM is translated by means of the Bussgang theorem and the central limit theorem (CLT) into attenuation of the data-carrying subcarriers at the receiver plus zero-mean complex-valued Gaussian noise. The attenuation factor and the variance of the non-linear distortion noise are derived in closed form, and they are accounted towards the received electrical SNR. Through pre-distortion with the inverse of the proposed piecewise polynomial function, the linear dynamic range of the transmitter is maximized, reducing the non-linear distortion to double-sided signal clipping.

Finally, the OWC schemes are compared in terms of spectral efficiency and electrical SNR requirement as the signal bandwidth exceeds the coherence bandwidth of the optical wireless channel for a practical $10$ dB linear dynamic range. Through optimum signal scaling and DC-biasing, DCO-OFDM is found to achieve the highest spectral efficiency for a target SNR, neglecting the additional DC bias power. When the DC bias power is counted towards the signal power, DCO-OFDM outperforms PAM with linear equalization, approaching the performance of the more computationally intensive PAM with non-linear equalization. In addition, the average optical power in O-OFDM is varied over dynamic ranges of $10$ dB, $20$ dB and $30$ dB. When the additional DC bias power is neglected, DCO-OFDM is shown to achieve the Shannon capacity, while ACO-OFDM exhibits a $3$ dB gap which grows with higher SNR targets. When the DC bias power is included, DCO-OFDM outperforms ACO-OFDM for the majority of average optical power levels with the increase of the SNR target or the dynamic range.

# Declaration of originality

I hereby declare that the research recorded in this thesis and the thesis itself was composed and originated entirely by myself in the Institute for Digital Communications (IDCOM) of the School of Engineering at The University of Edinburgh.

*Svilen Dimitrov*
Edinburgh, UK
August 2012

# Acknowledgements

I would like to express my deep gratitude to my supervisor, Prof. Harald Haas, from the Institute for Digital Communications (IDCOM) at the University of Edinburgh, UK. His academic excellence, enthusiasm for research and insatiable desire to pursue novel ideas have deeply inspired me. His pragmatic advices and continuous support were essential for the successful completion of my PhD.

In addition, I would like to thank my second supervisor, Dr. John Thompson, for his patience, guidance and support in my teaching activities. With his effort, engagement and care he is an admirable example of academic excellence.

Many thanks to my colleagues in IDCOM for their support, encouragement and entertainment. They truly turned the office into a cheerful, yet productive, environment. A special word of appreciation goes to Dr. Sinan Sinanovic. Our fruitful discussions were of major importance for the continuous progress of my research.

I gratefully acknowledge EADS Innovation Works UK in Newport for the support of this work. Special thanks to Mr. Patrick Geoffrey Williams for his continuous assistance.

This thesis is dedicated to my family and friends, the people who unconditionally stood by me. My deepest appreciation goes to their warming love, upbringing encouragement and motivation. My inexplicable gratitude belongs to my mother, Stefka, for her devotion and selfless care. Your being part of my life is invaluable to me, and words are insufficient to describe how thankful I am for this.

# Contents

# List of figures

# List of tables

# Acronyms and abbreviations

| | |
|---|---|
| AC | Alternating Current |
| ACO-OFDM | Asymmetrically Clipped Optical Orthogonal Frequency Division Multiplexing |
| A/D | Analog-to-Digital |
| AGC | Automatic Gain Control |
| AWGN | Additive White Gaussian Noise |
| BER | Bit-Error Ratio |
| BPSK | Binary Phase Shift Keying |
| CCDF | Complementary Cumulative Distribution Function |
| CP | Cyclic Prefix |
| CLT | Central Limit Theorem |
| D/A | Digital-to-Analog |
| DC | Direct Current |
| DCO-OFDM | Direct Current Biased Optical Orthogonal Frequency Division Multiplexing |
| DFE | Decision Feedback Equalizer |
| DMT | Discrete Multi-Tone |
| DSL | Digital Subscriber Line |
| DSP | Digital Signal Processor |
| FEC | Forward Error Correction |
| FFE | Feed-Forward Equalizer |
| FFT | Fast Fourier Transform |
| FOV | Field Of View |
| FSO | Free Space Optical |
| HPA | High-Power Amplifier |
| ICI | Inter-Carrier Interference |
| IEEE | Institute of Electrical and Electronics Engineers |
| IFFT | Inverse Fast Fourier Transform |
| IM/DD | Intensity Modulation and Direct Detection |
| IR | Infrared |
| IrDA | Infrared Data Association |
| ISI | Inter-Symbol Interference |

| | |
|---|---|
| LDPC | Low Density Parity Check |
| LED | Light Emitting Diode |
| LOS | Line Of Sight |
| MLSD | Maximum Likelihood Sequence Detection |
| MMSE | Minimum Mean Squared Error |
| $M$-PAM | Multi-level Pulse Amplitude Modulation |
| $M$-PAPM | Multi-level Pulse Amplitude and Position Modulation |
| $M$-PPM | Multi-level Pulse Position Modulation |
| $M$-QAM | Multi-level Quadrature Amplitude Modulation |
| NIR | Near Infrared |
| NLOS | Non-Line Of Sight |
| O/E | Optical-to-Electrical |
| O-OFDM | Optical Orthogonal Frequency Division Multiplexing |
| OOK | On-Off Keying |
| OWC | Optical Wireless Communication |
| P/S | Parallel-to-Serial |
| PAPR | Peak-to-Average-Power Ratio |
| PD | Photodiode |
| PDF | Probability Density Function |
| PIM | Pulse Interval Modulation |
| PSD | Power Spectral Density |
| PWM | Pulse Width Modulation |
| RF | Radio Frequency |
| RMS | Root Mean Square |
| SER | Symbol-Error Rate |
| SIR | Signal-to-Interference Ratio |
| SINR | Signal-to-Interference-and-Noise Ratio |
| SNR | Signal-to-Noise Ratio |
| S/P | Serial-to-Parallel |
| TIA | Transimpedance Amplifier |
| U-OFDM | Unipolar Orthogonal Frequency Division Multiplexing |
| VLC | Visible Light Communication |
| VLCC | Visible Light Communications Consortium |
| ZF | Zero Forcing |

# Nomenclature

| | |
|---|---|
| $*$ | Linear convolution operator |
| $\star$ | Linear discrete convolution operator |
| $a$ | Variable related to the RMS delay spread of the channel, $D$ |
| $\mathbf{b}$ | Bit loading vector in OFDM |
| $B$ | Double-sided signal bandwidth |
| BOTTOM | Shifted bottom clipping level |
| $B_{\mathrm{c}}$ | 3-dB double sided coherence bandwidth of the optical wireless channel |
| $c(t)$ | Chip |
| $\mathbf{c}$ | Chip vector |
| $C$ | Capacity/spectral efficiency |
| $\mathrm{Cov}\left[\cdot\right]$ | Covariance operator |
| $d$ | Distance |
| $D$ | RMS delay spread of the channel |
| $d_{\mathrm{s}}$ | Distance between an intended symbol and the closest interfering symbol |
| $\mathrm{E}\left[\cdot\right]$ | Expectation operator |
| $E_{\mathrm{b(elec)}}$ | Average electrical bit energy |
| $E_{\mathrm{s(elec)}}$ | Average electrical symbol energy |
| $f$ | Frequency variable |
| $\mathbf{f}$ | OFDM frame vector |
| $\widetilde{\mathbf{f}}$ | Distorted replica of the OFDM frame vector at the receiver |
| $F(\cdot)$ | Non-linear transfer function of the transmitter |
| $\mathbf{f}_{\mathrm{info}}$ | Vector with information-carrying subcarriers |
| $\widetilde{\mathbf{f}}_{\mathrm{info}}$ | Distorted replica of the vector with information-carrying subcarriers |
| $G_{\mathrm{B}}$ | Bandwidth utilization factor |
| $G_{\mathrm{DC}}$ | DC bias gain |
| $G_{\mathrm{EQ}}$ | Equalizer gain |
| $G_{\mathrm{GC}}$ | Gray coding gain |
| $g_{\mathrm{h(elec)}}$ | Electrical path gain |
| $g_{\mathrm{h(opt)}}$ | Optical path gain |
| $G_{\mathrm{T}}$ | Utilization factor for the information carrying time |

| | |
|---|---|
| $G_{\mathrm{TIA}}$ | Gain of the TIA |
| $h(t)$ | Impulse response of the optical wireless channel |
| $\mathbf{h}$ | Impulse response vector of the optical wireless channel |
| $H(f)$ | Fourier transform of $h(t)$ |
| $h_{\mathrm{norm}}(t)$ | Normalized impulse response of the optical wireless channel |
| $H_{\mathrm{norm}}(f)$ | Fourier transform of $h_{\mathrm{norm}}(t)$ |
| $i$ | Imaginary unit, *i.e.* $i = \sqrt{-1}$ |
| $I_{\mathrm{f}}$ | Forward current |
| $I_{\mathrm{in}}$ | Input current |
| $I_{\mathrm{max}}$ | Maximum forward current |
| $I_{\mathrm{max,norm}}$ | Normalized maximum forward current |
| $I_{\mathrm{min}}$ | Minimum forward current |
| $I_{\mathrm{min,norm}}$ | Normalized minimum forward current |
| $I_{\mathrm{out}}$ | Output current |
| $j$ | Index of polynomial function, $\psi(\cdot)$ |
| $J$ | Number of normalized clipping levels |
| $\hat{j}$ | Index of normalized clipping level, $\lambda$ |
| $k$ | Time domain sample index in OFDM |
| $K$ | Attenuation factor of non-linear distortion for information carrying subcarriers |
| $l$ | Symbol index |
| $L$ | Number of symbols per transmission vector |
| $m$ | Subcarrier index |
| $M$ | Modulation order |
| $n$ | Integer polynomial order |
| $N$ | Number of subcarriers, IFFT/FFT size |
| $N_0$ | Power spectral density of the AWGN |
| $N_{\mathrm{CP}}$ | Number of CP samples in OFDM |
| $N_{\mathrm{s}}$ | Average number of neighboring symbols |
| $p$ | Scaling factor for current levels in $M$-PAM |
| $\mathbf{p}$ | Power loading vector in OFDM |
| $P_{\mathrm{b(elec)}}$ | Average electrical bit power |
| $P_{\mathrm{elec}}$ | Dissipated electrical power |
| $P_{\mathrm{avg,norm}}$ | Normalized average optical power constraint |
| $P_{\mathrm{max,norm}}$ | Normalized maximum optical power constraint |

| | |
|---|---|
| $P_{\min,\mathrm{norm}}$ | Normalized minimum optical power constraint |
| $P_{\mathrm{opt}}$ | Radiated optical power |
| $P_{\mathrm{R}}$ | Optical power at receiver |
| $p_S(s)$ | PDF of clipped OFDM symbol |
| $p_{\hat{S}}(\hat{s})$ | PDF of unfolded clipped ACO-OFDM symbol |
| $P_{\mathrm{s(elec)}}$ | Average electrical symbol power |
| $P_{\mathrm{s(opt)}}$ | Average optical symbol power |
| $\mathrm{PL}(d)$ | Path loss at distance $d$ |
| $\mathrm{PL}(d_0)$ | Path loss at reference distance $d_0$ |
| $P_{\mathrm{T}}$ | Optical power of transmitter |
| $Q(\cdot)$ | CCDF of a standard normal distribution |
| $r(t)$ | Impulse response of matched filter at receiver |
| $r_{\mathrm{load}}$ | Load resistance |
| $R_{\mathrm{b}}$ | Bit rate |
| $R_{\mathrm{s}}$ | Symbol rate |
| $s(t)$ | Symbol |
| $\hat{s}(t)$ | Unfolded ACO-OFDM symbol |
| $\bar{s}(t)$ | Unfolded and debiased ACO-OFDM symbol |
| $\mathbf{s}$ | Symbol vector |
| $\widetilde{\mathbf{s}}$ | Distorted replica of symbol vector at the receiver |
| $S_{\mathrm{PD}}$ | responsivity of the PD |
| $\mathrm{SE}$ | Spectral efficiency of the modulation schemes for OWC |
| $\mathrm{SNR}$ | Electrical SNR on an enabled subcarrier in OFDM |
| $t$ | time variable |
| $T$ | Sampling period |
| $\mathrm{TOP}$ | Shifted top clipping level |
| $u$ | Dummy integration variable |
| $U(t)$ | Unit step function |
| $v(t)$ | Impulse response of the pulse shaping filter |
| $V(f)$ | Fourier transform of $v(f)$ |
| $V_{\mathrm{f}}$ | Forward voltage |
| $w(t)$ | AWGN at the receiver |
| $\mathbf{w}$ | AWGN vector at the receiver |
| $\mathbf{W}$ | AWGN vector at the frequency domain subcarriers |

| | |
|---|---|
| $w_{\text{clip}}(t)$ | Uncorrelated non-Gaussian time domain non-linear distortion noise |
| $\mathbf{W}_{\text{clip}}$ | Additive Gaussian non-linear distortion noise at the information-carrying subcarriers |
| $x(t)$ | Biased information carrying signal |
| $\mathbf{x}$ | Biased information carrying signal vector |
| $y(t)$ | Received signal |
| $\mathbf{y}$ | received signal vector |
| $z$ | Counter in summation of $W(f)$ |
| $Z_{\mathbf{x}}$ | Length of the biased information carrying signal vector |
| $Z_{\mathbf{h}}$ | Length of the impulse response vector of the optical wireless channel |
| $\alpha$ | Scaling factor of signal power |
| $\beta_{\text{DC}}$ | DC bias current |
| $\delta(\cdot)$ | Dirac delta function |
| $\gamma_{\text{b(elec)}}$ | Undistorted electrical SNR per bit at the transmitter |
| $\Gamma_{\text{b(elec)}}$ | Effective electrical SNR per bit at the receiver |
| $\zeta$ | Random variable with zero-mean log-normal distribution, shadowing component |
| $\lambda$ | Normalized clipping level |
| $\Lambda(f)$ | Variable related to $V(f)$ and $H(f)$ by (3.5) |
| $\lambda_{\text{bottom}}$ | Normalized bottom clipping level |
| $\lambda_{\text{top}}$ | Normalized top clipping level |
| $\mu$ | Mean of clipped DCO-OFDM symbol |
| $\xi$ | Path loss exponent |
| $\Xi(\cdot)$ | Piecewise polynomial transfer function of transmitter |
| $\pi$ | Number Pi, *i.e.* $\pi \approx 3.14$ |
| $\sigma$ | Standard deviation of OFDM time domain signal |
| $\sigma_{\text{AWGN}}$ | Standard deviation of the AWGN |
| $\sigma_{\text{clip}}$ | Standard deviation of non-linear distortion noise |
| $\tau$ | Dummy integration variable |
| $\phi(\cdot)$ | PDF of a standard normal distribution |
| $\Phi(\cdot)$ | Linearized transfer function of transmitter denoting double-sided signal clipping |
| $\psi(\cdot)$ | Polynomial function of non-negative integer order, $n$ |
| $\Psi(\cdot)$ | Normalized non-linear transfer function of transmitter |
| $\hat{\Psi}(\cdot)$ | Unfolded normalized non-linear transfer function in ACO-OFDM |
| $\mathcal{I}$ | Integral structure for calculation of non-linear distortion parameters |
| $\mathcal{N}(\mu, \sigma^2)$ | Normal distribution with mean $\mu$ and variance $\sigma^2$ of unclipped OFDM symbol |

# Chapter 1
# Introduction

## 1.1 Motivation

In optical wireless communication (OWC), the information is transmitted in the form of optical intensity. The signal occupies wavelengths in the visible light spectrum from $380$ nm to $750$ nm and/or the near infrared (NIR) spectrum from $750$ nm to $2.5$ $\mu$m. The total available bandwidth resource amounts to approximately $670$ THz which is a factor of $10,000$ larger than the radio frequency (RF) spectrum. In addition to being a complementary non-interfering solution alongside the RF technology, OWC has the advantage of a license-free unregulated operation over a huge spectrum resource. Due to the fact that light does not propagate through opaque objects, the data communication is hard to intercept or to eavesdrop. In addition, it is free of any health concerns as long as eye safety regulations are fulfilled [1]. Thus, OWC enables a secure data transmission in areas, where RF communication is physically impossible or prohibited. These include underwater communication, the aviation industry, hospitals and healthcare facilities, and hazardous environments such as oil and gas refineries.

With the increasing popularity of smartphones, the wireless data traffic of mobile devices is growing exponentially. By the year of $2015$, it is expected that the total wireless data traffic will reach $6$ Exabytes per month, potentially creating a $97\%$ gap between the traffic demand per device and the available data rate per device in the mobile networks [2]. Recently, the Wireless Gigabit Alliance has proposed the utilization of the mm-waves in the license-free $60$ GHz band, where the availability of $7$ GHz bandwidth enables $7$ Gbps short-range wireless links [3]. The $60$ GHz band has also been considered as a part of the IEEE $802.11$ad framework for the realization of very high throughput data links [4]. However, due to the high path loss of the radio waves in this spectrum range, $60$ GHz links are highly directional, and therefore, not directly applicable for mobile wireless networks. Fortunately, the RF spectrum can be relieved by an emerging technology, OWC. One branch of OWC is targeted at outdoor free-space optical (FSO) links over long distances which are generally realized through highly directional laser diodes as transmitters [5]. Another branch of OWC focuses on indoor mobile wireless networks, and it is realized through diffuse light emitting diodes (LEDs) as transmitters [6]. With

the advent of incoherent highly efficient high-power LEDs and highly sensitive photodiodes (PDs), OWC has become a viable candidate for medium-range indoor data transmission that can contribute to the cause of solving the spectrum deficit. The first indoor OWC system was reported by Gfeller and Bapst in $1979$ [6]. At a center wavelength of $950$ nm in the infrared (IR) spectrum, the system was capable of achieving $1$ Mbps using on-off keying (OOK) modulation and diffuse radiation for a coverage of an office room. In $1996$ Marsh and Kahn demonstrated an indoor diffuse OOK IR system with a data rate of $50$ Mbps [7]. Later in $2000$, Carruthers and Kahn presented a faster OOK IR system implementation with a data rate $70$ Mbps and a potential of up to $100$ Mbps [8]. Tanaka *et al.* first considered white LEDs to convey information in addition to serving the primary functionality of illumination in an indoor setup, and in $2003$ they presented a OOK system setup with up to $400$ Mbps data rate [9]. Recently, Vucic *et al.* ascertained the potential of visible light communication (VLC) systems with a demonstration of a $500$ Mbps data rate [10]. Their implementation was based on optical orthogonal frequency division multiplexing (O-OFDM) with bit and power loading and symmetric signal clipping. In this thesis, a single-carrier and multi-carrier modulation techniques are studied which can potentially enable indoor OWC at even higher data rates.

Indoor OWC is generally realized in a line-of-sight (LOS) or a non-line-of-sight (NLOS) communication setup [11, 12]. LOS links can be generally employed in static communication scenarios such as indoor sensor networks, where fixed position and alignment between the transmitter and receiver are maintained. In mobile environments such as commercial offices, mechanical or electronic beam steering [5] can be used to maintain an LOS connection. Such techniques, however, increase the cost of the optical front-ends. Therefore, in a mobile OWC network, where LOS links are likely to be blocked, transmission robustness can be facilitated through NLOS communication. Single-carrier pulse modulation techniques such as pulse width modulation (PWM), pulse interval modulation (PIM), pulse position modulation (PPM) and pulse amplitude modulation (PAM) suffer from inter-symbol interference (ISI) in the dispersive NLOS channel, and therefore, they have a limited throughput [5, 11, 13]. Because of its inherent robustness to multi-path fading, O-OFDM with multi-level quadrature amplitude modulation ($M$-QAM) is envisaged to enable NLOS communication, and therefore high-capacity wireless networking [14–16]. A major challenge in the implementation of an O-OFDM system is the optimum conditioning of the time domain signal within the limited dynamic range of the transmitter front-end, in order to minimize the resulting non-linear signal distortion and to maximize the system throughput [17–19]. In order to formulate this optimization problem,

the mathematical details of the optical-to-electrical (O/E) signal conversion of the unipolar O-OFDM signal are required. Since the energy efficiency of the system is measured by the amount of electrical power required for a given quality of service, a relationship with the output optical power needs to be established. Through pre-distortion of the signal with the inverse of the non-linear transfer function, the dynamic range of the transmitter can be linearized between levels of minimum and maximum radiated optical power [20]. Here, the non-linear distortion for a given signal biasing setup needs to be analyzed. Therefore, the achievable information rates of the O-OFDM system for a practical linear dynamic range of the transmitter under average electrical power and average optical power constraints is still an open issue.

## 1.2 Contributions

In this thesis, the spectral efficiency and information rates of multi-carrier O-OFDM transmission schemes are studied for a practical linear dynamic range of the transmitter front-end with minimum, average and maximum optical power constraint. In addition, a generalized non-linear transfer function is proposed, and the distortion of the information-carrying signal is analyzed. Finally, the spectral efficiency of multi-carrier modulation is compared with the spectral efficiency of single-carrier pulsed modulation in the flat fading optical wireless channel and the dispersive channel, where the signal bandwidth exceeds the channel coherence bandwidth. The results of the studies have been published in two journal papers in the *IEEE Transactions on Communications* and the *IEEE/OSA Journal on Lightwave Technology* [24, 25]. In addition, the results have been presented in five conference papers at *IEEE GLOBECOM*, *IEEE ICC*, *IEEE VTC* and *EuCAP* [21–23, 26, 52].

The optical front-ends impose minimum, average and maximum optical power constraints, as well as an average electrical power constraint, on the information-carrying signals. As a first contribution of this thesis, the electrical signal-to-noise ratio (SNR) requirement and the spectral efficiency of the modulation techniques for OWC, such as multi-carrier modulation realized through $M$-QAM O-OFDM and single-carrier pulse modulation realized through $M$-PPM and $M$-PAM, are analyzed. A signal shaping framework is proposed which enables the optimum scaling and DC-biasing of the optical signals, in order to condition them within the optical power constraints of the transmitter front-end. It includes the analysis of the optical-to-electrical (O/E) conversion in the physical layer of these communication schemes. The bit-error rate (BER) performance for a given electrical SNR at the receiver is derived, including or ex-

cluding the additional DC bias power required for a unipolar non-negative signal transmission. The detailed analysis is presented in Chapter 3, and it has been published in [25].

Because of the fact that the single-carrier pulse modulation signals have a probability density function (PDF) with a finite support and because of their respective demodulation procedures, they can fit within the optical power constraints of the transmitter without non-linear clipping distortion. However, the Gaussian and half-Gaussian DCO-OFDM and ACO-OFDM signals, respectively, suffer a double-sided time domain signal clipping. As a second contribution of this thesis, following the Bussgang theorem [27] and the central limit theorem (CLT) [28], the non-linear distortion of these signals is modeled as an attenuation of the received information-carrying subcarriers plus a zero-mean complex-valued Gaussian clipping noise. The attenuation factor and the variance of the clipping noise are determined in closed form for a generalized piecewise polynomial transfer function and for the particular case of double-sided signal clipping after pre-distortion [23, 24]. Furthermore, the non-linear distortion parameters are included in the derivation of the received electrical SNR. The theoretical BER performance of clipped ACO-OFDM and DCO-OFDM is verified through a Monte Carlo simulation for different clipping levels. Finally, the impact of the clipping distortion on higher order QAM modulation and higher number of subcarriers is discussed. The model for the non-linear signal distortion in O-OFDM is presented in Chapter 4, and it has been published in [21–24].

As a third contribution of this thesis, the analysis of the non-linear distortion in O-OFDM is employed in the formulation of the optimum signal scaling and DC-biasing in O-OFDM for a flat fading channel and for a dispersive channel, where the signal bandwidth exceeds the channel coherence bandwidth. First, the optimum biasing setup in the flat fading channel is defined, in order to achieve the minimum electrical SNR requirement for a target BER for a given combination of optical power constraints and a desired QAM order, $M$. Both alternating current (AC) power and DC power are included in the calculation of the electrical SNR requirement for average optical power levels varied over dynamic ranges of $10$ dB, $20$ dB and $30$ dB. For the majority of average optical power levels, DCO-OFDM is shown to have a lower minimum electrical SNR requirement for a target BER as compared to ACO-OFDM for modulation orders with similar spectral efficiencies as the dynamic range increases. Therefore, DCO-OFDM is proven to be the more flexible transmission scheme for OWC with an ability to sweep over more than $50\%$ of the dynamic range within a 3-dB SNR margin. In addition, the study is extended with the mutual information of the DCO-OFDM and ACO-OFDM systems with non-linear dis-

tortion. Since the non-linear distortion merely results in a modification of the electrical SNR, it can be directly translated into degradation of the mutual information in the Shannon framework. In this thesis, the minimization of the non-linear signal distortion, *i.e.* maximization of the received electrical SNR and maximization of the information rate, is formulated as an optimization problem. In addition to the minimum and maximum optical power constraints, an average optical power constraint is imposed, as well, and the information rate of the two O-OFDM systems is presented, excluding or including the additional DC bias power in the calculation of the electrical SNR. It is shown that DCO-OFDM can achieve the Shannon capacity, when the DC bias power is neglected, while ACO-OFDM exhibits a minimum gap of $3$ dB. When the DC bias power is included in the calculation of the electrical SNR, an optimum biasing setup is shown to minimize the SNR penalty for a given average optical power constraint. DCO-OFDM is shown to deliver the higher information rate as compared to ACO-OFDM for the majority of average optical power levels as the SNR target or the dynamic range increase. The optimization of the biasing setup in O-OFDM and the results are presented in Chapter 5, and they have been published in [26]. Finally, the single and multi-carrier OWC systems are compared in a novel fashion in terms of electrical SNR requirement and spectral efficiency in the dispersive optical wireless channel, excluding or including the DC bias power in the calculation of the electrical SNR. When the additional DC bias power is neglected, DCO-OFDM and PAM show the greatest spectral efficiency for a flat fading channel in the SNR region above $6.8$ dB. However, since O-OFDM with bit and power loading suffers a lower SNR penalty than PAM with non-linear equalization as the signal bandwidth exceeds the coherence bandwidth of the dispersive optical wireless channel, DCO-OFDM demonstrates a superior spectral efficiency. When the DC bias power is counted towards the electrical signal power, DCO-OFDM and ACO-OFDM suffer a greater SNR penalty due to the DC bias as compared to PAM and PPM, respectively. However, the presented optimum signal shaping framework enables O-OFDM to greatly reduce this penalty and minimize the gap to single-carrier transmission within $2$ dB in the flat fading channel. When the signal bandwidth exceeds the channel coherence bandwidth, DCO-OFDM outperforms PAM with linear equalization, and it approaches the spectral efficiency of the more computationally intensive PAM with non-linear equalization, while ACO-OFDM outperforms PPM with linear and non-linear equalization. The optimum biasing framework and the results of the studies are presented in Chapter 5, and they have been published in [25].

## 1.3 Thesis outline

The rest of the thesis is organized as follows. **Chapter 2** introduces the fundamentals of OWC, including front-end design, the variety of communication setups, the modulation formats and the existing literature on their capacity in the optical wireless channel with non-linear distortion in AWGN.

In **Chapter 3**, the general model of the transmission link in OWC is presented in Section 3.2. It includes the nonlinearity of the transmitter, the optical wireless channel and the AWGN at the receiver. Section 3.3 presents the mathematical details of the O/E conversion in the single-carrier modulation schemes, *i.e.* $M$-PPM and $M$-PAM, and the multi-carrier modulation schemes, *i.e.* $M$-QAM DCO-OFDM and $M$-QAM ACO-OFDM. The electrical SNR at the receiver is derived and translated into BER performance.

**Chapter 4** elaborates the derivation of the non-linear distortion parameters in O-OFDM, such as the attenuation factor and the variance of the additive non-linear Gaussian noise at the received subcarriers. The non-linear distortion is modeled by means of a piecewise polynomial transfer function in Section 4.2. In Section 4.3, the non-linear transfer characteristic is linearized by means of pre-distortion, and the non-linear distortion is reduced to double-sided signal clipping. The analytical modeling is verified through a Monte Carlo simulation.

**Chapter 5** discusses the achievable information rates of O-OFDM with non-linear distortion. In Section 5.2, the information rates of DCO-OFDM and ACO-OFDM are presented for the flat fading channel under minimum, average and maximum optical power constraints. Section 5.3 shows the maximum information rates of DCO-OFDM and ACO-OFDM with non-linear distortion in the Shannon framework. In Section 5.4, $M$-QAM O-OFDM with bit and power loading is compared with $M$-PPM and $M$-PAM with linear and non-linear equalization in terms of electrical SNR requirement and spectral efficiency in the dispersive channel.

Finally, **Chapter 6** concludes the thesis with the significant findings of this study. The limitations of the work are discussed, and an outlook with the future work is presented.

## 1.4 Chapter summary

Acknowledging the spectrum deficit in current RF technology and pointing out the immense license-free spectral resource available for OWC systems, some of the notable advances in

the achievable data rates of current OWC system implementations have been presented in this Chapter. The main challenges in improving the information rates of the OWC systems considering the limitations of off-the-shelf optical front-ends have been introduced. In this context, methods to maximize the information rates of multi-carrier OWC systems have been summarized as the contributions of this thesis. The Chapter concluded with the thesis outline.

# Chapter 2
# Background

## 2.1 Introduction

Optical communication is any form of telecommunication that uses light as the transmission medium. Examples of beacon fires and smoke signals to convey a message can be found in the history of any culture many centuries ago. Semaphore lines are the earliest form of technological application of optical wireless communication (OWC) [29]. The French engineer Claude Chappe built the first optical telegraph network back in 1792. A semaphore tower, similar to the one illustrated in Fig. 2.1, facilitates the transmission of 196 information symbols encoded in the position of the two arms connected by a crossbar. As another example of early OWC, the heliograph is a wireless solar telegraph that signals flashes of sunlight by pivoting a mirror or interrupting the beam with a shutter. After the invention of the Morse code in 1836, navy ships communicated by means of a signal lamp with on-shore lighthouses for navigation. In 1880, Alexander Graham Bell demonstrated the first implementation of a free-space optical (FSO) link in the form of the photophone [30]. By using a vibrating mirror at the transmitter a crystalline selenium cells at the focal point of a parabolic receiver, Bell was able to modulate a voice message onto a light signal.

The recent advancements in OWC technology gained significant pace after the pioneering work of Gfeller and Bapst in 1979 [6]. They showed the potential of OWC for realization of high-capacity in-house networks promising hundreds of terahertz bandwidth of electromagnetic spectrum in the optical domain. Originally targeted at the near infrared (NIR) spectrum [6, 11, 12, 31], the optical wireless link was meant for short range communications. Since 1993 a standardized set of protocols of the infrared data association (IrDA) [32] were implemented for wireless infrared communication in portable devices such as mobile phones, laptops, cameras, remote controls and many more. With the advancements of solid-state lighting technology in the recent years, light emitting diodes (LEDs) are replacing incandescent light bulbs because of their reliability and higher energy efficiency, *e.g.* $5\%$ *vs.* $30\%$ in favor of LEDs [33]. In addition to illumination, LEDs are also envisioned to provide high-capacity

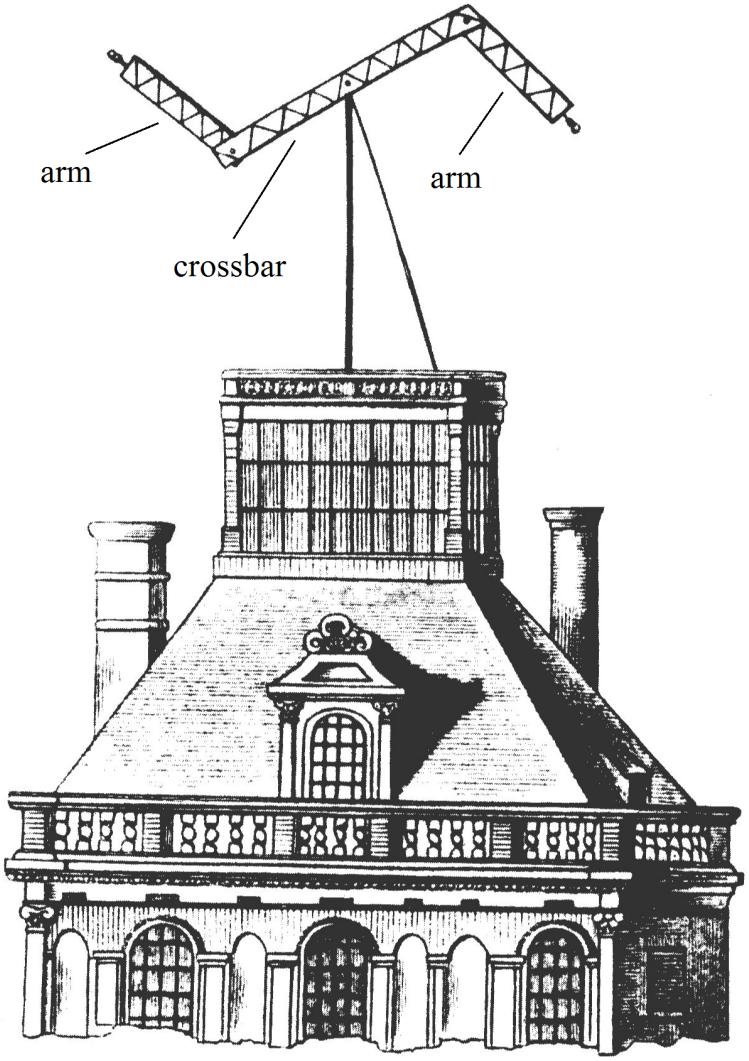


Figure 2.1: A semaphore tower at Louvre, France, invented by Claude Chappe in 1972. It is a part of the optical telegraph network covering the entire country, enabling the transmission of 196 symbols encoded in the position of the two arms connected by a crossbar on top of the tower [29].

wireless data broadcast capabilities [34–42]. Standardization of the visible light communication (VLC) research is strongly supported by the Visible Light Communications Consortium (VLCC) in Japan [43]. In 2011, the Institute of Electrical and Electronics Engineers (IEEE) published a standard for VLC, IEEE Std $802.15.7-2011$, "IEEE Standard for Local and Metropolitan Area Networks, Part 15.7: Short-Range Wireless Optical Communication Using Visible Light" [44]. In this Chapter, the details of the geometric setup and the capacity of different OWC system implementations are discussed.

## 2.2 Geometry of an OWC setup

The geometry of a wireless communication scenario is defined by the position and radiation/detection characteristics of the transmitters and receivers in an indoor or outdoor environment with certain reflection properties of the objects in the setup. Based on the propagation path of the light radiated by the transmitter and detected by the receiver, there are two general link arrangements, *i.e.* line-of-sight (LOS) and non-line-of-sight (NLOS) communications [12]. In addition, a cellular network can be deployed, in order to maximize the coverage and capacity over the area of the OWC setup [45–47]. In this Section, the building blocks of the transmitter and receiver front-ends are elaborated, and the general communication setup arrangements are discussed.

### 2.2.1 Front-ends

A generalized OWC link is illustrated in Fig. 2.2. The transmitter unit consists of a digital signal processor (DSP) which is responsible for the modulation of the information bits into a current signal. The current drives the optical emitter, *i.e.* an LED or an array of LEDs. Here, the information-carrying current signal is transformed into optical intensity. The optical signal can be passed through an optical system, in order to further shape the transmitted beam. Here, an optical amplifier lens, a collimator or a diffusor can be employed to concentrate or broaden the beam. The optical signal is then transmitted over the optical wireless channel. A portion of the optical energy is absorbed by the objects in the environment, and the rest is reflected back in a diffuse or specular fashion [47]. LOS and NLOS signal components arrive at the receiver. Here, an optical filter can be applied to select a portion of interest in the optical spectrum. In addition, the optical filter greatly reduces the interference from ambient light. Then, the optical signal is passed through a system of optical elements, *e.g.* collimator lenses, to amplify its strength and to align the impinging light in accordance with the detection characteristic of the photodetector [48, 49]. At the photodetector, *i.e.* a photodiode (PD) or an array of PDs, the optical signal is converted back to electrical current. The current signal is amplified through a transimpedance amplifier (TIA), and a DSP is employed for demodulation of the information bits.

The design of the transmitter unit is subject to eye safety regulations. According to the BS EN $62471:2008$ standard for photobiological safety of lamps and lamp systems [1], incoherent

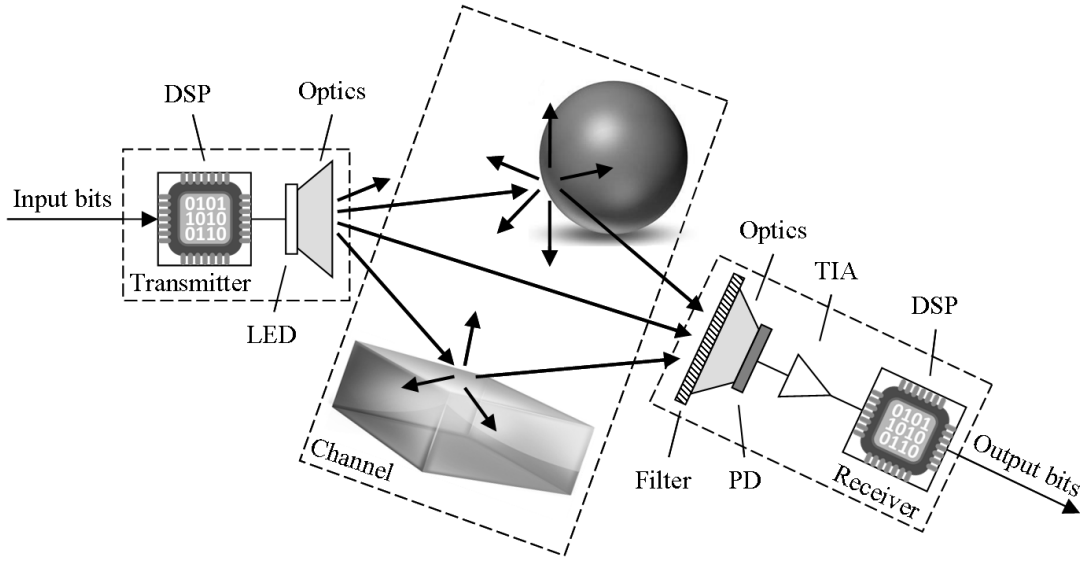


Figure 2.2: Transmission link in OWC. The general building blocks of the transmitter and receiver are presented. The optical wireless channel is illustrated, including several light rays and the reflecting objects in the setup.

diffuse continuous-wave-modulated LEDs belong to the exempt group classification and pose no photobiological hazard for the human eye, if the irradiance does not exceed $100$ W/m$^2$ at a distance of $0.2$ m from the optical source in the direction of maximal directivity within $1000s$. In general, a single LED has a generalized Lambertian radiation pattern [6, 12]. It has been shown in [47] that incoherent diffuse LEDs, *e.g.* Vishay TSHG8200 or OSRAM LCW W5SM Golden Dragon [50, 51], are inherently designed in accordance with the eye safety standard, and there is a significant room for intensity amplification through an optical system of lenses and collimators. In addition to the total output radiated optical power, the spectral response of the transmitter can be exploited in the design of high-capacity cellular OWC networks [52], where the access points in the different cells can be tuned to different center wavelengths, providing non-interfering modulation bandwidths. In OWC, this is achieved without tangible reduction in the total system capacity, because the modulation bandwidth in the order of a few tens of MHz is significantly smaller than the distance between two center frequencies. Recently, modulation bandwidth of an off-the-shelf inexpensive LED of up to $35$ MHz has been reported in [10] for realization of the currently fastest single diffuse link of $500$ Mbps. The non-linear transfer of input electrical power to output optical power is a further concern in the design of the transmitter, and it is analyzed in detail in Chapter 4.

The receiver unit has a generalized Lambertian detection pattern [6, 12]. A system of optical

elements, *e.g.* collimator lenses, can be employed to broaden the detection characteristic and enhance the strength of the received signal [49]. Furthermore, a large area PD such as the Hamamatsu S6967 [53] can be used to collect more of the total radiated signal optical power at the expense of a reduced modulation bandwidth due to the larger capacitance associated with the large-area element [52]. Alternatively, an array of PDs can be used to alleviate this trade-off. The spectral response of the receiver is determined by the spectral response of optical filter and the spectral response of the PD. Optical filters with a high transmittance coefficient at the center wavelength, *e.g.* Thorlabs bandpass filters [54], paired with PDs with high responsivity can be used in the design of high-capacity cellular OWC networks [52]. In addition, a large gain TIA, *e.g.* Analog Devices AD8015 TIA [55], with a low noise figure significantly contributes to the reduction of the electrical power of the additive white Gaussian noise (AWGN) at the receiver, and therefore to the reduction of the electrical signal-to-noise ratio (SNR) requirement. In general, because of the fact that the AWGN is directly proportional to the modulation bandwidth, a receiver matched to the transmitter in terms of modulation bandwidth can contribute to the reduction of AWGN, and therefore, to increased SNR and throughput of the OWC system. Furthermore, at the receiver, there is a linear transfer between the input optical power and output electrical power over a significantly larger dynamic range [53]. There is no signal clipping due to saturation of the PD because of the commonly employed automatic gain control (AGC).

### 2.2.2 Communication scenarios

Originally, Kahn and Barry categorize the indoor OWC scenarios based on the relative strength between the LOS and NLOS signal components [12]. In addition, based on the relative directivity between the transmitter and the receiver, the links are classified as directed and non-directed. While directed LOS links provide high irradiation intensity at the receiver and a wide channel coherence bandwidth, they are not suitable for scenarios, where high mobility of the users is required, and the link can be easily interrupted or blocked. On the other hand, even though non-directed NLOS communication provides a lower irradiation intensity at the receiver and a narrower channel coherence bandwidth, a NLOS scenario serves a greater mobility to the user, and it is significantly more robust to link blockage due to obstruction. Exploiting the reflection properties of the objects in the room, the irradiation intensity at the receiver in a NLOS communication setup can be enhanced by spot diffusing [56–58]. This is particularly beneficial for links in the infrared (IR) spectrum, where the material reflectivity is generally higher as compared to the visible light spectrum [47]. Since the primary functionality of VLC links is

illumination, a uniform light distribution over the topology of the room is desired [9]. Nonetheless, it is shown that the irradiation intensity at the receiver can be further enhanced by spot lighting [59]. There have been various studies on the optical wireless channel under different spatial conditions and optical configurations, based on direct measurements [49, 60–65] or ray-tracing simulations [12, 66–75]. It has been shown that the optical wireless channel can be well characterized by its root-mean-square (RMS) delay spread and path loss. RMS delay spread up to 13 ns and entire delay spread up to 100 ns have been reported for LOS and NLOS links, while optical path losses up to 80 dB can be experienced in an indoor setup.

In order to increase the capacity of a wireless system, a cellular network can be deployed [76]. A study conducted in [46] shows a configuration of hexagonal cells and wavelength reuse of 3 is co-channel interference limited for small cell radii and noise limited for large cell radii. Indoor peer-to-peer and client/server wireless infrared topologies have been analyzed in [45], where a noise limited network is assumed. A deployment of a cellular OWC network in an aircraft has been studied in [42, 47, 52, 77–80]. In general, the use of OWC technology within aircrafts can serve a variety of applications ranging from onboard inter-system communication, flight maintenance on the ground as well as flight entertainment. Significant amount of cabling can be saved which results in reduced weight and greater flexibility in cabin layout alterations. Measurements results reported in [77–79] demonstrate that data rates of several tens of Mbps are feasible within the cabin. Channel bandwidths of more than 50 MHz inside an aircraft cabin are reported in [49]. Comprehensive spatial signal-to-interference ratio (SIR) maps over the cabin topology are demonstrated in [47] by means of a Monte Carlo ray-tracing irradiation simulation for different wavelength reuse scenarios. By the use of a multi-beam transmitter [8, 81, 82], any radiation pattern can be obtained by combining Lambertian LEDs. In addition, light shaping diffusors can provide an even cell coverage [83] and reduce the RMS delay spread [84]. An omnidirectional radiation pattern of the transmitter and a nearly isotropic detection pattern of the receiver are employed as illustrated in Fig. 2.3. A methodology for optimization of the radiation/detection patterns in order to maximize the cell coverage is descried in [85].

The optical SIR maps can be converted into electrical signal-to-interference-and-noise ratio (SINR) maps as presented in [42, 52]. As a result, the throughput distribution over the cabin topology is obtained for wavelength reuse factors of 1, 2 and 3. It is shown that the cellular OWC network inside the aircraft cabin is interference limited due to the small cell size, employed to facilitate a high-capacity with a high link density. The results for a direct-current-

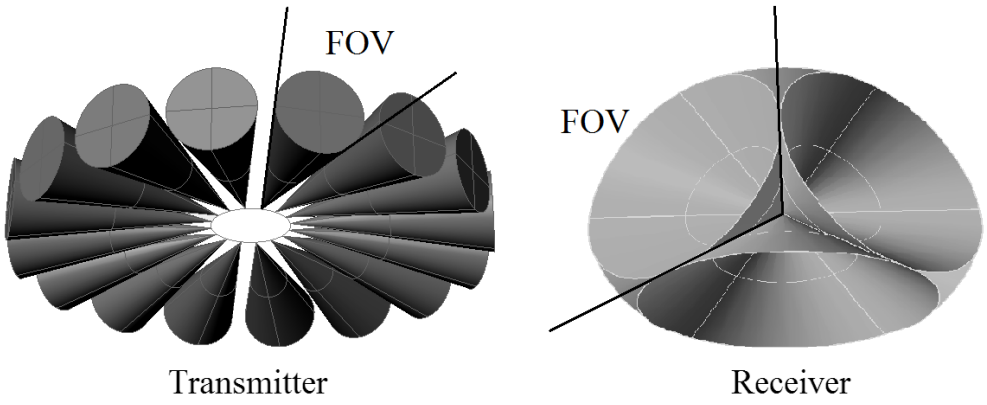


Figure 2.3: Omnidirectional radiation characteristic of a transmitter and a nearly isotropic detection pattern of a receiver. The field of view (FOV) of an individual LED and PD is illustrated.

biased optical orthogonal frequency division multiplexing (DCO-OFDM) OWC system implementation with adaptive modulation and coding are illustrated in Fig. 2.4 and Fig. 2.5 for wavelength reuse of 1 and 3, respectively. Data rates between 3 and 60 Mbps are demonstrated, and wavelength reuse factors of 3 or higher are required to ensure full cabin coverage.

From the spatial irradiation distribution in the aircraft cabin, mathematical models for the path loss in LOS and NLOS communication scenarios are obtained. It is confirmed that the optical path loss is linear over logarithmic distance, and it can be described by the following equation [47, 76, 80]:

$$\mathrm{PL}(d)[\mathrm{dB}] = 10\log_{10}\left(\frac{P_\mathrm{T}}{P_\mathrm{R}(d)}\right) = \mathrm{PL}(d_0) + 10\zeta\log_{10}\left(\frac{d}{d_0}\right) + \xi\ , \tag{2.1}$$

where $\mathrm{PL}(d_0)$ [dB] is the path loss at reference distance $d_0$ [m], $\zeta$ is the path loss exponent, $d$ [m] is the distance between transmitter and receiver, and $\xi$ [dB] is a random variable with zero-mean log-normal distribution that accounts for shadowing effects. The optical power radiated from the transmitter and the optical power impinging on the receiver are denoted by $P_\mathrm{T}$[W] and $P_\mathrm{R}$[W], respectively. Examples for LOS and NLOS path loss are presented in Fig. 2.6 and Fig. 2.7, respectively [47]. For the considered cabin setup, a LOS path loss between 27 dB and 69 dB with a path loss exponent of 1.94 and a standard deviation of the shadowing component of 0.57 dB is experienced over the distance between 0.04 m and 5.6 m. In addition, NLOS path loss between 64 dB and 72 dB with a path loss exponent of 1.28 and 0.7 dB standard deviation of the shadowing component can be observed over the distance between 1.45 m and 5.78 m. Since the NLOS path loss is comparable to the LOS path loss at larger distances, a

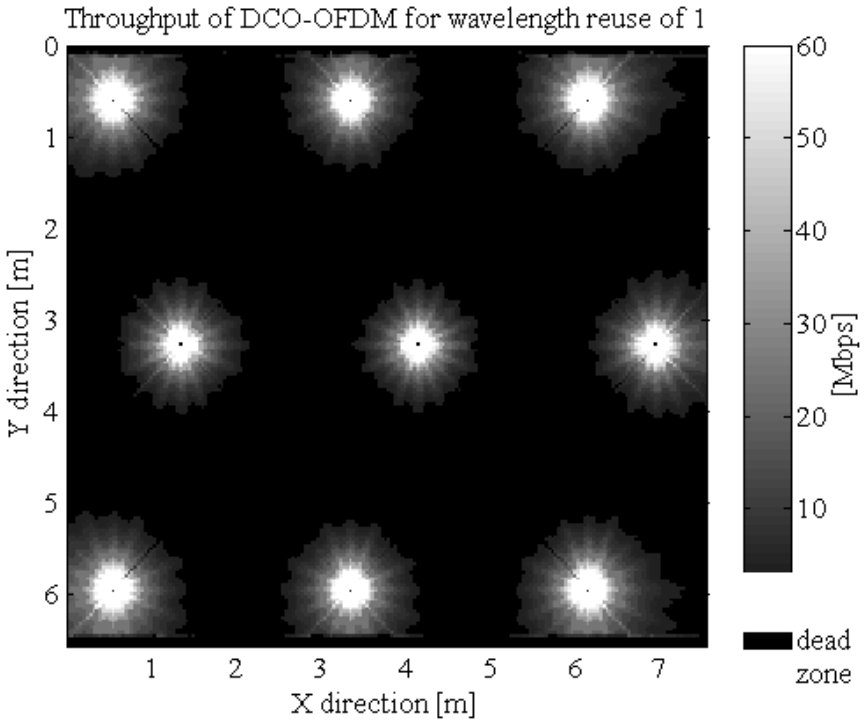


Figure 2.4: Throughput of DCO-OFDM in an aircraft cabin for wavelength reuse of 1 in the NIR spectrum.

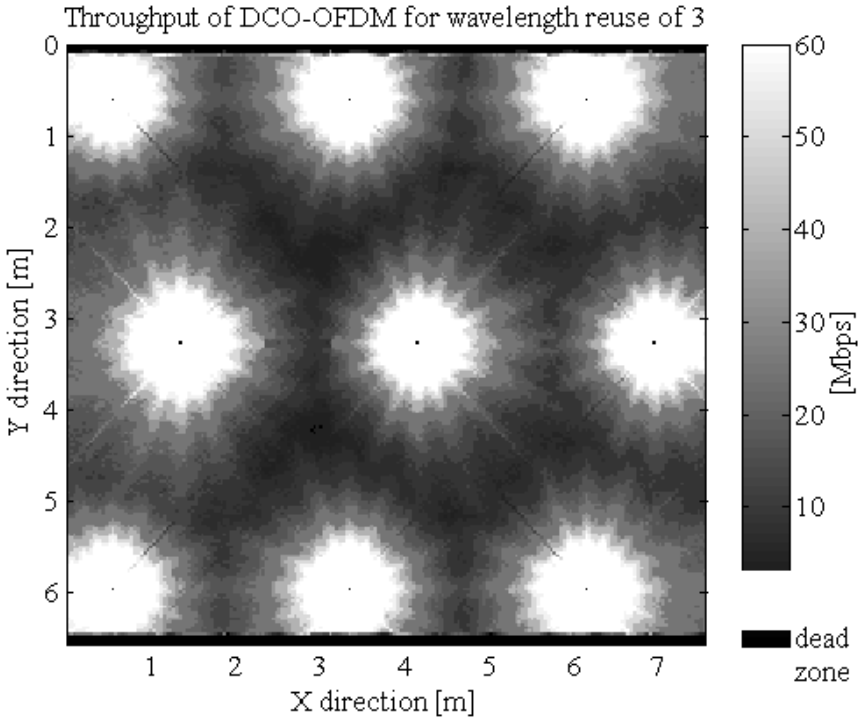


Figure 2.5: Throughput of DCO-OFDM in an aircraft cabin for wavelength reuse of 3 in the NIR spectrum.

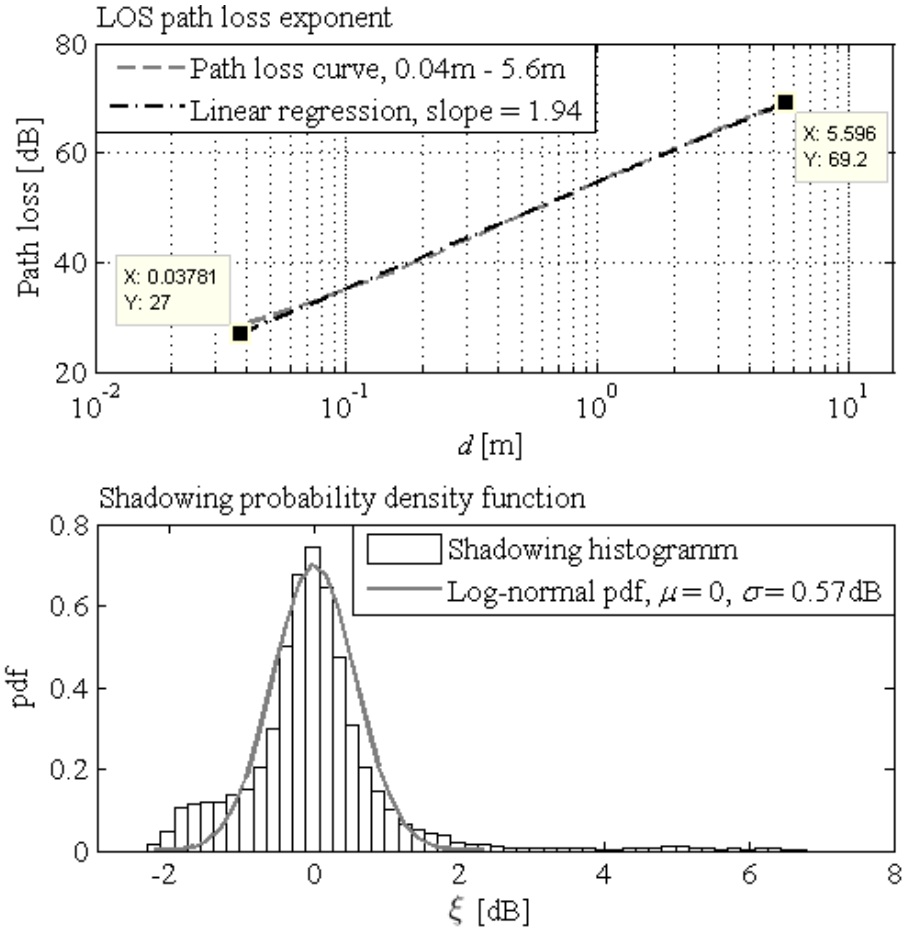


Figure 2.6: Infrared LOS path loss simulation in an aircraft cabin, including the estimation of the path loss exponent and the standard deviation of the shadowing component.

NLOS setup with higher robustness to link blockage and better mobility service is an appealing communication scenario for OWC.

## 2.3 Capacity of OWC

The capacity of a communication system is defined by Claude Shannon as the maximum number of bits per piece of bandwidth that can be successfully transmitted over a communication link [86]. The link impairments such as the non-linear transfer characteristics of the front-ends, the channel characteristics and the noise sources are the limiting factors for the system capacity. In practical system implementation, computational complexity of the signal processing and the nature of the front-ends, such as the electronic and optical components in an OWC system, impose constraints on the shape of the transmitted signals. In this Section, the challenges in the

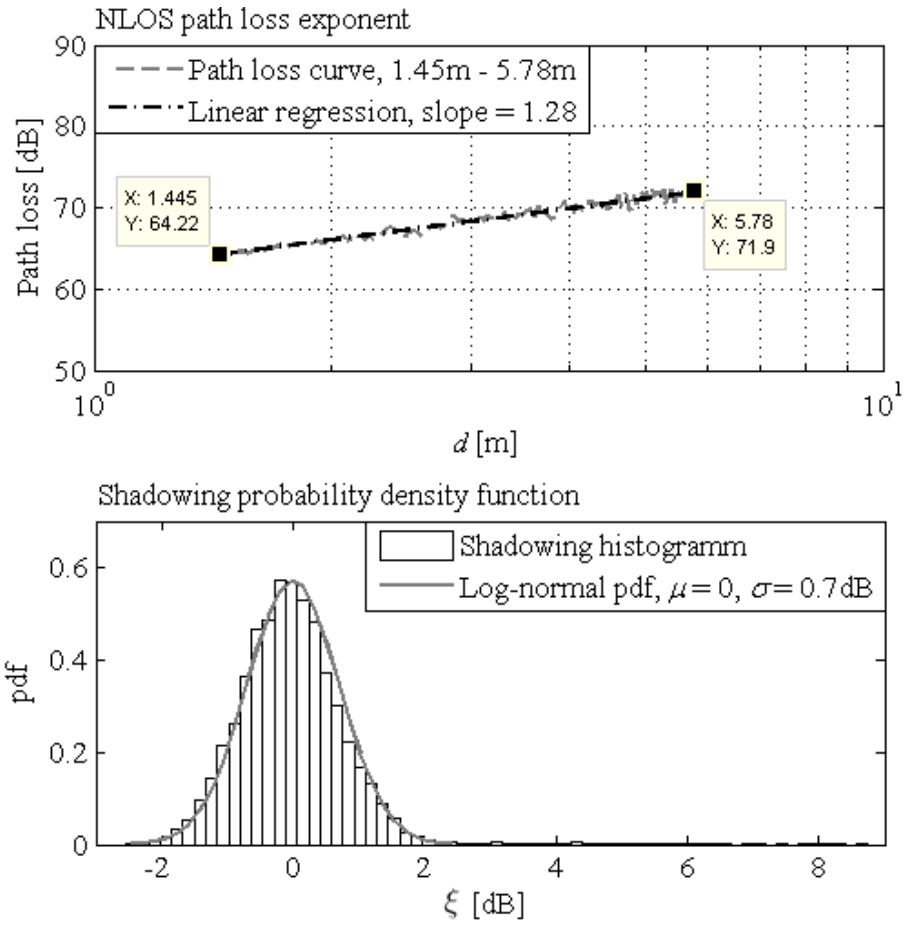


Figure 2.7: Infrared NLOS path loss simulation in an aircraft cabin, including the estimation of the path loss exponent and the standard deviation of the shadowing component.

maximization of the information rates and the capacity of practical OWC system implementations are discussed in the context of the existing literature.

### 2.3.1 Link impairments

Impairments in the optical wireless link result in signal distortion and capacity degradation. In this study, the signal distortion is accounted to the non-linear transfer characteristic of the transmitter, the dispersive optical wireless channel, and the AWGN at the receiver.

Because of the the non-negative dynamic range of the transmitter [50], signals with negative portions suffer from non-linear distortion due to signal clipping. In addition, imperfections of the optical front-ends due to the use of off-the-shelf components result in a non-linear transfer of the transmitted signal which introduces a further non-linear signal distortion. It is shown in [20]

that the non-linear transfer characteristic of the LED can be compensated by pre-distortion. A linear characteristic is obtainable, however, only over a limited range. Therefore, the transmitted signal is constrained between levels of minimum and maximum radiated optical power. Furthermore, the average optical power level is constrained by the eye safety regulations [1] and/or design requirements such as signal dimming. An example of the latter is OWC in an aircraft cabin [47] where the cabin illumination serves the dual purpose of VLC. In order to condition the signal in accordance with these constraints, signal scaling in the DSP and addition of a direct current (DC) bias in the analog circuitry is required.

In OWC with intensity modulation and direct detection (IM/DD), because of the fact that the light carrier wavelength is significantly smaller than the area of the photodetector, there is no fast fading in the channel due to effective spatial diversity [12], but rather only slow fading in the form of path loss and log-normal shadowing [47]. In addition, based on the geometry of the communication link, the optical wireless channel is dominated by LOS or NLOS/multipath signal components. The LOS channel has a very narrow power delay profile with a very broad 3-dB coherence bandwidth, which enables the transmission of signals with equally broad information bandwidth. It can be generally assumed as a frequency non-selective slow fading channel or a flat fading channel. The NLOS channel, however, has a very large RMS delay spread, and therefore a very narrow 3-dB coherence bandwidth. Thus, it can be modeled as a frequency selective slow fading channel or a dispersive channel. As a result, the transmission of a broadband signal suffers a data rate penalty. In general, a similar effect is also caused by the low-pass frequency response of the front-end components, such as LEDs, PDs and electronic amplifiers. However, as presented in Fig. 2.6 and Fig. 2.7 from [47], NLOS communication scenarios provide a irradiation intensity similar to LOS communication scenarios at larger distances because of the lower path loss exponent. Furthermore, a NLOS link is significantly more robust to physical link blockage due to obstruction by a mobile object or person. Therefore, multi-carrier transmission with an inherent robustness to multi-path dispersion is expected to deliver very high data rates and high quality of service is medium-range indoor communication scenarios with high mobility.

At the receiver, the signal is detected by a PD and pre-amplified by a transimpedance amplifier (TIA). Here, the ambient light produces shot noise, and thermal noise arises in the electronic circuitry. These noise components are generally white with a Gaussian distribution. As a result, the noise at the receiver can be modeled as AWGN.

### 2.3.2 Optical signals

As opposed to a radio frequency (RF) system, where the data-carrying signal modulates the complex-valued bipolar electric field radiated by an antenna, in an OWC system the signal modulates the intensity of the optical emitter, and therefore it needs to be real-valued and unipolar non-negative. Since LEDs are incoherent light sources, it is difficult to collect signal power in a single electromagnetic mode and to provide a stable carrier in an indoor OWC scenario. Therefore, it is infeasible to construct an efficient coherent receiver, such as the superheterodyne receiver commonly used in RF transmission. Practical low-cost optical carrier modulation for OWC is usually achieved through IM/DD in an incoherent fashion. The information is encoded in the envelope of the transmitted signal, and there is no frequency or phase information.

Single-carrier pulse modulation is a suitable candidate for data transmission in OWC. The information can be encoded in the duration of the pulse, such as pulse width modulation (PWM) or pulse interval modulation (PIM) [5, 87]. In addition, the information can be encoded in the position of the pulse, such as multi-level pulse position modulation ($M$-PPM) [11, 12]. Alternatively, the information can be encoded in the amplitude of the pulse, such as multi-level pulse amplitude modulation ($M$-PAM) [13]. In this study, the $M$-PPM and $M$-PAM are considered as benchmark schemes. Examples for binary and multi-level realizations of these single-carrier modulation techniques are given in Fig. 2.8 and Fig. 2.9, respectively. Here, a limited linear dynamic range of the transmitter between positive levels of minimum and maximum forward currents, *i.e.* $I_{\min}$ and $I_{\max}$, is considered, resulting in an additional DC bias requirement in $M$-PAM. By encoding the information in the position of the pulse within the transmitted symbol, $M$-PPM has been considered for OWC in [88] because of its ability to provide robust low-complexity low-rate transmission at very low SNR in the flat fading channel. Furthermore, trellis coding of the $M$-PPM signal is shown to increase the OWC system robustness and spectral efficiency also in a dispersive channel [89]. Here, a lower SNR requirement for a target bit-error ratio (BER) with a lower spectral efficiency is achieved by increasing the modulation order, $M$, where 2-PPM has the highest SNR requirement and spectral efficiency. Showing the same SNR requirement as 2-PPM, a binary on-off keying (OOK) transmission doubles the spectral efficiency, and therefore it has been the preferred candidate for the pursuit of higher data rates in an OWC system [6–9]. In addition, if the link budget accommodates higher SNR, the spectral efficiency of the single-carrier system can be increased by encoding the information in the amplitude of the pulse, *i.e.* amplitude of the transmitted symbol, such as multi-level

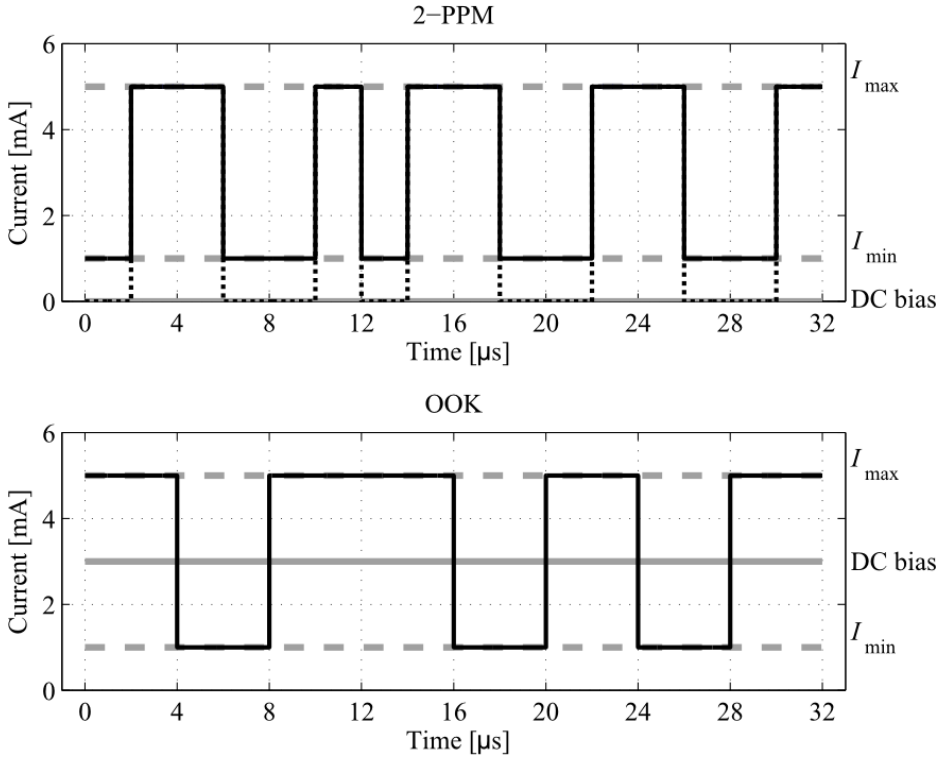


Figure 2.8: Single-carrier binary optical transmission.

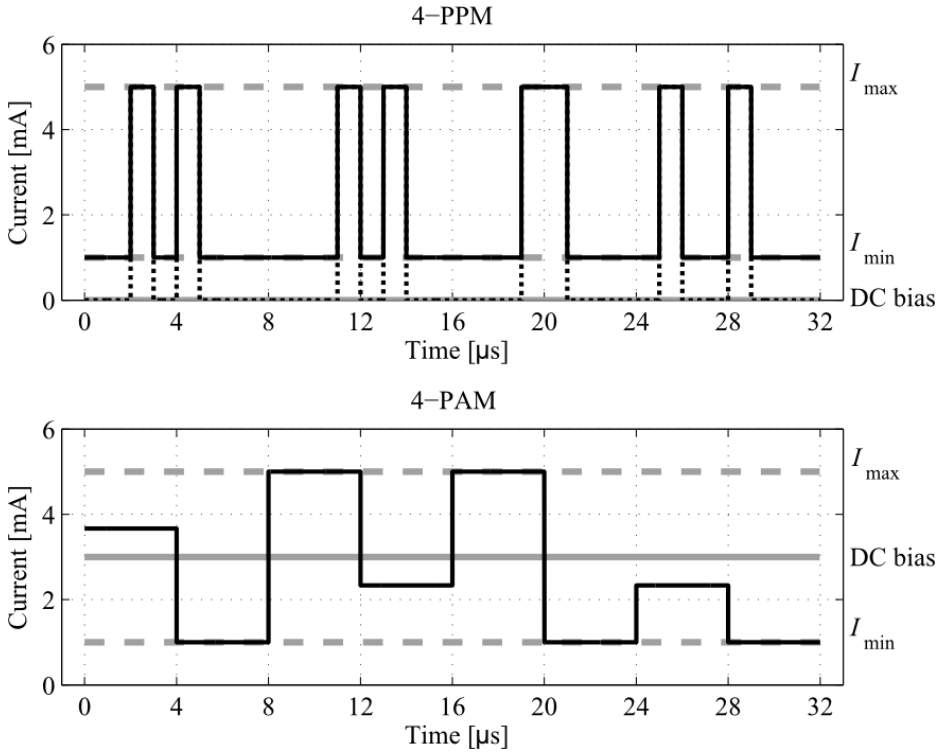


Figure 2.9: Single-carrier multi-level optical transmission.

$M$-PAM [13, 19]. The benefits of $M$-PPM and $M$-PAM are united in the hybrid system, *i.e.* multi-level pulse amplitude and position modulation ($M$-PAPM) [90].

At low data rates, the 3-dB coherence bandwidth of the dispersive channel is larger than the 3-dB bandwidth of the information-carrying pulse, and therefore the dispersive channel can be considered as flat fading over the pulse bandwidth. The challenge arises in the attempt to push high data rates through the dispersive channel. At high data rates, where the 3-dB bandwidth of the pulse exceeds the coherence 3-dB bandwidth of the optical wireless channel, the RMS delay spread of the channel impulse response exceeds the pulse duration. Therefore, such techniques suffer from severe inter-symbol interference (ISI), limiting their throughput. In general, a guard interval can be added to reduce the overlap between the information-carrying pulses [91] at the expense of a decreased system spectral efficiency. In order to compensate for the channel effect, the optimum receiver employs maximum likelihood sequence detection (MLSD) [12, 13]. Here, the MLSD algorithm chooses the sequence of symbols that maximizes the likelihood of the received symbols with the knowledge of the channel taps. Even though the Viterbi algorithm can be used for MLSD to reduce the computational effort, the complexity of MLSD still grows exponentially with the number of channel taps. Therefore, in practical system implementations, suboptimum equalization techniques with reduced complexity are used. These include the linear feed-forward equalizer (FFE) or the non-linear decision feedback equalizer (DFE) with zero forcing (ZF) or minimum mean squared error (MMSE) criteria [8, 13]. The superior BER performance at a lower SNR requirement of DFE comes at a significantly increased complexity as compared to FFE [13].

Multi-carrier modulation has inherent robustness to ISI, because the symbol duration is significantly longer than the RMS delay spread of the optical wireless channel. As a result, multi-level quadrature amplitude modulation ($M$-QAM) optical orthogonal frequency division multiplexing (O-OFDM) promises to deliver very high data rates [10, 16, 25]. Because of the common use of a cyclic prefix (CP), the channel frequency response can be considered as flat fading over the subcarrier bandwidth [92, 93]. Thus, single-tap linear FFE with low complexity paired with bit and power loading can be used to minimize the channel effect [94, 95]. In O-OFDM, the time domain signal envelope is utilized to modulate the intensity of the LED. For this purpose, the signal needs to be real-valued and non-negative. A real-valued signal is obtained when Hermitian symmetry is imposed on the OFDM subcarriers. One approach to obtain a non-negative signal, known as DCO-OFDM, is the addition of a DC bias [96, 97]. A closely

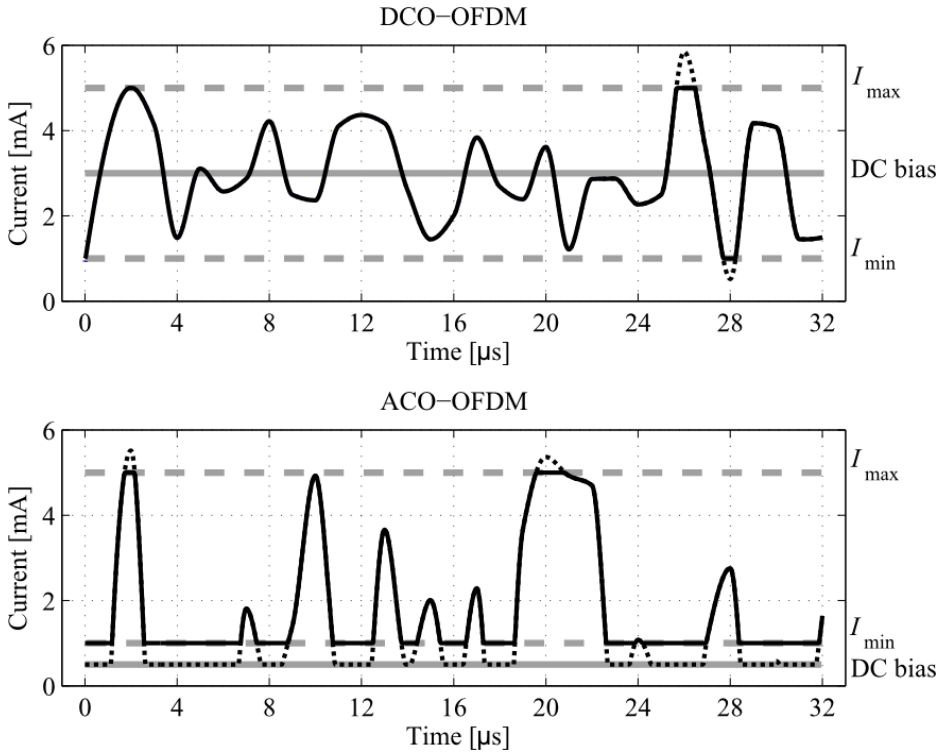


Figure 2.10: Multi-carrier multi-level optical transmission.

related technique, the discrete multi-tone (DMT), has been employed for digital subscriber line (DSL) data transmission [98]. Another approach, known as asymmetrically clipped O-OFDM (ACO-OFDM), is proposed by Armstrong *et al.* [93, 99, 100]. By enabling the odd subcarriers for data transmission and setting the even ones to zero, the negative part of the time domain signal can be clipped at the transmitter without any information loss at the odd subcarriers at the receiver. In comparison to DCO-OFDM, ACO-OFDM is expected to achieve a better spectral efficiency at low SNR at the expense of a $50\%$ reduction in spectral efficiency at high SNR. An example of O-OFDM transmission is illustrated in Fig. 2.10 for a limited linear dynamic range of the transmitter, resulting in non-linear signal clipping distortion [101, 102]. A modulation technique closely related to ACO-OFDM with similar electrical SNR requirement and spectral efficiency has been presented in [103] and named as PAM-DMT. The difference between the two lie within two steps of the modulation procedures. In PAM-DMT, only the imaginary part of the information-carrying odd subcarriers is modulated in an $M$-PAM fashion, while the real parts are set to zero, and there is no Hermitian symmetry imposed on the OFDM frame. Another unipolar modulation approach with similar SNR requirement and spectral efficiency is known as flip-OFDM [104]. By exploiting the symmetry within the time domain signal samples [99], the computational complexity can be reduced by $50\%$ by halving the number of fast

Fourier transform (FFT) operations.

In addition, there have been attempts to improve the electrical power efficiency of the unipolar half-Gaussian O-OFDM signals [105, 106]. Again by exploiting the symmetry within the time domain signal samples [99], the signal demodulation procedure of ACO-OFDM can be improved for a reduction in the electrical SNR requirement of approximately $1$ dB [105]. Moreover, the improved detector structure can be combined with the flip-OFDM structure to also achieve a $50\%$ reduction in the computational complexity. The combined modulation scheme is named as unipolar OFDM (U-OFDM) and presented in [106]. Since these improvements can be superimposed with the optimum signal scaling and DC-biasing to counter the non-linear signal distortion proposed in this study, only the general ACO-OFDM scheme is considered for the modeling and comparison purposes.

Since the $M$-PPM and $M$-PAM signals have a probability density function (PDF) with a finite support and because of their respective demodulation procedures, they can fit the minimum, average and maximum optical power constraints of the transmitter without effective non-linear clipping distortion. The O-OFDM systems employs the inverse FFT (IFFT) as a multiplexing technique at the transmitter. Therefore, for a large number of subcarriers the non-distorted time domain signals in DCO-OFDM and ACO-OFDM closely follow Gaussian and half-Gaussian distributions, respectively, according to the central limit theorem (CLT) [28]. A total subcarrier number as small as $64$ is sufficient to ensure Gaussianity [18]. Thus, signal scaling and DC-biasing in DCO-OFDM and ACO-OFDM result in a non-linear signal distortion which can be modeled by means of the Bussgang theorem [27] as an attenuation of the data-carrying signal plus a non-Gaussian uncorrelated clipping noise component [17–19]. At the receiver, the FFT is used for demultiplexing. Therefore, the CLT can be applied again, and the clipping noise component can be modeled as a Gaussian process. This methodology is used in [18], where the non-linear transfer effects due to the short dynamic range of high-power amplifiers (HPA) in OFDM-based RF systems are studied. Symmetric signal clipping due to the large peak-to-average-power ratio (PAPR) in RF OFDM is studied in [107, 108]. Equivalently, symmetric signal clipping in optical OFDM, *e.g.* DMT for DSL transmission, is investigated in [17, 19, 109, 110]. An optimal DC bias of a symmetrically clipped signal can be inferred from [110, 111]. It is shown in [110] that iterative decoding with clipping noise estimation and subtraction can reduce the BER for an increased computational complexity. In this study, a comprehensive analysis is presented for a generalized non-linear transfer function and for a double-sided signal

clipping at independent bottom and top levels after pre-distortion. In addition, the analysis is employed in the formulation of the optimum signal scaling and DC-biasing to minimize the required electrical SNR per bit for a target BER in a practical dynamic range of the transmitter.

OOK, essentially 2-PAM, and $M$-PPM have been compared in terms of electrical and optical power requirement in a dispersive channel with equalization in [12]. An increasing power requirement is demonstrated with the increase of the RMS channel delay spread or, equivalently, data rate. In a later study [112], $M$-PPM, $M$-PAM and multi-carrier $M$-QAM transmission, similar to $M$-QAM DCO-OFDM, have been compared assuming a flat fading channel in terms of optical power requirement and spectral efficiency. However, an unlimited non-negative dynamic range of the transmitter is considered which is hardly achievable in practice. In addition, the non-negative $M$-QAM signal is scaled down to accommodate the large PAPR, resulting in an increased optical power requirement. Recently, a similar comparison has been reported in [100] for the multi-carrier transmission schemes ACO-OFDM and DCO-OFDM with a tolerable clipping distortion. In this thesis, single-carrier and multi-carrier transmission schemes are compared in terms of spectral efficiency and electrical SNR requirement in a dispersive realistic optical wireless channel with optimum signal scaling and DC-biasing for a practical dynamic range of the transmitter, where the DC bias power is excluded or included in the calculation of the SNR.

### 2.3.3 Maximization of information rate and capacity

The optical wireless channel is a linear time-invariant channel, where the channel output can be obtained by a linear convolution of the impulse response of the channel and the transmitted signal [12]. In general, in OWC systems, the ambient light produces high-intensity shot noise at the receiver. In addition, thermal noise arises due to the electronic pre-amplifier in the receiver front-end. Both of these noise sources can be accurately modeled as AWGN which is independent from the transmitted signal [12]. Therefore, the OWC systems benefit from forward error correction (FEC) coding or channel coding procedures such as turbo codes or low density parity check (LDPC) codes to approach the Shannon capacity [86] under average electrical power constraint, where only the alternating current (AC) signal power is considered [113]. In general, in VLC systems, the additional DC bias power that may be required to facilitate a unipolar signal is employed for illumination as a primary functionality. Therefore, it can be excluded from the calculation of the electrical signal power invested in the complementary data

communication. In IR communication systems, the DC bias power is constrained by the eye safety regulations [1], and it is generally included in the calculation of the electrical SNR [25]. Therefore, the systems experience an SNR penalty because of the DC bias, and a framework for its minimization is proposed in this thesis.

The body of literature on the capacity of the band-limited linear optical wireless channel with AWGN mainly differs in the imposition of the constraints on the transmitted signals, *e.g.* average electrical power constraint, average optical power constraint, peak optical power constraint *etc*. Essiambre *et al.* [113] considers the validity of the Shannon capacity [86] as a function of the electrical SNR, when only an average electrical power constraint is imposed on the AC electrical power of single-carrier or multi-carrier signals and a linear transfer characteristic of the optical front-end. Hranilovic and Kschischang [114] assume signal non-negativity and an average optical power constraint. They derive an upper bound of the capacity as a function of the optical SNR, using Shannon sphere packing argument [115], and they present a lower bound of the capacity, using a maxentropic source distribution. Examples are given for PAM, QAM and signals in the form of prolate spheroidal waves. Later, Farid and Hranilovic [116, 117] tighten the upper and lower bounds, using an exact geometrical representation of signal spaces, and they add a peak optical power constraint. With the increasing popularity of multi-carrier systems, You and Kahn [118] presented the capacity of DCO-OFDM, using the sphere packing argument [115] under an average optical power constraint, infinite dynamic range of the transmitter and a sufficient DC bias to ensure non-negativity. In this case, there is a fixed ratio between the average optical power and the total electrical power, *i.e.* AC and DC electrical power, as presented in [24]. It is shown that the DCO-OFDM system capacity approaches the Shannon capacity [86] at high electrical SNR, leaving a 3-dB gap due to the DC bias penalty on the SNR given in [24]. Recently, Li *et al.* [119, 120] investigated the information rate of ACO-OFDM, confirming that it has a very similar form to the Shannon capacity [86]. They also assume an infinite dynamic range of the transmitter and an average optical power constraint. Similarly, there is a fixed ratio between the optical signal power and the electrical signal power which merely modifies the received electrical SNR, as generalized in [24]. It is shown that ACO-OFDM achieves half of the Shannon capacity due to the half bandwidth utilization, and there is a further 3-dB penalty on the electrical SNR due to the effective halving of the electrical power of an information-carrying subcarrier in ACO-OFDM.

Following the Bussgang decomposition, the mutual information of RF OFDM systems with

non-linear distortion has been studied in [18, 107, 121]. The maximum achievable rate of Gaussian signals with non-linear distortion has been presented in [122], considering the mutual information of the transmitted and received time domain signals. This information rate can be approached with iterative time-domain signal processing techniques, such as decision-aided signal reconstruction [123] or iterative non-linear noise estimation and cancelation [121, 124], for an increased computational complexity. In general, practical indoor O-OFDM system implementations aim to reduce the computational effort only to the IFFT/FFT operations, while the additional system parameters are computed offline and stored in look-up tables, for the sake of the realization of high data rate optical links [10]. In DCO-OFDM and ACO-OFDM, the information-carrying subcarriers are demodulated in the frequency domain, where the non-linear distortion is transformed into additive Gaussian noise. Since the transmitter biasing parameters, such as the signal standard deviation and the DC bias, directly influence the received electrical SNR [24], the optimum biasing setup for given minimum, average and maximum optical power constraints under an average electrical power constraint is essential for the OWC system information rate.

In this thesis, the achievable information rates of the DCO-OFDM and ACO-OFDM systems are formulated in the context of the non-linear signal distortion at the optical front-end. In addition to the minimum and maximum optical power constraints, an average optical power constraint is imposed, as well, and the information rates of the systems are presented, excluding or including the additional DC bias power in the calculation of the electrical SNR.

## 2.4 Chapter summary

In this Chapter, a brief summary of the history of OWC has been presented. The fundamentals of a wireless communication setup have been discussed, including the front-end design, the geometry of the wireless link and the resulting optical wireless channel. The typical building blocks of the transmitter and the receiver have been presented. In addition, the LOS and NLOS communication scenarios have been introduced, including ways to enhance the irradiance at the receiver in IR and VLC setups. The state-of-the-art in SINR modeling and maximization in cellular OWC systems has been discussed. Examples of throughput maps over the topology of the communication scenario have been presented for an aircraft cabin. In addition, realistic LOS and NLOS channel models have been shown, including path loss and log-normal shadowing.

In the second Section of the Chapter, the achievable capacity of an OWC link has been discussed. First, the limiting factors of the system capacity have been stated as the non-linear transfer characteristic of the transmitter, the limited coherence bandwidth of the optical wireless channel and the AWGN at the receiver. The common types of single-carrier and multi-carrier optical signals have been briefly discussed in the context of the existing literature on their performance and comparison, indicating the need for a comprehensive analytical treatment of practical OWC links in consideration of these capacity limiting factors. It was pointed out that multi-carrier transmission is expected to deliver higher data rates in the dispersive optical wireless channel in an NLOS communication setup because of its inherent robustness to multi-path fading. Finally, the literature on the capacity of the OWC systems has been summarized, where different types of signal constraints and an idealized infinite non-negative linear dynamic range of the transmitter have been considered.

# Chapter 3
# Modulation techniques for OWC

## 3.1 Introduction

The data transmission in optical wireless communication (OWC) with incoherent light sources is realized through intensity modulation and direct detection (IM/DD). For this purpose, the transmitted signal needs to be real-valued and non-negative. In practice, this is achieved through single-carrier modulation techniques, such as multi-level pulse position modulation ($M$-PPM) and multi-level pulse amplitude modulation ($M$-PAM), and through multi-carrier modulation such as multi-level quadrature amplitude modulation ($M$-QAM) optical orthogonal frequency division multiplexing (O-OFDM). Conventionally, the average optical power is defined as the first moment of the transmitted signal, while the average electrical power is defined as the second moment of the transmitted signal. In practice, the dynamic range can be linearized through pre-distortion only between levels of minimum and maximum radiated optical power. In addition, eye-safety regulations [1] and/or design requirements also impose an average optical power constraint. In accordance with these constraints, there is a fixed relation between average electrical power and the average optical power of the single-carrier and multi-carrier signals which varies with the change in the biasing setup, *i.e.* a combination of direct current (DC) bias and signal variance. The optical-to-electrical (O/E) conversion of the optical signals is elaborated in this Chapter. In this study, the electrical energy consumption of the OWC system is considered, and therefore the average electrical power carries the information. Here, the received electrical signal-to-noise ratio (SNR) is presented as a function of the channel equalization penalty, the DC bias penalty and the non-linear distortion parameters.

## 3.2 System model

OWC can be described by the following continuous-time model for a noisy communication link:

$$y = h * F(x) + w \ , \tag{3.1}$$

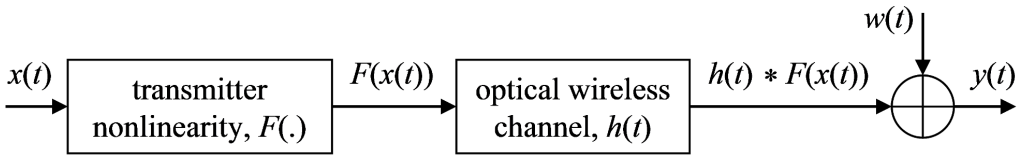


Figure 3.1: Generalized block diagram of the OWC link in the time domain, including the LED nonlinearity, the dispersive optical wireless channel and the AWGN.

where $y(t)$ represents the received distorted replica of the transmitted signal, $x(t)$, which is subjected to the non-linear distortion function, $F\big(x(t)\big)$, of the transmitter front-end. The non-linearly distorted transmitted signal is convolved with the channel impulse response, $h(t)$, and it is distorted by additive white Gaussian noise (AWGN), $w(t)$, at the receiver. Here, $*$ stands for linear convolution. The generalized model of the OWC link in the time domain is illustrated in Fig. 3.1. Since the OWC system is implemented by means of a digital signal processor (DSP), the following equivalent discrete model for a noisy communication link is employed in the system description:

$$\mathbf{y} = \mathbf{h} \star F(\mathbf{x}) + \mathbf{w} \ , \tag{3.2}$$

where $\star$ stands for discrete linear convolution. Here, the transmitted signal vector, $\mathbf{x}$, contains $Z_{\mathbf{x}}$ samples, the channel impulse response vector, $\mathbf{h}$, has $Z_{\mathbf{h}}$ samples, and as a result, the AWGN vector, $\mathbf{w}$, and the received signal vector, $\mathbf{y}$, have $Z_{\mathbf{x}} + Z_{\mathbf{h}} - 1$ samples [125]. The discrete signal vectors are obtained by sampling of the equivalent continuous-time signals. The sampling rates over a time period of $T$ differ in the considered systems, and the details are presented in Section 3.3.

### 3.2.1 Transmitter nonlinearity

A light emitting diode (LED) is biased by a constant current source which supports the entire range of forward voltages across the LED. The bias current is added to the data-carrying current, yielding the forward current through the LED, $I_{\mathrm{f}}$. The non-linear transfer characteristic of the LED can be described by the non-linear relation between the forward current, $I_{\mathrm{f}}$, and the forward voltage, $V_{\mathrm{f}}$, which can be translated into a non-linear relation between the dissipated electrical power, $P_{\mathrm{elec}}$, and the radiated optical power, $P_{\mathrm{opt}}$, as illustrated in Fig. 3.2. In this study, the nonlinearity is generalized as a relation between the input current, $I_{\mathrm{in}} = x$, linearly proportional to the square root of the dissipated electrical power, $P_{\mathrm{elec}}$, and the output current, $I_{\mathrm{out}} = F(x)$, linearly proportional to the radiated optical power, $P_{\mathrm{opt}}$. Therefore, the large

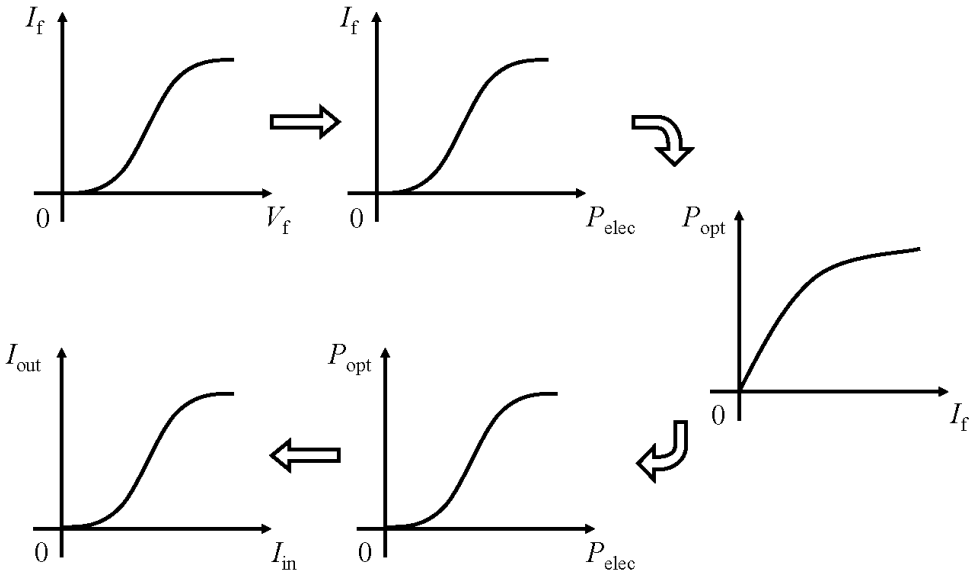


Figure 3.2: Typical non-linear transfer characteristic of an LED including the relations between the forward current, $I_\mathrm{f}$, the forward voltage, $V_\mathrm{f}$, the radiated optical power, $P_\mathrm{opt}$, and the dissipated electrical power, $P_\mathrm{elec}$. The model is generalized as a non-linear relation between the input and output information-carrying currents, $I_\mathrm{in}$ and $I_\mathrm{out}$.

peak-to-average-power ratio (PAPR) current signal, $x$, is subjected to a non-linear distortion function, $F(x)$, as it is passed through the front-end block.

Conventionally, the dynamic range of the transmitter to be modulated by the information-carrying signal is chosen as the portion of the transfer characteristic which can be considered as nearly linear. However, through signal pre-distortion with the inverse of the non-linear transfer function, the linear dynamic range of the transmitter can be maximized. As a result, the electrical alternating current (AC) power of the signal can be maximized at the transmitter for the sake of an increased electrical SNR at the receiver. This is illustrated in Fig. 3.3. A pre-distortion of the $V_\mathrm{f} - I_\mathrm{f}$ transfer characteristic of the optical transmitter has been considered in [20]. For the sake of a generalized nonlinearity model, the pre-distortion of the non-linear $I_\mathrm{in} - I_\mathrm{out}$ transfer characteristic, a superposition of the non-linear $V_\mathrm{f} - I_\mathrm{f}$ and $I_\mathrm{f} - P_\mathrm{opt}$ transfer characteristics, is considered in this study.

Two examples are presented in Fig. 3.4, one for a non-linear sigmoid function, $F(x) = \Xi(x)$, and one for a linearized function, $F(x) = \Phi(x)$. The linearization is obtained by pre-distortion of the signal with the inverse function $\Xi^{-1}(x)$. Because of the p-n junction barrier and the saturation effect of the LED, a linear transfer of the pre-distorted signal is obtainable only

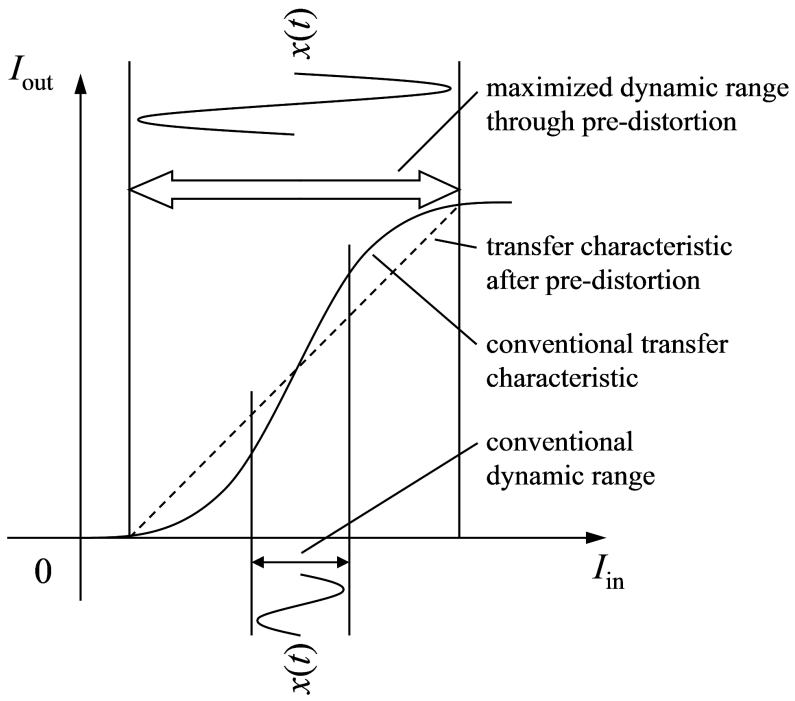


Figure 3.3: Dynamic range of the transmitter for signal modulation. The nearly linear dynamic range of a conventional non-linear transfer characteristic is illustrated, as well as the maximized linear dynamic range after signal pre-distortion.

between points of positive minimum and maximum input current, $I_{\min}$ and $I_{\max}$, resulting in a limited dynamic range of transmitter front-end. For the sake of generality, the input current is normalized to $I_{\max}$, *i.e.* $I_{\min,\mathrm{norm}} = I_{\min}/I_{\max}$ and $I_{\max,\mathrm{norm}} = 1$. In addition, the following normalized quantities are assumed for the boundaries of the dynamic range of the front-end in terms of normalized optical power and current: $P_{\min,\mathrm{norm}} = I_{\min,\mathrm{norm}}$ and $P_{\max,\mathrm{norm}} = I_{\max,\mathrm{norm}} = 1$. The eye safety regulations [1] and/or the design requirements constrain the level of radiated average optical power to $P_{\mathrm{avg,norm}}$. Through scaling and DC-biasing, $x$ can be conditioned within the dynamic range of the transmitter front-end in accordance with the average optical power constraint, and the details are presented in Section 3.3.

### 3.2.2 Optical wireless channel

The optical wireless channel has been shown to be a linear, time-invariant, memoryless system with an impulse response of a finite-duration [12]. Line-of-sight (LOS) and non-line-of-sight (NLOS) optical wireless channels can be accurately modeled by the rapidly decaying exponential impulse response function $h(t) = g_{\mathrm{h(opt)}} h_{\mathrm{norm}}(t)$, where $h_{\mathrm{norm}}(t) = U(t)6a^6/(t+a)^7$.

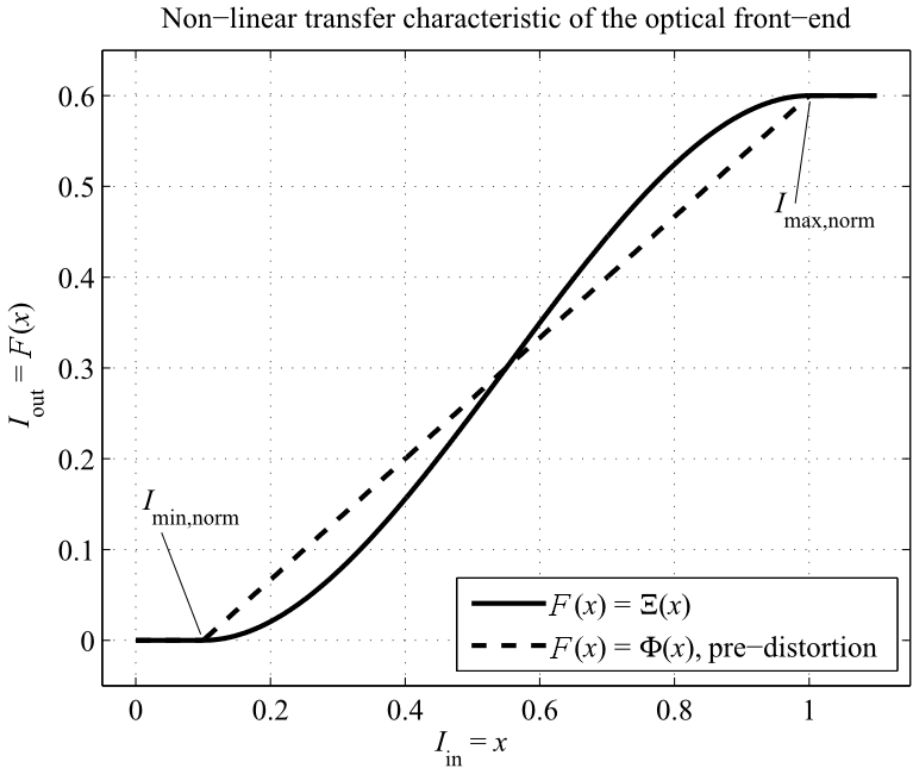


Figure 3.4: Non-linear transfer characteristic of the considered optical front-end, $\Xi(x)$, and the linearized characteristic after pre-distortion, $\Phi(x)$.

Here, $g_{\mathrm{h(opt)}}$ stands for the optical path gain coefficient, $U(\cdot)$ is the unit step function, and $a$ is related to the root-mean-square (RMS) delay spread, $D$, as follows: $a = D\sqrt{11/13}$. The 3-dB coherence bandwidth of the channel can be expressed as $B_{\mathrm{c}} = 1/(5D)$ [76]. RMS delay spreads between 1.3 ns and 12 ns are reported for LOS links, whereas RMS delay spreads between 7 and 13 ns are reported for NLOS links [12]. The channel taps in the vector $\mathbf{h}$ are obtained by sampling of the channel impulse response at the sampling frequency of the received signal, $\mathbf{y}$. The optical path gain can be expressed as $g_{\mathrm{h(opt)}} = P_{\mathrm{R}} S_{\mathrm{PD}} G_{\mathrm{TIA}} / (P_{\mathrm{T}} \sqrt{r_{\mathrm{load}}})$, where $P_{\mathrm{T}}$ is the average transmitted optical power, $P_{\mathrm{R}}$ is the average received optical power, $S_{\mathrm{PD}}$ is the responsivity of the photodiode (PD), $G_{\mathrm{TIA}}$ is the gain of the transimpedance amplifier (TIA), and $r_{\mathrm{load}}$ is the load resistance over which the received current is measured [47, 52]. In addition, the optical path gain can be related to the electrical path gain, $g_{\mathrm{h(elec)}}$, as follows:

$$g_{\mathrm{h(elec)}} = \frac{1}{B} \int_{-B/2}^{B/2} |H(f)|^2 \, df = g_{\mathrm{h(opt)}}^2 \frac{1}{B} \int_{-B/2}^{B/2} |H_{\mathrm{norm}}(f)|^2 \, df \ . \tag{3.3}$$

Here, $H(f)$ is the Fourier transform of the impulse response of the optical wireless channel, $h(t)$, $H_{\mathrm{norm}}(f)$ is the Fourier transform of $h_{\mathrm{norm}}(t)$, and $B$ is the double-sided signal band-

width. In general, it is unlikely that the signal is nonlinearly distorted at the receiver. For instance, the linear range of a Vishay TEMD5110X01 PD reaches up to $0.2$ mW of incident optical power at room temperature [126]. For a practical indoor path loss range between $50$ dB to $80$ dB [47, 80], the transmitter needs to radiate more than $20$ W of optical power, in order to drive the PD to saturation. Since such an amount significantly exceeds the limits imposed by the eye safety regulations [1, 47], it is assumed that the non-linear distortion occurs only at the transmitter.

Based on the optical center frequency, the optical emitter can be modulated within a certain bandwidth. Here, the multiplication of the bandwidth and the spectral efficiency of the system yields the system throughout. However, for a fixed SNR, the bit-error ratio (BER) performance is independent of the bandwidth, and consequently of the throughput. In this study, the BER performance of the OWC systems is compared for equal average electrical symbol power, $P_{\mathrm{s(elec)}}$, and equal bandwidth, $B$. In addition, the BER is assessed through the effective electrical SNR per bit at the receiver as a function of the undistorted electrical SNR per bit at the transmitter, *i.e.* the average electrical bit energy normalized to the power spectral density of the AWGN, $\gamma_{\mathrm{b(elec)}} = E_{\mathrm{b(elec)}}/N_0$.

In $M$-PPM and $M$-PAM, the RMS delay spread of the channel becomes comparable to or larger than the pulse duration at high data rates which causes a severe inter-symbol interference (ISI). Equivalently, the signal bandwidth exceeds the channel coherence bandwidth. In general, similar effects are also caused by the low-pass frequency response of the front-end components, such as LEDs, PDs and amplifiers. As a result, the BER performance is degraded, and the systems effectively incur an SNR penalty. In practical system implementations, a multi-tap linear feed-forward equalizer (FFE) and a non-linear decision feedback equalizer (DFE) with zero forcing (ZF) or minimum mean squared error (MMSE) criteria are deployed to reduce the SNR penalty. The theoretical limits for the least SNR penalty of the equalizers are discussed below. Because of the fact that in single-carrier modulation the RMS delay spread of the channel is comparable to or larger than the pulse duration at high data rates, a large number of channel taps are required to accurately represent the impulse response function, in order to counter its effect. As a result, the computational complexity of the equalization process is significantly increased. In addition, since the number of channel taps depends on the frequency at which the received signal, $\mathbf{y}$, is sampled, the received pulses are often oversampled, in order to increase the accuracy of the equalization process, leading to an even higher computational effort.

However, these approaches are fundamentally limited by the maximum sampling frequency of the analog-to-digital (A/D) converter employed. As a result, the theoretical limits for the SNR penalty are hardly achievable in practical system implementations. The gain of the equalizer is represented by the gain factor $G_{\mathrm{EQ}}$. For a linear FFE with the ZF criterion, the gain factor is given as follows [13]:

$$G_{\mathrm{EQ}} = \left( \frac{1}{B} \int_{-B/2}^{B/2} \frac{1}{\Lambda(f)} \, df \right)^{-1} . \tag{3.4}$$

Here, $\Lambda(f)$ is expressed as follows [13]:

$$\Lambda(f) = \sum_{z=-\infty}^{\infty} |V(f - zB)H(f - zB)|^2 \, , \tag{3.5}$$

where $V(f)$ is the Fourier transform of the impulse response of the pulse shaping filter at the transmitter, $v(t)$, and $z$ is the counter in the summation. For a linear FFE with the MMSE criterion, the gain factor is given as follows [13]:

$$G_{\mathrm{EQ}} = \left( \frac{1}{B} \int_{-B/2}^{B/2} \frac{1}{\Lambda(f) + \gamma_{\mathrm{b(elec)}}^{-1}} \, df \right)^{-1} . \tag{3.6}$$

For a non-linear DFE with the ZF criterion, the gain factor is given as follows [13]:

$$G_{\mathrm{EQ}} = \exp \left( \frac{1}{B} \int_{-B/2}^{B/2} \ln \left( \Lambda(f) \right) df \right) . \tag{3.7}$$

For a non-linear DFE with the MMSE criterion, the gain factor is given as follows [13]:

$$G_{\mathrm{EQ}} = \exp \left( \frac{1}{B} \int_{-B/2}^{B/2} \ln \left( \Lambda(f) + \gamma_{\mathrm{b(elec)}}^{-1} \right) df \right) . \tag{3.8}$$

The gain factor $G_{\mathrm{EQ}}$ represents the theoretical lower bound for the electrical SNR penalty which the BER performance incurs at high data rates. This lower bound is achieved when an infinite number of channel taps are considered in the FFE and DFE which is hardly achievable in practice. In general, ZF eliminates the ISI completely, but it results in AWGN amplification when the path gain decreases. Alternatively, MMSE equalization alleviates this issue as it provides a trade-off between AWGN amplification and residual ISI. Since, however, an equalizer with an MMSE criterion requires a higher computational effort, and it only reduces the SNR penalty by approximately $0.5$ dB as compared to the ZF criterion for the considered channel

model, ZF is considered in this study.

In multi-carrier systems such as OFDM-based OWC, the RMS delay spread is significantly shorter than the symbol duration, and therefore the equalization process is considerably simplified to single-tap equalization [93]. The ISI and the inter-carrier interference (ICI) are completely eliminated by the use of a large number of subcarriers and a cyclic prefix (CP) which has a negligible effect on the electrical SNR requirement and spectral efficiency [92]. Thus, the dispersive optical wireless channel is transformed into a flat fading channel over the subcarrier bandwidth [93]. For example, the ISI from maximum delay spreads of up to $100$ ns can be compensated by a CP of $2$ samples at a sampling rate of $20$ MHz. For a fast Fourier transform (FFT) size of $1024$, this results in a negligible reduction of the electrical SNR requirement with $0.01$ dB and a reduction of the spectral efficiency [92] of $0.2\%$. Therefore, the channel can be safely considered as flat fading over the entire OFDM frame for bandwidths up to $20$ MHz [12, 93], and it can be primarily characterized by the optical path gain coefficient, $g_{\mathrm{h(opt)}}$ [47, 80]. A large number of subcarriers, *e.g.* greater than $64$, also ensures that the time domain signal follows a close to Gaussian distribution [18]. This assumption greatly simplifies the derivations throughout the thesis. In addition, the CP transforms the linear convolution with the channel into a cyclic convolution, facilitating a single-tap linear FFE and eliminating the need for a non-linear DFE. Even though the channel can be considered as flat fading over the individual subcarriers, the non-flat channel frequency response over the entire OFDM frame in the case of a large frame bandwidth still leads to an SNR penalty for the average frame BER. The single-tap equalizer is generally paired with bit and power loading [94, 95], in order to minimize this SNR penalty. Here, the gain factor of the equalizer, $G_{\mathrm{EQ}}$, is obtained via a Monte Carlo simulation.

Link parameters such as the optical center frequency, the mutual orientation and position of the transmitter and receiver in an indoor setup and their field of view (FOV), the responsivity and the photosensitive area of the detector, and the average radiated optical power of the transmitter determine the optical path gain coefficient, $g_{\mathrm{h(opt)}}$ [47, 52], ant therefore, the electrical path gain coefficient, $g_{\mathrm{h(elec)}}$, from (3.3). Since, however, $g_{\mathrm{h(elec)}}$ is merely a factor in the equalization process, a change in $g_{\mathrm{h(elec)}}$ results in an equal SNR penalty for all the considered systems. Therefore, $g_{\mathrm{h(elec)}} = 1$ is assumed for simplicity. In general, the maximum information rate of the OWC system is achieved, when the coherence bandwidth of the channel is significantly larger than the signal bandwidth, *i.e.* when the channel is considered as flat fading with an

impulse response of $h(t) = \delta(t)$, where $\delta(\cdot)$ is the Dirac delta function. Equivalently, the maximum information rate is achievable for a channel frequency response of $|H(f)|^2 = 1$. In this study, a perfect synchronization between the transmitter and the receiver is assumed in the processing of the information-carrying signal. In addition, a perfect matched filtering and a perfect channel knowledge at the receiver and the transmitter are assumed for the purposes of equalization and bit and power loading.

### 3.2.3 Receiver noise

After passing through the optical wireless channel, the signal is received by the optical detector, a combination of a PD and an electronic pre-amplifier in the form of a TIA. In general, in OWC systems, the ambient light produces high-intensity shot noise at the receiver. In addition, thermal noise arises due to the electronic pre-amplifier in the receiver front-end [12]. Therefore, the additive noise component at the receiver, $w$, can be modeled as a random process with a zero-mean real-valued Gaussian distribution. After O/E conversion, the noise is transformed into a complex-valued AWGN with a double-sided electrical power spectral density (PSD) of $N_0/2$ per signal dimension [125]. Therefore, in $M$-PPM and $M$-PAM, $w$ has an electrical PSD of $N_0/2$ and an electrical power of $\sigma^2_{\text{AWGN}} = BN_0/2$. In optical OFDM with $M$-QAM, the electrical PSD of $w$ amounts to $N_0$ for an electrical power of $\sigma^2_{\text{AWGN}} = BN_0$ because of the two dimensional constellation [125].

## 3.3 Single-carrier and multi-carrier modulation

In single-carrier pulse modulation, the information is encoded either in the position of the pulse, *i.e.* $M$-PPM, or in the amplitude of the pulse, *i.e.* $M$-PAM. In multi-carrier modulation, the information is encoded on complex-valued subcarriers in an $M$-QAM fashion. Here, the inverse FFT (IFFT) is utilized as a multiplexing technique at the transmitter, and the FFT is utilized as a demultiplexing technique at the receiver. Through Hermitian symmetry on the OFDM frame, a real valued time domain signal is obtained. O-OFDM transmission is generally realized by a DC-biased Gaussian signal, *i.e.* DC-biased O-OFDM (DCO-OFDM), or a half-Gaussian signal with a $50\%$ reduction of the data rate, *i.e.* asymmetrically clipped O-OFDM (ACO-OFDM).

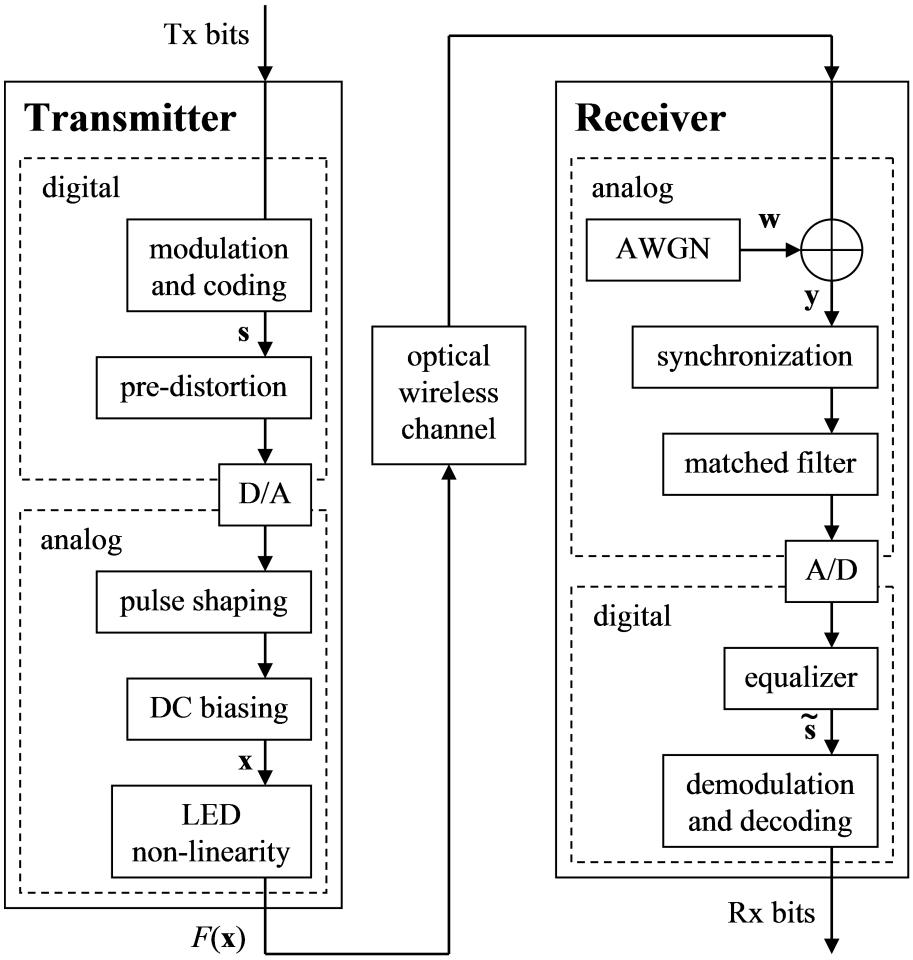


Figure 3.5: Block diagram of single-carrier transmission in OWC using PPM and PAM.

### 3.3.1 $M$-PPM

The block diagram of single-carrier transmission with pulse modulation is presented in Fig. 3.5. In $M$-PPM, $\log_2(M)$ equiprobable input bits form a time domain symbol. It is a sequence of $M$ chips, $\mathbf{c}$, where one chip has a current level of $\sqrt{MP_{\mathrm{s(elec)}}}$, and the other $M-1$ chips are set to zero. Here, $P_{\mathrm{s(elec)}}$ is the average electrical power of the $M$-PPM symbol, and it is related to the average electrical bit power, $P_{\mathrm{b(elec)}}$, as follows: $P_{\mathrm{s(elec)}} = P_{\mathrm{b(elec)}} \log_2(M)$. The respective energy per symbol, $E_{\mathrm{s(elec)}}$, and energy per bit, $E_{\mathrm{b(elec)}}$, are obtained via the symbol rate, $R_{\mathrm{s}}$, as follows: $E_{\mathrm{s(elec)}} = P_{\mathrm{s(elec)}}/R_{\mathrm{s}}$ and $E_{\mathrm{b(elec)}} = P_{\mathrm{b(elec)}}/R_{\mathrm{s}}$. Here, the $M$ chips with duration of $T/M$ fit within a time period of $T$. Therefore, the $M$-PPM symbol with a double-sided bandwidth of $B = M/T$ has a duration of $T$ for a symbol rate of $R_{\mathrm{s}} = B/M$, and it is grouped in the train of $L$ symbols, $\mathbf{s}_l$, where $l$, $l = 0, 1, ..., L-1$, is the symbol index. The spectral efficiency of a modulation scheme is determined by the number of bits that can be transmitted

per symbol duration and per symbol bandwidth, *i.e.* $\mathrm{SE} = R_\mathrm{b}/B$, where $R_\mathrm{b} = \log_2(M)R_\mathrm{s}$ is the bit rate. Thus, the spectral efficiency of $M$-PPM is $\log_2(M)/M$ bits/s/Hz [12, 13]. The train of symbols, $\mathbf{s}_l$, is pre-distorted by the inverse of the non-linear transfer function of the LED transmitter, and it is scaled by a factor, $\alpha$, in order to fit within the front-end optical power constraints. Next, the signal is passed through a digital-to-analog (D/A) converter to transform the train of digital chips into a train of continuous-time pulses. A pulse shaping filter with a real-valued impulse response of $v(t)$ is applied to obtain a band-limited signal. In $M$-PPM, because of the fact that the information-carrying pulse has an optical power level greater than $P_{\mathrm{min,norm}}$, zero bias is required. As a result, the transmitted signal vector, $F(\mathbf{x}_l)$, has a length of $Z_\mathbf{x} = LM$, and it can be expressed as follows:

$$F(\mathbf{x}_l) = \alpha \mathbf{s}_l \ , \tag{3.9}$$

where

$$\alpha = \min\Big(P_{\mathrm{max,norm}}, MP_{\mathrm{avg,norm}}\Big)/\sqrt{MP_{\mathrm{s(elec)}}} \ . \tag{3.10}$$

The transmitter front-end constrains $P_{\mathrm{min,norm}}$ and $P_{\mathrm{max,norm}}$, whereas $P_{\mathrm{avg,norm}}$ is independently imposed by the eye-safety regulations and/or the design requirements. In $M$-PPM, when $MP_{\mathrm{avg,norm}} < P_{\mathrm{max,norm}}$, the resulting pulse level, $MP_{\mathrm{avg,norm}}$, should be set greater than $P_{\mathrm{min,norm}}$, in order to turn on the transmitter. The average optical power of the signal is denoted as $\mathrm{E}\left[F(\mathbf{x}_l)\right]$ where $\mathrm{E}\left[\cdot\right]$ stands for the expectation operator. In general, constraining the average optical power level to $\mathrm{E}\left[F(\mathbf{x}_l)\right] \leq P_{\mathrm{avg,norm}}$ results in a suboptimal BER performance of the OWC systems. The best BER performance is obtained when this constraint is relaxed, *i.e.* when $\mathrm{E}\left[F(\mathbf{x}_l)\right]$ is allowed to assume any level in the dynamic range between $P_{\mathrm{min,norm}}$ and $P_{\mathrm{max,norm}}$.

In order to relate the average optical symbol power, $P_{\mathrm{s(opt)}}$, to the electrical symbol power, $P_{\mathrm{s(elec)}}$, the signal is subjected to O/E conversion defined as follows:

$$P_{\mathrm{s(elec)}} = \frac{\mathrm{E}\left[F(\mathbf{x}_l)^2\right]}{\mathrm{E}\left[F(\mathbf{x}_l)\right]^2} P_{\mathrm{s(opt)}}^2 \ , \tag{3.11}$$

where $\mathrm{E}\left[F(\mathbf{x}_l)\right]^2 = \min\Big(P_{\mathrm{max,norm}}/M, P_{\mathrm{avg,norm}}\Big)^2$ in $M$-PPM. In addition, the second moment is given as: $\mathrm{E}\left[F(\mathbf{x}_l)^2\right] = \min\Big(P_{\mathrm{max,norm}}, MP_{\mathrm{avg,norm}}\Big)^2/M$. Since the time domain signal in $M$-PPM has a probability density function (PDF) with a finite support and taking

into account its demodulation procedure elaborated below, it can be fitted within $P_{\min,\text{norm}}$ and $P_{\max,\text{norm}}$ without effective non-linear clipping distortion. Thus, the following holds for its average optical signal power: $\mathrm{E}\left[F(\mathbf{x}_l)\right] = P_{\text{s(opt)}} = \min\Big(P_{\max,\text{norm}}/M, P_{\text{avg,norm}}\Big) \leq P_{\text{avg,norm}}$.

After passing through the optical wireless channel, the signal is distorted by additive white Gaussian noise (AWGN), $\mathbf{w}_l$, at the receiver to obtain the received signal, $\mathbf{y}_l$. After synchronization, the signal is passed through a filter with an impulse response of $r(t) = v(\tau - t)$, matched to the impulse response of the pulse shaping filter at the transmitter, in order to maximize the received SNR. At the A/D converter, the signal is sampled at a frequency of $M/T$ [12, 13]. After equalization of the channel effect by means of linear FFE or non-linear DFE with ZF or MMSE criteria, the distorted replica of the transmitted symbol, $\widetilde{\mathbf{s}}_l$, is obtained. A hard-decision or soft-decision decoder can be employed to obtain the received bits.

The BER system performance in the optical wireless channel with AWGN and equalization has been discussed in [12]. The received $M$-PPM symbol can be treated as an on-off keying (OOK) sequence, and the information bits can be decoded by means of a hard-decision decoder. For this approach, an analytical union bound of the BER as a function of the electrical SNR per bit is presented and verified through simulation. Alternatively, the BER performance can be enhanced by means of soft-decision decoding based on the position of the chip with the maximum level within the received $M$-PPM symbol. The analytical BER performance of this decoder is presented in [13] as an integral that cannot be derived in closed form. In addition, it is considerably computationally intensive to evaluate it for higher order $M$-PPM. A tighter union bound for the symbol-error rate (SER) in soft-decision decoding can be obtained as a summation of the probabilities of $M-1$ chips of the total $M$ chips in the $M$-PPM symbol, being greater than an intended chip, $c_1$. Since chips in the chip vector, $\mathbf{c}$, are equally probable, a union bound for the SER can be expressed as follows:

$$\begin{aligned}\text{SER} &\leq (M-1)P(c_2|c_1) = (M-1)\int_{-\infty}^{\infty}\mathrm{P}(c_2|c_1=s)\mathrm{P}(c_1=s)\,ds \\ &= (M-1)\int_{-\infty}^{\infty}Q\left(\frac{s\sqrt{2}}{\sqrt{N_0}}\right)\frac{1}{\sqrt{\pi N_0}}\exp\left(-\frac{\left(s-\sqrt{G_{\text{EQ}}\log_2(M)E_{\text{b(elec)}}}\right)^2}{N_0}\right)ds\,,\end{aligned} \tag{3.12}$$

where $Q(\cdot)$ is the complementary cumulative distribution function (CCDF) of a standard normal

distribution with zero mean and unity variance. The BER can be obtained as follows:

$$\mathrm{BER} = \frac{M \log_2(M)}{2(M-1)} \mathrm{SER} \, . \tag{3.13}$$

### 3.3.2 $M$-PAM

The block diagram of $M$-PAM is presented in Fig. 3.5. Here, $\log_2(M)$ equiprobable input bits form a time domain symbol with a double-sided bandwidth of $B = 1/T$ and a duration of $T$ for a symbol rate of $R_\mathrm{s} = B$. The symbols are assigned to current levels of $p\sqrt{3P_{\mathrm{s(elec)}}}/\sqrt{(M-1)(M+1)}$, $p = \pm 1, \pm 3, ..., \pm M-1$, and these are grouped in the train of $L$ symbols, $\mathbf{s}_l$. Here, $E_{\mathrm{b(elec)}} = P_{\mathrm{b(elec)}}/B = P_{\mathrm{s(elec)}}/(\log_2(M)B)$. The resulting spectral efficiency of $M$-PAM is $\log_2(M)$ bits/s/Hz [12, 13]. The train of symbols is pre-distorted, scaled and passed through the D/A converter. A pulse shaping filter is applied. Since $\mathbf{s}_l$ is bipolar, it requires a DC bias, $\beta_\mathrm{DC}$, to fit within dynamic range of the front-end. The transmitted signal vector, $F(\mathbf{x}_l)$, has a length of $Z_\mathbf{x} = L$, and it can be expressed as follows:

$$F(\mathbf{x}_l) = \alpha \mathbf{s}_l + \beta_\mathrm{DC} \, , \tag{3.14}$$

where

$$\alpha = \sqrt{\frac{M+1}{3(M-1)P_{\mathrm{s(elec)}}}} \min\Big(P_{\mathrm{max,norm}} - \beta_\mathrm{DC}, \beta_\mathrm{DC} - P_{\mathrm{min,norm}}\Big). \tag{3.15}$$

In order to obtain the O/E conversion in $M$-PAM from (3.11), the second moment of $F(\mathbf{x}_l)$ can be expressed as follows:

$$\mathrm{E}\left[F(\mathbf{x}_l)^2\right] = \frac{M+1}{3(M-1)} \min\Big(P_{\mathrm{max,norm}} - \beta_\mathrm{DC}, \beta_\mathrm{DC} - P_{\mathrm{min,norm}}\Big)^2 + \beta_\mathrm{DC}^2 \, . \tag{3.16}$$

Because of the fact that the $M$-PAM time domain signal has a PDF with a finite support, it can be fitted within $P_{\mathrm{min,norm}}$ and $P_{\mathrm{max,norm}}$ without clipping. Thus, the following holds for its average optical power: $\mathrm{E}\left[F(\mathbf{x}_l)\right] = P_{\mathrm{s(opt)}} = \beta_\mathrm{DC} \leq P_{\mathrm{avg,norm}}$.

The signal is transmitted over the optical wireless channel, and it is distorted by AWGN, $\mathbf{w}_l$, at the receiver. The received signal, $\mathbf{y}_l$, is synchronized, and it is passed through a matched filter. At the A/D converter, the signal is sampled at a frequency of $1/T$ [12, 13]. Next, the signal is equalized by means of linear FFE or non-linear DFE with ZF or MMSE criteria, and the distorted replica of the transmitted symbol, $\widetilde{\mathbf{s}}_l$, is obtained. A hard-decision decoder

is employed to obtain the received bits. As a result, the effective electrical SNR per bit in $M$-PAM, $\Gamma_{\mathrm{b(elec)}}$, can be expressed as follows:

$$\Gamma_{\mathrm{b(elec)}} = \gamma_{\mathrm{b(elec)}} G_{\mathrm{EQ}} G_{\mathrm{DC}} \, . \tag{3.17}$$

Here, $G_{\mathrm{EQ}}$ is given in (3.4), (3.6), (3.7) and (3.8). The gain factor $G_{\mathrm{DC}}$ denotes the attenuation of the useful electrical signal power of $\mathbf{x}$ due to the DC component. In general, the addition of the DC bias influences the useful electrical power of the biased time domain signal. The total electrical power is a summation of the useful electrical AC power and the electrical DC power. Therefore, for a fixed total electrical power, the addition of the DC bias reduces the useful electrical AC power of the signal. The gain factor $G_{\mathrm{DC}}$ is given for $M$-PAM as follows:

$$G_{\mathrm{DC}} = \frac{\mathrm{E}\left[\left(F(\mathbf{x}_l) - F(\beta_{\mathrm{DC}})\right)^2\right]}{\mathrm{E}\left[F(\mathbf{x}_l)^2\right]} \, , \tag{3.18}$$

where

$$\mathrm{E}\left[\left(F(\mathbf{x}_l) - F(\beta_{\mathrm{DC}})\right)^2\right] = \frac{M+1}{3(M-1)} \min\Big(P_{\mathrm{max,norm}} - \beta_{\mathrm{DC}}, \beta_{\mathrm{DC}} - P_{\mathrm{min,norm}}\Big)^2 \, . \tag{3.19}$$

The exact closed form expression for the BER performance of $M$-PAM in AWGN has been presented in [127] as a summation of $M$ terms. A tight approximation for BER bellow $10^{-2}$ can be obtained when only considering the error contributed by the closest symbols in the constellation as follows [13]:

$$\mathrm{BER} = \frac{N_{\mathrm{s}}}{G_{\mathrm{GC}} \log_2(M)} Q\left(d_{\mathrm{s}} \sqrt{\log_2(M) \Gamma_{\mathrm{b(elec)}}}\right) . \tag{3.20}$$

In $M$-PAM, an intended symbol has an average number of $N_{\mathrm{s}} = 2(M-1)/M$ neighboring symbols. The gain introduced by Gray coding of the bits on the symbols is denoted by $G_{\mathrm{GC}} = 1$. The distance between an intended symbol and the closest interfering symbol is given by $d_{\mathrm{s}} = \sqrt{6/(M^2-1)}$ .

### 3.3.3 $M$-QAM O-OFDM

The block diagram for multi-carrier O-OFDM transmission is presented in Fig. 3.6. O-OFDM transmission can be realized through the bipolar DCO-OFDM with a DC bias [96] or through the unipolar ACO-OFDM [99]. In general, $N$ subcarriers form the $l$-th OFDM frame, $\mathbf{f}_{l,m}$,

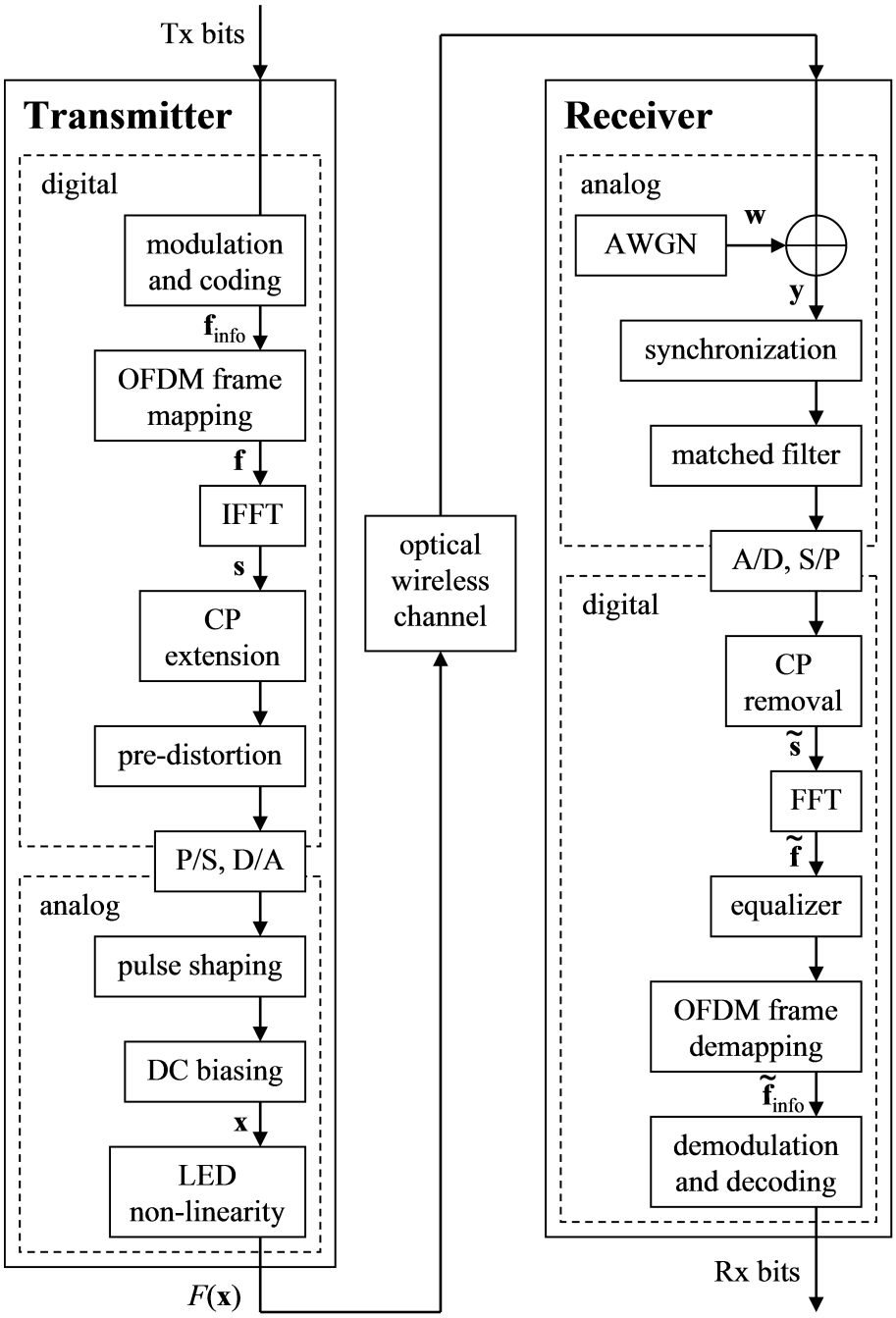


Figure 3.6: Block diagram of multi-carrier transmission in OWC using OFDM.

corresponding to the $l$-th OFDM symbol, where $m$, $m = 0, 1, ..., N-1$, is the subcarrier index. Each subcarrier occupies a bandwidth of $1/NT$ in a total OFDM frame double-sided bandwidth of $B = 1/T$. The two O-OFDM systems utilize a different portion of the available bandwidth, and the bandwidth utilization factor is denoted by $G_{\text{B}}$, where $G_{\text{B}} = (N-2)/N$ in DCO-OFDM and $G_{\text{B}} = 0.5$ in ACO-OFDM. In order to ensure a real-valued time domain

signal, both schemes have the Hermitian symmetry imposed on the OFDM frame, and the subcarriers with indices $m = \{0, N/2\}$ are set to zero. In DCO-OFDM, $N/2-1$ subcarriers in the first half of the frame, $m = 1, ..., N/2-1$, carry the information. In ACO-OFDM, only the odd subcarriers are enabled, while every even subcarrier is set to zero. Here, the $N/4$ subcarriers with indices $m = 1, 3, 5, ..., N/2-1$ carry the information. The information-carrying subcarriers are denoted as $\mathbf{f}_{\text{info}}^{l,m}$. In order to maintain the signal variance of $\sigma^2$, the electrical power of the enabled subcarriers is scaled through $\alpha = \sigma/\sqrt{G_{\text{B}}}$ to $P_{\text{s(elec)}}/G_{\text{B}}$, where $P_{\text{s(elec)}} = \sigma^2$. Both schemes can utilize bit and power loading of the frequency domain subcarriers, in order to optimally adapt the signal to the channel conditions. For a desired bit rate, the Levin-Campello algorithm [94, 95] can be applied, in order to maximize the received power margin, or equivalently, in order to minimize the required electrical SNR. The optimum solution achieved by the algorithm yields the $\mathbf{b}_m$ bits which modulate the complex-valued information-carrying frequency domain subcarrier from $\mathbf{f}_{l,m}$ in an $M$-QAM fashion. In addition, the algorithm provides subcarrier power scaling factors, $\mathbf{p}_m$, which ensure an equal maximized received power margin for every active subcarrier. Therefore, $\mathrm{E}[\mathbf{b}_m] G_{\text{B}}N$ bits on the $G_{\text{B}}N$ enabled subcarriers are transmitted per OFDM time domain symbol, $\mathbf{s}_l$. Without loss of generality, only integer average bit load, *i.e.* $\mathrm{E}[\mathbf{b}_m] = \log_2(M)$, is considered in this study. Thus, the average bit energy can be expressed as follows: $E_{\text{b(elec)}} = P_{\text{b(elec)}}/(G_{\text{T}}G_{\text{B}}B) = \sigma^2/(\log_2(M)G_{\text{T}}G_{\text{B}}B)$, where $P_{\text{b(elec)}}$ is the average electrical power of $G_{\text{B}}N$ bits. The $l$-th OFDM symbol in the train of $L$ symbols, $\mathbf{s}_l$, is obtained by the IFFT of the $l$-th OFDM frame in the train of $L$ frames, $\mathbf{f}_l$. Here, the unitary IFFT is utilized as a multiplexing technique at the transmitter, as follows:

$$\mathbf{s}_{l,k} = \frac{1}{\sqrt{N}} \sum_{m=0}^{N-1} \mathbf{f}_{l,m} \exp\left(\frac{i2\pi km}{N}\right), \tag{3.21}$$

where $i = \sqrt{-1}$ is the imaginary unit, and $k$, $k = 0, 1, ..., N-1$, denotes the time domain sample index within the $l$-th OFDM symbol. In addition, $N_{\text{CP}}$ samples from the end of each OFDM symbol are appended at the beginning of the symbol, creating the CP extension, in order to mitigate the ISI and the ICI [93, 125]. A large number of subcarriers and a CP transform the dispersive optical wireless channel into a flat fading channel over the subcarrier bandwidth, reducing the computational complexity of the equalization process at the receiver to a single-tap equalizer [125]. As a result, the time domain OFDM symbol with CP occupies a double-sided bandwidth of $B = 1/T$, and it has a duration of $(N+N_{\text{CP}})T$. The symbol rate amounts to $R_{\text{s}} = G_{\text{T}}G_{\text{B}}B$ [93, 125], where $G_{\text{T}} = N/(N + N_{\text{CP}})$ is the utilization factor for the information-

carrying time. Because of the Hermitian symmetry, the resulting spectral efficiency of $M$-QAM O-OFDM amounts to $\log_2(M)G_{\mathrm{T}}G_{\mathrm{B}}/2$ bits/s/Hz. The train of OFDM symbols with CPs follows a close to Gaussian distribution with zero mean and variance of $\sigma^2$ for FFT sizes greater than $64$ [18]. The non-linear transfer characteristic of the LED transmitter can be compensated by pre-distortion with the inverse of the non-linear transfer function [20]. The pre-distorted OFDM symbol is subjected to a parallel-to-serial (P/S) conversion, and it is passed through the D/A converter to obtain the continuous-time signal. A pulse shaping filter is applied. Since only the odd subcarriers are enabled in ACO-OFDM, the negative portion of the OFDM symbol can be clipped without loss of information at the received odd subcarriers. The signal is DC-biased by $\beta_{\mathrm{DC}}$ in the analog circuitry, and it is transmitted by the LED. The transmitted signal vector, $F(\mathbf{x}_l)$, with a length of $Z_{\mathbf{x}} = L(N + N_{\mathrm{CP}})$ can be expressed as follows:

$$F(\mathbf{x}_l) = \Phi(\mathbf{s}_l + \beta_{\mathrm{DC}}) \ , \tag{3.22}$$

where $\Phi(\cdot)$ represents the linearized transfer function of the LED transmitter which is reduced to the double-sided signal clipping operator discussed in Chapter 4. Effectively, the OFDM symbol, $\mathbf{s}_l$, is clipped at normalized bottom and top clipping levels of $\lambda_{\mathrm{bottom}}$ and $\lambda_{\mathrm{top}}$ relative to a standard normal distribution [24]. In DCO-OFDM, $\lambda_{\mathrm{bottom}} = \big(P_{\mathrm{min,norm}} - \beta_{\mathrm{DC}}\big)/\sigma$, while in ACO-OFDM, $\lambda_{\mathrm{bottom}} = \max\Big(\big(P_{\mathrm{min,norm}} - \beta_{\mathrm{DC}}\big)/\sigma, 0\Big)$. In both systems, $\lambda_{\mathrm{top}} = \big(P_{\mathrm{max,norm}} - \beta_{\mathrm{DC}}\big)/\sigma$. The clipping levels in DCO-OFDM can be negative and/or positive, whereas in ACO-OFDM, these are strictly non-negative. For reasons of plausibility, $\lambda_{\mathrm{top}} > \lambda_{\mathrm{bottom}}$. The Bussgang theorem [27] and the central limit theorem (CLT) [28] can be used to translate the non-linear distortion into an attenuation factor for the information-carrying subcarriers, $K$, plus uncorrelated zero-mean complex-valued Gaussian noise with variance of $\sigma^2_{\mathrm{clip}}$. The details of the analysis of these non-linear distortion parameters are presented in Chapter 4.

In addition to the distortion of the information-carrying subcarriers, the time domain signal clipping modifies the average optical power of the transmitted signal. The modified mean can be derived based on the statistics of a truncated Gaussian distribution [128]. Thus, the average optical power of the transmitted signal after double-sided signal clipping, $\mathrm{E}\left[\Phi(\mathbf{x}_l)\right]$, can be expressed as follows:

$$\mathrm{E}\left[\Phi(\mathbf{x}_l)\right] = \sigma\Big(\lambda_{\mathrm{top}}Q(\lambda_{\mathrm{top}}) - \lambda_{\mathrm{bottom}}Q(\lambda_{\mathrm{bottom}}) + \phi(\lambda_{\mathrm{bottom}}) - \phi(\lambda_{\mathrm{top}})\Big) + P_{\mathrm{bottom}} \ . \tag{3.23}$$

The details of the derivation of the result in (3.23) can be found in Section A.2 of Appendix A. In DCO-OFDM, $P_{\text{bottom}} = P_{\text{min,norm}}$. Because of the default zero-level clipping in ACO-OFDM, $P_{\text{bottom}} = \max\Big(P_{\text{min,norm}}, \beta_{\text{DC}}\Big)$. Here, $\phi(\cdot)$ stands for the PDF of a standard normal distribution with zero mean and unity variance. The eye safety regulations [1] and/or the design requirements such as signal dimming impose the average optical power constraint, $P_{\text{avg,norm}}$, *i.e.* $\mathrm{E}\left[\Phi(\mathbf{x}_l)\right] \leq P_{\text{avg,norm}}$. Thus, for a given set of front-end optical power constraints, one can obtain the target signal variance, $\sigma^2$, and the required DC bias, $\beta_{\text{DC}}$, from (3.23). The optimum choice of these design parameters is elaborated in Chapter 5.

Since the signal is clipped, the resulting average optical power of the signal, $\mathrm{E}\left[\Phi(\mathbf{x}_l)\right]$, differs from the undistorted optical power of the OFDM symbol, $P_{\text{s(opt)}}$. In general, $P_{\text{s(opt)}}$ is defined for the scenario with the least signal clipping which is given in DCO-OFDM as $\lambda_{\text{bottom}} = -\infty$ and $\lambda_{\text{top}} = +\infty$, and in ACO-OFDM as $\lambda_{\text{bottom}} = 0$ and $\lambda_{\text{top}} = +\infty$. In DCO-OFDM, $P_{\text{s(opt)}} = \beta_{\text{DC}}$, whereas in ACO-OFDM, $P_{\text{s(opt)}} = (\beta_{\text{DC}} + \sigma/\sqrt{2\pi})$. The O/E conversion is obtained in DCO-OFDM and ACO-OFDM, respectively, as follows:

$$P_{\text{s(elec)}} = \frac{\sigma^2 + \beta_{\text{DC}}^2}{\beta_{\text{DC}}^2} P_{\text{s(opt)}}^2 \ , \tag{3.24}$$

$$P_{\text{s(elec)}} = \frac{2\pi\beta_{\text{DC}}^2 + 2\sigma\beta_{\text{DC}}\sqrt{2\pi} + \pi\sigma^2}{2\pi\beta_{\text{DC}}^2 + 2\sigma\beta_{\text{DC}}\sqrt{2\pi} + \sigma^2} P_{\text{s(opt)}}^2 \ . \tag{3.25}$$

The signal $\mathbf{x}_{l,k}$ is transmitted over the optical wireless channel, and it is distorted by AWGN, $\mathbf{w}_{l,k}$, at the receiver. The received signal, $\mathbf{y}_{l,k}$, is synchronized, and it is passed through a matched filter. At the A/D converter, the signal is sampled at a frequency of $1/T$ [93, 125]. After serial-to-parallel (S/P) conversion, the CP extension of each OFDM symbol is removed to obtain the distorted replica of the OFDM symbol, $\widetilde{\mathbf{s}}_{l,k}$. Next, the signal is passed through an FFT block back to the frequency domain. Here, the demultiplexing is carried out by the use of the unitary FFT, as follows:

$$\widetilde{\mathbf{f}}_{l,m} = \frac{1}{\sqrt{N}} \sum_{k=0}^{N-1} \widetilde{\mathbf{s}}_{l,k} \exp\left(\frac{-i2\pi km}{N}\right), \tag{3.26}$$

where $\widetilde{\mathbf{f}}_{l,m}$ denotes the distorted replica of the OFDM frame, respectively. Here, the CLT can be applied, and the time domain additive uncorrelated non-Gaussian non-linear noise is transformed into additive uncorrelated zero-mean complex-valued Gaussian noise at the information-carrying subcarriers, $\mathbf{W}_{\text{clip}}^{l,m}$, preserving its variance of $\sigma_{\text{clip}}^2$. Because of the fact that the channel

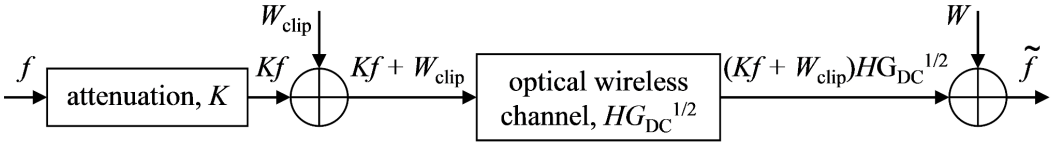


Figure 3.7: Generalized block diagram of the received information-carrying subcarriers in O-OFDM, including the attenuation factor and the additive Gaussian noise from the transmitter nonlinearity, the channel tap, the DC bias penalty and the AWGN.

frequency response can be considered as flat fading over the subcarrier bandwidth, the signal can be equalized by means of a single-tap linear FFE with ZF or MMSE criteria. As a result, the received distorted replica of the information-carrying subcarriers, $\widetilde{\mathbf{f}}_{\text{info}}^{l,m}$, can be expressed in DCO-OFDM and ACO-OFDM as follows:

$$\widetilde{\mathbf{f}}_{\text{info}}^{l,m} = \left(\sqrt{\mathbf{p}_{l,m}} K \mathbf{f}_{\text{info}}^{l,m} / \sqrt{G_{\text{B}}} + \mathbf{W}_{\text{clip}}^{l,m}\right) \sqrt{G_{\text{EQ}} G_{\text{DC}}} + \sqrt{G_{\text{B}}} \mathbf{W}_{l,m} \, . \tag{3.27}$$

Here, $G_{\text{EQ}}$ simplifies for the single-tap linear FFE with ZF or MMSE criteria, respectively, to $|H(f_{\text{info}})|^2$ and $|H(f_{\text{info}})|^2 + \gamma_{\text{b(elec)}}^{-1}$, where $H(f_{\text{info}})$ represents the channel frequency response on the information-carrying subcarrier. The zero-mean complex-valued AWGN with variance of $\sigma_{\text{AWGN}}^2 = BN_0$ is given by $\mathbf{W}_{l,m}$. The gain factor $G_{\text{DC}}$ denotes the attenuation of the useful electrical signal power due to the DC component, *i.e.* the penalty on the electrical SNR due to the DC component, and it can be expressed in DCO-OFDM and ACO-OFDM, respectively, as follows:

$$G_{\text{DC}} = \frac{\sigma^2}{\sigma^2 + \beta_{\text{DC}}^2} \, , \tag{3.28}$$

$$G_{\text{DC}} = \frac{\sqrt{2\pi}\sigma^2}{\sqrt{2\pi}\sigma^2 + 4\sigma\beta_{\text{DC}} + 2\sqrt{2\pi}\beta_{\text{DC}}^2} \, . \tag{3.29}$$

The generalized model of the received information-carrying subcarriers in O-OFDM is illustrated in Fig. 3.7. A hard-decision decoder is employed on the known OFDM frame structure to obtain the received bits. Thus, the electrical SNR on a received information-carrying subcarrier in DCO-OFDM and ACO-OFDM is given as follows:

$$\text{SNR}_m = \frac{\mathbf{p}_m K^2 P_{\text{s(elec)}} / G_{\text{B}}}{\sigma_{\text{clip}}^2 + \dfrac{G_{\text{B}} \sigma_{\text{AWGN}}^2}{G_{\text{EQ}} G_{\text{DC}}}} \, . \tag{3.30}$$

As a result, the effective electrical SNR per bit on an enabled subcarrier in O-OFDM, $\Gamma_{\text{b(elec)}}^m$,

| Modulation order | $N_{\mathrm{s}}$ | $G_{\mathrm{GC}}$ | $d_{\mathrm{s}}$ |
|---|---|---|---|
| BPSK | $1$ | $1$ | $2$ |
| $M = 2^{2n}$ $n = 1, 2, ...$ | $4 - \frac{4}{\sqrt{M}}$ | $1$ | $\sqrt{\frac{3}{M-1}}$ |
| $M = 8$ | $3$ | $\frac{4}{5}$ | $\sqrt{\frac{2}{3+\sqrt{3}}}$ |
| $M = 32$ | $\frac{13}{4}$ | $\frac{6}{7}$ | $\frac{1}{\sqrt{10}}$ |
| $M = 2^{2n+1}$ $n = 3, 4, ...$ | $4 - \frac{6}{\sqrt{2M}}$ | $\frac{6M}{6M + 3\sqrt{2M} + 2}$ | $\sqrt{\frac{96}{31M - 32}}$ |

Table 3.1: Parameters in (3.20) for square and cross $M$-QAM constellations [13, 127, 129, 130].

is given as follows:

$$\Gamma^{m}_{\mathrm{b(elec)}} = \frac{\mathbf{p}_m K^2 P_{\mathrm{b(elec)}}/G_{\mathrm{B}}}{\sigma^2_{\mathrm{clip}} + \frac{G_{\mathrm{B}}\sigma^2_{\mathrm{AWGN}}}{G_{\mathrm{EQ}}G_{\mathrm{DC}}}} = \frac{\mathbf{p}_m K^2}{\frac{\mathbf{b}_m G_{\mathrm{B}}\sigma^2_{\mathrm{clip}}}{P_{\mathrm{s(elec)}}} + \frac{G_{\mathrm{B}}\gamma^{-1}_{\mathrm{b(elec)}}}{G_{\mathrm{T}}G_{\mathrm{EQ}}G_{\mathrm{DC}}}} \,. \tag{3.31}$$

The exact closed form expression for the BER performance of square and cross $M$-QAM constellations in AWGN has been presented as a summation of $M$ terms in [127] and [129], respectively. However, the same tight approximation from (3.20) can be applied, and the respective parameters are given in TABLE 3.1 [13, 127, 129, 130], including binary phase shift keying (BPSK). Thus, the BER on the intended subcarrier, $\mathrm{BER}_m$, can be obtained by inserting (3.31) into (3.20), considering the parameters from TABLE 3.1 for the number of loaded bits. As a result, the link BER can be obtained as the average of the BER of all enabled subcarriers: $\mathrm{BER} = \mathrm{E}\left[\mathrm{BER}_m\right]$.

## 3.4 Chapter summary

In this Chapter, mathematical models of single-carrier and multi-carrier modulation schemes for practical OWC links have been presented in detail. First, the non-linear transfer of the input electrical power to output optical power at the transmitter has been introduced, and the optical power constraints of the transmitter have been defined as minimum, average and maximum radiated optical power. In addition, the model for the impulse response of the optical wireless

channel has been presented. Formulated as a function of the coherence bandwidth, the model has been shown to facilitate the study of the OWC system in narrow or broadband channels. In order to counter the channel effect, equalization has been employed, and the mathematical details of the equalizer penalty on the electrical SNR requirement have been presented in consideration of the AWGN at the receiver.

In the second Section of this Chapter, the BER performance of the single-carrier modulation formats $M$-PPM and $M$-PAM as well as the multi-carrier modulation formats $M$-QAM DCO-OFDM and $M$-QAM ACO-OFDM has been analyzed in detail. First the structure of the different signals has been presented. In the context of the positive limited dynamic range of the transmitter, the O/E signal conversion of the signals has been defined. Considering the additional DC bias requirement of some of the optical signals in order to be conditioned within the limited dynamic range, the DC bias penalty has been derived and included in calculation of the electrical SNR. The use of signal pre-distortion has been shown to linearize the dynamic range of the optical front-end between levels of minimum and maximum radiated optical power. In this way, the non-linear distortion has been avoided in the single-carrier pulse modulation schemes. In the multi-carrier modulation schemes, the non-linear distortion has been reduced to a double-sided signal clipping. The parameters of the non-linear distortion in O-OFDM have been included in the electrical SNR, and they have been derived in Chapter 4. Finally, the electrical SNR has been translated into BER performance.

# Chapter 4
# Non-linear distortion in O-OFDM

## 4.1 Introduction

Because of the p-n junction barrier and the saturation effect of the light emitting diode (LED), the transmitter front-end has a limited dynamic range, and it transfers the information-carrying signal in a non-linear fashion. This results in an increased bit-error rate (BER) or in an increased electrical signal-to-noise ratio (SNR) requirement. In order to alleviate this issue, signal pre-distortion with the inverse of the non-linear transfer function can be employed. Through pre-distortion, a linear signal transfer is obtainable between levels of minimum and maximum radiated optical power. However, the optical orthogonal frequency division multiplexing (O-OFDM) signals with a large peak-to-average-power ratio (PAPR) still suffer from double-sided signal clipping. In this Chapter, a generalized model is proposed for the non-linear distortion function of the transmitter front-end. The degradation of the electrical SNR is derived in closed form, and the model is verified through a Monte Carlo simulation. In addition, the effective received electrical SNR of the pre-distorted O-OFDM signals with double-sided signal clipping is also analyzed in closed form. Here, a verification of the model is also presented by means of a Monte Carlo simulation.

## 4.2 Generalized non-linear transfer function

In this study, the non-linear transfer function of the transmitter front-end is modeled by means of a piecewise polynomial function. This is a flexible yet general way to represent any non-linear function. It enables the derivation of the non-linear distortion parameters, such as the attenuation factor of the information-carrying subcarriers and the variance of the additive zero-mean Gaussian distortion noise. In addition, it facilitates the pre-distortion of the transmitted signal, in order to linearize the dynamic range of the transmitter and to reduce the non-linear distortion to double-sided signal clipping.

### 4.2.1 Analysis of the non-linear distortion

The non-linear distortion of the Gaussian and half-Gaussian OFDM symbols in direct-current-biased O-OFDM (DCO-OFDM) and asymmetrically clipped O-OFDM (ACO-OFDM), respectively, can be modeled by means of the Bussgang theorem [27] as an attenuation of the data-carrying signal plus a non-Gaussian uncorrelated noise component [18, 24]. Since the received signal is passed through a fast Fourier transform (FFT) at the receiver, the central limit theorem (CLT) [28] can be applied, and the additive uncorrelated noise from the non-linear distortion is transformed into additive uncorrelated complex-valued Gaussian noise with zero mean and variance of $\sigma^2_{\text{clip}}$. In order to derive the gain factor denoting the electrical power attenuation of the OFDM symbol, $K$, and the variance of the additive non-linear distortion noise, $\sigma^2_{\text{clip}}$, in DCO-OFDM and ACO-OFDM, a model for the non-linear transfer function of the optical front-end needs to be defined.

The undistorted and unclipped continuous-time OFDM symbol, $s$, follows a zero-mean Gaussian distribution with a variance of $\sigma^2 = P_{\text{s(elec)}}$, where $P_{\text{s(elec)}}$ is the average electrical symbol power. The DC-biased continuous-time signal to be transmitted through the optical front-end, $x$, can be expressed as $x = s + \beta_{\text{DC}}$, where $\beta_{\text{DC}}$ stands for the DC bias. Passing through the LED, the information-carrying signal, $x$, is subjected to the non-linear transfer function, $F(x)$. For the sake of generality, the non-linear transfer function of the transmitter front-end, $F(\cdot)$, is normalized, and the normalized non-linear transfer function, $\Psi(\cdot)$, is defined as follows: $\Psi(s) = F(x) - F(\beta_{\text{DC}})$. In this study, the following piecewise polynomial model for $\Psi(\cdot)$ is chosen as an accurate, flexible and generalized representation of the normalized non-linear transfer function:

$$\Psi(s) = \begin{cases} \sigma\lambda_1 & \text{if } s \leq \sigma\lambda_1, \\ \psi_1(s) & \text{if } \sigma\lambda_1 < s \leq \sigma\lambda_2, \\ \quad \vdots & \\ \psi_{J-1}(s) & \text{if } \sigma\lambda_{J-1} < s \leq \sigma\lambda_J, \\ \sigma\lambda_J & \text{if } s > \sigma\lambda_J. \end{cases} \tag{4.1}$$

Here, $\psi_j(s)$, $j = 1, ..., J-1$, are polynomial functions of non-negative integer order $n_j$. They facilitate the modeling of non-linear signal transfer through the LED and enable the derivation of the non-linear distortion parameters such as the attenuation factor, $K$, and the variance of the non-linear noise component, $\sigma^2_{\text{clip}}$. In addition, they enable the signal pre-distortion, where

the non-linear distortion is reduced to double-sided signal clipping. Here, $\lambda_{\hat{j}}$, $\hat{j} = 1, ..., J$, are real-valued normalized clipping levels relative to a standard normal distribution with zero mean and unity variance. They denote the end points of the polynomial functions, $\psi_j(s)$. In DCO-OFDM, the levels can be positive as well as negative, while in ACO-OFDM the levels are strictly non-negative because of the non-negative half-Gaussian signal distribution.

The non-linear distortion can be modeled by means of the Bussgang theorem for DCO-OFDM and ACO-OFDM, respectively, as follows:

$$\Psi(s) = Ks + w_{\text{clip}} \tag{4.2}$$

$$\Psi(s) = U(s)2Ks + w_{\text{clip}} \tag{4.3}$$

Here, $U(\cdot)$ stands for the unit step function which is used to denote the default zero-level clipping of the time domain signal in ACO-OFDM. The Bussgang theorem states that after the non-linear distortion the signal is attenuated by a factor, $K$, and an uncorrelated non-Gaussian noise, $w_{\text{clip}}$, is added. In ACO-OFDM the amplitude of the received odd subcarriers is reduced by $50\%$ because of the zero-level clipping and the symmetries discussed in [99]. Therefore, the attenuation factor $K$ is multiplied by a factor of 2 in (4.3). In addition, since the received signal is passed through an FFT, the additive non-linear noise, $w_{\text{clip}}$, is transformed into additive zero-mean complex-valued Gaussian noise at the information-carrying subcarriers, preserving its variance of $\sigma^2_{\text{clip}}$. In the following, $K$ and $\sigma^2_{\text{clip}}$ are derived for the considered DCO-OFDM and ACO-OFDM systems.

The attenuation factor of the non-linear distortion, $K$, can be generalized for DCO-OFDM and ACO-OFDM as follows:

$$\begin{aligned} K = {} & \lambda_J \phi(\lambda_J) - \lambda_1 \phi(\lambda_1) \\ & + \frac{1}{\sigma^2} \sum_{j=1}^{J-1} \int_{-\infty}^{\sigma\lambda_{j+1}} s\psi_j(s) \frac{1}{\sigma} \phi\left(\frac{s}{\sigma}\right) ds - \frac{1}{\sigma^2} \sum_{j=1}^{J-1} \int_{-\infty}^{\sigma\lambda_j} s\psi_j(s) \frac{1}{\sigma} \phi\left(\frac{s}{\sigma}\right) ds \,, \end{aligned} \tag{4.4}$$

where $\phi(\cdot)$ stands for the probability density function (PDF) of a standard normal distribution with zero mean and unity variance. The details of the derivation of the result in (4.4) can be found in Section A.1 of Appendix A. Since $s\psi_j(s)$ are polynomial functions of order $n_j + 1$, these integrals can be expressed as a linear combination of integrals with the following struc-

ture:

$$\int_{-\infty}^{\sigma\lambda} s^n \frac{1}{\sigma}\phi\left(\frac{s}{\sigma}\right)\, ds = \sigma^n \int_{-\infty}^{\lambda} u^n \phi(u)\, du = \sigma^n \mathcal{I}_n \ . \tag{4.5}$$

The integral, $\mathcal{I}_n$, can be solved, using the following recursive relation:

$$\mathcal{I}_n = -\lambda^{n-1}\phi(\lambda) + (n-1)\mathcal{I}_{n-2} \ , \tag{4.6}$$

where $\mathcal{I}_0 = 1 - Q(\lambda)$ and $\mathcal{I}_1 = -\phi(\lambda)$. Here, $Q(\cdot)$ is the complementary cumulative distribution function (CCDF) of a standard normal distribution with zero mean and unity variance.

In DCO-OFDM, the variance of the non-linear noise component, $\sigma^2_{\text{clip}}$, can be expressed for the generalized nonlinearity function, $\Psi(s)$, as follows:

$$\begin{aligned}\sigma^2_{\text{clip}} = {} & \sigma^2\lambda_1^2\big(1 - Q(\lambda_1)\big) + \sigma^2\lambda_J^2 Q(\lambda_J) - K^2\sigma^2 + \sum_{j=1}^{J-1}\int_{-\infty}^{\sigma\lambda_{j+1}} \psi_j(s)^2 \frac{1}{\sigma}\phi\left(\frac{s}{\sigma}\right)\, ds \\ & - \sum_{j=1}^{J-1}\int_{-\infty}^{\sigma\lambda_j} \psi_j(s)^2 \frac{1}{\sigma}\phi\left(\frac{s}{\sigma}\right)\, ds - \Big(\sigma\lambda_1\big(1 - Q(\lambda_1)\big) + \sigma\lambda_J Q(\lambda_J)\Big) \\ & + \sum_{j=1}^{J-1}\int_{-\infty}^{\sigma\lambda_{j+1}} \psi_j(s) \frac{1}{\sigma}\phi\left(\frac{s}{\sigma}\right)\, ds - \sum_{j=1}^{J-1}\int_{-\infty}^{\sigma\lambda_j} \psi_j(s) \frac{1}{\sigma}\phi\left(\frac{s}{\sigma}\right)\, ds\Big)^2 \ .\end{aligned} \tag{4.7}$$

In ACO-OFDM, using the unfolding and debiasing of the half-Gaussian distribution of $s$ elaborated in Section 4.3, $\sigma^2_{\text{clip}}$ can be expressed as follows:

$$\begin{aligned}\sigma^2_{\text{clip}} = {} & \sigma^2(\lambda_J - \lambda_1)^2 Q(\lambda_J) - 2K^2\sigma^2 + \sum_{j=1}^{J-1}\int_{-\infty}^{\sigma\lambda_{j+1}} \psi_j(s - \sigma\lambda_1)^2 \frac{1}{\sigma}\phi\left(\frac{s}{\sigma}\right)\, ds \\ & - \sum_{j=1}^{J-1}\int_{-\infty}^{\sigma\lambda_j} \psi_j(s - \sigma\lambda_1)^2 \frac{1}{\sigma}\phi\left(\frac{s}{\sigma}\right)\, ds \ .\end{aligned} \tag{4.8}$$

The details of the derivation of the results in (4.7) and (4.8) can be found in Section A.1 of Appendix A. The integrals in (4.7) and (4.8) can be solved, using the structure from (4.5) and (4.6). In addition, the expressions in (4.4), (4.7) and (4.8) do not exhibit a dominant term, and all of the addends are required to accurately model the non-linear distortion.

### 4.2.2 Verification of the model with a Monte Carlo simulation

The accuracy of the non-linear distortion modeling and the derived expression for the electrical SNR at the received subcarriers in (3.31) is verified by means of a Monte Carlo BER simulation. For this purpose, an IFFT/FFT size of 2048 and QAM orders, $M = \{16, 64, 256\}$, are chosen. The BER performance of DCO-OFDM and ACO-OFDM is evaluated as a function of the undistorted electrical SNR per bit, $\gamma_{\mathrm{b(elec)}}$. The analytical expression for the BER from (3.20) and TABLE 3.1 is used. The validity of the model is presented for the general non-linear piecewise polynomial transfer function, $F(x) = \Xi(x)$, considered in $\Psi(s) = F(x) - F(\beta_{\mathrm{DC}})$. An example for $\Xi(x)$, illustrated in Fig. 3.4, with increased precision of the polynomial coefficients for the sake of the accurate model verification is chosen as follows:

$$\Xi(x) = \begin{cases} 0 & \text{if } x \leq 0.1, \\ -1.6461x^3 + 2.7160x^2 & \\ -0.4938x + 0.0239 & \text{if } 0.1 < x \leq 1, \\ 0.6 & \text{if } x > 1. \end{cases} \tag{4.9}$$

The front-end biasing setup to condition the signal within this non-linear transfer function is defined through the DC bias, $\beta_{\mathrm{DC}}$, and the signal standard deviation, $\sigma$. In DCO-OFDM, $\beta_{\mathrm{DC}} = 0.5$ and $\sigma = 0.07$, while in ACO-OFDM, $\beta_{\mathrm{DC}} = 0.4$ and $\sigma = 0.24$. This setup results in an equal radiated average optical power of $0.25$ for both optical OFDM schemes. It enables ACO-OFDM to avoid the bottom knee of the non-linear transfer function and, therefore, to reduce the distortion of the half-Gaussian signal for the sake of a better BER performance. In DCO-OFDM, the signal is placed bellow the middle of the dynamic range as suggested in [26], in order to improve the electrical power efficiency. In addition, this setup provides moderate attenuation factor, $K$, and non-linear noise variance, $\sigma^2_{\mathrm{clip}}$, in order to validate the accuracy of the non-linear distortion model against higher order modulation. The BER performance of the DCO-OFDM and ACO-OFDM systems is presented in Fig. 4.1. It is ascertained that the theoretical and simulation results confirm a close match. Since only the odd subcarriers are modulated in ACO-OFDM, the electrical SNR requirement of $M$-QAM DCO-OFDM has to be compared with the one of $M^2$-QAM ACO-OFDM for an equal information rate. It is shown that ACO-OFDM suffers a greater BER degradation even though the bottom knee of the non-linear transfer function is avoided. DCO-OFDM consistently demonstrates a lower electrical SNR requirement as compared to ACO-OFDM for modulation orders with equal information

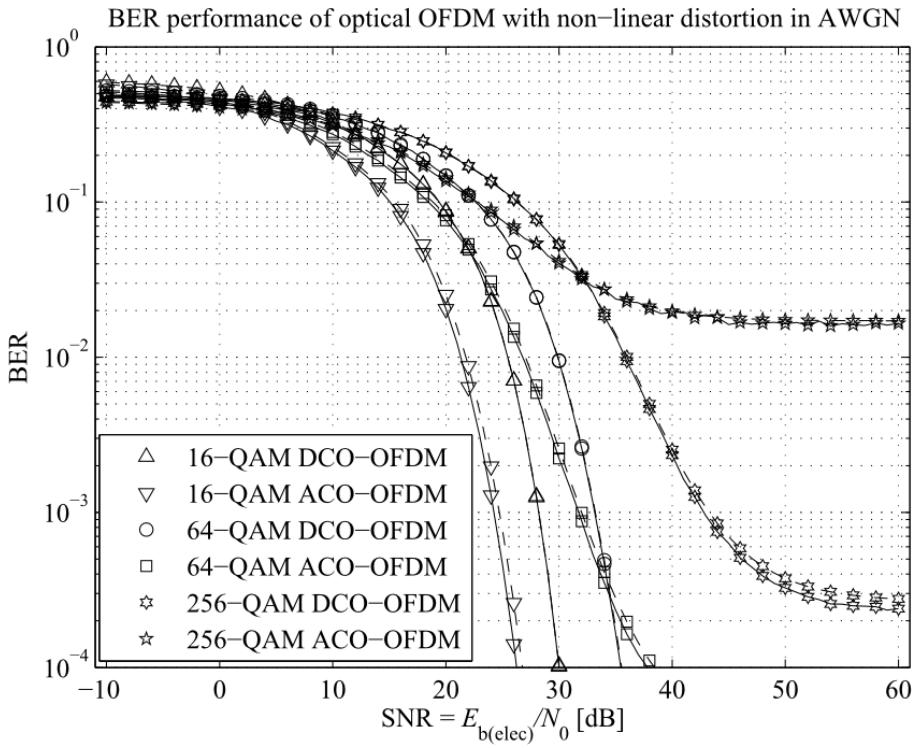


Figure 4.1: BER performance of DCO-OFDM and ACO-OFDM in AWGN with the non-linear distortion function $\Xi(x)$, simulation (solid lines) *vs.* theory (dashed lines).

rate, while higher order modulation proves to be more vulnerable to non-linear signal distortion.

## 4.3 Pre-distortion

Through pre-distortion, the dynamic range of the transmitter ca be maximized and linearized between levels of minimum and maximum radiated optical power. In this way, the single-carrier pulse modulation signals with a finite support in their PDF can be transmitted without non-linear distortion. However, the O-OFDM signals with a large PAPR and an infinite support in their PDF suffer a double-sided signal clipping.

### 4.3.1 Analysis of the double-sided signal clipping distortion

The non-linear signal distortion can be mitigated by pre-distortion of the signal with the inverse of the non-linear function $\Xi^{-1}(x)$. However, a linear dynamic range of the transmitter front-

end can only be obtained between points of minimum and maximum normalized input current, $I_{\text{min,norm}}$ and $I_{\text{max,norm}}$, as presented in Fig. 3.4. Using pre-distortion, a linear relation is established between the radiated optical power and the information-carrying input current over the limited dynamic range. Without loss of generality, the following normalized quantities are assumed for the boundaries of the dynamic range of the front-end in terms of normalized minimum and maximum optical power and current: $P_{\text{min,norm}} = I_{\text{min,norm}}$ and $P_{\text{max,norm}} = I_{\text{max,norm}} = 1$. Effectively, the time domain OFDM symbol, $s$, is subjected to double-sided clipping at normalized bottom and top clipping levels, $\lambda_{\text{bottom}}$ and $\lambda_{\text{top}}$. The resulting double-sided signal clipping after pre-distortion can be described by the non-linear distortion function $F(x) = \Phi(x)$, where $\Phi(x)$ is given as follows:

$$\Phi(x) = \begin{cases} P_{\text{min,norm}} & \text{if } x \leq P_{\text{min,norm}}, \\ x & \text{if } P_{\text{min,norm}} < x \leq P_{\text{max,norm}}, \\ P_{\text{max,norm}} & \text{if } x > P_{\text{max,norm}}. \end{cases} \tag{4.10}$$

Therefore, the normalized non-linear transfer function, $\Psi(s) = F(x) - F(\beta_{\text{DC}})$, can be obtained by the use of $F(x) = \Phi(x)$ also for the case of double-sided signal clipping after pre-distortion in O-OFDM. This linearized and clipped normalized transfer function can be used in (4.2) and (4.3) to obtain the clipping noise component, $w_{\text{clip}}$. In ACO-OFDM, $w_{\text{clip}}$ is non-negative, and it has a unipolar distribution, whereas in DCO-OFDM the clipping noise is bipolar. Passing through the FFT at the receiver, the clipping noise, $w_{\text{clip}}$, is transformed into additive zero-mean complex-valued Gaussian noise at the information-carrying subcarriers, preserving its variance of $\sigma^2_{\text{clip}}$. In the following, $K$ and $\sigma^2_{\text{clip}}$ are derived for case of double-sided signal clipping after pre-distortion in the considered DCO-OFDM and ACO-OFDM systems.

In both O-OFDM systems, the attenuation factor of the information-carrying subcarriers, $K$, can be expressed from (4.4) as follows:

$$K = Q(\lambda_{\text{bottom}}) - Q(\lambda_{\text{top}}) \, . \tag{4.11}$$

The details of the derivation of the result in (4.11) can be found in Section A.2 of Appendix A. Note that in ACO-OFDM and DCO-OFDM, since $s$ is real, $K$ is a real-valued function. It essentially represents the likelihood of samples not being clipped. In addition, it proves to be independent of the modulation scheme, $M$-QAM, and the FFT size, $N$. The attenuation factor

as a function of the normalized bottom and top clipping levels is illustrated in Fig. 4.2 and Fig. 4.3 for DCO-OFDM and ACO-OFDM, respectively. The signal clipping in DCO-OFDM exhibits a symmetric attenuation profile for clipping levels located symmetrically around the average optical power level. As suggested in [99, 100], the attenuation factor for ACO-OFDM approaches $0.5$ when the least signal clipping is present. Furthermore, the ACO-OFDM symbol suffers larger attenuation for downside clipping as compared to upside clipping.

The distorted DCO-OFDM symbol, $\Psi(s)$, is illustrated in Fig. 4.4. It follows a close to Gaussian distribution with zero mean and variance of $P_{\mathrm{s(elec)}}$, when the least signal clipping is present. Clipping the OFDM symbol at normalized bottom and top clipping levels, $\lambda_{\mathrm{bottom}}$ and $\lambda_{\mathrm{top}}$, in an asymmetric fashion, results in a non-zero-mean signal, $\Psi(s)$, which has a bias of $\mathrm{E}\left[\Psi(s)\right]$, where $\mathrm{E}\left[\cdot\right]$ stands for the expectation operator. After removing the bias of $\mathrm{E}\left[\Psi(s)\right]$ as shown in Fig. 4.4, $\sigma^2_{\mathrm{clip}}$ can be expressed in DCO-OFDM from (4.7) as follows:

$$\begin{aligned}\sigma^2_{\mathrm{clip}} = P_{\mathrm{s(elec)}}\Big(&K - K^2 + (1 - Q(\lambda_{\mathrm{bottom}}))\lambda^2_{\mathrm{bottom}} + Q(\lambda_{\mathrm{top}})\lambda^2_{\mathrm{top}} \\ &-\big(\phi(\lambda_{\mathrm{bottom}}) - \phi(\lambda_{\mathrm{top}}) + (1 - Q(\lambda_{\mathrm{bottom}}))\lambda_{\mathrm{bottom}} + Q(\lambda_{\mathrm{top}})\lambda_{\mathrm{top}}\big)^2 \\ &+\phi(\lambda_{\mathrm{bottom}})\lambda_{\mathrm{bottom}} - \phi(\lambda_{\mathrm{top}})\lambda_{\mathrm{top}}\Big)\,,\end{aligned} \tag{4.12}$$

The details of the derivation of the result in (4.12) can be found in Section A.2 of Appendix A.

The distorted ACO-OFDM symbol, $\Psi(s)$, is illustrated in Fig. 4.5. Here, the symmetries discussed in [99] allow for the unfolding of the truncated half-Gaussian distribution of $\Psi(s)$, the mirroring of the clipping levels around the origin and the redistribution of the signal samples. The resulting signal is symmetric with respect to the origin, and it follows a close to Gaussian distribution with zero mean and variance of $P_{\mathrm{s(elec)}}/2$, when the least signal clipping is present. However, the unfolded signal has a bias of $-\sigma\lambda_{\mathrm{bottom}}/\sqrt{2}$ on the negative samples and a bias of $\sigma\lambda_{\mathrm{bottom}}/\sqrt{2}$ on the positive ones. Since these biases are to be mounted on the first subcarrier in the ACO-OFDM frame after the FFT, they are irrelevant to the clipping noise variance on the data-carrying subcarriers. After removing these biases as shown in Fig. 4.5, $\sigma^2_{\mathrm{clip}}$ can be expressed in ACO-OFDM from (4.8) as follows:

$$\begin{aligned}\sigma^2_{\mathrm{clip}} = P_{\mathrm{s(elec)}}\Big(&K\big(\lambda^2_{\mathrm{bottom}} + 1\big) - 2K^2 - \lambda_{\mathrm{bottom}}\big(\phi(\lambda_{\mathrm{bottom}}) - \phi(\lambda_{\mathrm{top}})\big) \\ &-\phi(\lambda_{\mathrm{top}})\big(\lambda_{\mathrm{top}} - \lambda_{\mathrm{bottom}}\big) + Q(\lambda_{\mathrm{top}})\big(\lambda_{\mathrm{top}} - \lambda_{\mathrm{bottom}}\big)^2\Big)\,.\end{aligned} \tag{4.13}$$

The details of the derivation of the result in (4.13) can be found in Section A.2 of Appendix A.

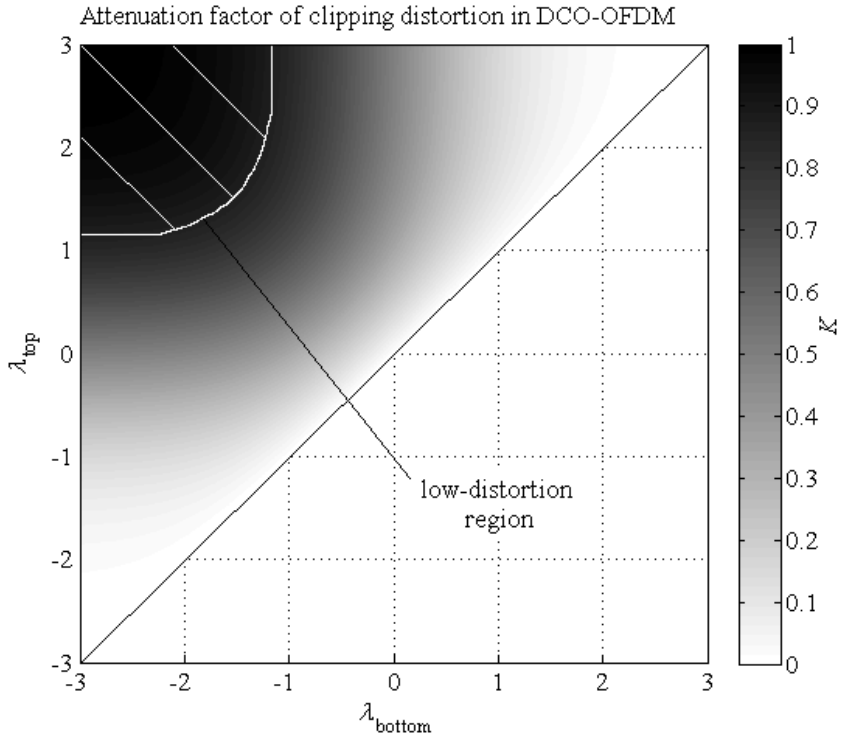


Figure 4.2: Attenuation factor of the clipping noise as a function of the normalized clipping levels in DCO-OFDM.

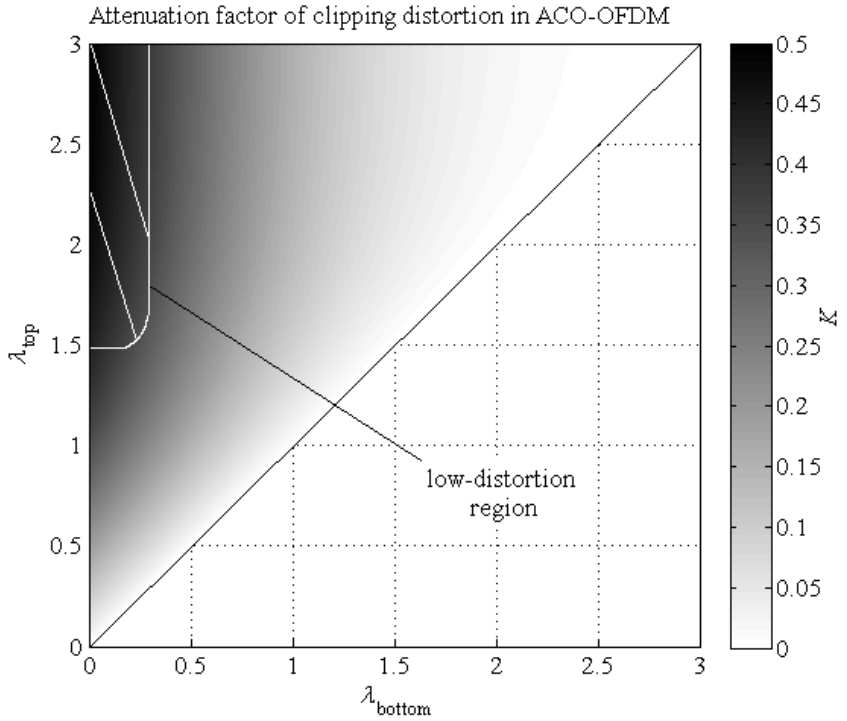


Figure 4.3: Attenuation factor of the clipping noise as a function of the normalized clipping levels in ACO-OFDM.

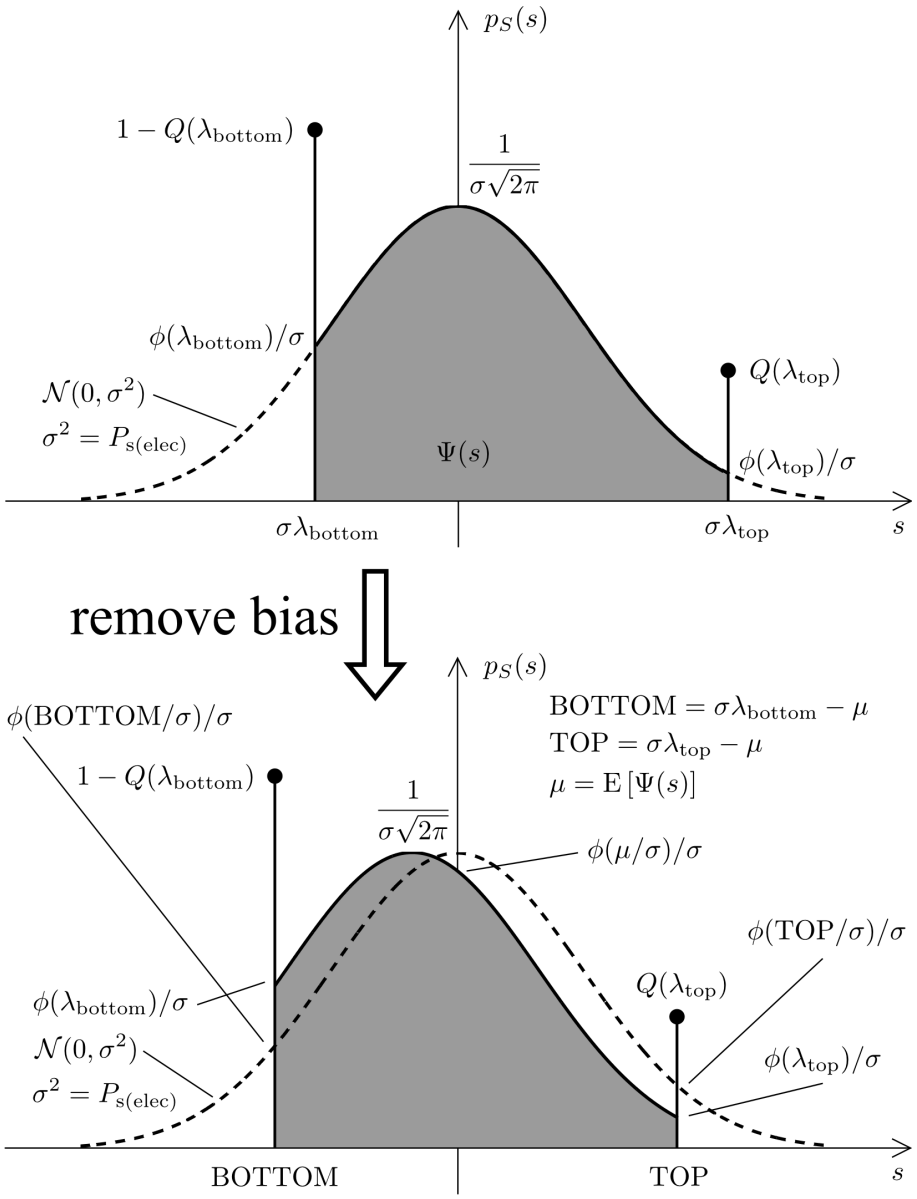


Figure 4.4: Double-sided clipping of the DCO-OFDM symbol after pre-distortion.

Note that similarly to the attenuation factor, $K$, the clipping noise variance, $\sigma^2_{\text{clip}}$, is independent of the modulation order, $M$, and the FFT size, $N$. It only depends on the normalized bottom and top clipping levels. This is illustrated in Fig. 4.7 and Fig. 4.6 for ACO-OFDM and DCO-OFDM, respectively. As expected, $\sigma^2_{\text{clip}}$ approaches zero for the least signal clipping. However, since $K$ and $\sigma^2_{\text{clip}}$ are coupled according to (4.2) and (4.3), as $K$ approaches zero, $\sigma^2_{\text{clip}}$ approaches zero, as well. Here, the large symbol distortion is defined for a small $K$ and a large $\sigma^2_{\text{clip}}$. Thus, Fig. 4.3 and Fig. 4.7 suggest that downside clipping introduces a larger ACO-OFDM symbol distortion than upside clipping. Expectedly, it is shown in Fig. 4.2

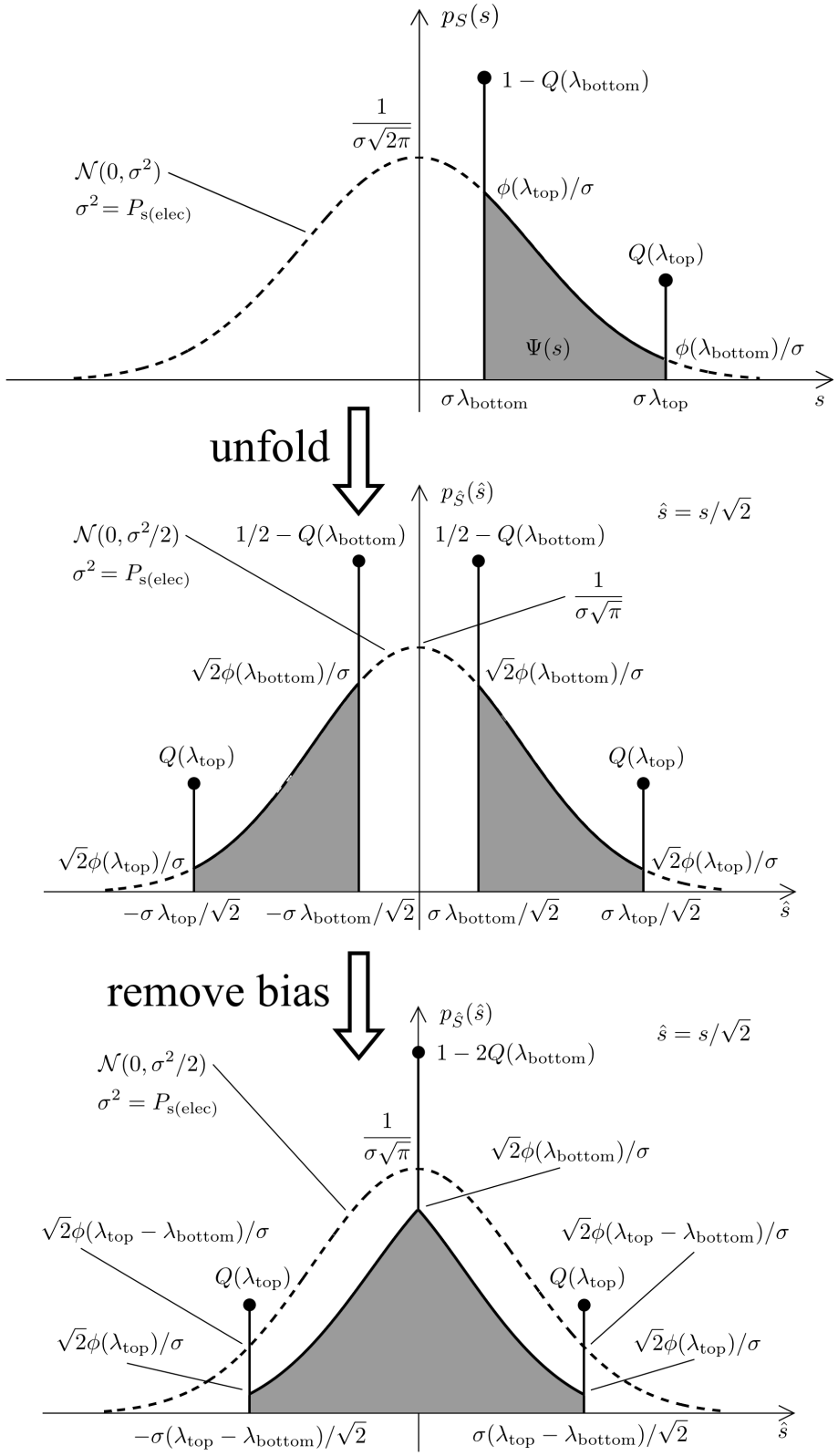


Figure 4.5: Double-sided clipping of the ACO-OFDM symbol after pre-distortion.

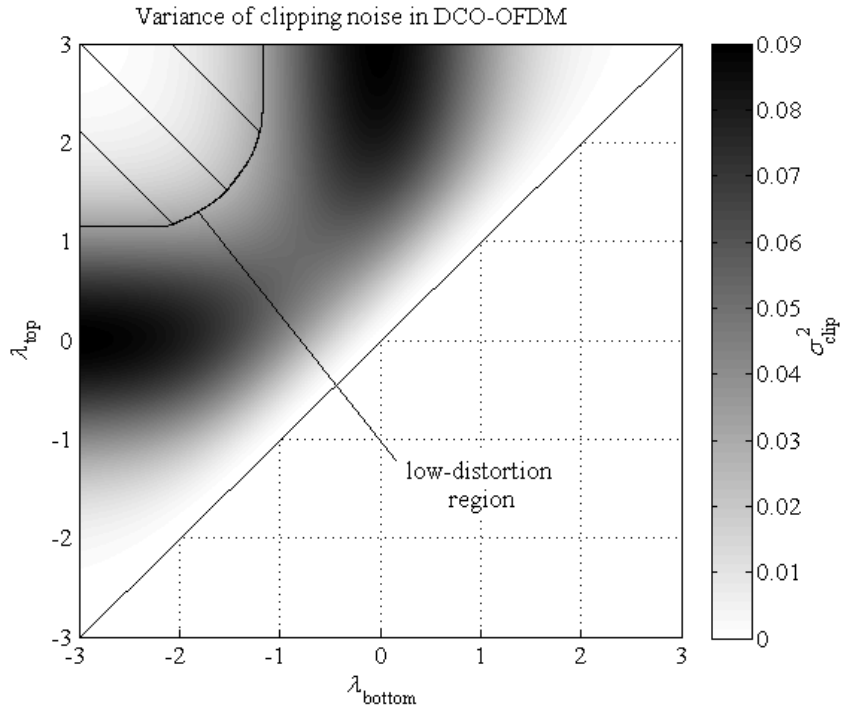


Figure 4.6: Variance of the clipping noise as a function of the normalized clipping levels in DCO-OFDM. Here, a scaled symbol power of $P_{\mathrm{s(elec)}}/G_{\mathrm{B}} = 1$ is assumed.

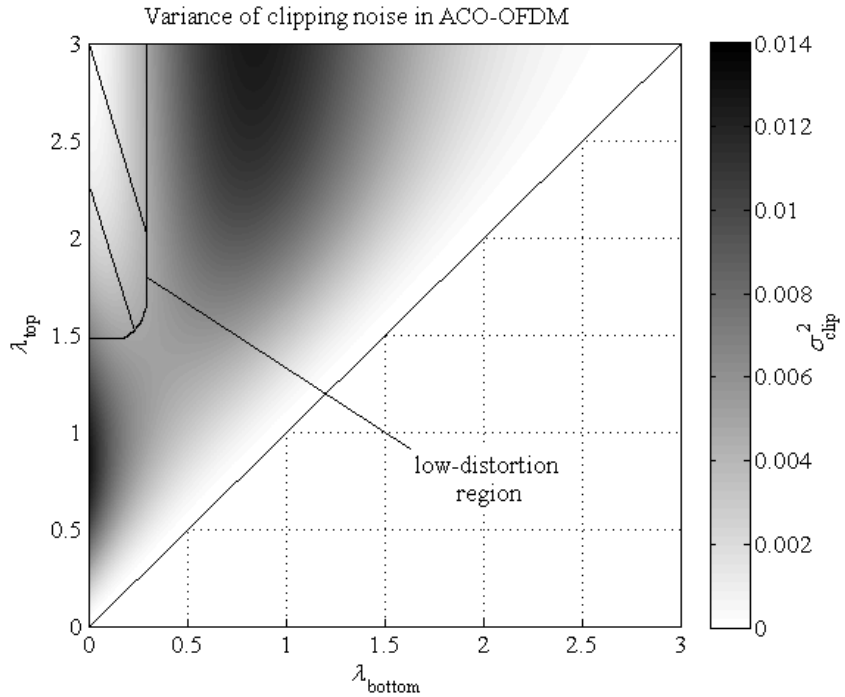


Figure 4.7: Variance of the clipping noise as a function of the normalized clipping levels in ACO-OFDM. Here, a scaled symbol power of $P_{\mathrm{s(elec)}}/G_{\mathrm{B}} = 1$ is assumed.

and Fig. 4.6 that the symbol distortion in DCO-OFDM can be minimized when symmetric normalized clipping levels are chosen. Since $K$ and $\sigma^2_{\text{clip}}$ are independent of $M$, they remain constant across the modulation orders for a particular choice of normalized bottom and top clipping levels. Nonetheless, the BER performance of the system depends on the granularity of the constellation, where higher order modulation is more vulnerable to Gaussian noise because of the shrinking of the decision regions. Therefore, the non-linear clipping distortion more significantly impacts the BER performance of higher order modulation, $M$-QAM.

### 4.3.2 Verification of the model with a Monte Carlo simulation

The accuracy of the analysis of the double-sided signal clipping distortion in O-OFDM is verified by means of a Monte Carlo BER simulation. For this purpose, an FFT size of $2048$ is chosen. The BER performance of DCO-OFDM and ACO-OFDM is evaluated as a function of the undistorted electrical SNR per bit, $\gamma_{\text{b(elec)}}$, in (3.31). The analytical expression for the BER from (3.20) and TABLE 3.1 is used. In general, because of the structure of the OFDM frame, ACO-OFDM achieves half the spectral efficiency of DCO-OFDM for equal modulation orders. Therefore, in addition to $4$-QAM ACO-OFDM with a spectral efficiency of $0.5$ bits/s/Hz, $16$-QAM ACO-OFDM is compared with $4$-QAM DCO-OFDM to evaluate the BER performance at a similar spectral efficiency of $1$ bit/s/Hz. Furthermore, the systems are constrained for equal average optical power of the transmitted signal. The linearized transfer characteristic with double-sided clipping, $F(x) = \Phi(x)$, is considered in $\Psi(s) = F(x) - F(\beta_{\text{DC}})$. Here, a practical $10$ dB linear dynamic range of a Vishay TSHG8200 LED at room temperature, *i.e.* $P_{\text{min,norm}} = 0.1$ and $P_{\text{max,norm}} = 1$, is considered the transmitter [50]. No clipping at the receiver is assumed. As benchmarks for a comparison with existing results, ideal cases for signal scaling and biasing are included from [100]. For any given fixed average optical power at the transmitter, $\mathrm{E}[\Phi(x)] = P_{\text{avg,norm}}$, the ACO-OFDM signal is clipped in the ideal case at $\lambda_{\text{bottom}} = 0$ and $\lambda_{\text{top}} = +\infty$. Here, $\beta_{\text{DC}} = 0$ and $\sigma = P_{\text{avg,norm}}\sqrt{2\pi}$. In DCO-OFDM, a widely used ideal case is defined for $\lambda_{\text{bottom}} = -2$ and $\lambda_{\text{top}} = +\infty$ [100]. Here, $\beta_{\text{DC}} = P_{\text{avg,norm}}$ and $\sigma = P_{\text{avg,norm}}/2$. In addition to the ideal case, two clipping scenarios which satisfy the average optical power constraint are considered for the verification of the analytical framework. Two average optical power constraints are chosen, *i.e.* $\mathrm{E}[\Phi(x)] = P_{\text{avg,norm}} = 0.2$ and $\mathrm{E}[\Phi(x)] = P_{\text{avg,norm}} = 0.3$. Here, the front-end biasing is defined through the parameters $\beta_{\text{DC}}$ and $\sigma$. They are obtained from (3.23) as a pair which yields the chosen $P_{\text{avg,norm}}$ for the given $P_{\text{min,norm}}$ and $P_{\text{max,norm}}$. In the first case,

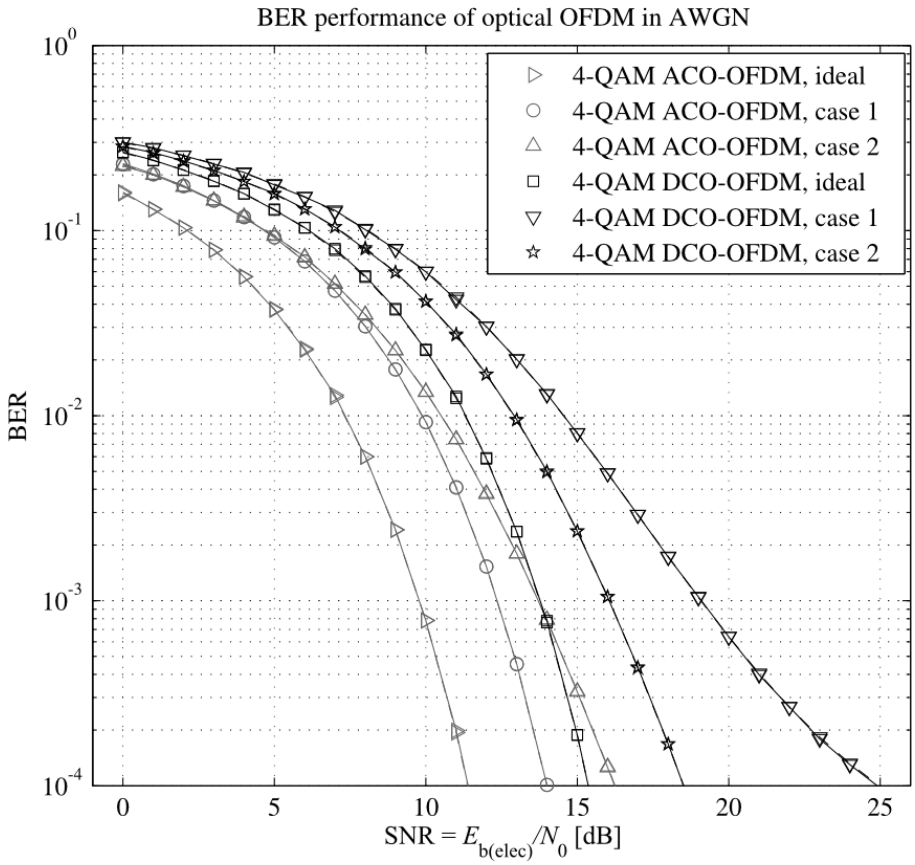


Figure 4.8: BER performance of optical OFDM in AWGN for a 10 dB dynamic range, 4-QAM ACO-OFDM *vs.* 4-QAM DCO-OFDM, simulation (solid lines) *vs.* theory (dashed lines).

$P_{\text{avg,norm}} = 0.2$ is realized in ACO-OFDM for $\beta_{\text{DC}} = 0.08$ and $\sigma = 0.29$, whereas $\beta_{\text{DC}} = 0.2$ and $\sigma = 0.1$ are required in DCO-OFDM. In the second case, $P_{\text{avg,norm}} = 0.3$ is obtained in ACO-OFDM for $\beta_{\text{DC}} = 0.06$ and $\sigma = 0.61$, while $\beta_{\text{DC}} = 0.3$ and $\sigma = 0.15$ are considered in DCO-OFDM. The two biasing setups yield the following normalized clipping levels. In ACO-OFDM, $\lambda_{\text{bottom}} = 0.06$ and $\lambda_{\text{top}} = 3.15$ in the first case, whereas $\lambda_{\text{bottom}} = 0.07$ and $\lambda_{\text{top}} = 1.54$ in the second case. In DCO-OFDM, $\lambda_{\text{bottom}} = -0.98$ and $\lambda_{\text{top}} = 8.2$ in the first case, whereas $\lambda_{\text{bottom}} = -1.32$ and $\lambda_{\text{top}} = 4.76$ in the second case. ACO-OFDM is expected to perform better in the first biasing setup because of the less severe upside clipping of the half-Gaussian signal distribution. On the contrary, DCO-OFDM is expected to perform better in the second biasing setup, because the normalized clipping levels are closer to a symmetric clipping of the Gaussian signal distribution.

The BER performance of the studied ACO-OFDM and DCO-OFDM systems is presented in Fig. 4.8 and Fig. 4.9. The theoretical and simulation results confirm a very close match. It is

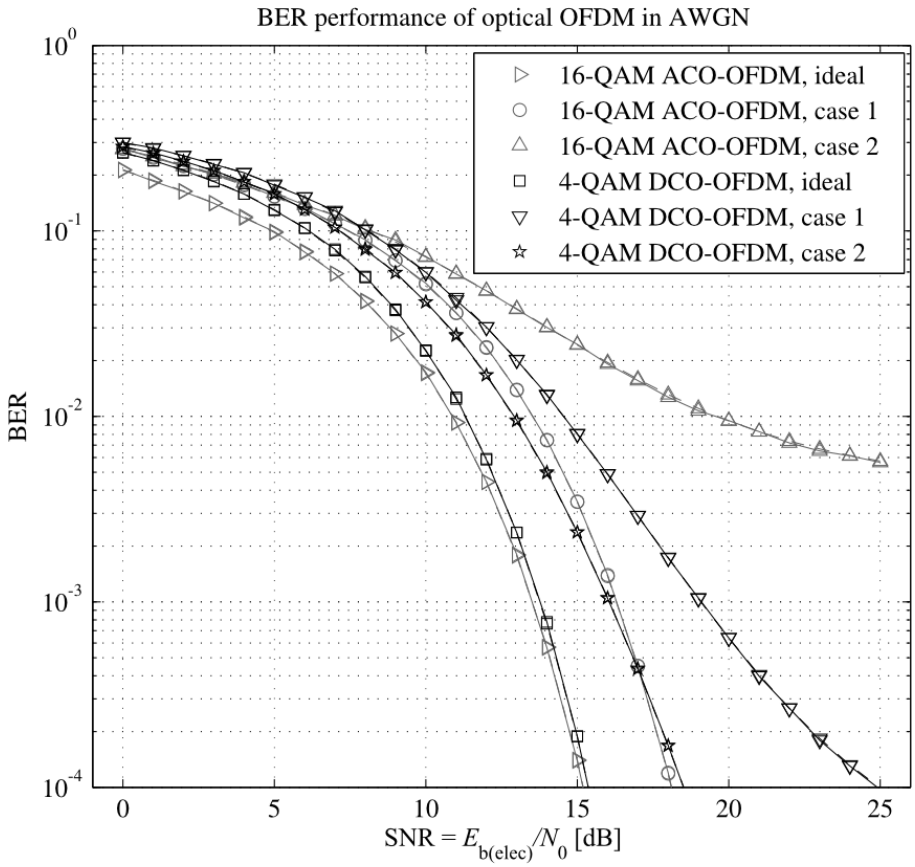


Figure 4.9: BER performance of optical OFDM in AWGN for a 10 dB dynamic range, 16-QAM ACO-OFDM *vs.* 4-QAM DCO-OFDM, simulation (solid lines) *vs.* theory (dashed lines).

shown that the existing simulation results from [100] for an ideal biasing scenario underestimate the BER performance of ACO-OFDM and DCO-OFDM in a biasing setup with a clipping distortion. However, the ideal biasing scenarios are not achievable in practice. In general, for identical QAM modulation orders ACO-OFDM demonstrates a better BER performance as compared to DCO-OFDM at the expense of $50\%$ reduction in spectral efficiency. In Fig. 4.8, even though 4-QAM ACO-OFDM shows the better BER performance for a corresponding clipping scenario, it is outperformed by 4-QAM DCO-OFDM in terms of spectral efficiency over the entire SNR region [21]. However, the results show that the biasing setup plays a significant role when comparing 16-QAM ACO-OFDM and 4-QAM DCO-OFDM. In general, a setup which accommodates a lower average optical power with respect to the given dynamic range is more suitable for ACO-OFDM. However, shifting the average optical power towards the middle of the dynamic range can potentially yield a better BER performance with DCO-OFDM and thereby a higher system throughput. This is because of the resulting front-end-induced signal clipping: in the first case DCO-OFDM is clipped more severely, whereas in the second

case ACO-OFDM is the one that suffers a greater signal degradation. This is confirmed by the BER results of 16-QAM ACO-OFDM and 4-QAM DCO-OFDM in Fig. 4.9. Whereas the first case of 16-QAM ACO-OFDM and the second case of 4-QAM DCO-OFDM perform similarly, the respective counterparts are more severely clipped, and their performance is degraded. However, a comparison between 4-QAM and 16-QAM ACO-OFDM suggests that higher order QAM modulation is more vulnerable to signal clipping. This is because, according to (3.31) the Gaussian clipping noise at the received data-carrying subcarriers is added independently of the QAM modulation order, $M$. Therefore, it is expected that $M$-QAM DCO-OFDM delivers a better BER performance, and therefore a higher throughput, as compared to $M^2$-QAM ACO-OFDM in a biasing setup with a higher average optical power. In addition, since the factors in (3.31) are independent of $N$ for practical FFT sizes, *i.e.* $N > 64$, the BER/throughput performance is independent of the total number of subcarriers.

## 4.4 Chapter summary

In this Chapter, the non-linear distortion of the large PAPR O-OFDM signals conditioned within the limited dynamic range of the transmitter has been analyzed in detail. First, a piecewise polynomial model has been proposed as a generalized representation of the non-linear transfer of the information-carrying current. The non-linear distortion has been translated by means of the Bussgang theorem and the CLT as an attenuation of the information-carrying subcarriers at the receiver plus zero-mean Gaussian uncorrelated noise. The non-linear distortion parameters such as the attenuation factor and the clipping noise variance have been derived in closed form. The model has been verified by means of a Monte Carlo simulation. The FFT size has been proven not to affect the non-linear distortion as long as Gaussianity of the O-OFDM time domain signal was ensured, *i.e.* $N > 64$. In addition, higher order $M$-QAM has been shown to suffer a larger BER degradation for a given signal biasing setup, *i.e.* signal scaling and DC bias.

In the second Section of this Chapter, the O-OFDM time domain signal has been subjected to pre-distortion with the inverse of the piecewise polynomial transfer function. As a result, the non-linear distortion has been reduced to double-sided signal clipping. The attenuation factor of the clipping distortion and the clipping noise variance have been derived in closed form. The model has been again verified by means of a Monte Carlo simulation. The non-linear distortion of the DCO-OFDM signal has been shown to be minimized for a symmetric clipping

setup, while in ACO-OFDM the bottom level clipping introduced a larger signal distortion as compared to top level clipping.

# Chapter 5
# Spectral efficiency and information rate of OFDM-based OWC with non-linear distortion

## 5.1 Introduction

In a practical communication setup, the electrical signal-to-noise ratio (SNR) requirement for a target bit-error ratio (BER) performance in additive white Gaussian noise (AWGN), the corresponding spectral efficiency and the information rate are figures of merit for a given modulation scheme. Here, the spectral efficiency of the modulation scheme is generally referred to as the uncoded bit rate per piece of bandwidth, while the information rate is based on the mutual information of transmitted and received data symbols. In a line-of-sight (LOS) communication scenario, where the optical wireless channel is dominated by the LOS signal component, the root-mean-square (RMS) delay spread of the channel is very small, and the 3-dB coherence bandwidth is very large. Such a scenario can be generally described as frequency non-selective slow fading channel or a flat fading channel. However, in a practical indoor setup, non-line-of-sight (NLOS) signal components can be reflected by the objects in room and detected at the receiver. In this case, the RMS delay spread of the channel increases, and the coherence bandwidth is reduced. Such a scenario can be generally described as frequency selective slow fading channel or a dispersive channel. Therefore, channel equalization at the receiver is required to recover the transmitted signal, which results in an increased SNR requirement to achieve a target BER. However, as shown in Fig. 2.6 and Fig. 2.7 from [47], NLOS communication links have similar received signal intensity to LOS communication links at larger distances because of the lower path loss exponent. In addition, NLOS communication is more robust to link blockage by a mobile object or person. Therefore, it is important to determine which digital modulation scheme for optical wireless communication (OWC) is most capable to deliver the highest spectral efficiency for a target electrical SNR for a practical dynamic range of the transmitter, when the bandwidth of the broadband signal exceeds the coherence bandwidth of the channel. In this Chapter, the achievable information rate of the multi-carrier modulation for OWC based

on optical orthogonal frequency division multiplexing (O-OFDM) with quadrature amplitude modulation ($M$-QAM) is presented for the flat fading channel under an average electrical power constraint, as well as minimum, average and maximum optical power constraints. The study is accommodated within the Shannon framework, in order to show the maximum information rate of O-OFDM in consideration of these constraints. In addition, the spectral efficiency of the multi-carrier modulation is compared with the spectral efficiency of single-carrier pulse modulation in the dispersive optical wireless channel for a practical dynamic range of the optical front-end.

## 5.2 $M$-QAM O-OFDM in the flat fading channel with AWGN

In this Section, the two general multi-carrier modulation schemes for OWC based on O-OFDM with $M$-QAM, *i.e.* direct-current-biased O-OFDM (DCO-OFDM) and asymmetrically clipped O-OFDM (ACO-OFDM), are compared in terms of electrical SNR requirement and spectral efficiency in a flat fading channel. By the use of pre-distortion, the non-linear signal distortion at the optical front-end can be reduce to double-sided signal clipping at normalized bottom and top clipping levels, $\lambda_{\mathrm{bottom}}$ and $\lambda_{\mathrm{top}}$. Practical linear dynamic ranges of $10$ dB, $20$ dB and $30$ dB are considered. An average optical power constraint is imposed, and it is varied over the entire dynamic range for the purpose of dimming of the radiated average optical power. The minimum electrical SNR requirement for a target BER of $M$-QAM O-OFDM is obtained through optimum signal scaling and DC-biasing. Through dimming of the average optical signal power, it is shown that there is still sufficient electrical signal power for communication.

### 5.2.1 Formulation of the biasing optimization

The choice of the optimum biasing parameters, such as the signal variance, $\sigma^2$, and the DC bias, $\beta_{\mathrm{DC}}$, in consideration of the front-end optical power constraints, such as the normalized minimum optical power constraint, $P_{\mathrm{min,norm}}$, the normalized maximum optical power constraint, $P_{\mathrm{max,norm}}$, and the normalized average optical power constraint, $P_{\mathrm{avg,norm}}$, for a given QAM modulation order, $M$, can be formulated as an optimization problem. The objective of the optimization is the minimization of the electrical SNR requirement to achieve a target BER which is summarized in TABLE 5.1. Here, the electrical SNR requirement is represented by

Given:

BER, $M$, $P_{\text{min,norm}}$, $P_{\text{max,norm}}$ and $P_{\text{avg,norm}}$

Find:

$$\underset{\substack{\sigma \geq 0 \\ \beta_{\text{DC}} \geq 0}}{\operatorname{argmin}} \ \gamma_{\text{b(elec)}}(\sigma, \beta_{\text{DC}}) \geq 0$$

where

ZF equalizer

$$\gamma_{\text{b(elec)}} = \frac{G_{\text{B}}}{|H(f_{\text{info}})|^2 G_{\text{T}} G_{\text{DC}}} \left( qK^2 - \frac{G_{\text{B}} \log_2(M) \sigma^2_{\text{clip}}}{P_{\text{s(elec)}}} \right)^{-1}$$

MMSE equalizer

$$\gamma_{\text{b(elec)}} = \frac{\dfrac{G_{\text{B}}}{G_{\text{T}} G_{\text{DC}}} - \left( qK^2 - \dfrac{G_{\text{B}} \log_2(M) \sigma^2_{\text{clip}}}{P_{\text{s(elec)}}} \right)}{|H(f_{\text{info}})|^2 \left( qK^2 - \dfrac{G_{\text{B}} \log_2(M) \sigma^2_{\text{clip}}}{P_{\text{s(elec)}}} \right)}$$

$$q = \frac{3 \log_2(M)}{M-1} \left( Q^{-1} \left( \frac{\text{BER} \sqrt{M} \log_2(M)}{4(\sqrt{M}-1)} \right) \right)^{-2}$$

Constraints: $\text{E}\left[\Phi(\mathbf{x}_l)\right] \leq P_{\text{avg,norm}}$

$\lambda_{\text{top}} > \lambda_{\text{bottom}}$ in DCO-OFDM

$\lambda_{\text{top}} > \lambda_{\text{bottom}} \geq 0$ in ACO-OFDM

Table 5.1: Minimization of $\gamma_{\text{b(elec)}}$ over $\sigma$ and $\beta_{\text{DC}}$ for given target BER, $M$, $P_{\text{min,norm}}$, $P_{\text{max,norm}}$ and $P_{\text{avg,norm}}$.

the electrical SNR per bit, $\gamma_{\text{b(elec)}} = E_{\text{b(elec)}}/N_0$, *i.e.* the average electrical bit energy normalized to the power spectral density of the AWGN. It is expressed from (3.20) by the use of the effective received electrical SNR per bit, $\Gamma_{\text{b(elec)}}$, from (3.31), where no bit and power loading is utilized. This is because of the considered flat fading channel with impulse response of $h(t) = \delta(t)$, where $\delta(\cdot)$ is the Dirac delta function, and a respective frequency response of $|H(f_{\text{info}})|^2 = 1$. In addition, only the modulation orders, $M$, of the even powers of 2 from TABLE 3.1 are used in (3.20) for simplicity. Here, the DC bias power is included in the calculation of the effective electrical SNR per bit, $\Gamma_{\text{b(elec)}}$. The DC bias gain, $G_{\text{DC}}$, is obtained from (3.28) and (3.29), and $G_{\text{DC}} < 1$. The bandwidth and time utilization factors are denoted in O-OFDM as $G_{\text{B}}$ and $G_{\text{T}}$, respectively. The clipping distortion parameters, such as the attenuation factor,

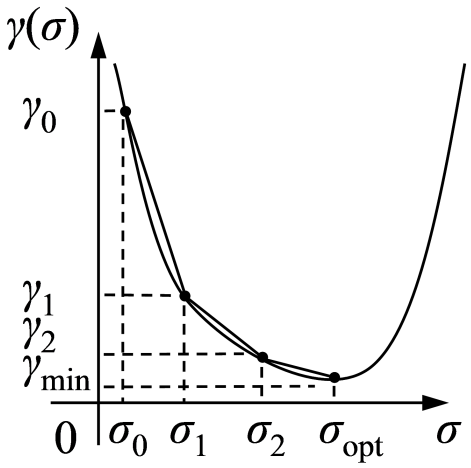


Figure 5.1: Example of an iterative optimization procedure based on the gradient descent method for a one-dimensional convex function, $\gamma(\sigma)$. Initial condition, $\sigma_0$, is chosen within the feasible region. The optimum solution, $(\sigma_{\mathrm{opt}}, \gamma_{\mathrm{min}})$, is illustrated.

$K$, and the clipping noise variance, $\sigma^2_{\mathrm{clip}}$, can be obtained in DCO-OFDM and ACO-OFDM from (4.11), (4.12) and (4.13). Here, $P_{\mathrm{s(elec)}} = \sigma^2$ stands for the average electrical symbol power, and $Q(\cdot)$ is the complementary cumulative distribution function (CCDF) of a standard normal distribution with zero mean and unity variance. The average optical power level of the transmitted O-OFDM signal is denoted as $\mathrm{E}\left[\Phi(\mathbf{x}_l)\right]$. It can be obtained from (3.23), and it is constrained to $P_{\mathrm{avg,norm}}$. The objective function is presented for the cases of a zero forcing (ZF) and a minimum mean squared error (MMSE) equalizer. The analytical approach to solve the minimization problem, such as for example the method of Lagrange multipliers [131], leads to a system of non-linear transcendental equations which does not have a closed-form solution. Therefore, a numerical optimization procedure is required, and the minimization can be carried out through a computer simulation for a particular choice of front-end optical power constraints. The formal proof of convexity of the objective function from TABLE 5.1 over the constrained function domain is equally intractable as the analytical minimization approach. However, the convexity can be illustrated by means of a computer simulation in Fig. 5.2 and Fig. 5.3 for a ZF equalizer in DCO-OFDM and ACO-OFDM, respectively. Therefore, an iterative optimization procedure based on the gradient descent method can be employed to find the optimum solution [131]. An example of the method is illustrated in Fig. 5.1 for a one-dimensional convex function with initial condition within the feasible region. In this thesis, the constrained optimization function *fmincon* from the Optimization Toolbox of the computation software MathWorks Matlab [132] is used.

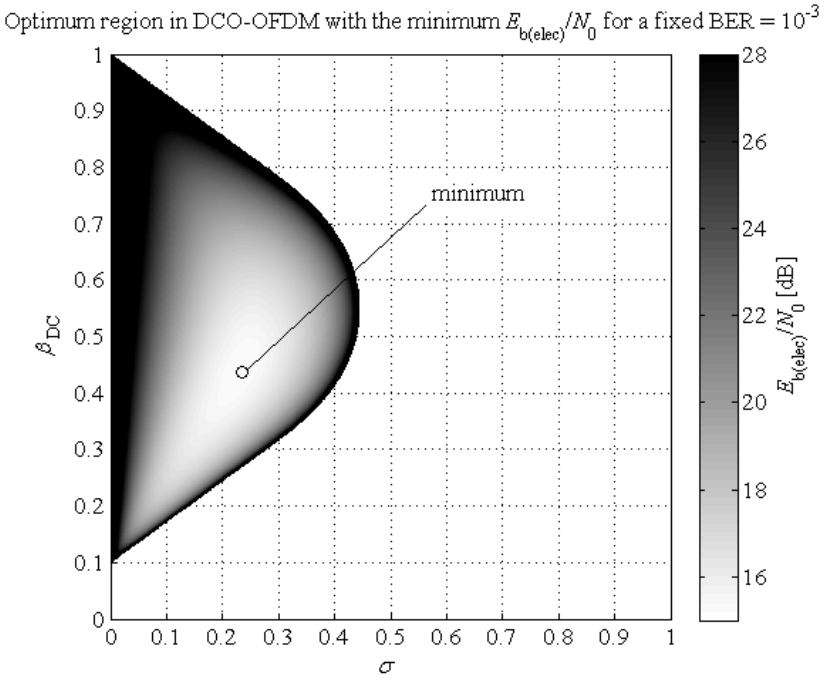


Figure 5.2: Convex objective function of $\sigma$ and $\beta_{\mathrm{DC}}$ in DCO-OFDM with the minimum $E_{\mathrm{b(elec)}}/N_0$ for a BER $= 10^{-3}$, 4-QAM with linear ZF equalizer, $h(t) = \delta(t)$, $P_{\mathrm{min,norm}} = 0.1$ and $P_{\mathrm{max,norm}} = 1$. DC bias power is included in the electrical SNR.

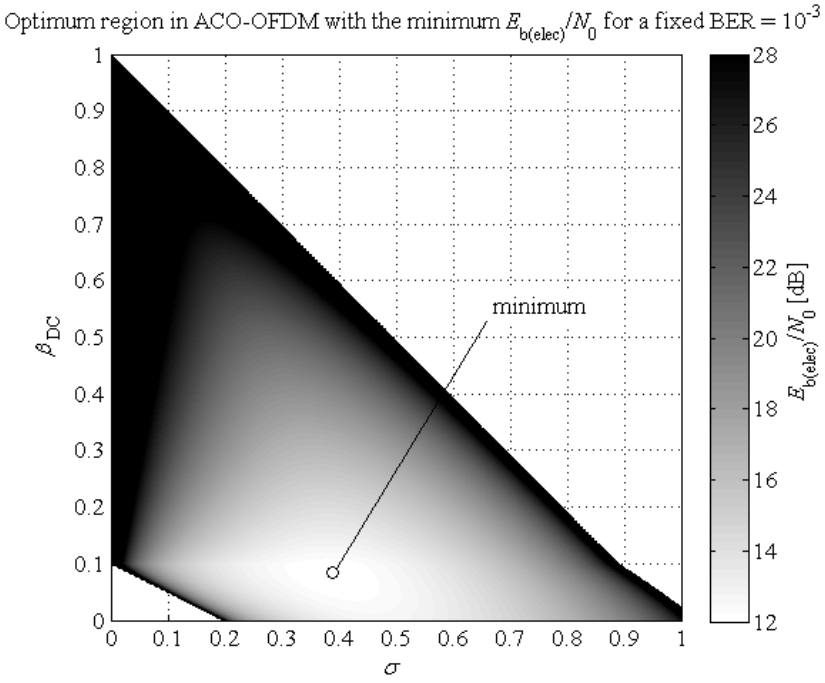


Figure 5.3: Convex objective function of $\sigma$ and $\beta_{\mathrm{DC}}$ in ACO-OFDM with the minimum $E_{\mathrm{b(elec)}}/N_0$ for a BER $= 10^{-3}$, 4-QAM with linear ZF equalizer, $h(t) = \delta(t)$, $P_{\mathrm{min,norm}} = 0.1$ and $P_{\mathrm{max,norm}} = 1$. DC bias power is included in the electrical SNR.

### 5.2.2 Spectral efficiency with an average optical power constraint

For the comparison of the SNR requirement of DCO-OFDM and ACO-OFDM under an average optical power constraint, the following QAM orders are chosen: $M = \{4, 16, 64, 256, 1024\}$. A target BER of $10^{-3}$ is considered as a minimum requirement to successfully enable forward error correction (FEC) coding or channel coding. In addition, the average optical power constraint in TABLE 5.1 is met with equality, *i.e.* $\mathrm{E}\left[\Phi(\mathbf{x}_l)\right] = P_{\mathrm{avg,norm}}$, in order to illustrate the influence of signal dimming on the electrical SNR requirement. Linear dynamic ranges of $10$ dB, $20$ dB and $30$ dB are considered, and therefore the normalized minimum optical power is set to $P_{\mathrm{min,norm}} = \{0.1, 0.01, 0.001\}$. For a large number of subcarriers, the inter-symbol interference (ISI) from maximum delay spreads up to $100$ ns can be compensated by a cyclic prefix (CP) of $2$ samples at a sampling rate of $20$ MHz with a negligible reduction of the electrical SNR requirement and the spectral efficiency [92]. A ZF equalizer is used.

The electrical SNR requirement for a target BER of $10^{-3}$ is presented in DCO-OFDM and ACO-OFDM for linear dynamic ranges of $10$ dB, $20$ dB and $30$ dB in Fig. 5.4, Fig. 5.5 and Fig. 5.6, respectively. As illustrated in Fig. 5.5, the small slopes of the graphs in the middle of the dynamic range suggest that average optical powers over more than $50\%$ and $25\%$ of the dynamic range can be supported by an SNR margin as low as $3$ dB in DCO-OFDM and ACO-OFDM, respectively. It is shown that for an equal modulation order, $M$, DCO-OFDM outperforms ACO-OFDM in terms of minimum electrical SNR requirement for average optical power levels in the upper part of the dynamic range, whereas ACO-OFDM prevails for lower average optical power levels because of the respective Gaussian and half-Gaussian distributions of the signals. In addition, the minimum electrical SNR requirement graphs exhibit an absolute minimum. This suggests that there is an average optical power level which allows for the best joint maximization of the signal variance, minimization of the clipping distortion and minimization of the DC-bias penalty from TABLE 5.1. For both systems, the absolute minimum electrical SNR requirement and the corresponding average optical power level are presented in Fig. 5.7. They decrease with the increase of the dynamic range because of the relaxed $P_{\mathrm{min,norm}}$ and $P_{\mathrm{max,norm}}$ constraints in the optimization. The details of the optimum biasing parameters for the $10$ dB dynamic range of the transmitter and QAM modulation orders, $M = \{4, 16, 64, 256, 1024\}$, with linear ZF equalizer in a flat fading channel are presented in TABLE 5.2. Considering the electrical power invested in the DC bias, it is shown that DCO-OFDM requires a non-symmetric clipping setup with the DC bias placed below the middle of

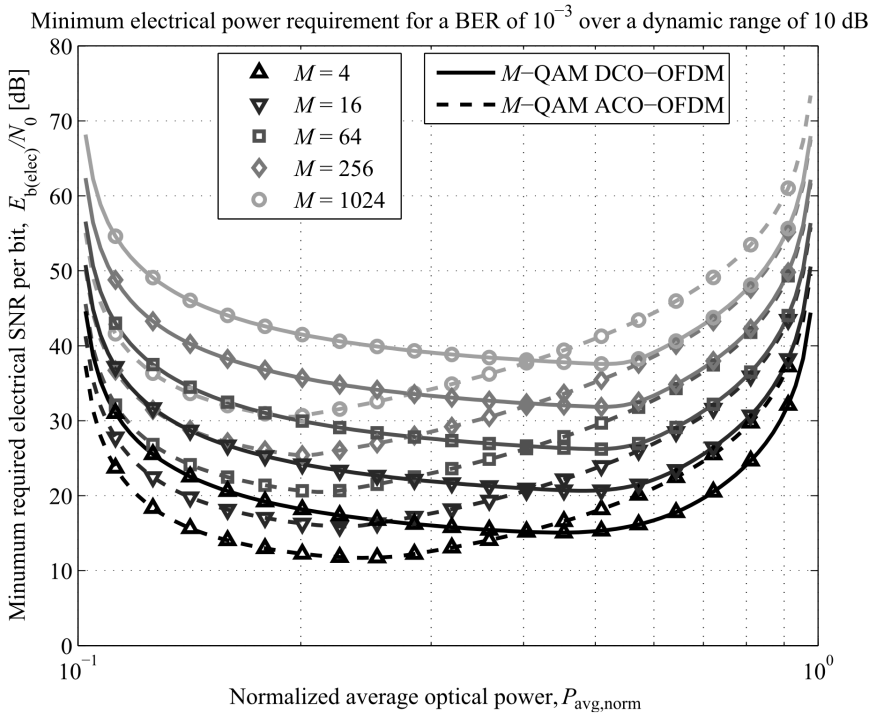


Figure 5.4: Minimum electrical SNR requirement for a BER of $10^{-3}$ *vs.* average optical power over a 10 dB dynamic range.

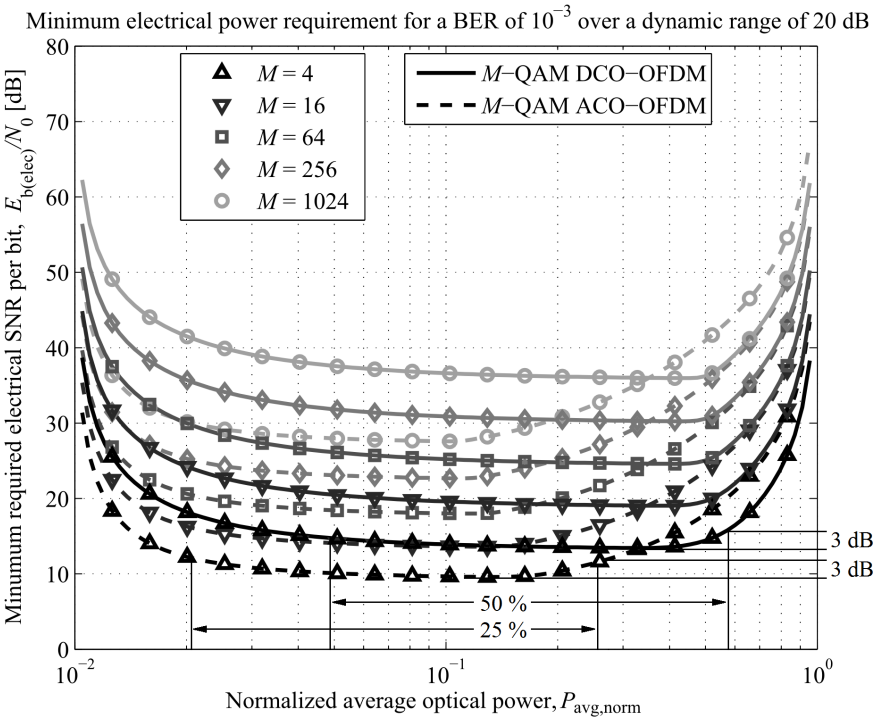


Figure 5.5: Minimum electrical SNR requirement for a BER of $10^{-3}$ *vs.* average optical power over a 20 dB dynamic range.

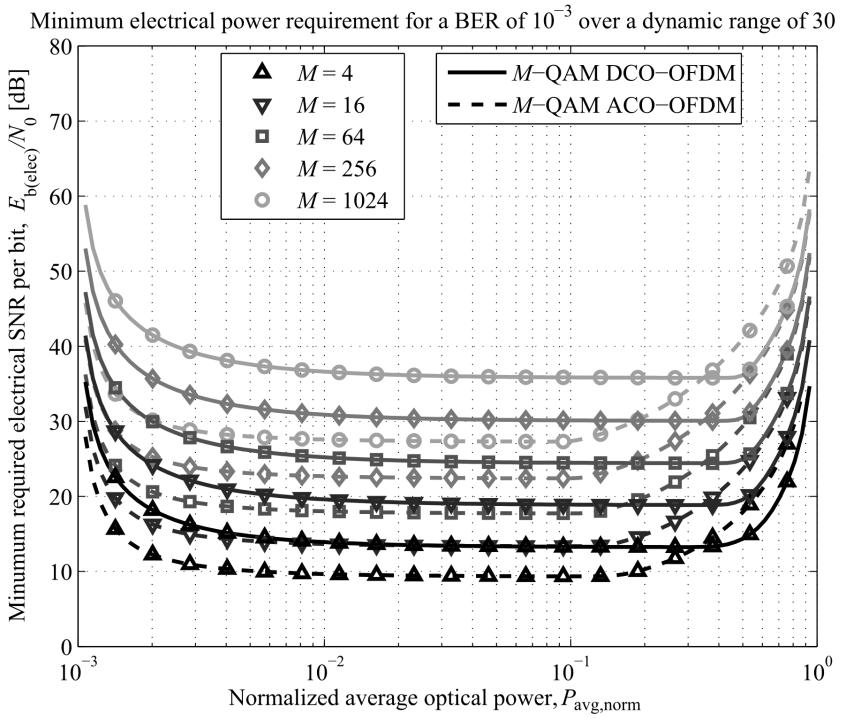


Figure 5.6: Minimum electrical SNR requirement for a BER of $10^{-3}$ *vs.* average optical power over a 30 dB dynamic range.

| Modulation order | ACO-OFDM | | | | DCO-OFDM | | | |
|---|---|---|---|---|---|---|---|---|
| | $\sigma$ | $\beta_{\mathrm{DC}}$ | $\lambda_{\mathrm{bottom}}$ | $\lambda_{\mathrm{top}}$ | $\sigma$ | $\beta_{\mathrm{DC}}$ | $\lambda_{\mathrm{bottom}}$ | $\lambda_{\mathrm{top}}$ |
| 4-QAM | 0.39 | 0.08 | 0.05 | 2.38 | 0.23 | 0.44 | $-1.47$ | 2.42 |
| 16-QAM | 0.33 | 0.09 | 0.01 | 2.76 | 0.18 | 0.48 | $-2.11$ | 2.87 |
| 64-QAM | 0.29 | 0.1 | 0 | 3.13 | 0.15 | 0.5 | $-2.6$ | 3.27 |
| 256-QAM | 0.26 | 0.1 | 0 | 3.48 | 0.14 | 0.51 | $-3.03$ | 3.63 |
| 1024-QAM | 0.24 | 0.1 | 0 | 3.81 | 0.12 | 0.52 | $-3.41$ | 3.97 |

Table 5.2: Optimum biasing parameters, $\sigma$ and $\beta_{\mathrm{DC}}$, and optimum normalized clipping levels, $\lambda_{\mathrm{bottom}}$ and $\lambda_{\mathrm{top}}$, in ACO-OFDM and DCO-OFDM with $M$-QAM and linear ZF equalizer for a 10 dB dynamic range and a $10^{-3}$ BER in a flat fading channel with impulse response $h(t) = \delta(t)$. DC bias power is included in the electrical SNR.

the dynamic range, in order to minimize the required $\gamma_{\mathrm{b(elec)}}$ for a target BER. The optimum performance of ACO-OFDM is obtained when the downside clipping is kept at minimum by setting the DC bias close to $P_{\mathrm{min,norm}}$.

In order to find out which system delivers the higher throughput for a given average optical power level, the spectral efficiency and the minimum electrical SNR requirement are shown in

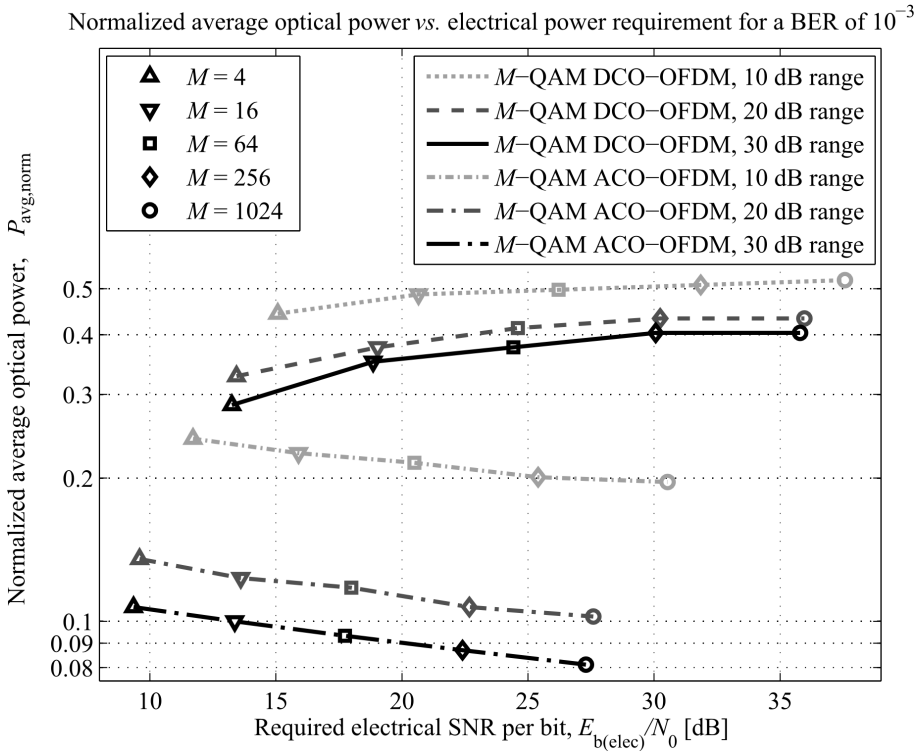


Figure 5.7: Normalized average optical power *vs.* absolute minimum electrical SNR requirement for a target BER of $10^{-3}$.

Fig. 5.8 for an average optical power level dimmed down to $20\%$. DCO-OFDM is expected to have a lower electrical SNR requirement and a superior spectral efficiency as compared to ACO-OFDM for average optical power levels in the upper part of the dynamic range. However, this is shown to be the case also for low average optical power levels, *i.e.* $P_{\text{avg,norm}} = 0.2$, as the dynamic range increases. Here, light emitting diodes (LEDs) with wider linear dynamic ranges are proven to be the enabling factor for OWC with low optical power radiation. In addition, DCO-OFDM demonstrates a lower minimum electrical SNR requirement for a target BER as compared to ACO-OFDM for modulation orders with similar spectral efficiencies for average optical power levels over more than $85\%$, $90\%$ and $95\%$ of the dynamic ranges of $10$ dB, $20$ dB and $30$ dB, respectively.

## 5.3 O-OFDM in the Shannon framework

In this Section, the information rate of DCO-OFDM and ACO-OFDM based on the mutual information between transmitted symbols and received symbols in the flat fading channel is presented for a practical linear dynamic range of the transmitter. In practice, the information

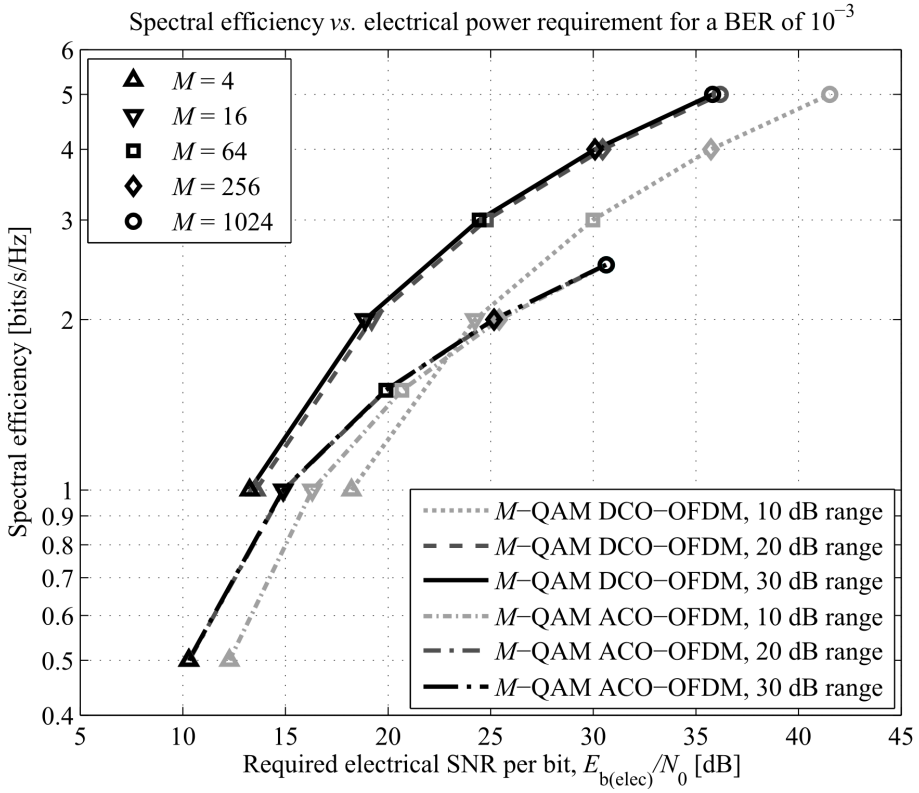


Figure 5.8: Spectral efficiency *vs.* minimum electrical SNR requirement for a target BER of $10^{-3}$. The average optical power level is set to $20\%$ of the maximum of the dynamic range.

rate of these modulation schemes can be achieved by means of FEC. Through pre-distortion, the non-linear distortion of the transmitter can be reduced to double-sided signal clipping. Since the clipping distortion merely results into an electrical SNR penalty, the information rate of O-OFDM with non-linear distortion can be accommodated within the Shannon framework. In addition, the average optical power constraint is imposed, and the information rate of O-OFDM with signal dimming is presented, including or excluding the additional DC bias power in the calculation of the electrical SNR.

### 5.3.1 Formulation of the biasing optimization

Passing through the transmitter front-end, the information-carrying O-OFDM signal, $\mathbf{x}_l$, is subjected to the non-linear distortion function $\Phi(\mathbf{x}_l)$. Because of the Gaussian signal distribution in O-OFDM the Bussgang theorem [27] can be applied, and the non-linear distortion can be modeled as an attenuation of the signal power and introduction of uncorrelated zero-mean non-Gaussian noise. After passing through the fast Fourier transform (FFT) at the receiver, the or-

thogonality of the attenuated information-carrying subcarriers is preserved, and the non-linear distortion noise is transformed into complex valued Gaussian noise according to the central limit theorem (CLT) [28]. The generalized model for the non-linear distortion of the received information-carrying subcarriers in O-OFDM is illustrated in Fig. 3.7. As a result, the non-linear distortion can be modeled as the transformation of the electrical SNR on an enabled subcarrier presented in (5.2). Because of the Hermitian symmetry within the O-OFDM frame, the DCO-OFDM and ACO-OFDM systems enable $G_{\mathrm{B}}N/2$ orthogonal complex-valued channels, the equivalent of $G_{\mathrm{B}}N$ orthogonal real-valued channels relevant for OWC. The information-carrying symbols on the orthogonal subcarriers, $f_{\mathrm{info}}$, generally have a uniform distribution since they are modulated in an $M$-QAM fashion. It has been shown in [133] that trough symbol shaping and coding such signals can also achieve the Shannon capacity. Therefore, the mutual information, $C$, in bits per real dimension (bits/dim) [125] as a function of the the undistorted electrical SNR per bit, $\gamma_{\mathrm{b(elec)}} = E_{\mathrm{b(elec)}}/N_0$, can be accommodated within the Shannon framework [86] for the two OFDM-based OWC systems with non-linear distortion for any given front-end biasing setup as follows:

$$C = \frac{R_{\mathrm{b}}}{B} = G_{\mathrm{T}}\frac{G_{\mathrm{B}}}{2}\log_2\left(1+\mathrm{SNR}\right) = G_{\mathrm{T}}\frac{G_{\mathrm{B}}}{2}\log_2\left(1+\frac{2K^2C/G_{\mathrm{B}}}{\dfrac{2C\sigma^2_{\mathrm{clip}}}{P_{\mathrm{s(elec)}}}+\dfrac{G_{\mathrm{B}}\gamma^{-1}_{\mathrm{b(elec)}}}{|H(f_{\mathrm{info}})|^2G_{\mathrm{T}}G_{\mathrm{DC}}}}\right), \tag{5.1}$$

The effective electrical SNR on an enabled subcarrier in O-OFDM is given as follows:

$$\mathrm{SNR} = \frac{K^2P_{\mathrm{s(elec)}}/G_{\mathrm{B}}}{\sigma^2_{\mathrm{clip}}+\dfrac{G_{\mathrm{B}}\sigma^2_{\mathrm{AWGN}}}{|H(f_{\mathrm{info}})|^2G_{\mathrm{DC}}}}, \tag{5.2}$$

where the variance of the AWGN is denoted as $\sigma^2_{\mathrm{AWGN}}$. The choice of the biasing parameters, such as the signal variance, $\sigma^2$, and the DC bias, $\beta_{\mathrm{DC}}$, to fit the signal within the limited linear dynamic range between $P_{\mathrm{min,norm}}$ and $P_{\mathrm{max,norm}}$ can be formulated as an optimization problem. The objective of the optimization is the minimization of the electrical SNR requirement, $\gamma_{\mathrm{b(elec)}}$, to achieve a target information rate, $C$, for a given average optical power constraint, $P_{\mathrm{avg,norm}}$. The minimum SNR requirement and the maximum information rate are achieved in a flat fading channel with impulse response of $h(t) = \delta(t)$ and a respective frequency response of $|H(f_{\mathrm{info}})|^2 = 1$. This optimization problem is summarized in TABLE 5.3. It has a trivial solution when the DC bias power is not included in the calculation of the effective electrical SNR

| |
|---|
| Given: $C$, $P_{\text{min,norm}}$, $P_{\text{max,norm}}$ and $P_{\text{avg,norm}}$ |
| Find: $\underset{\substack{\sigma \geq 0 \\ \beta_{\text{DC}} \geq 0}}{\text{argmin}} \ \gamma_{\text{b(elec)}}(\sigma, \beta_{\text{DC}}) \geq 0$<br>where<br>$\gamma_{\text{b(elec)}} = \frac{G_{\text{B}}^2}{2\lvert H(f_{\text{info}})\rvert^2 G_{\text{T}} G_{\text{DC}} C} \left( \frac{K^2}{2^{2C/(G_{\text{T}}G_{\text{B}})} - 1} - \frac{G_{\text{B}}\sigma_{\text{clip}}^2}{P_{\text{s(elec)}}} \right)^{-1}$ |
| Constraints: $\text{E}\left[\Phi(\mathbf{x}_l)\right] \leq P_{\text{avg,norm}}$<br>$\lambda_{\text{top}} > \lambda_{\text{bottom}}$ in DCO-OFDM<br>$\lambda_{\text{top}} > \lambda_{\text{bottom}} \geq 0$ in ACO-OFDM |

Table 5.3: Minimization of $\gamma_{\text{b(elec)}}$ over $\sigma$ and $\beta_{\text{DC}}$ for given $C$, $P_{\text{min,norm}}$, $P_{\text{max,norm}}$ and $P_{\text{avg,norm}}$.

in (5.2), *i.e.* when $G_{\text{DC}} = 1$. From (4.11) it follows that that $K^2$ decreases when the signal is more severely clipped. In addition, because of the fact that the clipping noise variance is non-negative, the effective electrical SNR and the information rate are maximized when the signal clipping is minimized. This is achieved by setting the normalized clipping levels, $\lambda_{\text{bottom}}$ and $\lambda_{\text{top}}$, farther apart as the information rate target increases, in order to accommodate the signal peaks [25].

However, the optimization problem has a non-trivial solution when the DC bias power is included in the calculation of the effective electrical SNR, *i.e.* when $G_{\text{DC}} < 1$. The analytical approach to solve the minimization problem leads to a system of non-linear transcendental equations which does not have a closed-form solution. Therefore, a numerical optimization procedure is required, and the minimization can be carried out through a computer simulation. In general, the formal proof of convexity of the objective function from TABLE 5.3 over the constrained function domain is equally intractable as the analytical minimization approach. However, the convexity can be illustrated by means of a computer simulation in Fig. 5.9 and Fig. 5.10 for DCO-OFDM and ACO-OFDM, respectively.

### 5.3.2 Maximum information rate without an average optical power constraint

The transmitter front-end constrains $P_{\text{min,norm}}$ and $P_{\text{max,norm}}$, while $P_{\text{avg,norm}}$ is independently imposed by the eye-safety regulations and/or the design requirements. In general, constraining

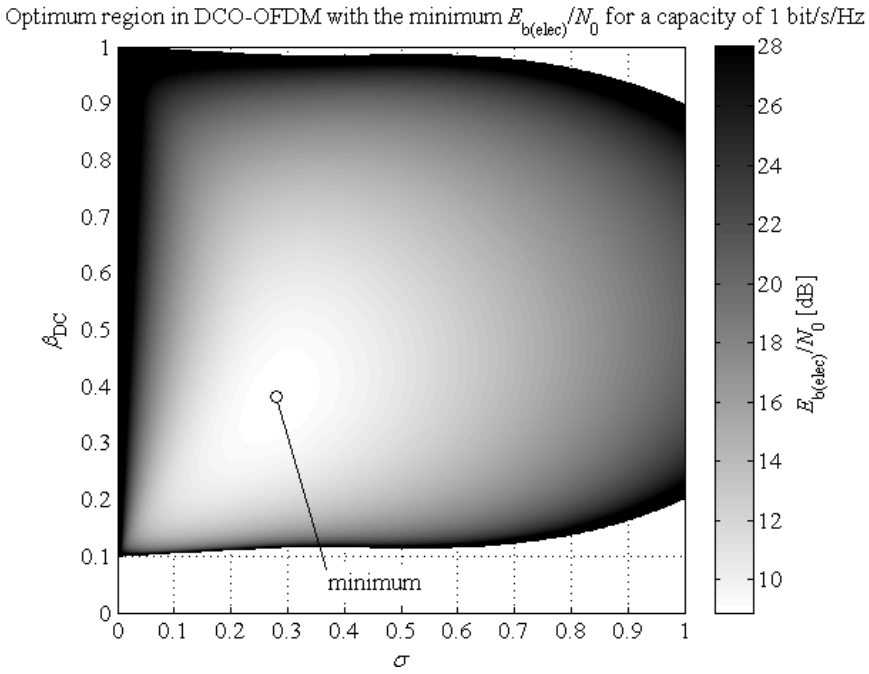


Figure 5.9: Convex objective function of $\sigma$ and $\beta_{\mathrm{DC}}$ in DCO-OFDM with the minimum $E_{\mathrm{b(elec)}}/N_0$ for a information rate of 1 bit/dim, $P_{\mathrm{min,norm}} = 0.1$ and $P_{\mathrm{max,norm}} = 1$. DC bias power is included in the electrical SNR.

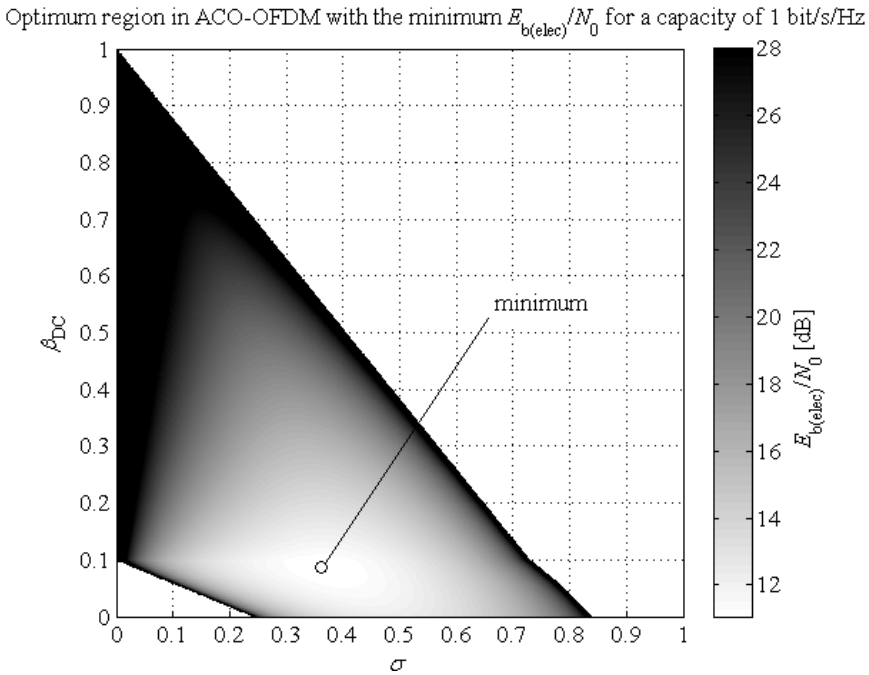


Figure 5.10: Convex objective function of $\sigma$ and $\beta_{\mathrm{DC}}$ in ACO-OFDM with the minimum $E_{\mathrm{b(elec)}}/N_0$ for a information rate of 1 bit/dim, $P_{\mathrm{min,norm}} = 0.1$ and $P_{\mathrm{max,norm}} = 1$. DC bias power is included in the electrical SNR.

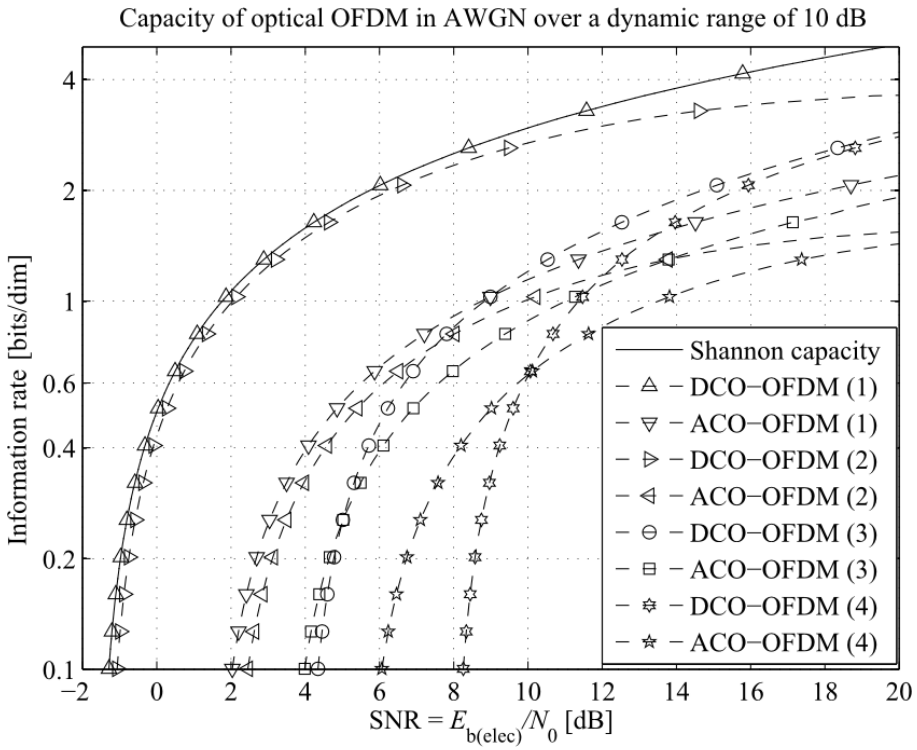


Figure 5.11: Mutual information in DCO-OFDM and ACO-OFDM *vs.* electrical SNR requirement for a 10 dB dynamic range without average optical power constraint: (1) with optimization, DC bias power not included; (2) without optimization, DC bias power not included; (3) with optimization, DC bias power included; (4) without optimization, DC bias power included.

the average optical power level to $\mathrm{E}\left[\Phi(\mathbf{x}_l)\right] \leq P_{\mathrm{avg,norm}}$ results in a suboptimal SNR requirement for a target information rate. The minimum SNR requirement is obtained when this constraint is relaxed, *i.e.* when $\mathrm{E}\left[\Phi(\mathbf{x}_l)\right]$ is allowed to assume any level in the dynamic range between $P_{\mathrm{min,norm}}$ and $P_{\mathrm{max,norm}}$. The optimized signal biasing setup is compared with a setup with a considerable signal clipping and suboptimal biasing. In DCO-OFDM, such a setup is realized, for instance, when $\beta_{\mathrm{DC}} = 0.55$ and $\sigma = 0.2$. In ACO-OFDM, the suboptimal biasing parameters are chosen as follows: $\beta_{\mathrm{DC}} = 0.2$ and $\sigma = 0.4$. The information rate for a 10 dB dynamic range of the optical front-end without an average optical power constraint is presented in Fig. 5.11. When the DC bias power is not counted towards the signal power, the optimized DCO-OFDM system achieves the Shannon capacity. Because of the effective halving of the electrical signal power and the half bandwidth utilization, the optimized ACO-OFDM system exhibits a 3-dB gap to the capacity which grows with the increase of the target information rate as presented in [99, 119]. In addition, it is shown that the severe signal clipping in the O-OFDM systems without optimization introduce a negligible SNR penalty reduction at low information rate targets, where the AWGN is dominant, and the SNR penalty grows with the increase of

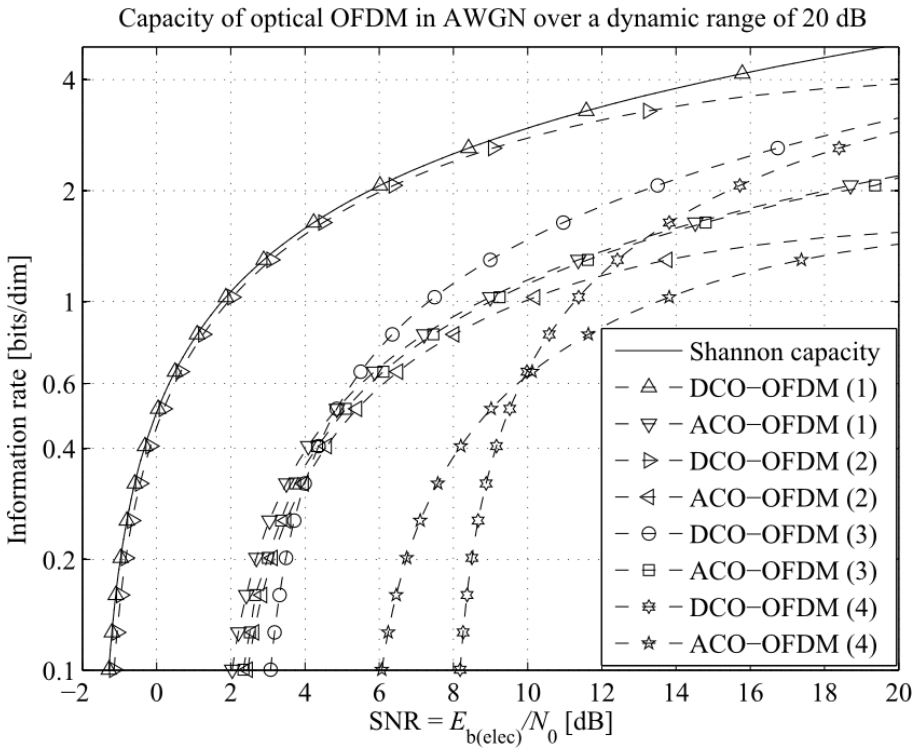


Figure 5.12: Mutual information in DCO-OFDM and ACO-OFDM *vs.* electrical SNR requirement for a 20 dB dynamic range without average optical power constraint: (1) with optimization, DC bias power not included; (2) without optimization, DC bias power not included; (3) with optimization, DC bias power included; (4) without optimization, DC bias power included.

the information rate target, where the clipping noise is dominant. When the DC bias power is added to the signal power, the systems incur an SNR penalty, because the DC bias reduces the useful alternating current (AC) signal power for a fixed total signal power. The optimized DCO-OFDM and ACO-OFDM systems exhibit a gap to the Shannon capacity of 5.6 dB and 5.3 dB, respectively, at 0.1 bits/dim, and 7.1 dB and 9.4 dB at 1 bit/dim. ACO-OFDM has a slightly lower SNR requirement as compared to DCO-OFDM at low information rate targets and a significantly higher SNR requirement at high information rate targets. It is shown that the optimization of the biasing setup can reduce the SNR penalty significantly. In this considered scenario a reduction of 4 dB and 2 dB is observed for DCO-OFDM and ACO-OFDM, respectively, at 0.1 bits/dim, and 2.5 dB at 1 bit/dim. With the increase of the linear dynamic range of the optical front-end to 20 dB presented in Fig. 5.12 the clipping distortion is reduced, and the O-OFDM systems without optimization have a slight increase of their information rate. The optimized O-OFDM systems preserve their maximum information rate in the case when the DC bias power is not included in the calculation of the electrical SNR. The increase of the dynamic range of the optical front-end further reduces the SNR requirement of the optimized

systems, when the DC bias power is counted towards the signal power. In DCO-OFDM and ACO-OFDM, the gap is reduced to $4.4$ dB and $3.6$ dB, respectively, at $0.1$ bits/dim, and to $5.6$ dB and $7.4$ dB at $1$ bit/dim.

### 5.3.3 Information rate with an average optical power constraint

In the next set of results, the average optical power constraint is imposed with equality and optimization is employed. DCO-OFDM is expected to have a lower electrical SNR requirement and a superior information rate as compared to ACO-OFDM for average optical power levels in the upper part of the dynamic range, while ACO-OFDM is expected to show a superior performance for average optical power levels in the lower part of the dynamic range. Therefore, optical power levels of $20\%$ and $50\%$ are chosen for the comparison of the optimized O-OFDM systems, and the results for a $10$ dB linear dynamic range are presented in Fig. 5.13. When the DC bias power is not counted towards the signal power, both systems achieve their maximum information rate for both average optical power levels, *i.e.* DCO-OFDM achieves the Shannon capacity, while ACO-OFDM has a 3-dB penalty which grows for higher information rate targets. When the DC bias power is included in the calculation of the electrical SNR, DCO-OFDM completely outperforms ACO-OFDM for the $50\%$ average optical power level. For the $20\%$ average optical power level, ACO-OFDM has a superior information rate as compared to DCO-OFDM only up to the cross-over point of $9.8$ dB at $0.8$ bits/dim. When the linear dynamic range is increased to $20$ dB and the DC bias power is counted towards the signal power, Fig. 5.14 shows that this cross-over point is shifted towards the lower SNR region, and DCO-OFDM has a superior information rate from $0.3$ bits/dim at $4$ dB onwards. While the increase of the dynamic range significantly increases the information rate for lower average optical power levels in an optimized biasing setup, the information rate of the higher optical power levels is only negligibly improved. This is because the increase of the dynamic range for a given average optical power level reduces the bottom level clipping which is already kept at minimum for high average optical power levels. For the $20\%$ average optical power level in the increased dynamic range of $20$ dB, DCO-OFDM and ACO-OFDM exhibit reduction of the SNR penalty of $2.3$ dB and $1.7$ dB, respectively, at $0.1$ bits/dim, and $3.8$ dB and $1.7$ dB at $1$ bit/dim. For the $50\%$ average optical power level, these values amount to merely $0.4$ dB and $0.1$ dB, respectively, at $0.1$ bits/dim, and $0.6$ dB and $0.1$ dB at $1$ bit/dim. When the DC bias power is excluded from the calculation of the electrical SNR, the optimized O-OFDM systems achieve their maximum information rate also for the increased $20$-dB dynamic range.

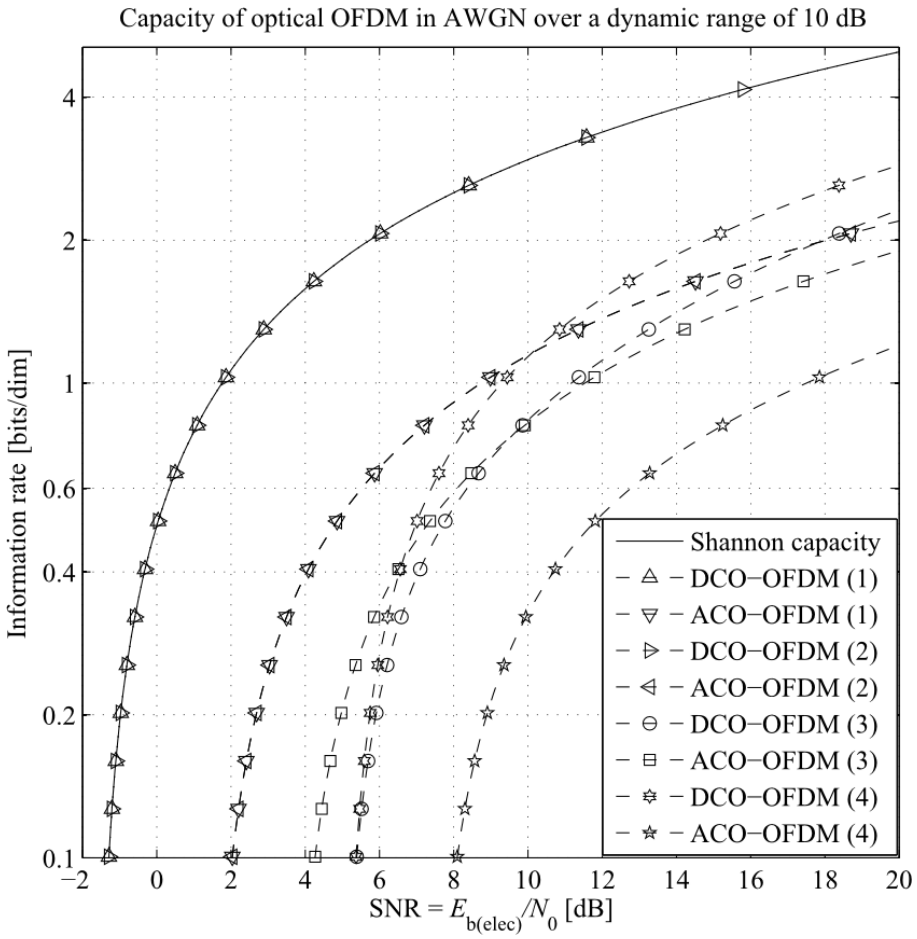


Figure 5.13: Mutual information in DCO-OFDM and ACO-OFDM *vs.* electrical SNR requirement for a 10 dB dynamic range with optimization: (1) $P_{\text{avg,norm}} = 0.2$, DC bias power not included; (2) $P_{\text{avg,norm}} = 0.5$, DC bias power not included; (3) $P_{\text{avg,norm}} = 0.2$, DC bias power included; (4) $P_{\text{avg,norm}} = 0.5$, DC bias power included.

In order to find out which system delivers the higher information rate for a any given average optical power level, the average optical power constraint is swept over the entire linear dynamic range. The solution of the optimization problem from TABLE 5.3 can be used to iteratively solve the dual problem, *i.e.* the maximization of the information rate, $C$, for a target SNR, $\gamma_{\text{b(elec)}}$, and a given average optical power constraint. The information rate of the optimized O-OFDM systems in this scenario is presented in Fig. 5.15 and in Fig. 5.16 for dynamic ranges of 10 dB and 20 dB, respectively. Here, SNR targets of $\gamma_{\text{b(elec)}} = 10$ dB and $\gamma_{\text{b(elec)}} = 15$ dB are chosen. When the DC bias power is not counted towards the signal power, the optimized O-OFDM systems consistently achieve their maximum information rate for average optical powers over the entire dynamic range, where DCO-OFDM delivers the higher information rate. When the DC bias power is included in the calculation of the electrical SNR,

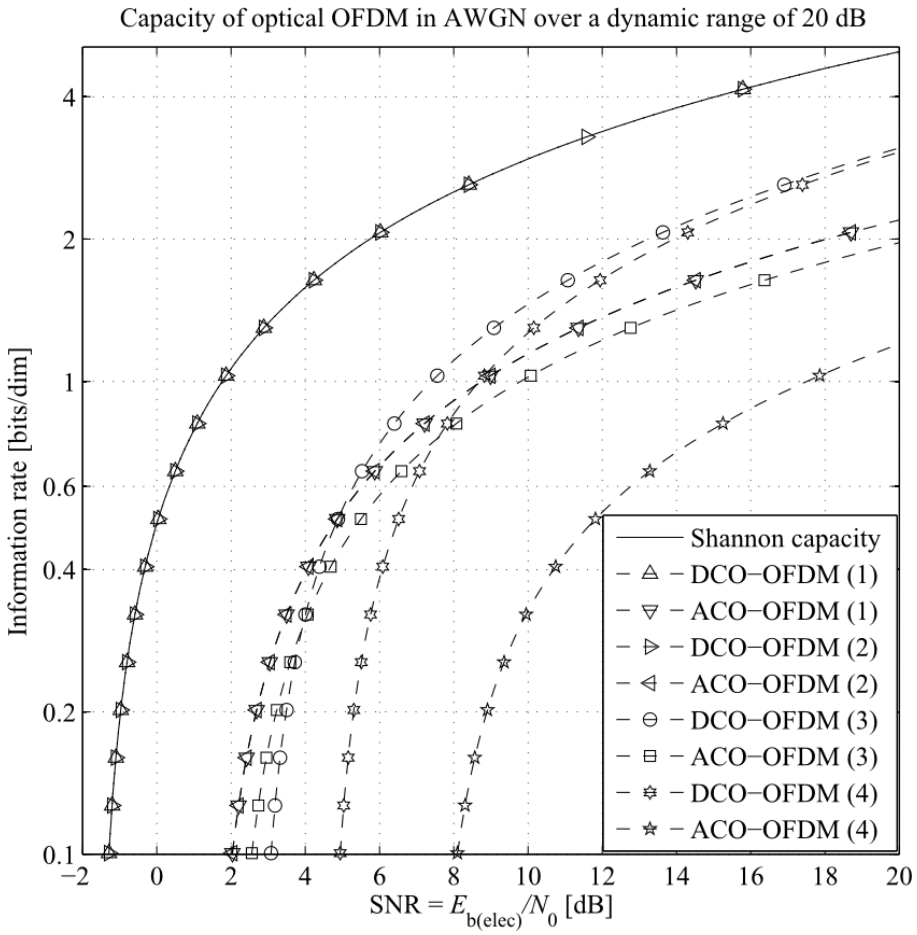


Figure 5.14: Mutual information in DCO-OFDM and ACO-OFDM *vs.* electrical SNR requirement for a 20 dB dynamic range with optimization: (1) $P_{\text{avg,norm}} = 0.2$, DC bias power not included; (2) $P_{\text{avg,norm}} = 0.5$, DC bias power not included; (3) $P_{\text{avg,norm}} = 0.2$, DC bias power included; (4) $P_{\text{avg,norm}} = 0.5$, DC bias power included.

DCO-OFDM is shown to have a superior information rate as compared to ACO-OFDM for average optical power levels in the upper part of the dynamic range, while ACO-OFDM shows a better performance for lower average optical power levels. This is because of the respective Gaussian and half-Gaussian distributions of the signals. However, as the dynamic range or the target SNR increase, DCO-OFDM is shown to dominate ACO-OFDM over a major part of the lower average optical power levels. Here, DCO-OFDM demonstrates a higher information rate as compared to ACO-OFDM for for average optical power levels over more than $89\%$ and $96\%$ of the $10$ dB dynamic range for the SNR targets of $10$ dB and $15$ dB, respectively, and over $99\%$ of the $20$ dB dynamic range. In addition, the information rate graphs exhibit an absolute maximum. This suggests that there is an average optical power level which allows for the best joint maximization of the signal variance, minimization of the clipping distortion and minimization

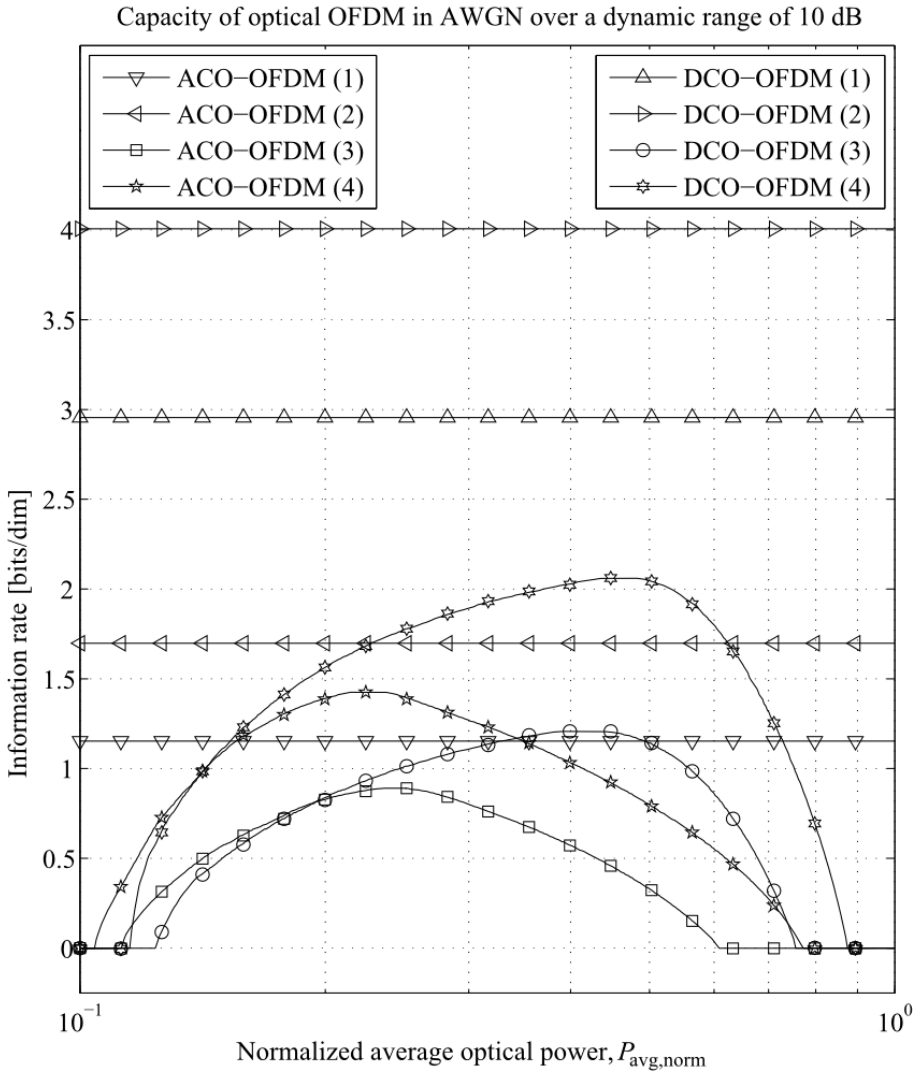


Figure 5.15: Mutual information in DCO-OFDM and ACO-OFDM *vs.* normalized average optical power for a 10 dB dynamic range with optimization: (1) $E_{\text{b(elec)}}/N_0 = 10$ dB, DC bias power not included; (2) $E_{\text{b(elec)}}/N_0 = 15$ dB, DC bias power not included; (3) $E_{\text{b(elec)}}/N_0 = 10$ dB, DC bias power included; (4) $E_{\text{b(elec)}}/N_0 = 15$ dB, DC bias power included.

of the DC-bias penalty from TABLE 5.3. As illustrated in Fig. 5.16, the small slopes of the graphs in the middle of the dynamic range suggest that average optical powers over more than $50\%$ and $25\%$ of the dynamic range can be supported at the expense of a mere $10\%$ decrease of information rate in DCO-OFDM and ACO-OFDM, respectively. Therefore, LEDs with wider linear dynamic ranges are proven to be the enabling factor for OWC with low optical power radiation in the case when the DC bias power is counted towards the signal power. It is important to mention that the DC bias penalty on the electrical SNR, $G_{\text{DC}}$, discussed in [25], is

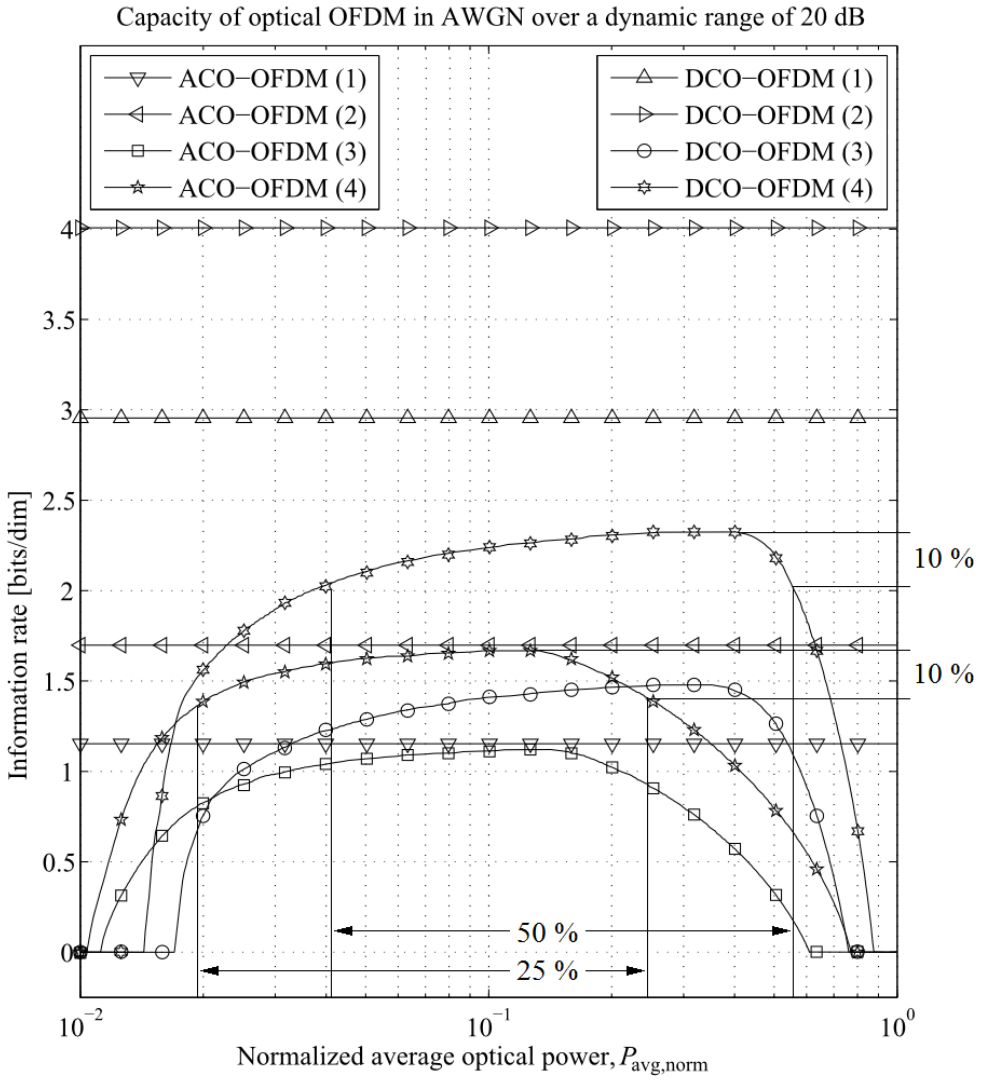


Figure 5.16: Mutual information in DCO-OFDM and ACO-OFDM *vs.* normalized average optical power for a 20 dB dynamic range with optimization: (1) $E_{\text{b(elec)}}/N_0 = 10$ dB, DC bias power not included; (2) $E_{\text{b(elec)}}/N_0 = 15$ dB, DC bias power not included; (3) $E_{\text{b(elec)}}/N_0 = 10$ dB, DC bias power included; (4) $E_{\text{b(elec)}}/N_0 = 15$ dB, DC bias power included.

minimized in the DCO-OFDM system as the dynamic range increases. In ACO-OFDM, the DC bias penalty almost goes to zero as shown in Fig. 5.15 and Fig. 5.16. As shown in the previous Section 5.3 the point of diminishing returns on the size of the dynamic range appears to be around 20 dB.

| |
|---|
| Given: $\gamma_{\mathrm{b(elec)}}$, $M$, $P_{\mathrm{min,norm}}$, $P_{\mathrm{max,norm}}$ and $P_{\mathrm{avg,norm}}$ |
| Find: $\underset{\substack{\sigma \geq 0 \\ \beta_{\mathrm{DC}} \geq 0}}{\operatorname{argmin}} \ \mathrm{BER}(\sigma, \beta_{\mathrm{DC}}) \geq 0$ |
| Constraints: $\mathrm{E}\left[\Phi(\mathbf{x}_l)\right] \leq P_{\mathrm{avg,norm}}$<br>$\lambda_{\mathrm{top}} > \lambda_{\mathrm{bottom}}$ in DCO-OFDM<br>$\lambda_{\mathrm{top}} > \lambda_{\mathrm{bottom}} \geq 0$ in ACO-OFDM |

Table 5.4: Minimization of BER over $\sigma$ and $\beta_{\mathrm{DC}}$ for given target $\gamma_{\mathrm{b(elec)}}$, $M$, $P_{\mathrm{min,norm}}$, $P_{\mathrm{max,norm}}$ and $P_{\mathrm{avg,norm}}$.

## 5.4 $M$-QAM O-OFDM in the dispersive channel with AWGN

In this Section, the spectral efficiency of $M$-QAM O-OFDM is obtained for the dispersive channel, including or excluding the additional DC bias power in the calculation of the electrical SNR. Through optimum signal scaling and DC-biasing the O-OFDM signal is conditioned within a 10 dB linear dynamic range. The spectral efficiency of $M$-QAM O-OFDM with bit and power loading is compared with the spectral efficiency of the single-carrier modulation techniques, multi-level pulse position modulation ($M$-PPM) and multi-level pulse amplitude modulation ($M$-PAM), with linear and non-linear equalization, when the signal bandwidth, $B$, exceeds the channel coherence bandwidth, $B_{\mathrm{c}}$.

### 5.4.1 Formulation of the biasing optimization

The choice of the optimum biasing parameters, such as the signal variance, $\sigma^2$, and the DC bias, $\beta_{\mathrm{DC}}$, which minimize the link BER for a target $\gamma_{\mathrm{b(elec)}}$ can be formulated as an optimization problem. Additional input parameters for the optimization are the front-end optical power constraints, $P_{\mathrm{min,norm}}$, $P_{\mathrm{max,norm}}$ and $P_{\mathrm{avg,norm}}$, and the desired average bit rate, equivalent to a QAM modulation order, $M$. This optimization problem is summarized in TABLE 5.4, and its solution can be used to iteratively solve the dual problem, *i.e.* the minimization of the $\gamma_{\mathrm{b(elec)}}$ for a target BER. The analytical expression for the BER from (3.20) is obtained by the use of TABLE 3.1 and the effective received electrical SNR per bit, $\Gamma_{\mathrm{b(elec)}}$, from (3.31) which is a function of $\gamma_{\mathrm{b(elec)}}$.

The optimization problem from TABLE 5.4 has a trivial solution when the DC bias power

is not included in the calculation of the effective electrical SNR per bit, $\Gamma_{\mathrm{b(elec)}}$, *i.e.* when $G_{\mathrm{DC}} = 1$. From (4.11) it follows that that $K^2$ decreases when the signal is more severely clipped. In addition, because of the fact that the clipping noise variance is non-negative, $\Gamma_{\mathrm{b(elec)}}$ is maximized and BER is minimized when the signal clipping is minimized. For instance, such a clipping scenario in DCO-OFDM is represented by $\lambda_{\mathrm{bottom}} = -4$ and $\lambda_{\mathrm{top}} = 4$. It is similar to the one used in [100], in order to minimize the clipping distortion. The equivalent scenario for ACO-OFDM is $\lambda_{\mathrm{bottom}} = 0$ and $\lambda_{\mathrm{top}} = 4$. These setups enable modulation orders as high as $M = 1024$ with a deviation from the true minimum required $\gamma_{\mathrm{b(elec)}}$ of only $0.1$ dB at BER of $10^{-3}$.

However, the optimization problem has a non-trivial solution when the DC bias power is included in the calculation of the effective electrical SNR per bit, $\Gamma_{\mathrm{b(elec)}}$, *i.e.* when $G_{\mathrm{DC}} < 1$. The analytical approach to solve the minimization problem leads to a system of non-linear transcendental equations which does not have a closed-form solution. Therefore, a numerical optimization procedure is required, and the minimization can be carried out through a computer simulation for a particular choice of front-end optical power constraints. In general, the formal proof of convexity of the objective function from TABLE 5.4 over the constrained function domain is equally intractable as the analytical minimization approach. However, the convexity can be illustrated by means of a computer simulation. A practical linear dynamic range of $10$ dB is assumed. In addition, the average optical power constraint is relaxed, in order to obtain the best BER system performance for the given dynamic range of the front-end. The objective function from TABLE 5.4 is illustrated in Fig. 5.17 and Fig. 5.18 for DCO-OFDM and ACO-OFDM, respectively, in the case of a flat fading channel with impulse response of $h(t) = \delta(t)$. It is shown that this objective function has a unique optimum convex region. In OFDM systems, the dispersive channel is represented by a superposition of orthogonal flat fading channels. Therefore, the objective average BER function can be obtained as the average of the BER functions for each flat fading channel which are shown to be convex. Since the expectation operator is a non-negative weighted summation, it preserves the convexity [131]. Therefore, the objective BER function in the dispersive channel remains convex.

### 5.4.2 The DC bias penalty

In this study, $M$-QAM O-OFDM in the dispersive channel is compared with $M$-PPM and $M$-PAM in terms of electrical SNR requirement, $\gamma_{\mathrm{b(elec)}}$, to achieve a target BER of $10^{-3}$

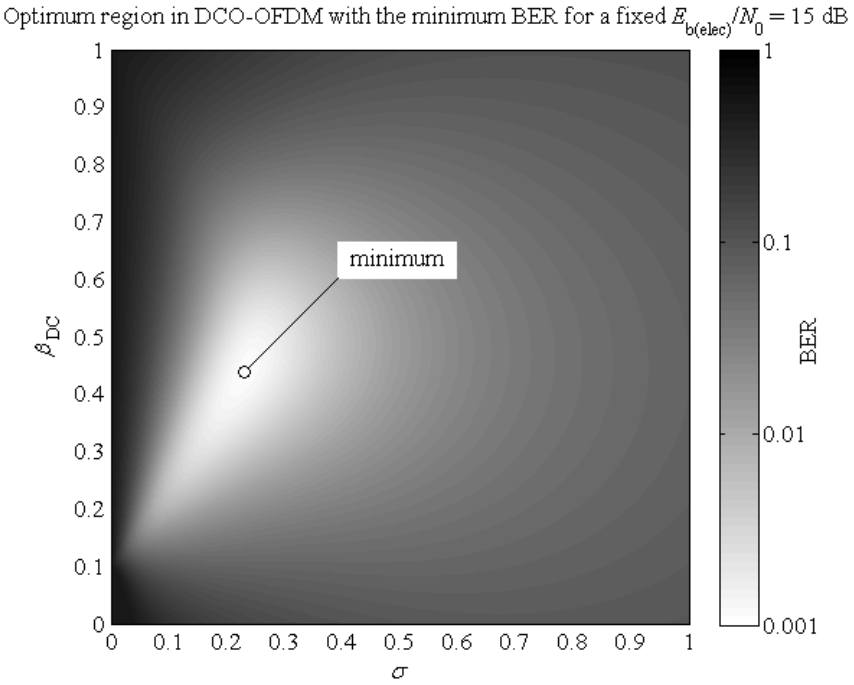


Figure 5.17: Convex objective function of $\sigma$ and $\beta_{\mathrm{DC}}$ in DCO-OFDM with the minimum BER for a fixed $E_{\mathrm{b(elec)}}/N_0 = 15$ dB, 4-QAM with linear ZF equalizer, $h(t) = \delta(t)$, $P_{\mathrm{min,norm}} = 0.1$ and $P_{\mathrm{max,norm}} = 1$. DC bias power is included in the electrical SNR.

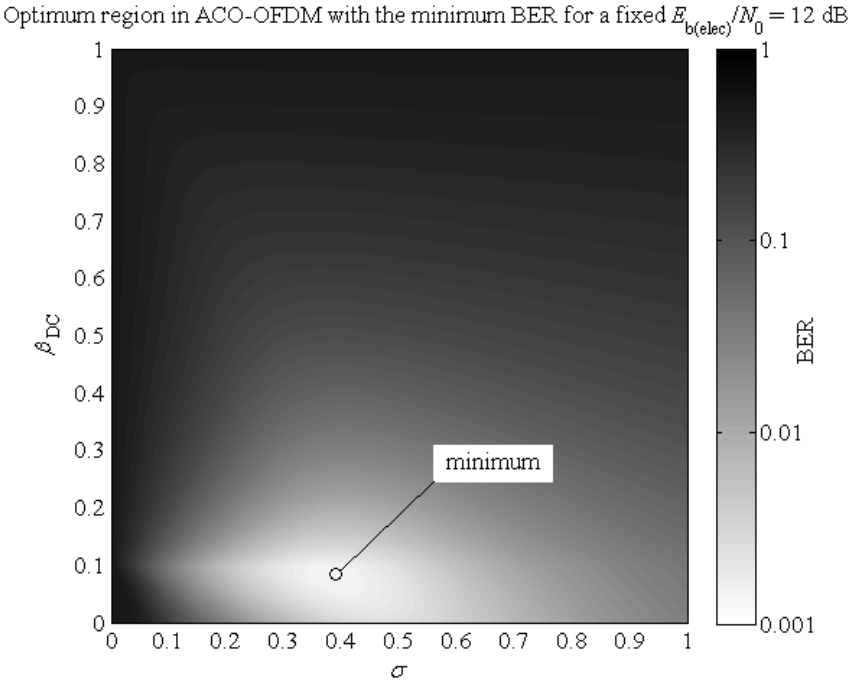


Figure 5.18: Convex objective function of $\sigma$ and $\beta_{\mathrm{DC}}$ in ACO-OFDM with the minimum BER for a fixed $E_{\mathrm{b(elec)}}/N_0 = 12$ dB, 4-QAM with linear ZF equalizer, $h(t) = \delta(t)$, $P_{\mathrm{min,norm}} = 0.1$ and $P_{\mathrm{max,norm}} = 1$. DC bias power is included in the electrical SNR.

and the corresponding spectral efficiency. In the first set of results, the DC bias power is not counted towards the signal power, and a flat fading channel without dispersion, *i.e.* $h(t) = \delta(t)$, is assumed. The following modulation orders are chosen: $M = \{2, 4, 16, 64, 256, 1024\}$. Here, single-carrier binary phase shift keying (BPSK) is identical to 2-PAM. A $10$ dB dynamic range of the optical front-end is assumed. The transmitted signal spans the entire dynamic range of optical power, and no constraint is imposed on the radiated average optical power, in order to obtain the best BER system performance for the given dynamic range. In single-carrier transmission, the non-linear signal distortion is avoided through pre-distortion. The average optical power level is set in $M$-PPM to $\mathrm{E}\left[F(\mathbf{x}_l)\right] = P_{\mathrm{max,norm}}/M$, and in $M$-PAM to $\mathrm{E}\left[F(\mathbf{x}_l)\right] = (P_{\mathrm{min,norm}} + P_{\mathrm{max,norm}})/2$. In multi-carrier transmission, a large number of subcarriers, *e.g.* $2048$, is chosen. Minimum signal clipping is assumed in O-OFDM, *i.e.* $\lambda_{\mathrm{bottom}} = -4$ and $\lambda_{\mathrm{top}} = 4$ in DCO-OFDM , and $\lambda_{\mathrm{bottom}} = 0$ and $\lambda_{\mathrm{top}} = 4$ in ACO-OFDM. In both systems, the average optical power level, $\mathrm{E}\left[\Phi(\mathbf{x}_l)\right]$, can be obtained from (3.23). The resulting spectral efficiency *vs.* electrical SNR requirement plot of the transmission schemes for OWC is presented in Fig. 5.19. It is shown that PPM is the only system which can operate at very low SNR in the range of $4.1 - 6.8$ dB. For a given higher SNR, DCO-OFDM and PAM demonstrate an equal highest spectral efficiency.

When the DC bias power is added to the signal power, the systems incur an SNR penalty, because the DC bias reduces the useful AC signal power for a fixed total signal power. Based on the different signal statistics, the compared systems incur a different SNR penalty due to the DC bias. The DC bias gain factor, $G_{\mathrm{DC}}$, can be obtained for $M$-PAM from (3.16), (3.18) and (3.19), and it is independent of the channel. In DCO-OFDM and ACO-OFDM, the DC bias gain is given in (3.28) and (3.29), respectively. Since bit and power loading in conjunction with the optimum signal biasing from TABLE 5.4 are employed in O-OFDM in order to minimize the electrical SNR requirement in the dispersive channel, the optimum $\sigma$ and $\beta_{\mathrm{DC}}$ are used in the calculation of $G_{\mathrm{DC}}$. The DC bias gain in the different modulation formats for OWC is presented in Fig. 5.20 as the signal bandwidth exceeds the channel coherence bandwidth. For the considered $10$ dB dynamic range, the optimum signal clipping reduces the SNR penalty by up to $6.5$ dB for DCO-OFDM and up to $1.4$ dB for ACO-OFDM as compared to minimum signal clipping. In addition, bit and power loading in combination with optimum signal clipping allow the DC bias gain to saturate above the DC bias gain in the minimum clipping case. Nevertheless, because of the close to Gaussian and half-Gaussian distribution of the signals, respectively, DCO-OFDM and ACO-OFDM still incur a larger SNR penalty as compared to

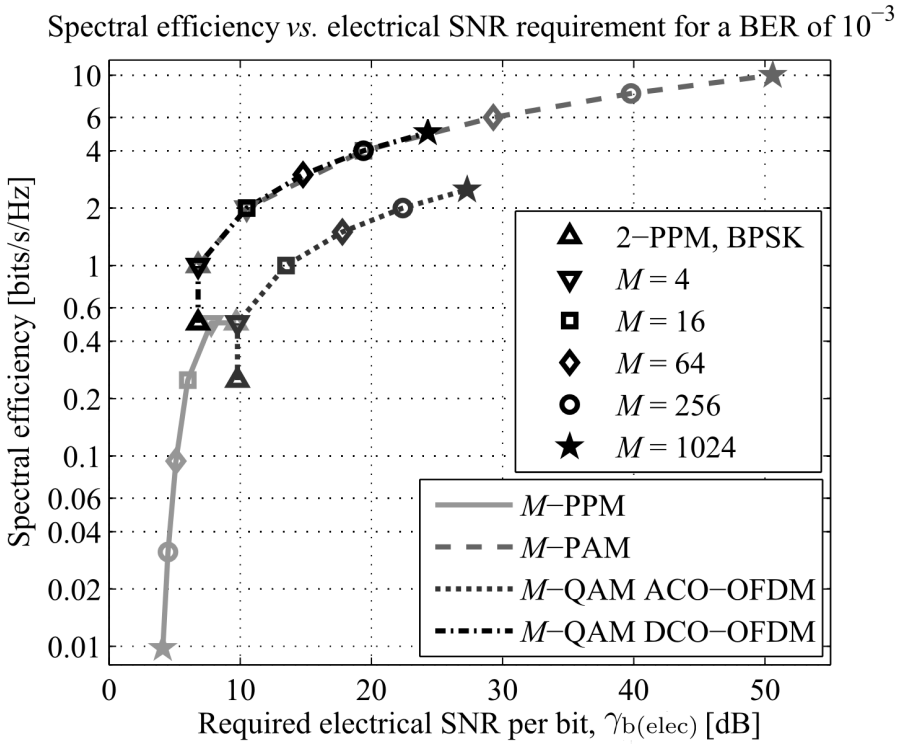


Figure 5.19: Spectral efficiency *vs.* electrical SNR requirement for a $10^{-3}$ BER of the OWC schemes in a flat fading channel with impulse response $h(t) = \delta(t)$ and neglected DC bias power.

PAM and PPM, respectively, which have distributions with finite support.

### 5.4.3 The equalizer penalty

In a practical non-flat channel with dispersion [12], the signal bandwidth becomes larger than the channel coherence bandwidth at high data rates. Therefore, the equalization process incurs an SNR penalty. In such a scenario, single-carrier transmission suffers a severe ISI. In multi-carrier transmission, a CP is employed which completely eliminates the ISI and the inter-carrier interference (ICI), and it has a negligible impact on the spectral efficiency and electrical SNR requirement [92]. It transforms the channel into a flat fading channel over the subcarrier bandwidth, and therefore single-tap equalization with bit and power loading [94, 95] can be performed, in order to minimize the channel effect. The equalizer gain factor, $G_{\mathrm{EQ}}$, can be obtained for single-carrier modulation from (3.4), (3.6), (3.7) or (3.8). In multi-carrier transmission, $G_{\mathrm{EQ}}$ is obtained from the Monte Carlo simulation of the optimum bit and power loading in the dispersive channel in conjunction with the optimum signal biasing from TABLE 5.4.

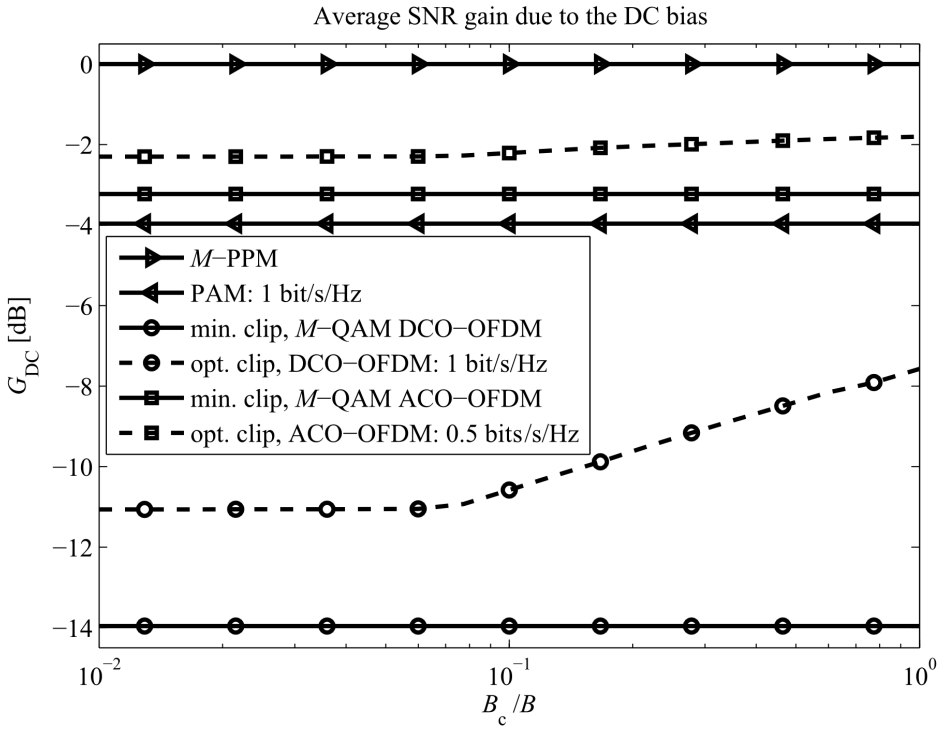


Figure 5.20: DC bias gain for signal bandwidth exceeding the channel coherence bandwidth and a 10 dB dynamic range.

Here, an electrical path gain of $g_{\mathrm{h(elec)}} = 1$ is considered for simplicity. The equalizer gain of multi-carrier transmission with bit and power loading and single-tap ZF equalizer is compared with the equalizer gain of single-carrier transmission with multi-tap ZF feed-forward equalizer (FFE) and ZF decision feedback equalizer (DFE) as the signal bandwidth grows larger than the channel coherence bandwidth. The result is presented in Fig. 5.21. It is shown that multi-carrier transmission incurs a lower SNR penalty in the equalization process.

### 5.4.4 Maximum spectral efficiency without an average optical power constraint

In order to obtain the electrical SNR requirement when the DC bias power is counted towards the signal power in a non-flat dispersive channel, the DC bias gain and the equalizer gain need to be subtracted from the electrical SNR requirement from Fig. 5.19. The result is presented in Fig. 5.22. It is shown that optimum signal clipping allows O-OFDM to close the gap to single-carrier transmission down to 2 dB in a flat fading channel when the DC bias power is included in the calculation of the SNR requirement. However, when the signal bandwidth exceeds the channel coherence bandwidth in a dispersive channel, ACO-OFDM shows a lower electrical SNR requirement as compared to PPM with both FFE and DFE. Equivalently, DCO-OFDM

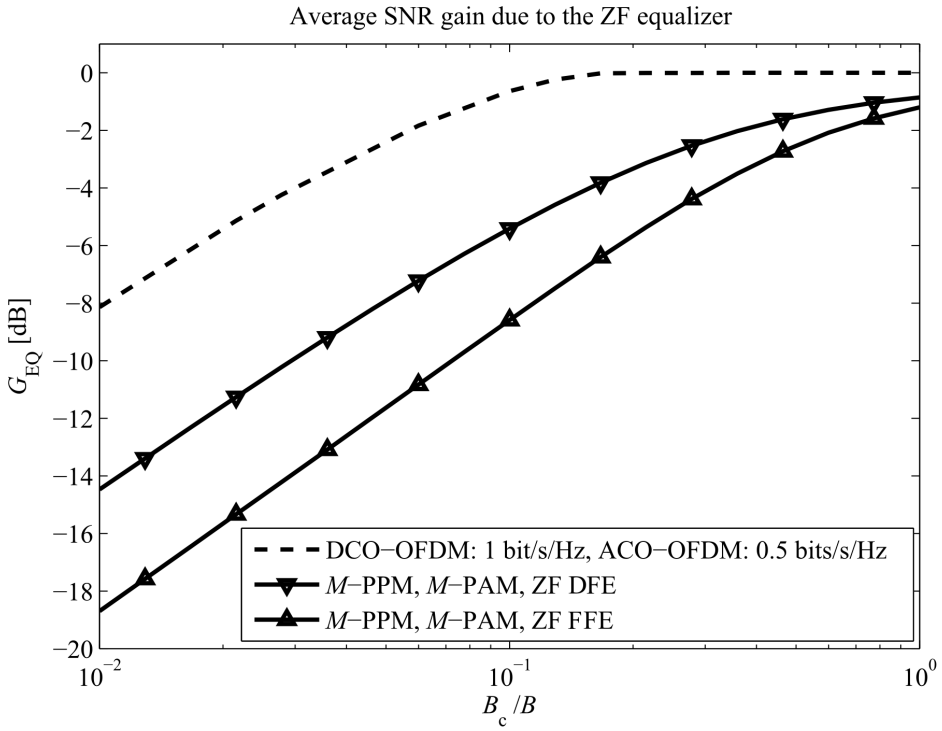


Figure 5.21: Equalizer gain for signal bandwidth exceeding the channel coherence bandwidth.

is shown to have a lower SNR requirement than PAM with FFE, and it approaches the SNR requirement of PAM with DFE.

By fixing the electrical SNR requirement, the relative performance of the systems can be obtained in terms of spectral efficiency. This is illustrated in Fig. 5.23 for $\gamma_{\mathrm{b(elec)}} = 25$ dB as the signal bandwidth exceeds the channel coherence bandwidth. When the DC power is not counted towards the electrical signal power, DCO-OFDM and ACO-OFDM show a superior spectral efficiency in the dispersive optical wireless channel as compared to PAM and PPM, respectively. When the DC power is included in the calculation of the electrical SNR, ACO-OFDM still outperforms PPM. DCO-OFDM outperforms PAM with FFE, and it approaches the performance of PAM with DFE. However, it has to be noted that the analysis of PAM with DFE represents an upper bound for the performance which is achieved when an infinite number of channel taps are considered in the equalizer. In a practical indoor optical wireless channel, where the impulse response only changes slowly, the channel taps and the required bit and power loading parameters with optimum signal shaping can be pre-computed and stored in look-up tables in memory. Therefore, the computational complexity at the receiver comes from the convolution operation of the DFE equalizer in single-carrier transmission and the FFT operation in multi-carrier transmission. It has been shown in [13] that the most efficient DFE

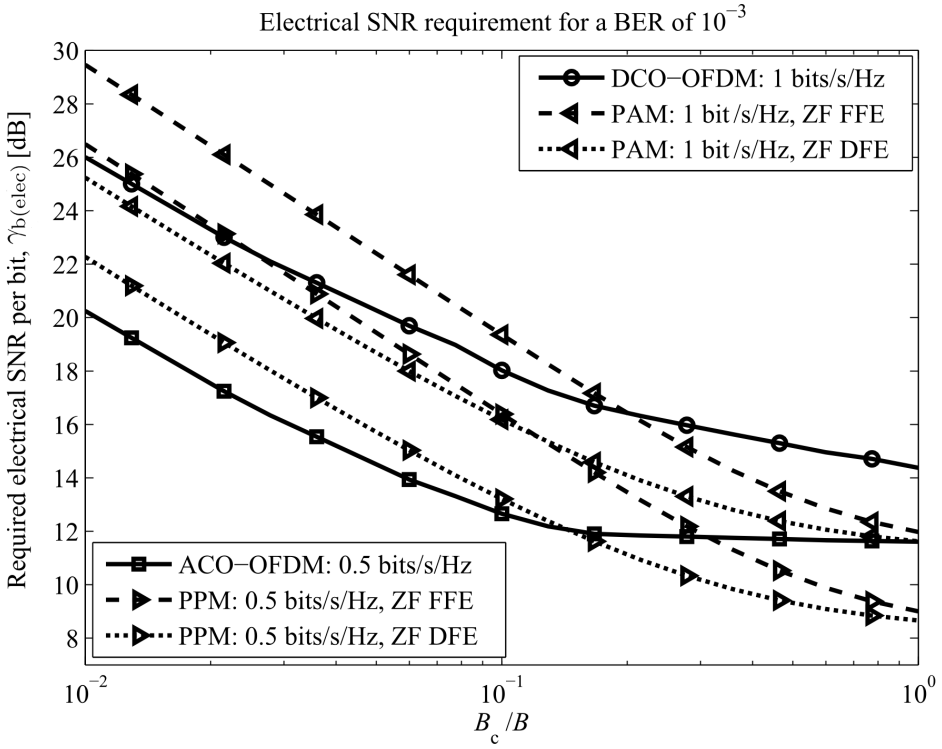


Figure 5.22: Required electrical SNR per bit for signal bandwidth exceeding the channel coherence bandwidth. The target BER is $10^{-3}$ for a 10 dB dynamic range.

implementation requires one FFT and one inverse FFT (IFFT) operation for $N$ channel taps. Therefore, for a fixed FFT size, O-OFDM is expected to require half of the computational complexity of single-carrier transmission with DFE.

## 5.5 Chapter summary

In this Chapter, the electrical SNR requirement for a target BER or information rate of the $M$-QAM O-OFDM schemes has been minimized by optimization of the biasing setup, *i.e.* signal scaling and DC bias, for a given limited positive linear dynamic range of the transmitter. In the first Section, linear dynamic ranges of 10 dB, 20 dB and 30 dB have been considered. In addition, an average optical power constraint has been imposed and varied over the entire dynamic range. Here, the additional DC bias power invested to condition the signal within the dynamic range has been included in the calculation of the electrical SNR. An optical power sweep over more than $50\%$ and $25\%$ of the dynamic range has been shown to be accommodated within an electrical SNR margin of 3 dB for DCO-OFDM and ACO-OFDM, respectively. Because of the Gaussian and half-Gaussian signal distributions, DCO-OFDM demonstrated an absolute mini-

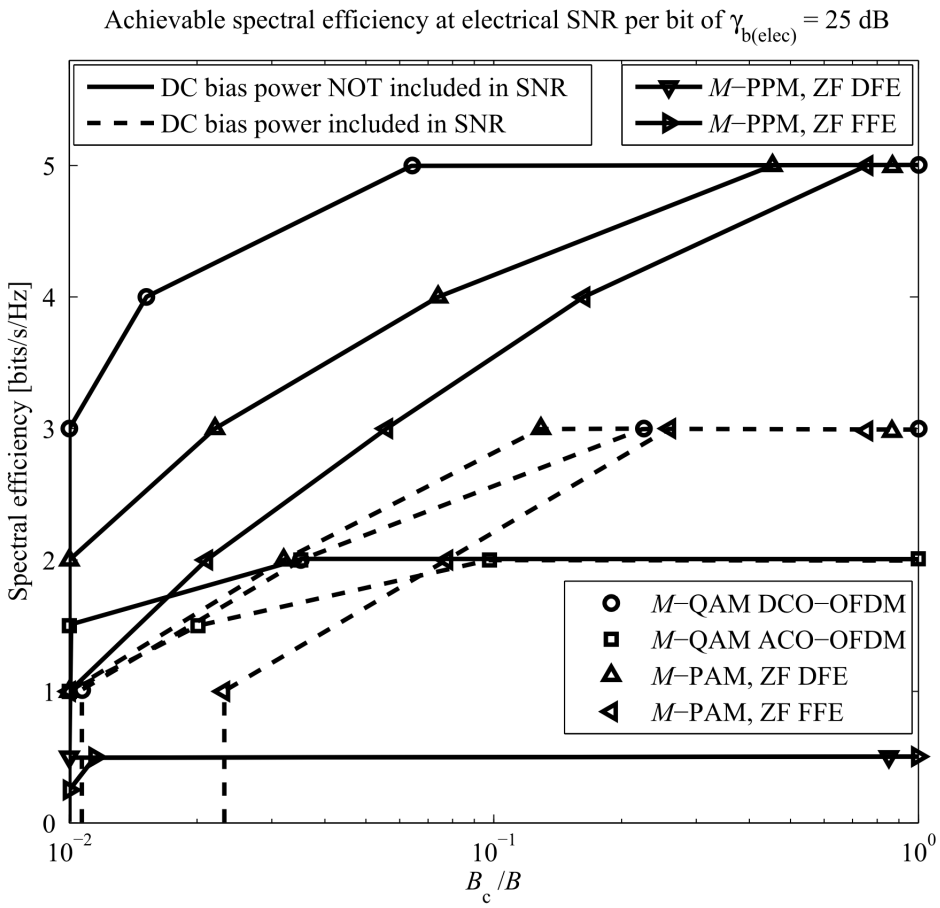


Figure 5.23: Spectral efficiency for signal bandwidth exceeding the channel coherence bandwidth. The target BER is $10^{-3}$ with an available electrical SNR per bit of $25$ dB.

mum SNR requirement towards the middle of the dynamic range, while ACO-OFDM proved to be most suitable for low optical power applications. Nonetheless, DCO-OFDM showed a lower SNR requirement for a similar spectral efficiency as compared to ACO-OFDM over more than $85\%$ of average optical power levels with the increase of the dynamic range.

In the second Section of this Chapter, the maximization of the information rate of the O-OFDM schemes has been studied within the Shannon framework under an average electrical power constraint and a limited linear dynamic range. Considering the DC bias penalty in the optimization of the biasing setup, DCO-OFDM demonstrated a superior information rate to ACO-OFDM over the majority of optical power levels with the increase of the dynamic range or the SNR target. Neglecting the DC bias penalty, DCO-OFDM has been shown to achieve the Shannon capacity with minimization of the non-linear distortion for any average optical power level, while ACO-OFDM exhibited a 3-dB gap which grows with higher information rate targets.

In the third Section of this Chapter, the spectral efficiency of $M$-QAM O-OFDM with bit and power loading has been compared with the spectral efficiency of $M$-PPM and $M$-PAM with equalization in the dispersive optical wireless channel. Here, the signal bandwidth has been increased beyond the channel coherence bandwidth. Through optimization of the biasing setup and neglecting the additional DC bias power, DCO-OFDM presented the highest spectral efficiency of all the considered modulation schemes for OWC. Including the DC bias power in the calculation of the electrical SNR, DCO-OFDM demonstrated a higher spectral efficiency than PAM with linear equalization, and it approached the performance of the more computationally intensive PAM with non-linear equalization.

# Chapter 6
# Conclusion

## 6.1 Main findings

This thesis presented a novel comprehensive analytical treatment of the performance of the intensity modulation schemes for optical wireless communication (OWC) based on orthogonal frequency division multiplexing (OFDM). A novel mathematical treatment of the non-linear distortion of the time domain OFDM signals at the transmitter front-end has been proposed. By means of pre-distortion, the effect of the non-linear transfer characteristic has been reduced to double-sided signal clipping. Thus, minimum and maximum radiated optical power constraints have been imposed by the optical front-end. In addition, an average optical power constraint has been imposed by the eye safety regulation and/or design requirements. The presented framework for non-linear distortion modeling enabled the formulation of the optimum signal biasing, *i.e.* signal scaling and direct current (DC) bias, in order to condition the signal within these constraints. The target of the optimization has been defined as minimization of the electrical signal-to-noise ratio (SNR) requirement, minimization of the bit-error ratio (BER) or maximization of the optical OFDM (O-OFDM) system information rate.

In the first part of the thesis, the analysis of the BER performance in additive white Gaussian noise (AWGN) of single-carrier modulation, such as multi-level pulse position modulation ($M$-PPM) and multi-level pulse amplitude modulation ($M$-PAM), and multi-carrier modulation, such as multi-level quadrature amplitude modulation ($M$-QAM) with DC-based O-OFDM (DCO-OFDM) and asymmetrically clipped O-OFDM (ACO-OFDM), has been presented. The optical-to-electrical (O/E) conversion of these OWC schemes has been defined for a given biasing setup within the limited linear dynamic range of the transmitter. The equalizer penalty on the electrical SNR has been included in the case a dispersive optical wireless channel, where the signal bandwidth has been increased beyond the channel coherence bandwidth. In addition, the DC bias penalty on the electrical SNR has been defined for every modulation scheme requiring additional DC bias power to condition the signals within the positive dynamic range of the transmitter.

The novel analysis of the non-linear distortion in O-OFDM, presented in the second part of the thesis, enabled the derivation of the electrical SNR at the receiver. The non-linear distortion has been translated by means of the Bussgang theorem and the central limit theorem (CLT) into attenuation of the information-carrying subcarriers plus zero-mean Gaussian uncorrelated noise. In addition, by the use of a piecewise polynomial model for the non-linear transfer function of the transmitter, the attenuation factor and the noise variance have been derived in closed form. Furthermore, this accurate and yet flexible representation of the transmitter nonlinearity enabled the signal pre-distortion, in order to linearize the dynamic range between points of minimum and maximum radiated optical power. While the single-carrier signals have been conditioned within these constraints without signal distortion, the Gaussian and half-Gaussian signals in DCO-OFDM and ACO-OFDM, respectively, have been shown to suffer a double-sided signal clipping. Practical fast Fourier transform (FFT) sizes greater than $64$, which ensure Gaussianity of the time domain O-OFDM signal, have been proven not to affect the attenuation factor and the clipping noise variance, and therefore the BER system performance. In addition, the BER performance of higher order modulation has been shown to be more severely degraded for a fixed biasing setup, and therefore optimization was required to ensure a target BER performance.

In the final part of the thesis, the maximization of the O-OFDM system spectral efficiency and information rate in AWGN has been studied under average electrical power constraint in conjunction with minimum, average and maximum optical power constraints, excluding or including the DC bias power in the calculation of the electrical SNR. Linear dynamic ranges of the transmitter of $10$ dB, $20$ dB and $30$ dB have been considered. Neglecting the additional DC bias power, DCO-OFDM has been shown to achieve the Shannon capacity for any average optical power level, while ACO-OFDM exhibited a minimum gap of $3$ dB which increased for higher information rate targets. Thus, DCO-OFDM has been proven to deliver the highest throughput in applications, where the additional DC bias power required to create a non-negative signal has been employed to serve a complementary functionality, such as illumination in visible light communication (VLC) systems. In infrared (IR) communication systems, where the DC power has been generally constrained by eye-safety regulations, and it has been included in the calculation of the electrical SNR, the optimum signal scaling and DC-biasing enabled O-OFDM to minimize the SNR penalty. In this case, a transmitter front-end with a wide linear dynamic range of $20$ dB or higher has been shown to provide sufficient electrical power to maintain OWC with optical power output close to the boundaries of the dynamic range, where the light emitting

diode (LED) appeared to be off or driven close to its maximum. In addition, an average optical power sweep over $50\%$ and $25\%$ of the dynamic range in DCO-OFDM and ACO-OFDM, respectively, has been accommodated within a mere $10\%$ reduction of information rate or within a 3-dB electrical SNR margin. DCO-OFDM has been shown to deliver the higher information rate as compared to ACO-OFDM for the majority of average optical power levels, *e.g.* more than $90\%$, with the increase of the SNR target or the dynamic range. In addition, a novel comparison has been presented between the single-carrier $M$-PPM and $M$-PAM schemes with the multi-carrier O-OFDM in terms of electrical SNR requirement and spectral efficiency in AWGN. The systems have been compared in a flat fading channel and in a dispersive channel, where the signal bandwidth has been increased beyond the channel coherence bandwidth. Equalization has been employed in single-carrier systems, in order to counter the channel effect, while bit and power loading has been considered in multi-carrier systems. Neglecting the additional DC bias power, DCO-OFDM and ACO-OFDM demonstrated a superior spectral efficiency in the dispersive optical wireless channel as compared to PAM and PPM. Including the DC bias power in the calculation of the electrical SNR, the optimum signal clipping enabled O-OFDM to reduce the SNR requirement gap to single-carrier transmission down to 2 dB in the flat fading channel, showing an improvement of $6.5$ dB and $1.4$ dB in DCO-OFDM and ACO-OFDM, respectively, as compared to a conventional minimum-distortion front-end biasing. When the signal bandwidth has been increased beyond the channel coherence bandwidth, DCO-OFDM showed a higher spectral efficiency than PAM with linear equalization, and it approached the performance of the more computationally intensive PAM with non-linear equalization.

## 6.2 Limitations of work, outlook and future work

The analytical model for the non-linear distortion caused by the optical front-end in OFDM-based OWC systems has been shown to be in very close agreement with an equivalent Monte Carlo simulation. However, there are a couple of essential assumptions which have been made for the sake of straightforward derivations. The violation of these assumptions in some system implementations is not envisioned as a fundamental limiting factor for the performance of the OWC system, although it can lead to a suboptimum biasing setup for the transmitted signal and a suboptimum system performance. The following suggestions can be considered to improve the OWC system capacity in practical single-link and multi-user implementation setups.

First, the model of the non-linear distortion at the optical front-end in OFDM-based OWC relies on the assumption that the time-domain OFDM signal follows a close to Gaussian distribution. This is achieved for a total number of subcarriers greater than $64$. However, in system implementations, where the computational resources of the electronics are limited, only a smaller number of FFT operations may be feasible for the sake of a real-time processing with a reasonable data rates. Therefore, a mathematical model is still to be derived for FFT sizes below $64$, in order to include it in the optimization of the biasing setup. Furthermore, the overhead on the information rate related to the synchronization between the transmitter and the receiver, as well as to the pulse shaping and matched filtering, is neglected in this study. Moreover, channel knowledge at the receiver and the transmitter is assumed for the purposes of equalization and bit and power loading, and the quantization noise in the digital-to-analog (D/A) and analog-to-digital (A/D) conversions is neglected. A study of the influence of these system building blocks on the front-end biasing setup can be considered in future work.

In addition, the spectral efficiency and electrical SNR requirement of single-carrier and multi-carrier modulation schemes in a flat fading channel and a dispersive channel under an average electrical power constraint and minimum, average and maximum optical power constraints have been compared in this thesis. Taking into account the total invested electrical signal power, *i.e.* alternating current (AC) and DC power, it has been shown that there is still room for improvement of the existing digital modulation formats and the detection algorithms. Even though some modulation schemes perform better in some of the studied channels, there is no absolute and unanimous favorite. Therefore, the research of novel digital modulation formats for OWC is still open for new schemes which combine the strengths sans the shortcomings of the current formats. Future work can include the improvement of the information rate in O-OFDM through iterative cancelation of the additive noise component due to the nonlinearity of the optical front-end.

Finally, the system model and the optimum front-end biasing setup are currently tailored only to a single-link OWC scenario. Capacity enhancing techniques, where multiple LEDs are employed at the transmitter and multiple photodiodes (PDs) are employed at the receiver, are still an open issue. Future work can include an investigation of the mechanisms that increase the probability of detection of the individual signals and the associated diversity techniques. Furthermore, the study of the OWC systems is to be expanded with the simulation and optimization of multiple access scenarios in a network of mobile users. Current OWC systems with intensity

modulation and direct detection (IM/DD) can hardly utilize the entire available optical spectrum. In addition, because of the fact that the center wavelength is significantly larger than the modulation bandwidth of the optical front-ends, wavelength reuse in cellular OWC systems can be performed without a reduction of capacity as opposed to radio frequency (RF) cellular systems. Therefore, a larger insight is to be gained into the maximization of the capacity of cellular OWC networks with a transition towards autonomous self-organizing interference-aware networks.

# Appendix A
# Mathematical derivations

## A.1 Generalized non-linear distortion parameters

The gain factor denoting the electrical power attenuation of an information-carrying subcarrier in O-OFDM, $K$, can be expressed in DCO-OFDM and ACO-OFDM from [27] as follows:

$$K = \frac{\mathrm{Cov}\left[s, \Psi(s)\right]}{\sigma^2} \,, \tag{A.1}$$

where $\mathrm{Cov}\left[\cdot\right]$ stands for the covariance operator. Since the OFDM symbol, $s$, is a zero mean Gaussian random variable, $K$ can be derived as follows:

$$K = \frac{\mathrm{E}\left[s\Psi(s)\right]}{\sigma^2} = \frac{1}{\sigma^2}\int_{-\infty}^{+\infty} s\Psi(s)\frac{1}{\sigma}\phi\left(\frac{s}{\sigma}\right)\, ds \,, \tag{A.2}$$

where $\mathrm{E}\left[\cdot\right]$ stands for the expectation operator. Using the structure of the normalized non-linear distortion function, $\Psi(s)$, from (4.1), the piecewise integration can be performed by the use of the general structure of the individual integrals and their solutions given in (4.5) and (4.6), respectively. Therefore, the attenuation factor of the non-linear distortion, $K$, can be generalized for DCO-OFDM and ACO-OFDM as follows:

$$\begin{aligned} K = {} & \lambda_J\phi(\lambda_J) - \lambda_1\phi(\lambda_1) \\ & + \frac{1}{\sigma^2}\sum_{j=1}^{J-1}\int_{-\infty}^{\sigma\lambda_{j+1}} s\psi_j(s)\frac{1}{\sigma}\phi\left(\frac{s}{\sigma}\right)\, ds - \frac{1}{\sigma^2}\sum_{j=1}^{J-1}\int_{-\infty}^{\sigma\lambda_j} s\psi_j(s)\frac{1}{\sigma}\phi\left(\frac{s}{\sigma}\right)\, ds \,, \end{aligned} \tag{A.3}$$

This result is given in (4.4) in Section 4.2 of Chapter 4.

In DCO-OFDM, the non-linear distortion noise component, $w_{\mathrm{clip}}$, can be expressed from (4.2). Thus, the variance of the non-linear noise, $\sigma^2_{\mathrm{clip}}$, can be derived for the generalized non-linear

distortion function, $\Psi(s)$, in DCO-OFDM as follows:

$$\begin{aligned}\sigma^2_{\text{clip}} &= \mathrm{E}\left[\big(\Psi(s)-Ks\big)^2\right] - \mathrm{E}\left[\Psi(s)-Ks\right]^2 = \mathrm{E}\left[\Psi(s)^2\right] - \mathrm{E}\left[\Psi(s)\right]^2 - K^2\sigma^2 \\ &= \int_{-\infty}^{+\infty} \Psi(s)^2 \frac{1}{\sigma}\phi\left(\frac{s}{\sigma}\right)\, ds - \left(\int_{-\infty}^{+\infty} \Psi(s)\frac{1}{\sigma}\phi\left(\frac{s}{\sigma}\right)\, ds\right)^2 - K^2\sigma^2 \,.\end{aligned} \tag{A.4}$$

Using (4.1), (4.5) and (4.6), the variance of the non-linear distortion noise, $\sigma^2_{\text{clip}}$, can be generalized for DCO-OFDM as follows:

$$\begin{aligned}\sigma^2_{\text{clip}} = \sigma^2\lambda_1^2\big(1-Q(\lambda_1)\big) + \sigma^2\lambda_J^2 Q(\lambda_J) - K^2\sigma^2 + \sum_{j=1}^{J-1}\int_{-\infty}^{\sigma\lambda_{j+1}} \psi_j(s)^2\frac{1}{\sigma}\phi\left(\frac{s}{\sigma}\right)\, ds \\ - \sum_{j=1}^{J-1}\int_{-\infty}^{\sigma\lambda_j} \psi_j(s)^2\frac{1}{\sigma}\phi\left(\frac{s}{\sigma}\right)\, ds - \Big(\sigma\lambda_1\big(1-Q(\lambda_1)\big) + \sigma\lambda_J Q(\lambda_J)\Big) \\ + \sum_{j=1}^{J-1}\int_{-\infty}^{\sigma\lambda_{j+1}} \psi_j(s)\frac{1}{\sigma}\phi\left(\frac{s}{\sigma}\right)\, ds - \sum_{j=1}^{J-1}\int_{-\infty}^{\sigma\lambda_j} \psi_j(s)\frac{1}{\sigma}\phi\left(\frac{s}{\sigma}\right)\, ds\Big)^2 \,.\end{aligned} \tag{A.5}$$

This result is given in (4.7) in Section 4.2 of Chapter 4.

In order to derive the variance of the non-linear noise component in ACO-OFDM, the half-Gaussian distribution of $s$ is unfolded as elaborated in Section 4.3 of Chapter 4 and illustrated in Fig. 4.5. The resulting unfolded symbol, $\hat{s}$, follows a zero-mean real-valued Gaussian distribution with a variance of $\sigma^2/2$. The corresponding unfolded non-linear distortion function, $\hat{\Psi}(\hat{s})$, is symmetric with respect to the origin, and it can be written as follows:

$$\hat{\Psi}(\hat{s}) = \begin{cases} \Psi\left(s/\sqrt{2}\right) & \text{if } \hat{s} \geq 0 \,, \\ \Psi\left(-s/\sqrt{2}\right) & \text{if } \hat{s} < 0 \,. \end{cases} \tag{A.6}$$

The unfolded signal, $\hat{s}$, has a bias of $-\sigma\lambda_1/\sqrt{2}$ on the negative samples and a bias of $\sigma\lambda_1/\sqrt{2}$ on the positive ones. Since these biases are to be mounted on the first subcarrier in the ACO-OFDM frame after the fast Fourier transformation (FFT) block at the receiver, they are irrelevant to the non-linear noise variance on the data-carrying subcarriers. Therefore, these biases are removed as follows:

$$\bar{s} = \begin{cases} \hat{s} - \sigma\lambda_1/\sqrt{2} & \text{if } \hat{s} \geq 0 \,, \\ \hat{s} + \sigma\lambda_1/\sqrt{2} & \text{if } \hat{s} < 0 \,. \end{cases} \tag{A.7}$$

As a result, the variance of the non-linear noise component, $\sigma^2_{\text{clip}}$, can be derived for the generalized non-linear distortion function, $\Psi(s)$, in ACO-OFDM from (4.3) as follows:

$$\begin{aligned}\sigma^2_{\text{clip}} &= \mathrm{E}\left[\left(\hat{\Psi}(\bar{s}) - 2K\hat{s}\right)^2\right] - \mathrm{E}\left[\hat{\Psi}(\bar{s}) - 2K\hat{s}\right]^2 \\ &= \mathrm{E}\left[\hat{\Psi}(\bar{s})^2\right] - 4K\mathrm{E}\left[\hat{\Psi}(\bar{s})\hat{s}\right] + 4K^2\mathrm{E}\left[\hat{s}^2\right] \\ &\quad -\mathrm{E}\left[\hat{\Psi}(\bar{s})\right]^2 + 4K\mathrm{E}\left[\hat{\Psi}(\bar{s})\right]\mathrm{E}\left[\hat{s}\right] - 4K^2\mathrm{E}\left[\hat{s}\right]^2 \ .\end{aligned} \tag{A.8}$$

Given that $\mathrm{E}\left[\hat{s}\right] = 0$, $\mathrm{E}\left[\hat{\Psi}(\bar{s})\right] = 0$, $\mathrm{E}\left[\hat{\Psi}(\bar{s})\hat{s}\right] = K\sigma^2$ and $\mathrm{E}\left[\hat{\Psi}(\bar{s})^2\right] = \mathrm{E}\left[\Psi(s-\sigma\lambda_1)^2\right]$, $\sigma^2_{\text{clip}}$ can be expressed in ACO-OFDM as follows:

$$\sigma^2_{\text{clip}} = \mathrm{E}\left[\Psi(s-\sigma\lambda_1)^2\right] - 2K^2\sigma^2 = \int_{-\infty}^{+\infty} \Psi(s-\sigma\lambda_1)^2 \frac{1}{\sigma}\phi\left(\frac{s}{\sigma}\right)\, ds - 2K^2\sigma^2 \ . \tag{A.9}$$

Using (4.1), (4.5) and (4.6), the variance of the non-linear distortion noise, $\sigma^2_{\text{clip}}$, can be generalized for ACO-OFDM as follows:

$$\begin{aligned}\sigma^2_{\text{clip}} = \sigma^2(\lambda_J - \lambda_1)^2 Q(\lambda_J) - 2K^2\sigma^2 &+ \sum_{j=1}^{J-1} \int_{-\infty}^{\sigma\lambda_{j+1}} \psi_j(s-\sigma\lambda_1)^2 \frac{1}{\sigma}\phi\left(\frac{s}{\sigma}\right)\, ds \\ &- \sum_{j=1}^{J-1} \int_{-\infty}^{\sigma\lambda_j} \psi_j(s-\sigma\lambda_1)^2 \frac{1}{\sigma}\phi\left(\frac{s}{\sigma}\right)\, ds \ .\end{aligned} \tag{A.10}$$

This result is given in (4.8) in Section 4.2 of Chapter 4.

## A.2 Double-sided signal clipping distortion parameters

The non-linear transfer function of the optical front-end is given in (4.10) for the case of double-sided signal clipping after pre-distortion in O-OFDM. Therefore, the normalized non-linear distortion function, $\Psi(s)$, can be expressed as follows:

$$\Psi(s) = \begin{cases} \sigma\lambda_{\text{bottom}} & \text{if } s \leq \sigma\lambda_{\text{bottom}}, \\ s & \text{if } \sigma\lambda_{\text{bottom}} < s \leq \sigma\lambda_{\text{top}}, \\ \sigma\lambda_{\text{top}} & \text{if } s > \sigma\lambda_{\text{top}}. \end{cases} \tag{A.11}$$

In DCO-OFDM and ACO-OFDM, the attenuation factor of the information-carrying subcarriers, $K$, can be expressed from (A.2) and (A.3) using (4.5) and (4.6) as follows:

$$\begin{aligned} K &= \lambda_{\text{top}}\phi(\lambda_{\text{top}}) - \lambda_{\text{bottom}}\phi(\lambda_{\text{bottom}}) \\ &\quad + \frac{1}{\sigma^2}\int_{-\infty}^{\sigma\lambda_{\text{top}}} s^2 \frac{1}{\sigma}\phi\left(\frac{s}{\sigma}\right) ds - \frac{1}{\sigma^2}\int_{-\infty}^{\sigma\lambda_{\text{bottom}}} s^2 \frac{1}{\sigma}\phi\left(\frac{s}{\sigma}\right) ds \\ &= Q(\lambda_{\text{bottom}}) - Q(\lambda_{\text{top}}) \, . \end{aligned} \tag{A.12}$$

This result is given in (4.11) in Section 4.3 of Chapter 4.

In DCO-OFDM, the clipping noise variance, $\sigma^2_{\text{clip}}$, can be derived for the normalized non-linear distortion function of double-sided signal clipping from (A.11) by the use of (A.4) and (A.5). Here, the integrals for $\mathrm{E}\left[\Psi(s)^2\right]$ and $\mathrm{E}\left[\Psi(s)\right]$ can be solved by means of (4.5) and (4.6) for (A.11) as follows:

$$\begin{aligned} \mathrm{E}\left[\Psi(s)^2\right] = P_{\text{s(elec)}}\Big(&K + \phi(\lambda_{\text{bottom}})\lambda_{\text{bottom}} - \phi(\lambda_{\text{top}})\lambda_{\text{top}} \\ &+\big(1 - Q(\lambda_{\text{bottom}})\big)\lambda^2_{\text{bottom}} + Q(\lambda_{\text{top}})\lambda^2_{\text{top}}\Big) \, , \end{aligned} \tag{A.13}$$

$$\mathrm{E}\left[\Psi(s)\right] = \sqrt{P_{\text{s(elec)}}}\Big(\phi(\lambda_{\text{bottom}}) - \phi(\lambda_{\text{top}}) + \big(1 - Q(\lambda_{\text{bottom}})\big)\lambda_{\text{bottom}} + Q(\lambda_{\text{top}})\lambda_{\text{top}}\Big) \, . \tag{A.14}$$

As a result, the clipping noise variance, $\sigma^2_{\text{clip}}$, in DCO-OFDM can be expressed as follows:

$$\begin{aligned} \sigma^2_{\text{clip}} = P_{\text{s(elec)}}\Big(&K - K^2 + (1 - Q(\lambda_{\text{bottom}}))\lambda^2_{\text{bottom}} + Q(\lambda_{\text{top}})\lambda^2_{\text{top}} \\ &-\big(\phi(\lambda_{\text{bottom}}) - \phi(\lambda_{\text{top}}) + (1 - Q(\lambda_{\text{bottom}}))\lambda_{\text{bottom}} + Q(\lambda_{\text{top}})\lambda_{\text{top}}\big)^2 \\ &+\phi(\lambda_{\text{bottom}})\lambda_{\text{bottom}} - \phi(\lambda_{\text{top}})\lambda_{\text{top}}\Big) \, . \end{aligned} \tag{A.15}$$

This result is given in (4.12) in Section 4.3 of Chapter 4.

In ACO-OFDM, the clipping noise variance, $\sigma^2_{\text{clip}}$, can be derived for the normalized non-linear distortion function of double-sided signal clipping from (A.11) by the use of (A.9) and (A.10). Here, the integral for $\mathrm{E}\left[\Psi(s - \sigma\lambda_{\text{bottom}})^2\right]$ can be solved by means of (4.5)

and (4.6) for (A.11) as follows:

$$\mathrm{E}\left[\Psi(s-\sigma\lambda_{\mathrm{bottom}})^2\right] = P_{\mathrm{s(elec)}}\Big(K\big(\lambda_{\mathrm{bottom}}^2+1\big)+Q(\lambda_{\mathrm{top}})\big(\lambda_{\mathrm{top}}-\lambda_{\mathrm{bottom}}\big)^2 \\ +2\phi(\lambda_{\mathrm{top}})\lambda_{\mathrm{bottom}}-\phi(\lambda_{\mathrm{top}})\lambda_{\mathrm{top}}-\phi(\lambda_{\mathrm{bottom}})\lambda_{\mathrm{bottom}}\Big)\,. \tag{A.16}$$

As a result, the clipping noise variance, $\sigma_{\mathrm{clip}}^2$, in ACO-OFDM can be expressed as follows:

$$\sigma_{\mathrm{clip}}^2 = P_{\mathrm{s(elec)}}\Big(K\big(\lambda_{\mathrm{bottom}}^2+1\big)-2K^2-\lambda_{\mathrm{bottom}}\big(\phi(\lambda_{\mathrm{bottom}})-\phi(\lambda_{\mathrm{top}})\big) \\ -\phi(\lambda_{\mathrm{top}})\big(\lambda_{\mathrm{top}}-\lambda_{\mathrm{bottom}}\big)+Q(\lambda_{\mathrm{top}})\big(\lambda_{\mathrm{top}}-\lambda_{\mathrm{bottom}}\big)^2\Big)\,. \tag{A.17}$$

This result is given in (4.13) in Section 4.3 of Chapter 4.

# Appendix B
# Publications

## B.1 Journal papers

S. Dimitrov, S. Sinanovic, and H. Haas, Clipping Noise in OFDM-based Optical Wireless Communication Systems, *IEEE Transactions on Communications (IEEE TCOM)*, vol. 60, pp. 1072-1081, Apr. 2012.

S. Dimitrov, S. Sinanovic, and H. Haas, Signal Shaping and Modulation for Optical Wireless Communication, *IEEE/OSA Journal on Lightwave Technology (IEEE/OSA JLT)*, vol. 30, pp. 1319-1328, May 2012.

## B.2 Conference papers

S. Dimitrov and H. Haas, On the Clipping Noise in an ACO-OFDM Optical Wireless Communication System, in *Proc. of IEEE Global Communications Conference (IEEE GLOBECOM 2010)*, Miami, Florida, USA, 6-10 Dec. 2010.

S. Dimitrov, H. Haas, M. Cappitelli, and M. Olbert, On the Throughput of an OFDM-based Cellular Optical Wireless System for an Aircraft Cabin, in *Proc. of European Conference on Antennas and Propagation (EuCAP 2011)*, Rome, Italy, 11-15 Apr. 2011. Invited Paper.

S. Dimitrov, S. Sinanovic, and H. Haas, Double-sided Signal Clipping in ACO-OFDM Wireless Communication Systems, in *Proc. of IEEE International Conference on Communications (IEEE ICC 2011)*, Kyoto, Japan, 5-9 June 2011.

S. Dimitrov, S. Sinanovic, and H. Haas, A Comparison of OFDM-based Modulation Schemes for OWC with Clipping Distortion, in *Proc. of the 2nd Optical Wireless Communications (OWC) Workshop in conjunction with IEEE Global Telecommunications Conference (IEEE GLOBECOM 2011)*, Houston, Texas, USA, 5-9 Dec. 2011.

S. Dimitrov and H. Haas, Optimum Signal Shaping in OFDM-based Optical Wireless Communication Systems, in *Proc. of the IEEE Vehicular Technology Conference (IEEE VTC Fall)*, Quebec City, Canada, Sept. 3-6 2012.

1072 IEEE TRANSACTIONS ON COMMUNICATIONS, VOL. 60, NO. 4, APRIL 2012

# Clipping Noise in OFDM-Based Optical Wireless Communication Systems

Svilen Dimitrov, *Student Member, IEEE,* Sinan Sinanovic, *Member, IEEE,* and Harald Haas, *Member, IEEE*

***Abstract*—In this paper, the impact of clipping noise on optical wireless communication (OWC) systems employing orthogonal frequency division multiplexing (OFDM) is investigated. The two existing optical OFDM (O-OFDM) transmission schemes, asymmetrically clipped optical OFDM (ACO-OFDM) and direct-current-biased optical OFDM (DCO-OFDM), are studied. Time domain signal clipping generally results from direct current (DC) biasing and/or from physical limitations of the transmitter front-end. These include insufficient forward biasing and the maximum power driving limit of the emitter. The clipping noise can be modeled according to the Bussgang theorem and the central limit theorem (CLT) as attenuation of the data-carrying subcarriers at the receiver and addition of zero-mean complex-valued Gaussian noise. Analytical expressions for the attenuation factor and the clipping noise variance are determined in closed-form and employed in the derivation of the electrical signal-to-noise ratio (SNR). The validity of the model is verified through a Monte Carlo bit-error ratio (BER) simulation. Finally, the BER performance of ACO-OFDM with DCO-OFDM is compared for different clipping levels and multi-level quadrature amplitude modulation ($M$-QAM) schemes.**

***Index Terms*—Wireless communication, optical devices, OFDM, Gaussian processes, non-linear distortion.**

## I. Introduction

With the advent of incoherent high-power light emitting diodes (LEDs) and highly sensitive photodiodes (PDs), OWC has become a viable candidate for medium range indoor data transmission [1]. As opposed to a radio frequency (RF) system, where the data-carrying signal modulates the electric field radiated by an antenna, in an OWC system the signal modulates the intensity of the optical emitter. Pulsed modulation schemes such as pulse position modulation (PPM), pulse width modulation (PWM) or pulse amplitude modulation (PAM) are often used in OWC systems with intensity modulation and direct detection (IM/DD) [2, 3]. However, the time dispersion of the optical wireless channel in an indoor setup is a major throughput limiting factor for these modulation schemes because of the severe inter-symbol interference (ISI) at high data rates.

A well known modulation technique with an inherent robustness to multi-path dispersion is the OFDM transmission scheme [1, 4]. In O-OFDM, the time domain signal envelope is utilized to modulate the intensity of the LED [4]. For this purpose, the signal needs to be real and non-negative. A real-valued time domain signal is obtained when Hermitian symmetry is imposed on the OFDM subcarriers. One approach to obtain a non-negative signal, known as DCO-OFDM, is the addition of a DC bias [5]. A closely related technique, the discrete multi-tone (DMT) modulation, has been employed for digital subscriber line (DSL) data transmission [6]. Another approach, known as ACO-OFDM, is proposed by Armstrong *et al.* [7–9]. In comparison to DCO-OFDM, ACO-OFDM achieves an increase in the optical power efficiency at the expense of a $50\%$ reduction in spectral efficiency. By enabling the odd subcarriers for data transmission and setting the even ones to zero, the negative part of the time domain signal can be clipped at the transmitter without any information loss. The information can be still successfully decoded from the odd subcarriers at the receiver.

Imperfections of the optical front-ends due to the use of off-the-shelf components result in a non-linear distortion of the transmitted signal such as non-linear transfer effects or signal clipping. An OFDM system employs the inverse fast Fourier transform (IFFT) as a multiplexing technique at the transmitter. Therefore, the non-distorted time domain signal follows a close to Gaussian distribution for large IFFT sizes according to the CLT [10]. A total subcarrier number as small as $64$ is sufficient to ensure Gaussianity [11]. As a result, the non-linear distortion can be modeled by means of the Bussgang theorem [12] as an attenuation of the data-carrying signal plus a non-Gaussian uncorrelated clipping noise component [11, 13, 14]. At the receiver, the fast Fourier transform (FFT) is used for demultiplexing. Therefore, the CLT can be applied again, and the clipping noise component can be modeled as a Gaussian process. This methodology is used in [11], where the non-linear transfer effects due to the short dynamic range of high-power amplifiers (HPA) in OFDM-based RF systems are studied. In OWC, the non-linear transfer characteristic of the LED can be compensated by pre-distortion [15]. Symmetric signal clipping due to the large peak-to-average-power ratio (PAPR) in RF OFDM is studied in [16, 17]. Equivalently, symmetric signal clipping in optical OFDM, *e.g.* DMT for DSL transmission, is investigated in [13, 14, 18]. An optimal DC bias of a symmetrically clipped signal can be inferred from [19]. In a previous study [20], bottom level single-sided time domain signal clipping in ACO-OFDM is investigated and the clipping noise statistics are derived in a semi-analytical fashion. However, in OWC the time domain signal is likely to be clipped double-sidedly, *i.e.* to have downside and upside clipping, because of insufficient

Paper approved by W. Shieh, the Editor for Optical Transmission and Switching of the IEEE Communications Society. Manuscript received September 6, 2010; revised March 21, 2011 and July 28, 2011.

This work was presented in part at the *IEEE International Communications Conference ICC 2011*, Kyoto, Japan and at the *IEEE Global Communications Conference GLOBECOM 2011*, Houston, Texas, USA.

The authors are with the University of Edinburgh, Institute for Digital Communications, Joint Research Institute for Signal and Image Processing, Edinburgh EH9 3JL, UK (e-mail: {s.dimitrov, s.sinanovic, h.haas}@ed.ac.uk).

Digital Object Identifier 10.1109/TCOMM.2012.022712.100493

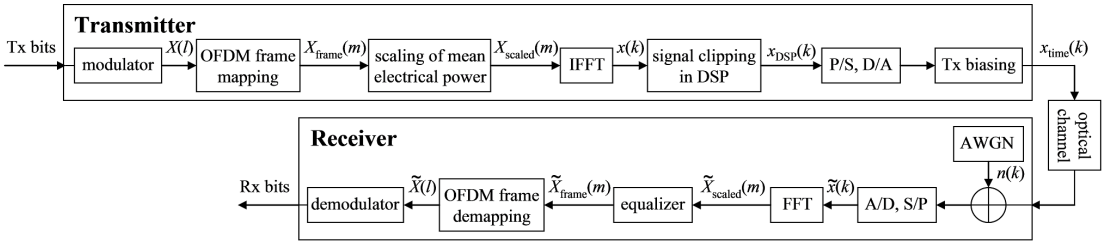


Fig. 1. Block diagram of the OFDM-based OWC system.

forward biasing and the maximum power driving limit of the transmitter front-end. Since, in addition, the eye safety regulations [21] constrain the level of radiated average optical power, the real-valued Gaussian time domain signal in OFDM-based OWC systems is likely to be clipped at independent bottom and top levels.

In this paper, double-sided time domain signal clipping at the transmitter front-end is studied for ACO-OFDM and DCO-OFDM. The attenuation factor and the variance of the complex-valued Gaussian clipping noise at the received data-carrying subcarriers are determined in closed-form and included in the derivation of the electrical SNR. The theoretical BER performance of clipped ACO-OFDM and DCO-OFDM is verified through a Monte Carlo simulation for different clipping levels. Finally, the impact of the clipping distortion on higher order modulation and higher IFFT/FFT sizes is discussed. As a result, the developed framework for signal shaping and biasing in ACO-OFDM and DCO-OFDM can be used to translate the signal scaling and DC biasing for a given dynamic range of the emitter into electrical SNR, and therefore, to BER performance.

The rest of the paper is organized as follows. Section II presents the model of the OFDM-based OWC system. Section III explains the derivation of the clipping noise statistics and the electrical SNR. BER performance results are discussed in Section IV. Finally, Section V concludes the paper.

## II. OFDM-BASED OWC SYSTEM MODEL

The system model considered in this study is illustrated in Fig. 1. For simplicity, subscripts indicating the ACO-OFDM and DCO-OFDM signals are omitted in this paper, but they can be clearly inferred from the context. First, the input bit stream at the transmitter is mapped to complex symbols, $X(l)$, according to the chosen modulation scheme, *e.g.* $M$-QAM. For an IFFT/FFT of size $N$, $N$ subcarriers form an OFDM frame, $X_{\mathrm{frame}}(m)$, $m = 0, ..., N-1$. The two existing multi-carrier optical wireless transmission schemes, ACO-OFDM and DCO-OFDM, utilize a different frame structure. In ACO-OFDM, $N/4$ symbols in $X(l)$, $l = 0, ..., N/4-1$, are mapped onto half of the odd subcarriers, $X_{\mathrm{frame}}(m)$, $m = 1, 3, 5, ..., N/2-1$, whereas the even subcarriers are set to zero. In DCO-OFDM, $N/2-1$ symbols in $X(l)$, $l = 0, ..., N/2-2$, modulate the first half of $X_{\mathrm{frame}}(m)$ leaving the first subcarrier set to zero, *i.e* $m = 1, ..., N/2-1$. In both systems, Hermitian symmetry of the subcarriers is imposed on the second half of the OFDM frame, $X_{\mathrm{frame}}(m)$, $m = N/2, ..., N-1$, in order to ensure a real-valued time domain signal, $x(k)$, $k = 0, ..., N-1$, at the expense of $50\%$ reduction in spectral efficiency. Here, the utilization factor for the double-sided bandwidth $B$ of the OFDM frame is denoted by $G_{\mathrm{B}}$, where $G_{\mathrm{B}} = 0.5$ in ACO-OFDM and $G_{\mathrm{B}} = (N-2)/N$ in DCO-OFDM. Note that because of the different frame structure of ACO-OFDM and DCO-OFDM $x(k)$ has different statistics which are discussed in the next paragraph. In general, in the OFDM framework there exists the flexibility to employ QAM symbols from different modulation orders, $M$, across the OFDM frame. Square $M$-QAM constellations, *e.g.* $\{4\mathrm{-QAM}, 16\mathrm{-QAM}, 64\mathrm{-QAM}, ...\}$, are considered. The $G_{\mathrm{B}}N$ $M$-QAM symbols on the enabled subcarriers have an average electrical power of $P_{\mathrm{s(elec)}} = P_{\mathrm{b(elec)}} \log_2(M)$, where $P_{\mathrm{b(elec)}}$ is the average electrical power of $G_{\mathrm{B}}N$ bits. Because of the fact that the clipping noise is added equally to each symbol in the OFDM frame, irrespectively of the modulation order [11], and for the sake of simplicity, in this study the same modulation order, $M$, is chosen for the symbols in the OFDM frame.

Conventionally, in OWC the average optical power of the transmitted signal, $x_{\mathrm{time}}(k)$, is defined in the time domain as $\mathrm{E}\left[x_{\mathrm{time}}(k)\right]$. Here, $\mathrm{E}[\cdot]$ stands for the expectation operator. The average electrical power of the signal, however, is defined in the frequency domain as $\mathrm{E}\left[|X_{\mathrm{frame}}(m)|^2\right]$. According to [8], the mean electrical signal power is proportional to the variance of $x(k)$, $\sigma^2_{x(k)}$. Therefore, in order to fix a certain electrical SNR, $\sigma^2_{x(k)}$ needs to be specified accordingly. For this purpose, the subcarriers at the transmitter require a pre-scaling by a factor, $\alpha$, to obtain $X_{\mathrm{scaled}}(m)$. Following the Parseval theorem and using an unbiased estimator for the variance of $x(k)$, the factor, $\alpha$, is expressed as follows:

$$\alpha = \sigma_{x(k)} \sqrt{\frac{N-1}{\sum_{m=0}^{N-1} |X_{\mathrm{frame}}(m)|^2}}. \tag{1}$$

For practical IFFT/FFT sizes, *i.e.* $N > 64$, $\mathrm{E}\left[\alpha^2\right]$ can be simplified to $\mathrm{E}\left[\alpha^2\right] = \sigma^2_{x(k)}/G_{\mathrm{B}}$. Before the scaling clock, the average electrical power of the enabled subcarriers, $X_{\mathrm{frame,info}}(m)$, amounts to $P_{\mathrm{s(elec)}} = P_{\mathrm{b(elec)}} \log_2(M) = 1$. Therefore, a time domain signal, $x(k)$, with a variance of $\sigma^2_{x(k)}$ is obtained when the power of the enabled subcarriers is scaled to $P_{\mathrm{s(elec)}}/G_{\mathrm{B}}$, where $P_{\mathrm{s(elec)}} = \sigma^2_{x(k)}$. As a result, the average bit energy, $E_{\mathrm{b(elec)}}$, can be expressed as follows: $E_{\mathrm{b(elec)}} = \sigma^2_{x(k)} / \left(\log_2(M) G_{\mathrm{B}} B\right)$.

Next, the scaled subcarriers are passed through an IFFT block. Without loss of generality, the unitary transform is employed [9]:

$$x(k) = \frac{1}{\sqrt{N}} \sum_{m=0}^{N-1} X_{\text{scaled}}(m) \exp\left(\frac{j2\pi km}{N}\right). \quad (2)$$

In general, a cyclic prefix (CP) is included in OFDM-based systems to combat ISI and inter-carrier interference (ICI). In addition, the CP transforms the dispersive optical wireless channel into a flat fading channel over the subcarrier bandwidth [9]. However, in OWC the CP is shown to have a negligible impact on the electrical SNR requirement and the spectral efficiency [22]. Therefore, for simplicity, it is omitted in the derivations in this study.

In order to efficiently utilize the dynamic range of the digital-to-analog (D/A) converter, any structure-specific signal clipping needs to be performed in the digital signal processor (DSP). Moreover, in order to facilitate a power efficient D/A conversion, further DC biasing is performed in the analog circuitry. Therefore, the constraints imposed by the emitter front-end need to be pre-set in the DSP signal shaping block which results in signal pre-clipping. In general, the LED is biased by a constant current source which supports the entire range of forward voltages across the LED. The bias current is added to the data-carrying current, yielding the forward current through the LED. Since the radiated optical power is directly proportional to the forward current, the signal and the constraints imposed by the transmitter front-end are described in terms of optical power in the rest of the paper. It is shown in [15] that the non-linear $I$-$V$ characteristic of the LED can be compensated by pre-distortion. A linear characteristic is obtainable, however, only over a limited range between $i_{\min}$ and $i_{\max}$. Therefore, in this paper, a linear dynamic range of the LED is assumed between a corresponding point of minimum optical power, $P_{\text{Tx,min}}$, and a point of maximum optical power, $P_{\text{Tx,max}}$. The amount of optical power needed to bias the time domain signal is denoted as $P_{\text{Tx,bias}}$.

Because of the time domain signal structure in ACO-OFDM and DCO-OFDM, different combinations of front-end biasing parameters, *i.e.* $\sigma_{x(k)}$ and $P_{\text{Tx,bias}}$, are chosen for a particular linear dynamic range, $P_{\text{Tx,min}}$ to $P_{\text{Tx,max}}$. Therefore, in the two systems the time domain signal, $x(k)$, is pre-clipped at different bottom and top levels, $\varepsilon_{\text{bottom}}$ and $\varepsilon_{\text{top}}$. In ACO-OFDM, in the case of insufficient forward biasing, *i.e.* $P_{\text{Tx,bias}} < P_{\text{Tx,min}}$, the signal is pre-clipped at a positive bottom level defined as $\varepsilon_{\text{bottom}} = P_{\text{Tx,min}} - P_{\text{Tx,bias}}$. In the opposite case, *i.e.* $P_{\text{Tx,bias}} \geq P_{\text{Tx,min}}$, $\varepsilon_{\text{bottom}}$ is kept at zero, in order to facilitate the structure-specific asymmetric zero-level signal clipping in ACO-OFDM. Therefore, $\varepsilon_{\text{bottom}} = \max\Big(P_{\text{Tx,min}} - P_{\text{Tx,bias}}, 0\Big)$. In addition, the signal is pre-clipped at a top level, $\varepsilon_{\text{top}} = P_{\text{Tx,max}} - P_{\text{Tx,bias}}$. Since the plausible clipping levels satisfy the inequality $\varepsilon_{\text{bottom}} < \varepsilon_{\text{top}}$, the clipping levels in ACO-OFDM assume only non-negative values. Here, the scenario with the least signal clipping is defined as: $\varepsilon_{\text{bottom}} = 0$ and $\varepsilon_{\text{top}} = +\infty$. In DCO-OFDM, in the case of insufficient forward biasing, *i.e.* $P_{\text{Tx,bias}} < P_{\text{Tx,min}}$, the signal is pre-clipped at a bottom level $\varepsilon_{\text{bottom}} = P_{\text{Tx,min}} - P_{\text{Tx,bias}}$. Moreover, the signal is pre-clipped at a top level, $\varepsilon_{\text{top}} = P_{\text{Tx,max}} - P_{\text{Tx,bias}}$. In DCO-OFDM, the clipping levels can be negative and/or positive as long as the inequality $\varepsilon_{\text{bottom}} < \varepsilon_{\text{top}}$ is satisfied for reasons of plausibility. Here, the scenario with the least signal clipping is defined as: $\varepsilon_{\text{bottom}} = -\infty$ and $\varepsilon_{\text{top}} = +\infty$. As a result of the signal pre-clipping in the DSP, the discrete signal $x_{\text{DSP}}(k)$ is obtained. After parallel-to-serial (P/S) and D/A conversion and addition of the biasing optical power, $P_{\text{Tx,bias}}$, the signal is passed to the optical emitter. In both systems, the DC bias is employed to facilitate the minimum signal clipping. While the unipolar ACO-OFDM signal requires the DC bias only to overcome the minimum required optical power, $P_{\text{Tx,min}}$, the bipolar DCO-OFDM needs a larger DC bias, in order to have its mean placed in the middle of the dynamic range, ensuring minimum bottom and top level clipping [6]. Biasing of both ACO-OFDM and DCO-OFDM time domain signals reveals the trade-off between downside and upside clipping distortion which is discussed in the following Section III. Particular examples for signal biasing are discussed in Section IV. Furthermore, it is important to mention that the addition of the DC bias influences the useful electrical power of the biased time domain signal, $x_{\text{time}}(k) = x_{\text{DSP}}(k) + P_{\text{Tx,bias}}$, to be transmitted. The total electrical power, $\mathrm{E}\left[x_{\text{time}}(k)^2\right]$, is a summation of the useful electrical alternating current (AC) power and the electrical DC power. Therefore, for a fixed total electrical power, the addition of the DC bias reduces the useful electrical AC power of the signal. The attenuation factor, $G_{\text{DC}}$, for the useful electrical AC power is derived at the end of Section IV.

The biased time domain signal, $x_{\text{time}}(k)$, represents the OFDM symbol to be transmitted. After passing through the optical wireless channel, it is received by the optical detector, a combination of a PD and a transimpedance amplifier (TIA). The impulse response of the optical wireless channel can be modeled by a rapidly decaying exponential function with root-mean-square (RMS) delay spreads between 1.3 ns and 13 ns for line-of-sight (LOS) and non-line-of-sight (NLOS) links [2]. In O-OFDM, the ISI from maximum delay spreads of up to 100 ns can be compensated by a CP of 2 samples at a sampling rate of 20 MHz for a negligible reduction of the electrical SNR requirement and the spectral efficiency [22]. Therefore, the channel can be safely considered as flat fading over the entire OFDM frame for bandwidths up to 20 MHz [2, 9], and it can be primarily characterized by the optical path gain coefficient, $g_{\text{h(opt)}}$ [23, 24]. Here, $g_{\text{h(opt)}} = I_{\text{PD}} S_{\text{PD}} \rho_{\text{PD}} G_{\text{TIA}} / (\mathrm{E}\left[x_{\text{time}}(k)\right] \sqrt{r_{\text{load}}})$, where $I_{\text{PD}}$ denotes the average irradiance of the PD, $S_{\text{PD}}$ is the photosensitive area of the PD, $\rho_{\text{PD}}$ is the responsivity of the PD, $G_{\text{TIA}}$ is the gain of the transimpedance amplifier (TIA), $\mathrm{E}\left[x_{\text{time}}(k)\right]$ is the average transmitted optical power, and $r_{\text{load}}$ is the load resistance over which the received current is measured [24, 25]. Furthermore, it is unlikely that the signal is upside-clipped at the receiver. For instance, the linear range of a Vishay TEMD5110X01 PD reaches up to 0.2 mW of incident optical power at room temperature [26]. For a practical indoor path loss range between 50 dB to 80 dB [23, 24], the transmitter needs to radiate more than 20 W of optical power, in order to drive the PD to saturation. Since such an amount significantly exceeds the limits imposed by the eye safety regulations [21,

24], it is assumed that the upside clipping occurs only at the transmitter. At the detector, the signal is distorted by a zero-mean real-valued bipolar additive white Gaussian noise (AWGN), $n_{\mathrm{AWGN}}(k)$ [8]. It accounts for the shot noise and the thermal noise at the receiver. After optical-to-electrical conversion at the received unequalized constellation, it can be modeled as a zero-mean complex-valued AWGN with a two-sided power spectral density of $N_0/2$ per complex dimension and a variance of $\sigma^2_{\mathrm{AWGN}} = BN_0$ [2, 27].

After serial-to-parallel (S/P) and analogue-to-digital (A/D) conversion the signal is passed through a unitary FFT block back to the frequency domain [9]:

$$\widetilde{X}_{\mathrm{scaled}}(m) = \frac{1}{\sqrt{N}} \sum_{k=0}^{N-1} \widetilde{x}(k) \exp\left(\frac{-j2\pi km}{N}\right). \quad (3)$$

According to [7, 8], in ACO-OFDM the asymmetric clipping at the transmitter results in halving of the amplitude of the odd subcarriers at the receiver. In DCO-OFDM, the subcarrier amplitude is inherently preserved. Therefore, further clipping at the front-ends introduces further attenuation. In general, in the OFDM framework, pilot tones are used for channel estimation and equalization. Thus, by the use of pilot tones within the OFDM frame, the equalization block is able to compensate for the effect of the optical wireless channel and the attenuation due to the signal clipping. Finally, the data-carrying symbols in $\widetilde{X}_{\mathrm{frame}}(m)$ can be extracted due to the known frame structure, and the symbols are demodulated using a maximum likelihood (ML) detector.

## III. Assessment of the Clipping Noise Statistics

The clipping of an OFDM time domain signal modifies its mean and consequently its average optical power. Since the non-distorted signal follows a close to Gaussian distribution, the modified mean can be derived based on the statistics of a truncated Gaussian distribution [28]. Thus, the average optical power of the transmitted signal after front-end-induced clipping, $\mathrm{E}\left[x_{\mathrm{time}}(k)\right]$, can be expressed as follows:

$$\mathrm{E}\left[x_{\mathrm{time}}(k)\right] = \sigma_{x(k)}\Big(\phi(\lambda_{\mathrm{bottom}}) - \phi(\lambda_{\mathrm{top}}) + \lambda_{\mathrm{top}}Q(\lambda_{\mathrm{top}}) - \lambda_{\mathrm{bottom}}Q(\lambda_{\mathrm{bottom}})\Big) + P_{\mathrm{bottom}}\ , \quad (4)$$

where

$$\lambda_{\mathrm{bottom}} = \frac{\varepsilon_{\mathrm{bottom}}}{\sigma_{x(k)}}\ , \quad (5)$$

$$\lambda_{\mathrm{top}} = \frac{\varepsilon_{\mathrm{top}}}{\sigma_{x(k)}}\ , \quad (6)$$

$$\phi(u) = \frac{1}{\sqrt{2\pi}} \exp\left(\frac{-u^2}{2}\right) \quad (7)$$

and

$$Q(u) = \frac{1}{\sqrt{2\pi}} \int_u^{\infty} \exp\left(-\frac{v^2}{2}\right)\, dv\ . \quad (8)$$

In DCO-OFDM, $P_{\mathrm{bottom}} = P_{\mathrm{Tx,min}}$. In ACO-OFDM, $P_{\mathrm{bottom}} = \max\Big(P_{\mathrm{Tx,min}}, P_{\mathrm{Tx,bias}}\Big)$ because of the default zero-level clipping in the DSP. In general, the eye safety regulations [21] and/or the design requirements constrain the level of radiated average optical power to $P_{\mathrm{Tx,mean}}$. Therefore, $\mathrm{E}\left[x_{\mathrm{time}}(k)\right] \leq P_{\mathrm{Tx,mean}}$. Here, $\lambda_{\mathrm{bottom}}$ and $\lambda_{\mathrm{top}}$ are the normalized bottom and top clipping levels relative to a standard normal distribution. In addition, $\phi(\cdot)$ and $Q(\cdot)$ are the respective probability density function (PDF) and complementary cumulative distribution function (CCDF). Plausible clipping levels satisfy the inequality $\lambda_{\mathrm{bottom}} < \lambda_{\mathrm{top}}$. In addition, lower $\lambda_{\mathrm{top}}$ results in larger signal clipping, whereas the opposite holds for $\lambda_{\mathrm{bottom}}$. The scenario with the least signal clipping is defined in ACO-OFDM for $\lambda_{\mathrm{bottom}} = 0$ and $\lambda_{\mathrm{top}} = +\infty$. In DCO-OFDM, the least signal clipping is obtained for $\lambda_{\mathrm{bottom}} = -\infty$ and $\lambda_{\mathrm{top}} = +\infty$. For a given dynamic range of the transmitter, $P_{\mathrm{Tx,min}}$ to $P_{\mathrm{Tx,max}}$, the variables in (4) depend only on $P_{\mathrm{Tx,bias}}$ and $\sigma_{x(k)}$. It can, therefore, be ascertained that the average optical power of the transmitted signal, $\mathrm{E}\left[x_{\mathrm{time}}(k)\right]$, is only a function of the front-end biasing parameters, $\sigma_{x(k)}$ and $P_{\mathrm{Tx,bias}}$. In addition, because of the fact that the time domain signal is clipped, the resulting average optical power, $\mathrm{E}\left[x_{\mathrm{time}}(k)\right]$, differs from the undistorted optical power of the OFDM symbol, $P_{\mathrm{s(opt)}}$. In general, $P_{\mathrm{s(opt)}}$, is defined for the least signal clipping scenario. In ACO-OFDM, $P_{\mathrm{s(opt)}} = (P_{\mathrm{Tx,bias}} + \sigma_{x(k)}/\sqrt{2\pi})$, whereas in DCO-OFDM, $P_{\mathrm{s(opt)}} = P_{\mathrm{Tx,bias}}$. Combined with (4), these equations can be used to obtain the relation between $\mathrm{E}\left[x_{\mathrm{time}}(k)\right]$ and the undistorted optical power of the OFDM symbol, $P_{\mathrm{s(opt)}}$. Therefore, in O-OFDM, for a given set of front-end optical power constraints, $P_{\mathrm{Tx,min}}$, $P_{\mathrm{Tx,mean}}$ and $P_{\mathrm{Tx,max}}$, one can obtain the signal scaling factor, $\alpha$, for a target signal variance, $\sigma^2_{x(k)}$, and the required DC bias, $P_{\mathrm{Tx,bias}}$, from (1) and (4).

In addition to the modification of the average optical signal power, the front-end-induced signal clipping distorts the data-carrying symbols. An expression for the distorted scaled data-carrying subcarriers at the receiver, $\widetilde{X}_{\mathrm{scaled,info}}(m)$, is derived by the use of the Bussgang theorem and the CLT. First, the Bussgang theorem is used to obtain $\widetilde{x}(k)$ in ACO-OFDM and DCO-OFDM, respectively, as follows:

$$\widetilde{x}(k) = U\big(x(k)\big)g_{\mathrm{h(opt)}}Ax(k) + g_{\mathrm{h(opt)}}n_{\mathrm{c}}(k) + g_{\mathrm{h(opt)}}P_{\mathrm{Tx,bias}} + n_{\mathrm{AWGN}}(k)\ , \quad (9)$$

$$\widetilde{x}(k) = g_{\mathrm{h(opt)}}Ax(k) + g_{\mathrm{h(opt)}}n_{\mathrm{c}}(k) + g_{\mathrm{h(opt)}}P_{\mathrm{Tx,bias}} + n_{\mathrm{AWGN}}(k)\ . \quad (10)$$

Here, $U(\cdot)$ stands for the unit step function which is used to denote the default zero-level clipping of the time domain signal in ACO-OFDM. The theorem states that after the nonlinear clipping distortion the signal is attenuated by a factor, $A$, and an uncorrelated non-Gaussian clipping noise, $n_{\mathrm{c}}(k)$, is added. In ACO-OFDM, $n_{\mathrm{c}}(k)$ is non-negative and it has a unipolar distribution, whereas in DCO-OFDM the clipping noise component is bipolar. In addition, in ACO-OFDM the amplitude of the received odd subcarriers is reduced by $50\%$ because of the zero-level clipping and the symmetries discussed in [7]. Therefore, in the presence of double-sided clipping in ACO-OFDM, the effective attenuation factor at the received odd subcarriers, $K$, is related to $A$ as $K = A/2$, where $A = 1$ in the least signal clipping scenario. In DCO-OFDM, $K = A$. Below $K$ is derived for the considered ACO-OFDM and DCO-OFDM systems. Further on, $\widetilde{x}(k)$ is passed through an FFT. Applying the CLT, the distorted scaled

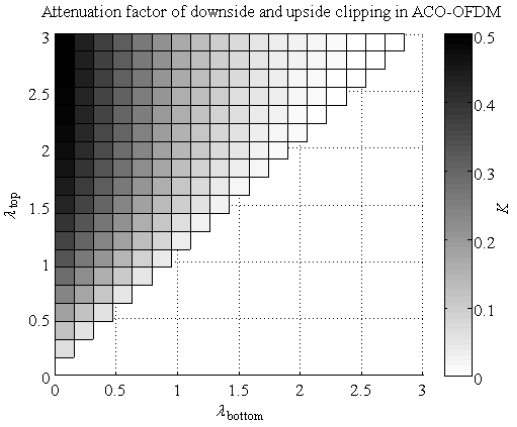


Fig. 2. Attenuation factor of the clipping noise as a function of the normalized clipping levels in ACO-OFDM.

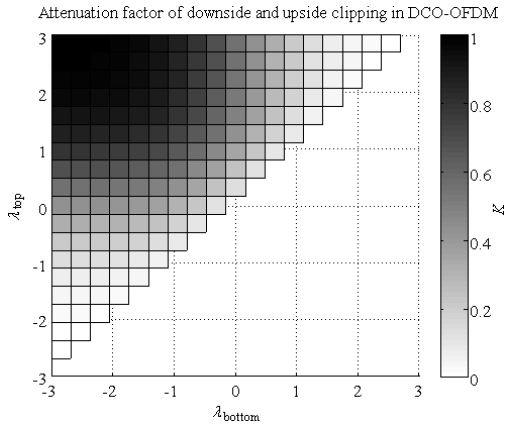


Fig. 3. Attenuation factor of the clipping noise as a function of the normalized clipping levels in DCO-OFDM.

data-carrying subcarriers, $\widetilde{X}_{\text{scaled,info}}(m)$, can be expressed as a function of the transmitted data-carrying subcarriers, $X_{\text{frame,info}}(m)$, in ACO-OFDM and DCO-OFDM as follows:

$$\begin{aligned}\widetilde{X}_{\text{scaled,info}}(m) &= \alpha g_{\text{h(opt)}} K X_{\text{frame,info}}(m) \\ &\quad + g_{\text{h(opt)}}\sigma_{\text{clip}} N_{\mathcal{CN}}(m) + \sigma_{\text{AWGN}} N_{\mathcal{CN}}(m)\ ,\end{aligned} \tag{11}$$

where $\sigma_{\text{clip}}$ is the standard deviation of the complex-valued Gaussian clipping noise at the data-carrying subcarriers. Below we also derive $\sigma_{\text{clip}}$ for the considered ACO-OFDM and DCO-OFDM systems. $N_{\mathcal{CN}}(m)$ is a sample of a complex-valued Gaussian distribution with zero mean and unity variance. Here, in order to recover $X_{\text{frame,info}}(m)$, a zero forcing (ZF) equalizer is employed [3]. Even though ZF is an equalization technique widely used in OFDM-based systems, it results in AWGN amplification when the path gain decreases. Alternatively, minimum mean-squared error (MMSE) equalization can be employed to alleviate this issue [3].

Applying the assumption of Gaussianity of $x(k)$, the attenuation factor, $K$, is expressed as follows [14]:

$$K = \frac{\text{Cov}\left[x(k), x_{\text{DSP}}(k)\right]}{\sigma^2_{x(k)}} = Q(\lambda_{\text{bottom}}) - Q(\lambda_{\text{top}})\ , \tag{12}$$

where $\text{Cov}[\cdot]$ stands for the covariance operator. Note that in ACO-OFDM and DCO-OFDM, since $x_{\text{time}}(k)$ is real, $K$ is a real-valued function. It essentially represents the likelihood of samples not being clipped. In addition, it proves to be independent of the modulation scheme, $M$-QAM, and the IFFT/FFT size, $N$. The attenuation factor as a function of the normalized bottom and top clipping levels is illustrated in Fig. 2 and Fig. 3 for ACO-OFDM and DCO-OFDM, respectively. As suggested in [7, 8], the attenuation factor for ACO-OFDM approaches $0.5$ when the least signal clipping is present. Furthermore, the ACO-OFDM symbol suffers larger attenuation for downside clipping as compared to upside clipping. On the contrary, the signal clipping in DCO-OFDM exhibits a symmetric attenuation profile for clipping levels located symmetrically around the average optical power level.

According to (9) and (10) the time domain clipping noise, $n_{\text{c}}(k)$, is an independent component and can be estimated separately. The time domain signal, subject only to double-sided clipping, $x_{\text{DSP}}(k)$, can be written in ACO-OFDM and DCO-OFDM, respectively, as follows:

$$\begin{aligned}x_{\text{DSP}}(k) &= U\big(x(k)\big)x(k) - \Delta_x(k) \\ &= U\big(x(k)\big)2Kx(k) + n_{\text{c}}(k)\ ,\end{aligned} \tag{13}$$

$$x_{\text{DSP}}(k) = x(k) - \Delta_x(k) = Kx(k) + n_{\text{c}}(k)\ . \tag{14}$$

Here, $\Delta_x(k)$ is the clipped signal portion. Therefore, the time domain clipping noise component, $n_{\text{c}}(k)$, can be expressed in ACO-OFDM and DCO-OFDM, respectively, as follows:

$$n_{\text{c}}(k) = U\big(x(k)\big)(1-2K)x(k) - \Delta_x(k)\ , \tag{15}$$

$$n_{\text{c}}(k) = (1-K)x(k) - \Delta_x(k)\ . \tag{16}$$

Because of the unitary FFT at the receiver, $n_{\text{c}}(k)$ is transformed into a zero-mean Gaussian noise component at the data-carrying subcarriers according to the CLT. In order to obtain the clipping noise variance, $\sigma^2_{\text{clip}}$, the time domain signal in the DSP, $x_{\text{DSP}}(k)$, is required. The later signal is depicted in Fig. 4 and Fig. 5 in ACO-OFDM and DCO-OFDM, respectively. In ACO-OFDM, the symmetries discussed in [7] allow the unfolding of the truncated half Gaussian distribution of $x_{\text{DSP}}(k)$, the mirroring of the clipping levels around the origin and the redistribution of the signal samples. The resulting signal is denoted as $\hat{x}_{\text{DSP}}(k)$, and it is depicted in Fig. 6. It is a symmetric signal with respect to the origin, and it follows a close to Gaussian distribution with zero mean and variance of $P_{\text{s(elec)}}/2$ when the least signal clipping is present. However, $\hat{x}_{\text{DSP}}(k)$ has a bias of $-\sigma_{x(k)}\lambda_{\text{bottom}}/\sqrt{2}$ on the negative samples and a bias of $\sigma_{x(k)}\lambda_{\text{bottom}}/\sqrt{2}$ on the positive ones. Since these biases are to be mounted on the first subcarrier in the ACO-OFDM frame after the FFT, they are irrelevant to the clipping noise variance on the data-carrying subcarriers. Thus, $\hat{x}_{\text{DSP}}(k)$ is debiased to obtain $\hat{x}_{\text{DSP,debiased}}(k)$ as illustrated in Fig. 7. Using the statistics of a truncated Gaussian distribution, $\sigma^2_{\text{clip}}$ can be expressed in ACO-OFDM as follows:

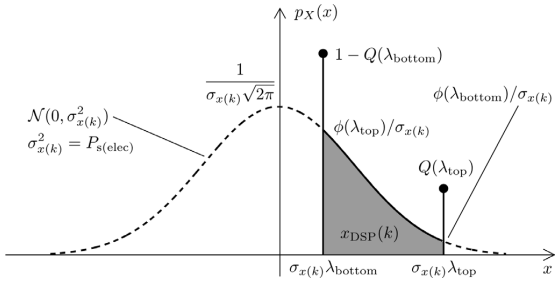


Fig. 4. Time domain signal in DSP, $x_{\text{DSP}}(k)$, in ACO-OFDM.

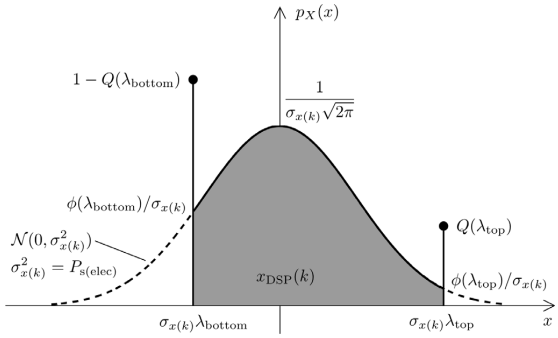


Fig. 5. Time domain signal in DSP, $x_{\text{DSP}}(k)$, in DCO-OFDM.

$$\sigma^2_{\text{clip}} = \frac{P_{\text{s(elec)}}}{2}(1 - 4K^2) - \Delta\sigma^2 \ , \tag{17}$$

where

$$\Delta\sigma^2 = \frac{P_{\text{s(elec)}}}{2} - \text{E}\left[\hat{x}_{\text{DSP,debiased}}(k)^2\right] \ , \tag{18}$$

$$\begin{aligned}\text{E}\left[\hat{x}_{\text{DSP,debiased}}(k)^2\right] = \frac{P_{\text{s(elec)}}}{2}\Big(&4\phi(\lambda_{\text{top}})\lambda_{\text{bottom}} \\ &-2\phi(\lambda_{\text{top}})\lambda_{\text{top}} - 2\phi(\lambda_{\text{bottom}})\lambda_{\text{bottom}} \\ &+\big(\lambda^2_{\text{bottom}} + 1\big)\big(1 - 2Q(\lambda_{\text{top}})\big) \\ &-\big(\lambda^2_{\text{bottom}} + 1\big)\big(1 - 2Q(\lambda_{\text{bottom}})\big) \\ &+2Q(\lambda_{\text{top}})\big(\lambda_{\text{top}} - \lambda_{\text{bottom}}\big)^2\Big) \ .\end{aligned} \tag{19}$$

In DCO-OFDM, $x_{\text{DSP}}(k)$ follows a close to Gaussian distribution with zero mean and variance of $P_{\text{s(elec)}}$ when the least signal clipping is present. After removing the bias of $\text{E}\left[x_{\text{DSP}}(k)\right]$, the debiased time domain signal, $x_{\text{DSP,debiased}}(k)$, is obtained as illustrated in Fig. 8. Similarly, using the statistics of a truncated Gaussian distribution, $\sigma^2_{\text{clip}}$ can be expressed in DCO-OFDM as follows:

$$\sigma^2_{\text{clip}} = P_{\text{s(elec)}}(1 - K^2) - \Delta\sigma^2 \ , \tag{20}$$

where

$$\Delta\sigma^2 = P_{\text{s(elec)}} - \text{E}\left[x_{\text{DSP,debiased}}(k)^2\right] \ , \tag{21}$$

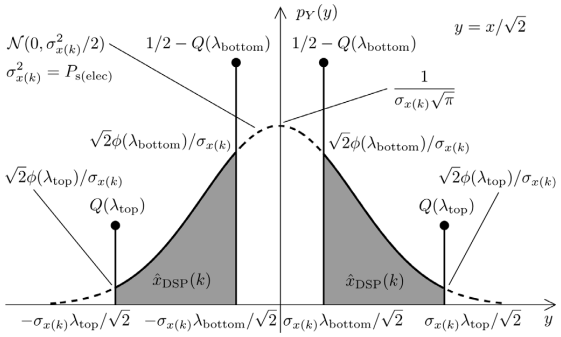


Fig. 6. Unfolded time domain signal in DSP, $\hat{x}_{\text{DSP}}(k)$, in ACO-OFDM.

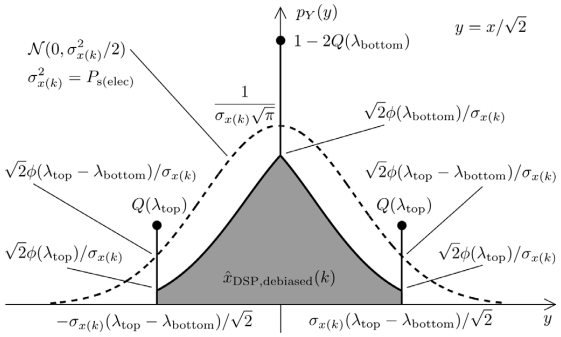


Fig. 7. Debiased and unfolded time domain signal in DSP, $\hat{x}_{\text{DSP,debiased}}(k)$, in ACO-OFDM.

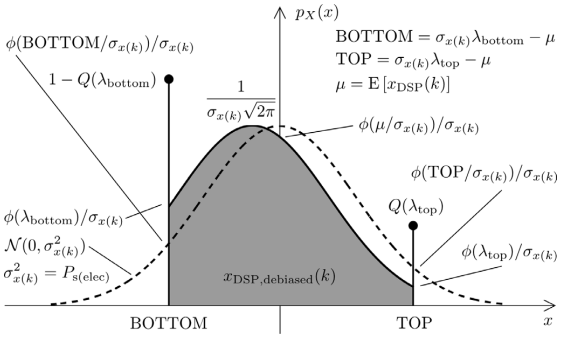


Fig. 8. Debiased time domain signal in DSP, $x_{\text{DSP,debiased}}(k)$, in DCO-OFDM.

$$\text{E}\left[x_{\text{DSP,debiased}}(k)^2\right] = \text{E}\left[x_{\text{DSP}}(k)^2\right] - \text{E}\left[x_{\text{DSP}}(k)\right]^2 \ , \tag{22}$$

$$\begin{aligned}\text{E}\left[x_{\text{DSP}}(k)\right] = \sqrt{P_{\text{s(elec)}}}\Big(&\phi(\lambda_{\text{bottom}}) - \phi(\lambda_{\text{top}}) \\ &+\big(1 - Q(\lambda_{\text{bottom}})\big)\lambda_{\text{bottom}} + Q(\lambda_{\text{top}})\lambda_{\text{top}}\Big) \ ,\end{aligned} \tag{23}$$

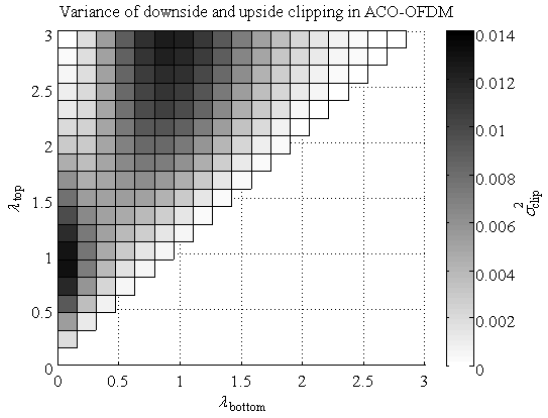


Fig. 9. Variance of the clipping noise as a function of the normalized clipping levels in ACO-OFDM. Here, a scaled symbol power of $P_{\text{s(elec)}}/G_{\text{B}} = 1$ is assumed.

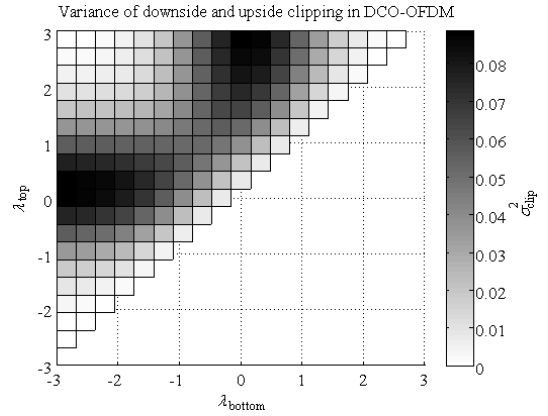


Fig. 10. Variance of the clipping noise as a function of the normalized clipping levels in DCO-OFDM. Here, a scaled symbol power of $P_{\text{s(elec)}}/G_{\text{B}} = 1$ is assumed.

$$\begin{aligned}\mathrm{E}\left[x_{\text{DSP}}(k)^2\right] = P_{\text{s(elec)}}\Big(&Q(\lambda_{\text{bottom}}) - Q(\lambda_{\text{top}}) \\ &+\phi(\lambda_{\text{bottom}})\lambda_{\text{bottom}} - \phi(\lambda_{\text{top}})\lambda_{\text{top}} \\ &+\big(1 - Q(\lambda_{\text{bottom}})\big)\lambda^2_{\text{bottom}} + Q(\lambda_{\text{top}})\lambda^2_{\text{top}}\Big)\,.\end{aligned} \tag{24}$$

Note that similarly to the attenuation factor, $K$, the clipping noise variance, $\sigma^2_{\text{clip}}$, is independent of the modulation order, $M$, and the IFFT/FFT size, $N$. It only depends on the normalized bottom and top clipping levels. This is illustrated in Fig. 9 and Fig. 10 for ACO-OFDM and DCO-OFDM, respectively. As expected, $\sigma^2_{\text{clip}}$ approaches zero for the least signal clipping scenario. However, since $K$ and $\sigma^2_{\text{clip}}$ are coupled according to (11), as $K$ approaches zero, $\sigma^2_{\text{clip}}$ approaches zero, as well. Here, the large symbol distortion is defined for a small $K$ and a large $\sigma^2_{\text{clip}}$. Thus, Fig. 2 and Fig. 9 suggest that downside clipping introduces a larger ACO-OFDM symbol distortion than upside clipping. Expectedly, it is shown in Fig. 3 and Fig. 10 that the symbol distortion in DCO-OFDM can be minimized when symmetric normalized clipping levels are chosen. Since $K$ and $\sigma^2_{\text{clip}}$ are independent of $M$, they remain constant across the modulation orders for a particular choice of normalized bottom and top clipping levels. Nonetheless, the BER performance of the system depends on the granularity of the constellation, where higher order modulation is more vulnerable to Gaussian noise because of the shrinking of the decision regions. Therefore, for a given biasing setup in the dynamic range of the transmitter front-end, the resulting additive noise term of the non-linear clipping distortion more significantly impacts the BER performance of higher order modulation, $M$-QAM, as shown in Section IV.

Using (11), (12), (17) and (20), an analytical expression for the effective electrical SNR per bit in OFDM-based OWC, $\Gamma_{\text{b(elec)}}$, can be expressed for ZF as a function of the undistorted electrical SNR per bit, $\gamma_{\text{b(elec)}} = E_{\text{b(elec)}}/N_0$, as follows:

$$\Gamma_{\text{b(elec)}} = \frac{K^2 P_{\text{b(elec)}}/G_{\text{B}}}{\sigma^2_{\text{clip}} + \dfrac{G_{\text{B}}\sigma^2_{\text{AWGN}}}{g^2_{\text{h(opt)}} G_{\text{DC}}}} = \frac{K^2}{\dfrac{G_{\text{B}}\sigma^2_{\text{clip}}}{P_{\text{b(elec)}}} + \dfrac{G_{\text{B}}\gamma^{-1}_{\text{b(elec)}}}{g^2_{\text{h(opt)}} G_{\text{DC}}}}\,. \tag{25}$$

The factor $G_{\text{DC}}$ denotes the attenuation of the useful electrical signal power of $x_{\text{time}}(k)$ due to the biasing of the transmitter front-end by $P_{\text{Tx,bias}}$ in the least signal clipping scenario. The factor $G_{\text{DC}}$ is defined for ACO-OFDM as follows:

$$\begin{aligned}G_{\text{DC}} &= \frac{\mathrm{E}\left[x_{\text{DSP,least}}(k)^2\right]}{\mathrm{E}\left[x_{\text{time,least}}(k)^2\right]} \\ &= \frac{\sqrt{2\pi}\sigma^2_{x(k)}}{\sqrt{2\pi}\sigma^2_{x(k)} + 4\sigma_{x(k)}P_{\text{Tx,bias}} + 2\sqrt{2\pi}P^2_{\text{Tx,bias}}}\,.\end{aligned} \tag{26}$$

In DCO-OFDM, $G_{\text{DC}}$ is given by:

$$G_{\text{DC}} = \frac{\sigma^2_{x(k)}}{\sigma^2_{x(k)} + P^2_{\text{Tx,bias}}}\,. \tag{27}$$

In addition, because of the bias added to the ACO-OFDM signal, $P_{\text{Tx,bias}}$, the electrical-to-optical conversion in [8] has to be generalized as follows:

$$\begin{aligned}P_{\text{s(opt)}} &= \sqrt{\frac{\mathrm{E}\left[x_{\text{time,least}}(k)\right]^2}{\mathrm{E}\left[x_{\text{time,least}}(k)^2\right]}}P_{\text{s(elec)}} \\ &= \sqrt{\frac{2\pi P^2_{\text{Tx,bias}} + 2\sigma_{x(k)}P_{\text{Tx,bias}}\sqrt{2\pi} + \sigma^2_{x(k)}}{2\pi P^2_{\text{Tx,bias}} + 2\sigma_{x(k)}P_{\text{Tx,bias}}\sqrt{2\pi} + \pi\sigma^2_{x(k)}}}P_{\text{s(elec)}}\,.\end{aligned} \tag{28}$$

The conversion in DCO-OFDM given in [8] can be generalized as follows:

$$P_{\text{s(opt)}} = \sqrt{\frac{P^2_{\text{Tx,bias}}}{\sigma^2_{x(k)} + P^2_{\text{Tx,bias}}}}P_{\text{s(elec)}}\,. \tag{29}$$

## IV. BER Performance of O-OFDM

The performance of the ACO-OFDM and DCO-OFDM systems in the presence of double-sided signal clipping and AWGN is assessed in terms of BER. The exact closed form expression for the BER performance of $M$-QAM in AWGN has been presented in [29] as a summation of $M$ terms. A

very good approximation can be obtained by using only the first two terms and neglecting the rest. Therefore, an analytical expression for the BER performance of $M$-QAM O-OFDM can be obtained as follows:

$$\mathrm{BER} = \frac{4(\sqrt{M}-1)}{\sqrt{M}\log_2(M)} Q\left(\sqrt{\frac{3\log_2(M)}{M-1}\Gamma_{\mathrm{b(elec)}}}\right) + \frac{4(\sqrt{M}-2)}{\sqrt{M}\log_2(M)} Q\left(3\sqrt{\frac{3\log_2(M)}{M-1}\Gamma_{\mathrm{b(elec)}}}\right). \quad (30)$$

The BER performance of O-OFDM with double-sided signal clipping is evaluated as a function of the undistorted electrical SNR per bit, $\gamma_{\mathrm{b(elec)}}$, through the effective electrical SNR per bit in O-OFDM, $\Gamma_{\mathrm{b(elec)}}$. The accuracy of the derived expression for $\Gamma_{\mathrm{b(elec)}}$ is verified by means of a Monte Carlo BER simulation. For this purpose, an IFFT/FFT size of $2048$ is chosen. Link parameters such as the optical center frequency, the mutual orientation and position of the transmitter and receiver in an indoor setup and their field of view (FOV), the responsivity and the photosensitive area of the detector, and the average radiated optical power of the transmitter determine the optical path gain coefficient, $g_{\mathrm{h(opt)}}$ [24, 25]. Since, however, $g_{\mathrm{h(opt)}}$ is merely a factor in the equalization process as shown in (11) and (25), a change in $g_{\mathrm{h(opt)}}$ results in an equal SNR penalty in ACO-OFDM and DCO-OFDM. Therefore, $g_{\mathrm{h(opt)}} = 1$ is assumed for simplicity. In addition, based on the optical center frequency, the optical emitter can be modulated within a certain modulation bandwidth. Here, the multiplication of the modulation bandwidth and the spectral efficiency of the system yields the system throughout. However, for a fixed SNR, the BER performance is independent of the bandwidth, and consequently of the throughput. Therefore, the ACO-OFDM and DCO-OFDM systems are constrained for unity bandwidth. In general, because of the structure of the OFDM frame, ACO-OFDM achieves half the spectral efficiency of DCO-OFDM for equal modulation orders. Therefore, in addition to $4$-QAM ACO-OFDM with a spectral efficiency of $0.5$ bits/s/Hz, $16$-QAM ACO-OFDM is compared with $4$-QAM DCO-OFDM to evaluate the BER performance at a similar spectral efficiency of $1$ bit/s/Hz. Furthermore, the systems are constrained for equal average optical power of the transmitted signal. A practical linear dynamic range of a Vishay TSHG8200 LED between $P_{\mathrm{Tx,min}} = 5$ mW and $P_{\mathrm{Tx,max}} = 50$ mW at room temperature is considered the transmitter [30]. No clipping at the receiver is assumed. As benchmarks for a comparison with existing results, ideal cases for signal scaling and biasing are included from [8]. For any given fixed average optical power at the transmitter, $\mathrm{E}[x_{\mathrm{time}}(k)] = P_{\mathrm{Tx,mean}}$, the ACO-OFDM signal is clipped in the ideal case at $\lambda_{\mathrm{bottom}} = 0$ and $\lambda_{\mathrm{top}} = +\infty$. Here, $P_{\mathrm{Tx,bias}} = 0$ and $\sigma_{x(k)} = P_{\mathrm{Tx,mean}}\sqrt{2\pi}$. In DCO-OFDM, a widely used ideal case is defined for $\lambda_{\mathrm{bottom}} = -2$ and $\lambda_{\mathrm{top}} = +\infty$ [8]. Here, $P_{\mathrm{Tx,bias}} = P_{\mathrm{Tx,mean}}$ and $\sigma_{x(k)} = P_{\mathrm{Tx,mean}}/2$. In addition to the ideal case, two clipping scenarios which satisfy the average optical power constraint are considered for the verification of the analytical framework, following the guidelines for signal scaling, clipping and biasing discussed in Section II. Thus, two average optical power constraints are chosen, *i.e.* $\mathrm{E}[x_{\mathrm{time}}(k)] = P_{\mathrm{Tx,mean}} = 10$ mW and $\mathrm{E}[x_{\mathrm{time}}(k)] = P_{\mathrm{Tx,mean}} = 15$ mW. Here, the front-end biasing is defined through the parameters $P_{\mathrm{Tx,bias}}$ and $\sigma_{x(k)}$. They are obtained from (4) as a pair which yields the chosen $P_{\mathrm{Tx,mean}}$ for the given $P_{\mathrm{Tx,min}}$ and $P_{\mathrm{Tx,max}}$. In the first case, $P_{\mathrm{Tx,mean}} = 10$ mW is realized in ACO-OFDM for $P_{\mathrm{Tx,bias}} = 4.2$ mW and $\sigma_{x(k)} = 14.5$ mW, whereas $P_{\mathrm{Tx,bias}} = 9.8$ mW and $\sigma_{x(k)} = 4.9$ mW are required in DCO-OFDM. In the second case, $P_{\mathrm{Tx,mean}} = 15$ mW is obtained in ACO-OFDM for $P_{\mathrm{Tx,bias}} = 2.8$ mW and $\sigma_{x(k)} = 30.6$ mW, while $P_{\mathrm{Tx,bias}} = 14.8$ mW and $\sigma_{x(k)} = 7.4$ mW are considered in DCO-OFDM. The two biasing setups yield the following normalized clipping levels. In ACO-OFDM, $\lambda_{\mathrm{bottom}} = 0.06$ and $\lambda_{\mathrm{top}} = 3.15$ in the first case, whereas $\lambda_{\mathrm{bottom}} = 0.07$ and $\lambda_{\mathrm{top}} = 1.54$ in the second case. In DCO-OFDM, $\lambda_{\mathrm{bottom}} = -0.98$ and $\lambda_{\mathrm{top}} = 8.2$ in the first case, whereas $\lambda_{\mathrm{bottom}} = -1.32$ and $\lambda_{\mathrm{top}} = 4.76$ in the second case. Since ACO-OFDM is more efficient in terms of optical power, it is expected to perform better in the first biasing setup because of the less severe upside clipping. On the contrary, DCO-OFDM is expected to perform better in the second biasing setup, because the normalized clipping levels are closer to a symmetric clipping.

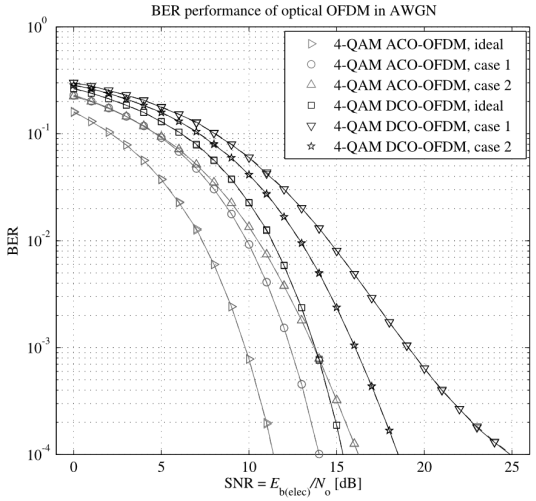


Fig. 11. BER performance of optical OFDM in AWGN, 4-QAM ACO-OFDM *vs.* 4-QAM DCO-OFDM, simulation (solid lines) *vs.* theory (dashed lines).

The BER performance of the studied ACO-OFDM and DCO-OFDM systems is presented in Fig. 11 and Fig. 12. The theoretical and simulation results confirm a very close match. It is shown that the existing simulation results from [8] for an ideal biasing scenario underestimate the BER performance of ACO-OFDM and DCO-OFDM in a biasing setup with a clipping distortion. However, the ideal biasing scenarios are not achievable in practice. In general, for identical QAM modulation orders ACO-OFDM demonstrates a better BER performance as compared to DCO-OFDM at the expense of $50\%$ reduction in spectral efficiency. In Fig. 11, even though $4$-QAM ACO-OFDM shows the better BER performance for a

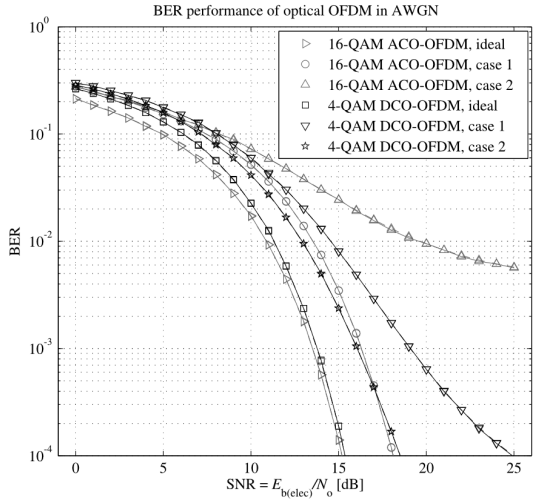


Fig. 12. BER performance of optical OFDM in AWGN, 16-QAM ACO-OFDM *vs.* 4-QAM DCO-OFDM, simulation (solid lines) *vs.* theory (dashed lines).

corresponding clipping scenario, it is outperformed by $4$-QAM DCO-OFDM in terms of spectral efficiency over the entire SNR region [20]. However, the results show that the biasing setup plays a significant role when comparing $16$-QAM ACO-OFDM and $4$-QAM DCO-OFDM. In general, a setup which accommodates a lower average optical power with respect to the given dynamic range is more suitable for ACO-OFDM. However, shifting the average optical power towards the middle of the dynamic range can potentially yield a better BER performance with DCO-OFDM and thereby a higher system throughput. This is because of the resulting front-end-induced signal clipping: in the first case DCO-OFDM is clipped more severely, whereas in the second case ACO-OFDM is the one that suffers a greater signal degradation. This is confirmed by the BER results of $16$-QAM ACO-OFDM and $4$-QAM DCO-OFDM in Fig. 12. Whereas the first case of $16$-QAM ACO-OFDM and the second case of $4$-QAM DCO-OFDM perform similarly, the respective counterparts are more severely clipped and show a degraded performance. However, a comparison between $4$-QAM and $16$-QAM ACO-OFDM suggests that higher order QAM modulation is more vulnerable to signal clipping. This is because, according to (11) the Gaussian clipping noise at the received data-carrying subcarriers is added independently of the QAM modulation order, $M$. Therefore, it is expected that $M$-QAM DCO-OFDM delivers a better BER performance and, therefore a higher throughput, as compared to $M^2$-QAM ACO-OFDM in a biasing setup with a higher average optical power. In addition, since the factors in (11) are independent of $N$ for practical IFFT/FFT sizes, *i.e.* $N > 64$, the BER/throughput performance is independent of the total number of subcarriers.

## V. Conclusion

In this paper, double-sided signal clipping in ACO-OFDM and DCO-OFDM OWC systems due to biasing issues and physical limitations of the transmitter front-end is studied. In accord with the Bussgang theorem and the CLT, the statistics of the clipping noise at the received data-carrying subcarriers are derived in closed-form as a function of the normalized bottom and top clipping levels. An expression for the effective electrical SNR per bit in O-OFDM is presented, and it proves to closely match the Monte Carlo BER simulation. The derived SNR shows that, unlike in OFDM-based RF systems, an SNR increase is not achievable simply by increasing the average electrical and/or optical power at the transmitter. In OWC, such a measure leads to a larger clipping distortion, and therefore, to a larger SNR penalty which is exactly quantified in (25). In general, the presented system model includes the power limitations imposed by the transmitter front-end, and it provides means for time domain signal shaping, *i.e.* signal scaling and biasing, to condition the signal within these constraints. It is shown that the BER performance of OFDM-based OWC is more severely degraded with the increase of the modulation order for a particular double-sided signal clipping scenario. In addition, practical IFFT/FFT sizes greater than $64$ do not affect the BER performance. Finally, the ACO-OFDM and DCO-OFDM systems are studied for different normalized clipping levels. It is found that ACO-OFDM is more robust to the clipping effects than DCO-OFDM for similar modulation schemes at the expense of a $50\%$ reduction in spectral efficiency. Therefore, ACO-OFDM is more suitable for applications with lower radiated average optical power, whereas DCO-OFDM promises to deliver higher throughput.

## Acknowledgement

We gratefully acknowledge EADS UK Ltd. for the support of this research. Professor Haas acknowledges the Scottish Funding Council support of his position within the Edinburgh Research Partnership in Engineering and Mathematics between the University of Edinburgh and Heriot Watt University.

## References

[1] Y. Tanaka, T. Komine, S. Haruyama, and M. Nakagawa, "Indoor visible communication utilizing plural white LEDs as lighting," in *Proc. 2001 IEEE International Symp. Personal, Indoor Mobile Radio Commun.*, vol. 2, pp. 81–85.

[2] J. M. Kahn and J. R. Barry, "Wireless infrared communications," *Proc. IEEE*, vol. 85, no. 2, pp. 265–298, Feb. 1997.

[3] J. G. Proakis, *Digital Communications*, 4th edition, ser. McGraw-Hill Series in Electrical and Computer Engineering, S. W. Director, editor. McGraw-Hill Higher Education, Dec. 2000.

[4] H. Elgala, R. Mesleh, H. Haas, and B. Pricope, "OFDM visible light wireless communication based on white LEDs," in *Proc. 2007 IEEE Veh. Technol. Conf. – Spring*.

[5] J. B. Carruthers and J. M. Kahn, "Multiple-subcarrier modulation for nondirected wireless infrared communication," *IEEE J. Sel. Areas Commun.*, vol. 14, no. 3, pp. 538–546, Apr. 1996.

[6] P. Golden, H. Dedieu, and K. Jacobsen, *Fundamentals of DSL Technology*. Auerbach Publications, 2006.

[7] J. Armstrong and A. Lowery, "Power efficient optical OFDM," *Electron. Lett.*, vol. 42, no. 6, pp. 370–372, Mar. 16, 2006.

[8] J. Armstrong and B. J. C. Schmidt, "Comparison of asymmetrically clipped optical OFDM and DC-biased optical OFDM in AWGN," *IEEE Commun. Lett.*, vol. 12, no. 5, pp. 343–345, May 2008.

[9] J. Armstrong, "OFDM for optical communications," *J. Lightwave Technol.*, vol. 27, no. 3, pp. 189–204, Feb. 2009.

[10] J. Rice, *Mathematical Statistics and Data Analysis*, 2nd edition. Duxbury Press, 1995.

[11] D. Dardari, V. Tralli, and A. Vaccari, "A theoretical characterization of nonlinear distortion effects in OFDM systems," *IEEE Trans. Commun.*, vol. 48, no. 10, pp. 1755–1764, Oct. 2000.

[12] J. Bussgang, "Cross correlation function of amplitude-distorted Gaussian signals," Research Laboratory for Electronics, Massachusetts Institute of Technology, Cambridge, MA, Technical Report 216, Mar. 1952.

[13] Q. Pan and R. J. Green, "Bit-error-rate performance of lightwave hybrid AM/OFDM systems with comparison with AM/QAM systems in the presence of clipping impulse noise," *IEEE Photon. Technol. Lett.*, vol. 8, no. 2, pp. 278–280, Feb. 1996.

[14] S. Randel, F. Breyer, S. C. J. Lee, and J. W. Walewski, "Advanced modulation schemes for short-range optical communications," *IEEE J. Sel. Topics Quantum Electron.*, vol. PP, no. 99, pp. 1–10, 2010.

[15] H. Elgala, R. Mesleh, and H. Haas, "Non-linearity effects and predistortion in optical OFDM wireless transmission using LEDs," *Inderscience Intenational J. Ultra Wideband Commun. Syst.*, vol. 1, no. 2, pp. 143–150, 2009.

[16] H. Ochiai and H. Imai, "Performance analysis of deliberately clipped OFDM signals," *IEEE Trans. Commun.*, vol. 50, no. 1, pp. 89–101, Jan. 2002.

[17] A. Bahai, M. Singh, A. Goldsmith, and B. Saltzberg, "A new approach for evaluating clipping distortion in multicarrier systems," *IEEE J. Sel. Areas Commun.*, vol. 20, no. 5, pp. 1037–1046, June 2002.

[18] D. J. G. Mestdagh, P. Spruyt, and B. Biran, "Analysis of clipping effect in DMT-based ADSL systems," in *Proc. 1994 IEEE International Conf. Commun.*, vol. 1, pp. 293–300.

[19] S. C. J. Lee, F. Breyer, S. Randel, H. P. A. van der Boom, and A. M. J. Koonen, "High-speed transmission over multimode fiber using discrete multitone modulation," *J. Optical Netw.*, vol. 7, no. 2, pp. 183–196, Feb. 2008.

[20] S. Dimitrov and H. Haas, "On the clipping noise in an ACO-OFDM optical wireless communication system," in *Proc. 2010 IEEE Global Commun. Conf.*.

[21] BS EN 62471:2008, Photobiological Safety of Lamps and Lamp Systems, BSI British Standards Std., Sep. 2008.

[22] H. Elgala, R. Mesleh, and H. Haas, "Practical considerations for indoor wireless optical system implementation using OFDM," in *Proc. 2009 IEEE International Conf. Telecommun.*

[23] S. Dimitrov, R. Mesleh, H. Haas, M. Cappitelli, M. Olbert, and E. Bassow, "Path loss simulation of an infrared optical wireless system for aircraft," in *Proc. 2009 IEEE Global Commun. Conf.*

[24] ——, "On the SIR of a cellular infrared optical wireless system for an aircraft," *IEEE J. Sel. Areas Commun.*, vol. 27, no. 9, pp. 1623–1638, Dec. 2009.

[25] S. Dimitrov, H. Haas, M. Cappitelli, and M. Olbert, "On the throughput of an OFDM-based cellular optical wireless system for an aircraft cabin," in *Proc. 2011 European Conf. Antennas Propagat.*

[26] Vishay Semiconductors, "Datasheet: TEMD5110X01 Silicon PIN Photodiode," retrieved July 26, 2011 from http://www.vishay.com/docs/84658/temd5110.pdf, May 2009.

[27] D. Tse and P. Viswanath, *Fundamentals of Wireless Communication*. Cambridge University Press, 2005.

[28] N. Johnson, S. Kotz, and N. Balakrishnan, *Continuous Univariate Distributions*, 2nd edition. John Wiley & Sons Ltd., 1994, vol. 1.

[29] J. Li, X. Zhang, Q. Gao, Y. Luo, and D. Gu, "Exact BEP analysis for coherent M-arry PAM and QAM over AWGN and Rayleigh fading channels," in *Proc. 2008 IEEE Veh. Technol. Conf. – Spring*, pp. 390–394.

[30] Vishay Semiconductors, "Datasheet: TSHG8200 High Speed Infrared Emitting Diode, 830 nm, GaAlAs Double Hetero," retrieved July 26, 2011 from http://www.vishay.com/docs/84755/tshg8200.pdf, July 2008.


**Svilen Dimitrov** (S'09) received the BSc degree in electrical engineering and computer science in 2008, and the MSc degree in communications, systems, and electronics in 2009 from Jacobs University, Bremen, Germany. He wrote his BSc thesis (2007 – 2008) with the department of Pre-Development of Cabin Electronic Systems of Airbus Germany on a simulation model for reproduction of infrared wireless path loss distribution in an aircraft cabin, using a Monte Carlo Ray-tracing algorithm. During his MSc study (2008 – 2009), he extended the work on the characterization of the optical wireless channel with the department of Simulation and Graphical Technologies of EADS Innovation Works Germany. Currently, he is working towards his PhD degree in electrical engineering at the University of Edinburgh, UK. His main research interests are in the area of computer-aided system design, test and optimization with emphasis on wireless communication systems.

**Sinan Sinanovic** (S'98-M'07) obtained his Ph.D. in electrical and computer engineering from Rice University, Houston, Texas, in 2006. In the same year, he joined Jacobs University Bremen in Germany as a post doctoral fellow. In 2007, he joined the University of Edinburgh in the UK where he currently works as a research fellow in the Institute for Digital Communications (IDCOM). While working with Halliburton Energy Services, he developed acoustic telemetry receiver which was patented. He also worked for Texas Instruments. He is a member of the Tau Beta Pi engineering honor society and a member of Eta Kappa Nu electrical engineering honor society. He won an honourable mention at the International Math Olympiad in 1994.

**Professor Harald Haas** (S'98-A'00-M'03) received his PhD degree from the University of Edinburgh in 2001. His main research interests are in the areas of wireless system design and analysis as well as digital signal processing, with a particular focus on interference coordination in wireless networks, spatial modulation and optical wireless communication. From 2001 to 2002, Prof. Haas was project manager at Siemens AG (Information and Communication Mobile Networks) for an international research project. He joined International University Bremen, now Jacobs University Bremen, in September 2002 as Associate Professor of Electrical Engineering before returning to the University of Edinburgh in June 2007. He now holds the personal Chair of Mobile Communications in the Institute for Digital Communications (IDCOM). Prof. Haas holds 18 patents in the area of wireless communications. He has published more than 50 journal papers including a Science Article, which is cited more than 400 times, and more than 150 peer-reviewed conference papers. Nine of his papers are invited papers. Prof. Haas has co-authored a book entitled *Next Generation Mobile Access Technologies: Implementing TDD* with Cambridge University Press. This textbook is now being translated into Chinese. His work on optical wireless communication was selected for publication in "100 Produkte der Zukunft (100 Products of the Future)" authored by Nobel Laureate T. W. Hänsch. He was an invited speaker at the TED Global conference 2011. Since 2007 Haas has been a Regular High Level Visiting Scientist supported by the Chinese "111 program" at Beijing University of Posts and Telecommunications (BUPT).

JOURNAL OF LIGHTWAVE TECHNOLOGY 1319

# Signal Shaping and Modulation for Optical Wireless Communication

Svilen Dimitrov, *Student Member, IEEE*, Sinan Sinanovic, *Member, IEEE*, and Harald Haas, *Member, IEEE*

***Abstract*—In this paper, a signal shaping framework for optical wireless communication (OWC) is proposed. The framework is tailored to the single-carrier pulse modulation techniques, such as multi-level pulse position modulation ($M$-PPM) and multi-level pulse amplitude modulation ($M$-PAM), and to multi-carrier transmission realized through multi-level quadrature amplitude modulation ($M$-QAM) with orthogonal frequency division multiplexing (OFDM). Optical OFDM (O-OFDM) transmission is generally accomplished via direct-current-biased optical OFDM (DCO-OFDM) or asymmetrically clipped optical OFDM (ACO-OFDM). Through scaling and DC-biasing the transmitted signal is optimally conditioned in accord with the optical power constraints of the transmitter front-end, i.e., minimum, average and maximum radiated optical power. The OWC systems are compared in a novel fashion in terms of electrical signal-to-noise ratio (SNR) requirement and spectral efficiency as the signal bandwidth exceeds the coherence bandwidth of the optical wireless channel. In order to counter the channel effect at high data rates, computationally feasible equalization techniques such as linear feed-forward equalization (FFE) and nonlinear decision-feedback equalization (DFE) are employed for single-carrier transmission, while multi-carrier transmission combines bit and power loading with single-tap equalization. It is shown that DCO-OFDM has the highest spectral efficiency for a given electrical SNR at high data rates when the additional direct current (DC) bias power is neglected. When the DC bias power is counted towards the signal power, DCO-OFDM outperforms PAM with FFE, and it approaches the performance of the more computationally intensive PAM with DFE.**

***Index Terms*—Optical devices, orthogonal frequency division multiplexing (OFDM), pulse modulation, signal processing, wireless communication.**

## I. Introduction

OPTICAL wireless communication (OWC) has proven to be a promising candidate for medium range high-speed data transmission with a potential to deliver several hundreds of Mbps data rate [1], [2]. In addition to being a complementary non-interfering solution alongside radio frequency (RF) technology, OWC has the advantage of license-free operation over a significantly wider spectrum.

The data transmission in OWC is achieved through intensity modulation and direct detection (IM/DD). Suitable candidates for data modulation are the single-carrier pulse modulation schemes such as $M$-PPM and $M$-PAM [3], [4]. At high data rates, where the 3-dB bandwidth of the pulse exceeds the coherence 3-dB bandwidth of the optical wireless channel, the RMS delay spread of the channel impulse response exceeds the pulse duration. Therefore, such techniques suffer from severe inter-symbol interference (ISI), limiting their throughput. In order to compensate for the channel effect, the optimum receiver employs maximum likelihood sequence detection (MLSD) [4]. Here, the MLSD algorithm chooses the sequence of symbols that maximizes the likelihood of the received symbols with the knowledge of the channel taps. Even though the Viterbi algorithm can be used for MLSD to reduce the computational effort, the complexity of MLSD still grows exponentially with the number of channel taps. Therefore, in practical system implementations, suboptimum equalization techniques with feasible complexity are used. These include the linear FFE or the nonlinear DFE with zero forcing (ZF) or minimum mean squared error (MMSE) criteria [4]. The superior bit-error ratio (BER) performance at a lower SNR requirement of DFE comes at a significantly increased complexity as compared to FFE [4].

Multi-carrier modulation has inherent robustness to ISI, because the symbol duration is significantly longer than the RMS channel delay spread. As a result, $M$-QAM O-OFDM promises to deliver very high data rates [2]. Because of the common use of a cyclic prefix (CP), the channel frequency response can be considered as flat fading over the subcarrier bandwidth [5], [6]. Thus, single-tap linear FFE with low complexity paired with bit and power loading can be used to minimize the channel effect [7], [8]. In the literature, two possible O-OFDM system realizations can be found: DCO-OFDM [9] and ACO-OFDM [10]. ACO-OFDM shows a greater optical power efficiency at the expense of a 50% reduction in spectral efficiency as compared to DCO-OFDM.

Imperfections of the optical front-ends due to the use of off-the-shelf components result in a limited linear dynamic range of radiated optical power [11]. Therefore, the transmitted signal is constrained between levels of minimum and maximum optical power. In addition, the average optical power level is constrained by the eye safety regulations [12] and/or the design requirements. In order to condition the signal in accord with these constraints, signal scaling in the digital signal processor (DSP) and DC-biasing in the analog circuitry is required. Since the $M$-PPM and $M$-PAM signals have a probability density function (PDF) with a finite support, they can fit the constraints without signal clipping. However, scaling and DC-biasing of the Gaussian time domain signals in ACO-OFDM and DCO-OFDM result in a nonlinear signal distortion which is precisely analyzed in [13]. In this paper, the analysis is employed in the formulation of the optimum signal scaling and DC-biasing to

Manuscript received August 16, 2011; revised November 18, 2011 and January 26, 2012; accepted January 26, 2012. Date of publication February 16, 2012; date of current version April 04, 2012. This work was supported by EADS UK Ltd. The work of H. Haas was supported by the Scottish Funding Council within the Edinburgh Research Partnership in Engineering and Mathematics between the University of Edinburgh and Heriot Watt University.

The authors are with the Institute for Digital Communications, Joint Research Institute for Signal and Image Processing, University of Edinburgh, Edinburgh EH9 3JL, U.K. (e-mail: s.dimitrov@ed.ac.uk; s.sinanovic@ed.ac.uk; h.haas@ed.ac.uk).

Digital Object Identifier 10.1109/JLT.2012.2188376

minimize the required electrical SNR per bit for a target BER. In general, in visible light communication (VLC) systems, the DC bias power is employed for illumination as a primary functionality. Therefore, it can be excluded from the calculation of the electrical signal power invested in the complementary data communication. In infrared (IR) communication systems, the DC bias power is constrained by the eye safety regulations [12], and it is generally included in the calculation of the electrical SNR.

On-off keying (OOK), essentially 2-PAM, and $M$-PPM have been compared in terms of electrical and optical power requirement in a dispersive channel with equalization in [3]. An increasing power requirement is demonstrated with the increase of the RMS channel delay spread or, equivalently, data rate. In a later study [14], $M$-PPM, $M$-PAM and multi-carrier $M$-QAM transmission, similar to $M$-QAM DCO-OFDM, have been compared assuming a flat fading channel in terms of optical power requirement and spectral efficiency. However, an unlimited non-negative dynamic range of the transmitter is considered which is hardly achievable in practice. Here, the non-negative $M$-QAM signal is scaled down to accommodate the large peak-to-average-power ratio (PAPR), resulting in an increased optical power requirement. Recently, a similar comparison has been reported in [15] for the multi-carrier transmission schemes ACO-OFDM and DCO-OFDM with a tolerable clipping distortion. To the best of the authors' knowledge, there is no comprehensive framework in literature which enables the comparison of single-carrier and multi-carrier transmission schemes in terms of spectral efficiency and electrical SNR requirement in a dispersive realistic optical wireless channel. In addition, a study on signal shaping for a practical dynamic range of the transmitter front-end, where the DC bias power is excluded or included in the calculation of the SNR is still considered an open issue.

In this paper, a signal shaping framework is proposed for $M$-PPM, $M$-PAM and $M$-QAM O-OFDM which through scaling and DC-biasing conditions the signals to fit within the optical power constraints of the transmitter front-end. For the Gaussian O-OFDM signals in particular, the signal shaping is optimum, i.e., the required electrical SNR is minimized. The systems are compared in a novel fashion in terms of electrical SNR requirement and spectral efficiency in the dispersive optical wireless channel, excluding or including the DC bias power in the calculation of the electrical SNR. When the additional DC bias power is neglected, DCO-OFDM and PAM show the greatest spectral efficiency for a flat fading channel in the SNR region above 6.8 dB. However, since O-OFDM with bit and power loading suffers a lower SNR penalty than PAM with DFE as the signal bandwidth exceeds the coherence bandwidth of the dispersive optical wireless channel, DCO-OFDM demonstrates a superior spectral efficiency. When the DC bias power is counted towards the electrical signal power, DCO-OFDM and ACO-OFDM suffer a greater SNR penalty due to the DC bias as compared to PAM and PPM, respectively. However, the presented optimum signal shaping framework enables O-OFDM to greatly reduce this penalty and minimize the gap to single-carrier transmission within 2 dB in the flat fading channel. When the signal bandwidth exceeds the channel coherence bandwidth, DCO-OFDM outperforms PAM with FFE, and it approaches the spectral efficiency of the more computationally intensive PAM with DFE, while ACO-OFDM outperforms PPM with FFE and DFE.

The rest of the paper is organized as follows. Section II presents the system model and the signal shaping framework for $M$-PPM, $M$-PAM and $M$-QAM O-OFDM. Single-carrier and multi-carrier transmission are compared in terms of electrical SNR requirement and spectral efficiency in Section III. Finally, Section IV concludes the paper.

## II. System Model and Signal Shaping

The conventional discrete model for a noisy communication link is employed in this study:

$$\mathbf{y} = \mathbf{h} * \mathbf{x} + \mathbf{n} \tag{1}$$

where $\mathbf{y}$ represents the received replica of the transmitted signal, $\mathbf{x}$, which is convolved with the channel impulse response, $\mathbf{h}$, and it is distorted by additive white Gaussian noise (AWGN), $\mathbf{n}$, at the receiver. In OWC, $\mathbf{n}$ has a zero-mean real-valued Gaussian distribution. After optical-to-electrical (O/E) conversion, it has an electrical power spectral density (PSD) of $N_0/2$ in $M$-PPM and $M$-PAM. In optical OFDM with $M$-QAM, the PSD of $\mathbf{n}$ amounts to $N_0$ because of the two-dimensional constellation [16]. Here, $*$ stands for discrete linear convolution. Without loss of generality, the system analysis is presented in terms of discrete signal vectors. Here, $\mathbf{x}$ contains $Z_{\mathbf{x}}$ samples, $\mathbf{h}$ has $Z_{\mathbf{h}}$ samples, and as a result, $\mathbf{n}$ and $\mathbf{y}$ have $Z_{\mathbf{x}} + Z_{\mathbf{h}} - 1$ samples [16]. The discrete signal vectors are obtained by sampling of the equivalent continuous-time signals. The sampling rates over a time period of $T$ differ in the considered systems, and the details are presented below. Through scaling and DC-biasing, $\mathbf{x}$ can be conditioned within the optical power constraints of the transmitter front-end. The nonlinear transfer characteristic of the LED can be compensated by pre-distortion [17]. A linear dynamic range of the transmitter is obtainable, however, only between levels of minimum and maximum radiated optical power, $P_{\mathrm{Tx,min}}$ and $P_{\mathrm{Tx,max}}$ [13]. Furthermore, the eye safety regulations [12] and/or the design requirements constrain the level of radiated average optical power to $P_{\mathrm{Tx,avg}}$. The signal scaling and DC-biasing are discussed in detail for OWC schemes below.

It has been shown in [3] that line-of-sight (LOS) and non-line-of-sight (NLOS) optical wireless channels can be accurately modeled by the impulse response function $h(t) = g_{\mathrm{h(opt)}} f(t)$, where $f(t) = U(t) 6a^6/(t+a)^7$. Here, $g_{\mathrm{h(opt)}}$ stands for the optical path gain coefficient, $U(\cdot)$ is the unit step function, and $a$ is related to the RMS delay spread, $D$, by $a = D\sqrt{11/13}$. The 3-dB coherence bandwidth of the channel can be expressed as $B_{\mathrm{c}} = 1/(5D)$ [18]. RMS delay spreads between 1.3 ns and 12 ns are reported for LOS links, whereas RMS delay spreads between 7 and 13 ns are reported for NLOS links [3]. The channel taps in the vector $\mathbf{h}$ are obtained by sampling of the channel impulse response at the sampling frequency of the received signal, $\mathbf{y}$. The optical path gain can be expressed as $g_{\mathrm{h(opt)}} = I_{\mathrm{PD}} S_{\mathrm{PD}} \rho_{\mathrm{PD}} G_{\mathrm{TIA}} / (\mathrm{E}[\mathbf{x}] \sqrt{r_{\mathrm{load}}})$, where $I_{\mathrm{PD}}$ denotes the average irradiance of the PD, $S_{\mathrm{PD}}$ is the photosensitive area of the PD, $\rho_{\mathrm{PD}}$ is the responsivity of the PD, $G_{\mathrm{TIA}}$ is the gain of the transimpedance amplifier (TIA), $\mathrm{E}[\mathbf{x}]$

is the average transmitted optical power, where $\mathrm{E}[\cdot]$ stands for the expectation operator, and $r_{\mathrm{load}}$ is the load resistance over which the received current is measured [19], [20]. In addition, the optical path gain can be related to the electrical path gain, $g_{\mathrm{h(elec)}}$, as follows:

$$g_{\mathrm{h(elec)}} = g_{\mathrm{h(opt)}}^2 \frac{1}{B} \int_{-B/2}^{B/2} |F(f)|^2 \, df \tag{2}$$

where $F(f)$ is the Fourier transform of $f(t)$, and $B$ is the double-sided signal bandwidth.

In $M$-PPM and $M$-PAM, the RMS delay spread of the channel becomes comparable to or larger than the pulse duration at high data rates which causes a severe ISI. Equivalently, the signal bandwidth exceeds the channel coherence bandwidth. In general, similar effects are also caused by the low-pass frequency response of the front-end components, such as LEDs, PDs, and amplifiers. As a result, the BER performance is degraded, and the systems effectively incur an SNR penalty. In practical system implementations, multi-tap linear FFE and nonlinear DFE with ZF or MMSE criteria are deployed to reduce the SNR penalty. Since an equalizer with an MMSE criterion requires a higher computational effort, and it only reduces the SNR penalty by approximately 0.5 dB as compared to the ZF criterion, ZF is generally employed. The gain factor, $G_{\mathrm{EQ}}$, of a linear ZF FFE is given as follows [4]:

$$G_{\mathrm{EQ}} = \left( \frac{1}{B} \int_{-B/2}^{B/2} \frac{1}{W(f)} \, df \right)^{-1} \tag{3}$$

where $W(f)$ is expressed as follows:

$$W(f) = \sum_{n=-\infty}^{\infty} |V(f - nB) H(f - nB)|^2. \tag{4}$$

Here, $V(f)$ and $H(f)$ are the Fourier transforms of the impulse responses of the pulse shaping filter at the transmitter, $v(t)$, and the optical wireless channel, $h(t)$, respectively. The gain factor of a nonlinear ZF DFE is given as follows [4]:

$$G_{\mathrm{EQ}} = \exp\left( \frac{1}{B} \int_{-B/2}^{B/2} \ln(W(f)) \, df \right). \tag{5}$$

The gain factor $G_{\mathrm{EQ}}$ represents the theoretical lower bound for the electrical SNR penalty which the BER performance incurs at high data rates. This lower bound is achieved when an infinite number of channel taps are considered in the FFE and DFE which is hardly achievable in practice because of the significantly increased computational complexity.

In multi-carrier systems such as OFDM-based OWC, the RMS delay spread is significantly shorter than the symbol duration, and therefore the equalization process is considerably simplified to single-tap equalization [6]. The ISI and the inter-carrier interference (ICI) are completely eliminated by the use of a large number of subcarriers and a CP which has a negligible effect on the electrical SNR requirement and spectral efficiency [5]. A large number of subcarriers, e.g., greater than 64, also ensures that the time domain signal follows a close to Gaussian distribution [21]. This assumption greatly simplifies the derivations throughout the paper. In addition, the CP transforms the linear convolution with the channel into a cyclic convolution, facilitating a single-tap linear FFE and eliminating the need for a nonlinear DFE. Even though the channel can be considered as flat fading over the individual subcarriers, the non-flat channel frequency response over the entire OFDM frame still leads to an SNR penalty for the average frame BER. Here, the single-tap equalizer is generally paired with bit and power loading [7], [8], in order to minimize this SNR penalty. Here, the gain factor of the equalizer, $G_{\mathrm{EQ}}$, is obtained via a Monte Carlo simulation.

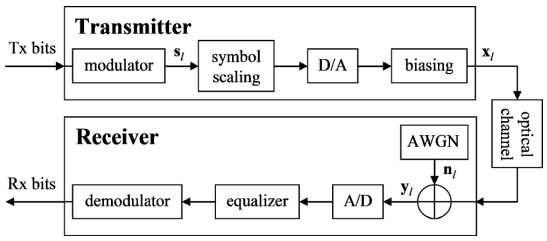


Fig. 1. Block diagram of single-carrier transmission in OWC using pulse modulation.

### A. M-PPM

The block diagram of single-carrier transmission with pulse modulation is presented in Fig. 1. In $M$-PPM, $\log_2(M)$ equiprobable input bits form a time domain symbol. It is a sequence of $M$ chips, where one chip has a current level of $\sqrt{MP_{\mathrm{s(elec)}}}$, and the other $M-1$ chips are set to zero. Here, $P_{\mathrm{s(elec)}}$ is the average electrical power of the $M$-PPM symbol, and it is related to the average electrical energy per bit, $E_{\mathrm{b(elec)}}$, as follows: $E_{\mathrm{b(elec)}} = MP_{\mathrm{s(elec)}}/(\log_2(M)B)$. The $M$-PPM symbol with a double-sided bandwidth of $B = M/T$ has a duration of $T$, and it is grouped in the train of $L$ symbols, $\mathbf{s}_l$, where $l$, $l = 0, 1, \ldots, L-1$, is the symbol index. Thus, the spectral efficiency of $M$-PPM is $\log_2(M)/M$ bits/s/Hz [3], [4]. The train of symbols, $\mathbf{s}_l$, is scaled by a factor, $\alpha$, in order to fit within the front-end optical power constraints. Next, the signal is passed through a digital-to-analog (D/A) converter. Here, a pulse shaping filter with a real-valued impulse response of $v(t)$ is applied to transform the train of digital chips into a train of continuous-time pulses. In $M$-PPM, because of the fact that the information carrying pulse has an optical power level greater than $P_{\mathrm{Tx,min}}$, zero bias is required. As a result, the transmitted signal vector, $\mathbf{x}$, has a length of $Z_{\mathbf{x}} = LM$, and it can be expressed as follows:

$$\mathbf{x}_l = \alpha \mathbf{s}_l \tag{6}$$

where

$$\alpha = \min(P_{\mathrm{Tx,max}}, MP_{\mathrm{Tx,avg}}) / \sqrt{MP_{\mathrm{s(elec)}}}. \tag{7}$$

The transmitter front-end constrains $P_{\mathrm{Tx,min}}$ and $P_{\mathrm{Tx,max}}$, whereas $P_{\mathrm{Tx,avg}}$ is independently imposed by the eye-safety regulations and/or the design requirements. In general, constraining the average optical power level to $\mathrm{E}[\mathbf{x}_l] \leq P_{\mathrm{Tx,avg}}$ results in a suboptimal BER performance of the OWC systems. The best BER performance is obtained when this constraint is relaxed, i.e., when $\mathrm{E}[\mathbf{x}_l]$ is allowed to assume any level in the dynamic range between $P_{\mathrm{Tx,min}}$ and $P_{\mathrm{Tx,max}}$.

In order to relate the average optical symbol power, $P_{\mathrm{s(opt)}}$, to the electrical symbol power, $P_{\mathrm{s(elec)}}$, the signal is subjected to O/E conversion defined as follows:

$$P_{\mathrm{s(elec)}} = \frac{\mathrm{E}[\mathbf{x}_l^2]}{\mathrm{E}[\mathbf{x}_l]^2} P_{\mathrm{s(opt)}}^2 \tag{8}$$

where $\mathrm{E}[\mathbf{x}_l]^2 = \min(P_{\mathrm{Tx,max}}/M, P_{\mathrm{Tx,avg}})^2$ and $\mathrm{E}[\mathbf{x}_l^2] = \min(P_{\mathrm{Tx,max}}, MP_{\mathrm{Tx,avg}})^2/M$ in $M$-PPM. Since the time domain signal in $M$-PPM has a PDF with a finite support, it can be fitted within $P_{\mathrm{Tx,min}}$ and $P_{\mathrm{Tx,max}}$ without clipping. Thus, the following holds for its average optical signal power: $\mathrm{E}[\mathbf{x}_l] = P_{\mathrm{s(opt)}} = \min(P_{\mathrm{Tx,max}}/M, P_{\mathrm{Tx,avg}}) \leq P_{\mathrm{Tx,avg}}$.

In this paper, the BER performance of the OWC systems is compared for equal average electrical signal power, $P_{\mathrm{s(elec)}}$, and equal bandwidth, $B$. In addition, the BER is assessed as a function of the electrical SNR per bit, i.e., the average electrical bit energy normalized to the power spectral density of the AWGN, $\gamma_{\mathrm{b(elec)}} = E_{\mathrm{b(elec)}}/N_0$.

In $M$-PPM, the received signal, $\mathbf{y}_l$, is passed through a matched filter, and at the analog-to-digital (A/D) converter it is sampled at a frequency of $M/T$ or higher [3], [4]. The BER system performance in the optical wireless channel with AWGN and equalization has been discussed in [3]. The received $M$-PPM symbol can be treated as an on-off-keying (OOK) sequence, and the information bits can be decoded by means of a hard-decision decoder. For this approach, an analytical union bound of the BER as a function of the electrical SNR per bit is presented and verified through simulation. Alternatively, the BER performance can be enhanced by means of soft-decision decoding based on the position of the chip with the maximum level within the received $M$-PPM symbol. However, the analytical BER performance of this decoder is not derived. A union bound for the symbol error rate (SER) in soft-decision decoding can be obtained as a summation of the probabilities of chips $c_i, i = 2, 3, \ldots, M$, being greater than an intended chip $c_1$ within the $M$-PPM symbol. Since $c_i$ are equally probable, a union bound for the SER can be expressed as follows:

$$\begin{aligned}\mathrm{SER} &\leq (M-1)P(c_2|c_1) \\ &= (M-1)\int_{-\infty}^{\infty} Q\left(\frac{s\sqrt{2}}{\sqrt{N_0}}\right)\frac{1}{\sqrt{\pi N_0}} \\ &\quad \times \exp\left(-\frac{\left(s-\sqrt{G_{\mathrm{EQ}}\log_2(M)E_{\mathrm{b(elec)}}}\right)^2}{N_0}\right) ds\end{aligned} \tag{9}$$

where $Q(\cdot)$ is the complementary cumulative distribution function (CCDF) of a standard normal distribution with zero mean and unity variance. The BER can be obtained as follows:

$$\mathrm{BER} = \frac{M\log_2(M)}{2(M-1)}\mathrm{SER}. \tag{10}$$

### B. M-PAM

The block diagram of $M$-PAM is presented in Fig. 1. Here, $\log_2(M)$ equiprobable input bits form a time domain symbol with a double-sided bandwidth of $B = 1/T$ and a duration of $T$. The symbols are assigned to current levels of $p\sqrt{3P_{\mathrm{s(elec)}}}/\sqrt{(M-1)(M+1)}$, $p = \pm 1, \pm 3, \ldots, \pm M-1$, and these are grouped in the train of $L$ symbols, $\mathbf{s}_l$. Here, $E_{\mathrm{b(elec)}} = P_{\mathrm{s(elec)}}/(\log_2(M)B)$. The resulting spectral efficiency of $M$-PAM is $\log_2(M)$ bits/s/Hz [3], [4]. The train of symbols is scaled and passed through the D/A converter. Since $\mathbf{s}_l$ is bipolar, it requires a DC bias, $\beta_{\mathrm{DC}}$, to fit within the front-end optical power constraints. The transmitted signal vector, $\mathbf{x}$, has a length of $Z_{\mathbf{x}} = L$, and it can be expressed as follows:

$$\mathbf{x}_l = \alpha\mathbf{s}_l + \beta_{\mathrm{DC}} \tag{11}$$

where

$$\alpha = \sqrt{\frac{M+1}{3(M-1)P_{\mathrm{s(elec)}}}} \times \min(P_{\mathrm{Tx,max}} - \beta_{\mathrm{DC}}, \beta_{\mathrm{DC}} - P_{\mathrm{Tx,min}}). \tag{12}$$

In order to obtain the E/O conversion in $M$-PAM from (8), the second moment of $\mathbf{x}$ can be expressed as follows:

$$\mathrm{E}\left[\mathbf{x}_l^2\right] = \frac{M+1}{3(M-1)}\min(P_{\mathrm{Tx,max}} - \beta_{\mathrm{DC}}, \beta_{\mathrm{DC}} - P_{\mathrm{Tx,min}})^2 + \beta_{\mathrm{DC}}^2. \tag{13}$$

Because of the fact that the $M$-PAM time domain signal has a PDF with a finite support, it can be fitted within $P_{\mathrm{Tx,min}}$ and $P_{\mathrm{Tx,max}}$ without clipping. Thus, the following holds for its average optical power: $\mathrm{E}[\mathbf{x}_l] = P_{\mathrm{s(opt)}} = \beta_{\mathrm{DC}} \leq P_{\mathrm{Tx,avg}}$.

The received signal, $\mathbf{y}_l$, is passed through a matched filter, and at the A/D converter it is sampled at a frequency of $1/T$ or higher [3], [4]. After equalization of the channel effect, a hard-decision decoder can be employed to obtain the received bits. As a result, the effective electrical SNR per bit in $M$-PAM, $\Gamma_{\mathrm{b(elec)}}$, can be expressed as follows:

$$\Gamma_{\mathrm{b(elec)}} = \gamma_{\mathrm{b(elec)}} G_{\mathrm{EQ}} G_{\mathrm{DC}}. \tag{14}$$

Here, $G_{\mathrm{EQ}}$ is given in (3) and (5). The gain factor $G_{\mathrm{DC}}$ denotes the attenuation of the useful electrical signal power of $\mathbf{x}$ due to the DC component, and it is given as follows [13]:

$$G_{\mathrm{DC}} = \frac{\mathrm{E}[(\mathbf{x}_l - \beta_{\mathrm{DC}})^2]}{\mathrm{E}\left[\mathbf{x}_l^2\right]}. \tag{15}$$

The exact closed form expression for the BER performance of $M$-PAM in AWGN has been presented in [22] as a summation of $M$ terms. A tight approximation for BER bellow $10^{-2}$ can be obtained when only considering the error contributed by the closest symbols in the constellation as follows [4]:

$$\mathrm{BER} = \frac{N_{\mathrm{s}}}{G_{\mathrm{GC}}\log_2(M)} Q\left(d_{\mathrm{s}}\sqrt{\log_2(M)\Gamma_{\mathrm{b(elec)}}}\right). \tag{16}$$

In $M$-PAM, an intended symbol has an average number of $N_{\mathrm{s}} = 2(M-1)/M$ neighboring symbols. The gain introduced by Gray coding of the bits on the symbols is denoted by $G_{\mathrm{GC}} = 1$. The distance between an intended symbol and the closest interfering symbol is given by $d_{\mathrm{s}} = \sqrt{6/(M^2-1)}$.

### C. M-QAM O-OFDM

The block diagram for multi-carrier O-OFDM transmission is presented in Fig. 2. The two O-OFDM realizations known as DCO-OFDM [9] and ACO-OFDM [10] are studied. In general,

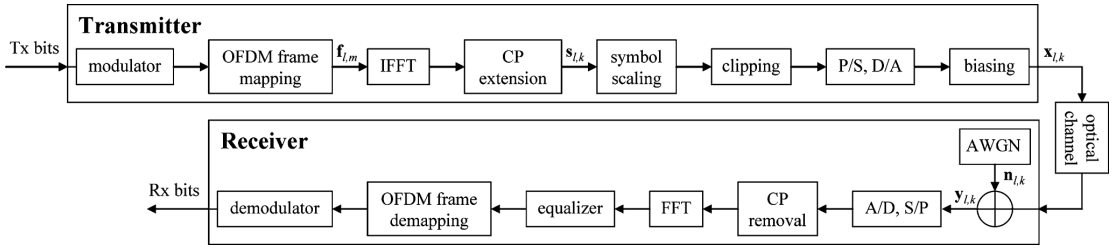


Fig. 2. Block diagram of multi-carrier transmission in OWC using OFDM.

$N$ subcarriers form the $l$th OFDM frame, $\mathbf{f}_{l,m}$, corresponding to the $l$th OFDM symbol, where $m$, $m = 0, 1, \ldots, N-1$, is the subcarrier index. Each subcarrier occupies a bandwidth of $1/NT$ in a total OFDM frame double-sided bandwidth of $B = 1/T$. The two O-OFDM systems utilize a different portion of the available bandwidth, and the bandwidth utilization factor is denoted by $G_{\mathrm{B}}$, where $G_{\mathrm{B}} = (N-2)/N$ in DCO-OFDM and $G_{\mathrm{B}} = 0.5$ in ACO-OFDM. In order to ensure a real-valued time domain signal, both schemes have the Hermitian symmetry imposed on the OFDM frame, and the subcarriers with indices $m = \{0, N/2\}$ are set to zero. In DCO-OFDM, $(N-2)/2$ subcarriers in the first half of the frame carry the information. In ACO-OFDM, only the odd subcarriers are enabled, while every even subcarrier is set to zero. Both schemes can utilize bit and power loading of the frequency domain subcarriers, in order to optimally adapt the signal to the channel conditions. For a desired bit rate, the Levin-Campello algorithm [7], [8] can be applied, in order to maximize the received power margin, or equivalently, in order to minimize the required electrical SNR. The optimum solution achieved by the algorithm yields the $\mathbf{b}_m$ bits which modulate the complex-valued information carrying frequency domain subcarrier from $\mathbf{f}_{l,m}$ in an $M$-QAM fashion. In addition, the algorithm provides subcarrier power scaling factors, $\mathbf{w}_m$, which ensure an equal maximized received power margin for every active subcarrier. Without loss of generality, only integer average bit rates, i.e., $\mathrm{E}[\mathbf{b}_m] = \log_2(M)$, are considered in this study. In both systems, the unitary inverse fast Fourier transform (IFFT) and fast Fourier transform (FFT) are utilized as multiplexing and demultiplexing techniques at the transmitter and the receiver, respectively [6]. The $l$th OFDM symbol in the train of $L$ symbols, $\mathbf{s}_l$, is obtained by the IFFT of the $l$th OFDM frame in the train of $L$ frames, $\mathbf{f}_l$. Next, $N_{\mathrm{CP}}$ samples from the end of each OFDM symbol are appended at the beginning of the symbol, creating the CP extension, in order to remove the ISI and ICI [6], [16]. Here, the time domain sample index within the $l$th OFDM symbol with CP, $\mathbf{s}_{l,k}$, is denoted by $k$, $k = 0, 1, \ldots, N + N_{\mathrm{CP}} - 1$. As a result, the time domain OFDM symbol with CP occupies a double-sided bandwidth of $B = 1/T$, and it has a duration of $(N + N_{\mathrm{CP}})T$. Because of the Hermitian symmetry, the resulting spectral efficiency of $M$-QAM O-OFDM amounts to $\log_2(M)G_{\mathrm{T}}G_{\mathrm{B}}/2$ bits/s/Hz, where $G_{\mathrm{T}} = N/(N+N_{\mathrm{CP}})$ is the utilization factor for the information carrying time. The train of OFDM symbols with CPs, $\mathbf{s}_{l,k}$, follows a close to Gaussian distribution for IFFT/FFT sizes greater than 64 [21]. In order to fit the signal within the optical power constraints of the transmitter, the train of OFDM symbols is scaled and clipped at normalized bottom and top clipping levels of $\lambda_{\mathrm{bottom}}$ and $\lambda_{\mathrm{top}}$ relative to a standard normal distribution [13]. In DCO-OFDM, $\lambda_{\mathrm{bottom}} = (P_{\mathrm{Tx,min}} - \beta_{\mathrm{DC}})/\sigma$, whereas in ACO-OFDM, $\lambda_{\mathrm{bottom}} = \max((P_{\mathrm{Tx,min}} - \beta_{\mathrm{DC}})/\sigma, 0)$. Here, $\sigma$ is the target standard deviation of the non-clipped time domain signal. In both schemes, $\lambda_{\mathrm{top}} = (P_{\mathrm{Tx,max}} - \beta_{\mathrm{DC}})/\sigma$. The clipping levels in DCO-OFDM can be negative and/or positive, whereas in ACO-OFDM, these are strictly non-negative. For reasons of plausibility, $\lambda_{\mathrm{top}} > \lambda_{\mathrm{bottom}}$. Next, the train of symbols with CPs is subjected to a parallel-to-serial (P/S) conversion, and it is passed through the D/A converter. Here, a pulse shaping filter is applied to obtain the continuous-time signal. As a next step in the signal shaping framework to fit the front-end optical power constraints, the signal is DC biased by $\beta_{\mathrm{DC}}$. Therefore, the transmitted signal vector, $\mathbf{x}$, with a length of $Z_{\mathbf{x}} = L(N + N_{\mathrm{CP}})$ can be expressed as follows:

$$\mathbf{x}_{l,k} = \mathrm{CLIP}[\alpha \mathbf{s}_{l,k}] + \beta_{\mathrm{DC}} \tag{17}$$

where

$$\alpha = \sigma \sqrt{\frac{N-1}{\sum_{m=0}^{N-1} |\mathbf{f}_{l,m}|^2}}. \tag{18}$$

Before the scaling clock, the average electrical power of the $G_{\mathrm{B}}N$ QAM symbols on the enabled subcarriers amounts to $P_{\mathrm{s(elec)}} = 1$. In order to maintain the signal variance of $\sigma^2$, the power of the enabled subcarriers is scaled through $\alpha$ to $P_{\mathrm{s(elec)}}/G_{\mathrm{B}}$, where $P_{\mathrm{s(elec)}} = \sigma^2$. Thus, the average bit energy can be expressed as follows: $E_{\mathrm{b(elec)}} = \sigma^2/(\log_2(M)G_{\mathrm{T}}G_{\mathrm{B}}B)$. The nonlinear clipping distortion represented by the $\mathrm{CLIP}[\cdot]$ operator can be translated by means of the Bussgang theorem [23] and the central limit theorem [24] into a gain factor, $K$, representing the attenuation of the information carrying subcarriers plus a zero-mean complex Gaussian noise component with a variance of $\sigma^2_{\mathrm{clip}}$. In DCO-OFDM and ACO-OFDM, $K$ is given as follows [13]:

$$K = Q(\lambda_{\mathrm{bottom}}) - Q(\lambda_{\mathrm{top}}). \tag{19}$$

The variance of the clipping noise in DCO-OFDM and ACO-OFDM, respectively, can be expressed as follows [13]:

$$\begin{aligned}\sigma^2_{\mathrm{clip}} = P_{\mathrm{s(elec)}} \big(K - K^2 - (\phi(\lambda_{\mathrm{bottom}}) - \phi(\lambda_{\mathrm{top}}) \\ + (1 - Q(\lambda_{\mathrm{bottom}}))\lambda_{\mathrm{bottom}} + Q(\lambda_{\mathrm{top}})\lambda_{\mathrm{top}})^2 \\ + (1 - Q(\lambda_{\mathrm{bottom}}))\lambda^2_{\mathrm{bottom}} + Q(\lambda_{\mathrm{top}})\lambda^2_{\mathrm{top}} \\ + \phi(\lambda_{\mathrm{bottom}})\lambda_{\mathrm{bottom}} - \phi(\lambda_{\mathrm{top}})\lambda_{\mathrm{top}})\end{aligned} \tag{20}$$

$$\sigma^2_{\text{clip}} = P_{\text{s(elec)}} \left( K(\lambda^2_{\text{bottom}} + 1) - 2K^2 - \lambda_{\text{bottom}}(\phi(\lambda_{\text{bottom}}) - \phi(\lambda_{\text{top}})) - \phi(\lambda_{\text{top}})(\lambda_{\text{top}} - \lambda_{\text{bottom}}) + Q(\lambda_{\text{top}})(\lambda_{\text{top}} - \lambda_{\text{bottom}})^2 \right) \quad (21)$$

where $\phi(\cdot)$ stands for the PDF of a standard normal distribution. In addition to the distortion of the information carrying subcarriers, time domain signal clipping modifies the average optical power of the transmitted signal as follows:

$$\text{E}[\mathbf{x}_l] = \sigma(\lambda_{\text{top}} Q(\lambda_{\text{top}}) - \lambda_{\text{bottom}} Q(\lambda_{\text{bottom}}) + \phi(\lambda_{\text{bottom}}) - \phi(\lambda_{\text{top}})) + P_{\text{bottom}} \leq P_{\text{Tx,avg}}. \quad (22)$$

In DCO-OFDM, $P_{\text{bottom}} = P_{\text{Tx,min}}$, while in ACO-OFDM, $P_{\text{bottom}} = \max(P_{\text{Tx,min}}, \beta_{\text{DC}})$ because of the default zero-level clipping. Thus, for a given set of front-end optical power constraints, one can obtain the signal scaling factor, $\alpha$, for a target signal variance, $\sigma^2$, and the required DC bias, $\beta_{\text{DC}}$, from (18) and (22). The optimum choice of these design parameters is elaborated below.

Since the signal is clipped, the resulting average optical power of the signal, $\text{E}[\mathbf{x}_l]$, differs from the undistorted optical power of the OFDM symbol, $P_{\text{s(opt)}}$. In DCO-OFDM, $P_{\text{s(opt)}} = \beta_{\text{DC}}$, whereas in ACO-OFDM, $P_{\text{s(opt)}} = (\beta_{\text{DC}} + \sigma/\sqrt{2\pi})$. The O/E conversion is obtained in DCO-OFDM and ACO-OFDM, respectively, as follows:

$$P_{\text{s(elec)}} = \frac{\sigma^2 + \beta^2_{\text{DC}}}{\beta^2_{\text{DC}}} P^2_{\text{s(opt)}} \quad (23)$$

$$P_{\text{s(elec)}} = \frac{2\pi\beta^2_{\text{DC}} + 2\sigma\beta_{\text{DC}}\sqrt{2\pi} + \pi\sigma^2}{2\pi\beta^2_{\text{DC}} + 2\sigma\beta_{\text{DC}}\sqrt{2\pi} + \sigma^2} P^2_{\text{s(opt)}}. \quad (24)$$

The received signal, $\mathbf{y}_{l,k}$, is passed through a matched filter, and at the A/D converter it is sampled at a frequency of $1/T$ or higher [6], [16]. Next, the CP extension of every OFDM symbol is removed, and after serial-to-parallel (S/P) conversion the signal is passed through an FFT block back to the frequency domain. A single-tap equalizer and a hard-decision decoder are employed to obtain the received bits. Thus, the effective electrical SNR per bit on an enabled subcarrier in O-OFDM, $\Gamma^m_{\text{b(elec)}}$, is given for linear ZF FFE as follows:

$$\Gamma^m_{\text{b(elec)}} = \frac{\mathbf{w}_m K^2}{\frac{\mathbf{b}_m G_{\text{B}} \sigma^2_{\text{clip}}}{P_{\text{s(elec)}}} + \frac{G_{\text{B}} \gamma^{-1}_{\text{b(elec)}}}{G_{\text{T}} G_{\text{DC}} |H(f)|^2}} \quad (25)$$

where $H(f)$ is the channel frequency response on the intended subcarrier. The factor $G_{\text{DC}}$ can be expressed in DCO-OFDM and ACO-OFDM, respectively, as follows [13]:

$$G_{\text{DC}} = \frac{\sigma^2}{\sigma^2 + \beta^2_{\text{DC}}} \quad (26)$$

$$G_{\text{DC}} = \frac{\sqrt{2\pi}\sigma^2}{\sqrt{2\pi}\sigma^2 + 4\sigma\beta_{\text{DC}} + 2\sqrt{2\pi}\beta^2_{\text{DC}}}. \quad (27)$$

The exact closed form expression for the BER performance of square and cross $M$-QAM constellations in AWGN has been presented as a summation of $M$ terms in [22] and [25], respectively. However, the same tight approximation from (16) can be applied, and the respective parameters are given in Table I [4], [26]. Thus, the BER on the intended subcarrier, $\text{BER}_m$, can be obtained by inserting (25) into (26), considering the parameters from Table I for the number of loaded bits. As a result, the link BER can be obtained as the average of the BER of all enabled subcarriers: $\text{BER} = \text{E}[\text{BER}_m]$.

TABLE I
PARAMETERS IN (16) FOR $M$-QAM

| | $N_{\text{s}}$ | $G_{\text{GC}}$ | $d_{\text{s}}$ |
|---|---|---|---|
| BPSK | 1 | 1 | 2 |
| $M = 2^{2i}$, $i = 1, 2, ...$ | $4 - \frac{4}{\sqrt{M}}$ | 1 | $\sqrt{\frac{3}{M-1}}$ |
| $M = 8$ | 3 | $\frac{4}{5}$ | $\sqrt{\frac{2}{3+\sqrt{3}}}$ |
| $M = 32$ | $\frac{13}{4}$ | $\frac{6}{7}$ | $\frac{1}{\sqrt{10}}$ |
| $M = 2^{2i+1}$, $i = 3, 4, ...$ | $4 - \frac{6}{\sqrt{2M}}$ | $\frac{6M}{6M + 3\sqrt{2M} + 2}$ | $\sqrt{\frac{96}{31M - 32}}$ |

The choice of the biasing parameters, such as the signal variance, $\sigma^2$, and the DC bias, $\beta_{\text{DC}}$, which minimize the link BER for a target $\gamma_{\text{b(elec)}}$ can be formulated as an optimization problem. Additional input parameters for the optimization are the front-end optical power constraints, $P_{\text{Tx,min}}$, $P_{\text{Tx,max}}$ and $P_{\text{Tx,avg}}$, and the desired average bit rate, equivalent to a QAM modulation order, $M$. This optimization problem is summarized in Table II, and its solution can be used to iteratively solve the dual problem, i.e., the minimization of the $\gamma_{\text{b(elec)}}$ for a target BER.

The optimization problem from Table II has a trivial solution when the DC bias power is not included in the calculation of the effective electrical SNR per bit, $\Gamma_{\text{b(elec)}}$, i.e., when $G_{\text{DC}} = 1$. From (19) it follows that $K^2$ decreases when the signal is more severely clipped. In addition, because of the fact that the clipping noise variance is non-negative, $\Gamma_{\text{b(elec)}}$ is maximized and BER is minimized when the signal clipping is minimized. For instance, such a clipping scenario in DCO-OFDM is represented by $\lambda_{\text{bottom}} = -4$ and $\lambda_{\text{top}} = 4$. It is similar to the one used in [15], in order to minimize the clipping distortion. The equivalent scenario for ACO-OFDM is $\lambda_{\text{bottom}} = 0$ and $\lambda_{\text{top}} = 4$. These setups enable modulation orders as high as $M = 1024$ with a deviation from the true minimum required $\gamma_{\text{b(elec)}}$ of only 0.1 dB at BER of $10^{-3}$.

However, the optimization problem has a non-trivial solution when the DC bias power is included in the calculation of the effective electrical SNR per bit, $\Gamma_{\text{b(elec)}}$, i.e., when $G_{\text{DC}} < 1$. The analytical approach to solve the minimization problem leads to a system of nonlinear transcendental equations which does not have a closed-form solution. Therefore, a numerical optimization procedure is required, and the minimization can be carried out through a computer simulation for a particular choice of front-end optical power constraints. In general, the formal proof of convexity of the objective function from Table II over the constrained function domain is equally intractable as the analytical minimization approach. However, the convexity can be illustrated by means of a computer simulation. A practical linear dynamic range of a Vishay TSHG8200 LED between $P_{\text{Tx,min}} = 5$ mW and $P_{\text{Tx,max}} = 50$ mW at room temperature is assumed at the transmitter [11]. It can be inferred from [19] that this LED is eye-safe, even if the average optical power

TABLE II
MINIMIZATION OF BER OVER $\sigma$ AND $\beta_{\mathrm{DC}}$ FOR GIVEN TARGET $\gamma_{\mathrm{b(elec)}}$, $M$, $P_{\mathrm{Tx,min}}$, $P_{\mathrm{Tx,max}}$ AND $P_{\mathrm{Tx,avg}}$

| | |
|---|---|
| Given: | $\gamma_{\mathrm{b(elec)}}$, $M$, $P_{\mathrm{Tx,min}}$, $P_{\mathrm{Tx,max}}$ and $P_{\mathrm{Tx,avg}}$ |
| Find: | $\underset{\substack{\sigma \geq 0 \\ \beta_{\mathrm{DC}} \geq 0}}{\operatorname{argmin}} \ \mathrm{BER}(\sigma, \beta_{\mathrm{DC}}) \geq 0$ |
| Constraints: | $\mathrm{E}[\mathbf{x}_l] \leq P_{\mathrm{Tx,avg}}$<br>$\lambda_{\mathrm{top}} > \lambda_{\mathrm{bottom}}$ in DCO-OFDM<br>$\lambda_{\mathrm{top}} > \lambda_{\mathrm{bottom}} \geq 0$ in ACO-OFDM |

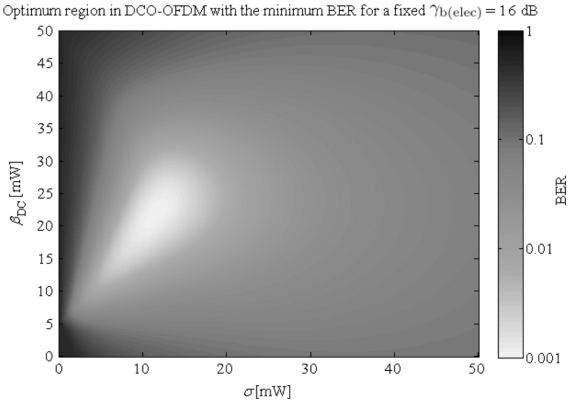


Fig. 3. Minimum BER in DCO-OFDM as a function of $\sigma$ and $\beta_{\mathrm{DC}}$ for a fixed $\gamma_{\mathrm{b(elec)}} = 16$ dB, 4-QAM with linear ZF FFE, $h(t) = \delta(t)$, $P_{\mathrm{Tx,min}} = 5$ mW and $P_{\mathrm{Tx,max}} = 50$ mW. DC bias power is included in the electrical SNR.

level is set to the maximum of the dynamic range. Therefore, the average optical power constraint is relaxed, in order to obtain the best BER system performance for the given dynamic range of the front-end. The objective function from Table II is illustrated in Figs. 3 and 4 for DCO-OFDM and ACO-OFDM, respectively, in the case of a flat fading channel with impulse response of $h(t) = \delta(t)$, where $\delta(\cdot)$ is the Dirac delta function. It is shown that the objective function for a flat fading channel has a unique optimum convex region. In OFDM systems, the dispersive channel is represented by a superposition of orthogonal flat fading channels. Therefore, the objective average BER function can be obtained as the average of the BER functions for each flat fading channel which are shown to be convex. Since the expectation operator is a non-negative weighted summation, it preserves the convexity [27]. Therefore, the objective BER function in the dispersive channel remains convex.

The details of the optimum biasing parameters for the above-mentioned dynamic range of the transmitter front-end and QAM modulation orders, $M = \{4, 16, 64, 256, 1024\}$, with linear ZF FFE in a flat fading channel are presented in Table III. Considering the electrical power invested in the DC bias, it is shown that DCO-OFDM requires a non-symmetric clipping setup with the DC bias placed below the middle of the dynamic range, in order to minimize the required $\gamma_{\mathrm{b(elec)}}$ for a target BER. The optimum performance of ACO-OFDM is obtained when the downside clipping is kept at minimum by setting the DC bias close to $P_{\mathrm{Tx,min}}$.

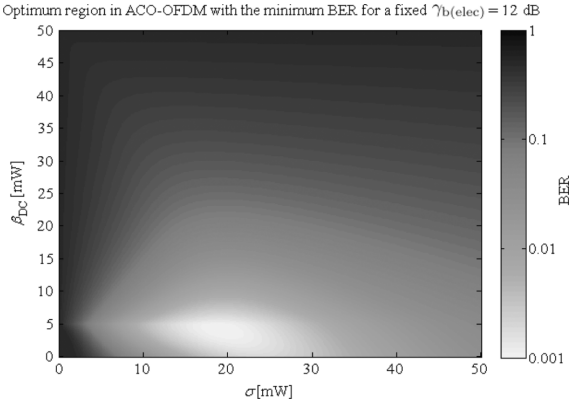


Fig. 4. Minimum BER in ACO-OFDM as a function of $\sigma$ and $\beta_{\mathrm{DC}}$ for a fixed $\gamma_{\mathrm{b(elec)}} = 12$ dB, 4-QAM with linear ZF FFE, $h(t) = \delta(t)$, $P_{\mathrm{Tx,min}} = 5$ mW and $P_{\mathrm{Tx,max}} = 50$ mW. DC bias power is included in the electrical SNR.

## III. SINGLE-CARRIER VERSUS MULTI-CARRIER TRANSMISSION

The performance of $M$-PPM and $M$-PAM versus $M$-QAM optical OFDM is assessed in terms of electrical SNR requirement, $\gamma_{\mathrm{b(elec)}}$, to achieve a target BER of $10^{-3}$ and the corresponding spectral efficiency. In the first set of results, the DC bias power is not counted towards the signal power, and a flat fading channel without dispersion, i.e., $h(t) = \delta(t)$, is assumed. The following modulation orders are chosen: $M = \{2, 4, 16, 64, 256, 1024\}$. Here, single-carrier BPSK is identical to 2-PAM. The above mentioned eye-safe linear dynamic range of the transmitter LED between $P_{\mathrm{Tx,min}} = 5$ mW and $P_{\mathrm{Tx,max}} = 50$ mW is assumed for the comparison of the OWC systems. The transmitted signal spans the entire dynamic range of optical power, and no constraint is imposed on the radiated average optical power, in order to obtain the best BER system performance for the given dynamic range. In single-carrier transmission, no signal clipping is assumed. As a result, the average optical power level is set in $M$-PPM to $\mathrm{E}[\mathbf{x}_l] = 50/M$ mW, and in $M$-PAM to $\mathrm{E}[\mathbf{x}_l] = 27.5$ mW. In multi-carrier transmission, a large number of subcarriers, e.g., 2048, is chosen. Minimum signal clipping is assumed in O-OFDM, i.e., $\lambda_{\mathrm{bottom}} = -4$ and $\lambda_{\mathrm{top}} = 4$ in DCO-OFDM, and $\lambda_{\mathrm{bottom}} = 0$ and $\lambda_{\mathrm{top}} = 4$ in ACO-OFDM. In both systems, the average optical power level, $\mathrm{E}[\mathbf{x}_l]$, can be obtained from (22). The resulting spectral efficiency versus electrical SNR requirement plot of the transmission schemes for OWC is presented in Fig. 5. It is shown that PPM is the only system which can operate at very low SNR in the range of 4.1–6.8 dB. For a given higher SNR, DCO-OFDM, and PAM demonstrate an equal highest spectral efficiency.

However, in a practical non-flat channel with dispersion [3], the signal bandwidth becomes larger than the channel coherence bandwidth at high data rates. Therefore, the equalization process incurs an SNR penalty. In such a scenario, single-carrier transmission suffers a severe ISI. In multi-carrier transmission, a CP is employed which completely eliminates ISI and ICI, and it has a negligible impact on the spectral efficiency and electrical SNR requirement [5]. It transforms the channel into

TABLE III
OPTIMUM BIASING PARAMETERS, $\sigma$ AND $\beta_{\mathrm{DC}}$, AND OPTIMUM NORMALIZED CLIPPING LEVELS, $\lambda_{\mathrm{bottom}}$ AND $\lambda_{\mathrm{top}}$, IN ACO-OFDM AND DCO-OFDM WITH $M$-QAM AND LINEAR ZF FFE FOR $P_{\mathrm{Tx,min}} = 5$ MW, $P_{\mathrm{Tx,max}} = 50$ MW AND A $10^{-3}$ BER IN A FLAT FADING CHANNEL WITH IMPULSE RESPONSE $h(t) = \delta(t)$. DC BIAS POWER IS INCLUDED IN THE ELECTRICAL SNR

| | ACO-OFDM | | | | DCO-OFDM | | | |
|---|---|---|---|---|---|---|---|---|
| | $\sigma$ [mW] | $\beta_{\mathrm{DC}}$ [mW] | $\lambda_{\mathrm{bottom}}$ | $\lambda_{\mathrm{top}}$ | $\sigma$ [mW] | $\beta_{\mathrm{DC}}$ [mW] | $\lambda_{\mathrm{bottom}}$ | $\lambda_{\mathrm{top}}$ |
| 4-QAM | 19.25 | 4.12 | 0.05 | 2.38 | 11.58 | 22 | $-1.47$ | 2.42 |
| 16-QAM | 16.4 | 4.78 | 0.01 | 2.76 | 9.04 | 24.07 | $-2.11$ | 2.87 |
| 64-QAM | 14.39 | 4.95 | 0 | 3.13 | 7.66 | 24.95 | $-2.6$ | 3.27 |
| 256-QAM | 12.92 | 4.99 | 0 | 3.48 | 6.75 | 25.47 | $-3.03$ | 3.63 |
| 1024-QAM | 11.81 | 5 | 0 | 3.81 | 6.1 | 25.81 | $-3.41$ | 3.97 |

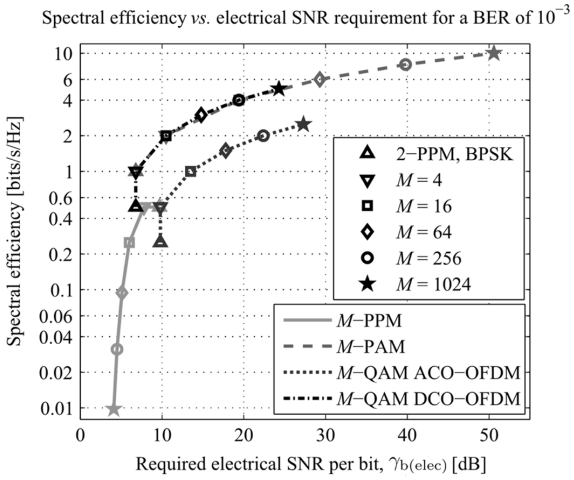


Fig. 5. Spectral efficiency versus electrical SNR requirement for a $10^{-3}$ BER of the OWC schemes in a flat fading channel with impulse response $h(t) = \delta(t)$ and neglected DC bias power.

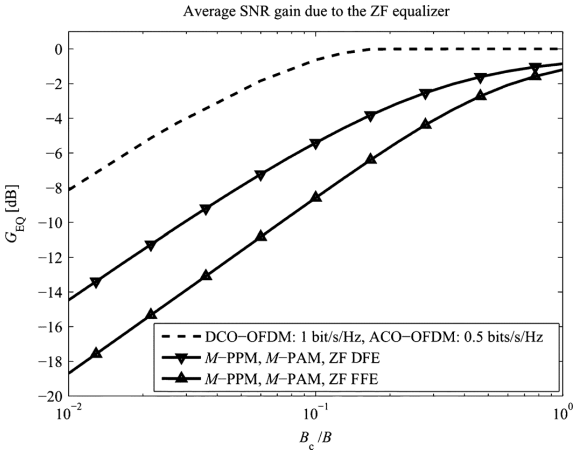


Fig. 6. Equalizer gain for signal bandwidth exceeding the channel coherence bandwidth.

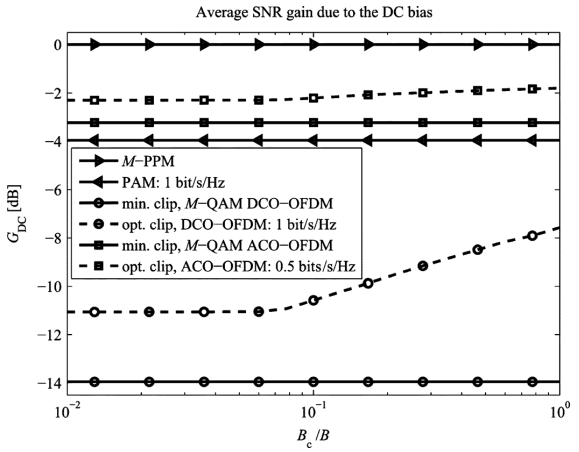


Fig. 7. DC bias gain for signal bandwidth exceeding the channel coherence bandwidth. A dynamic range of the transmitter between $P_{\mathrm{Tx,min}} = 5$ mw and $P_{\mathrm{Tx,max}} = 50$ mW is assumed.

a flat fading channel over the subcarrier bandwidth, and therefore single-tap equalization with bit and power loading [7], [8] can be performed, in order to minimize the channel effect. In addition, since the electrical path gain coefficient, $g_{\mathrm{h(elec)}}$, is merely a factor in the equalization process, it directly translates into an SNR penalty, $g_{\mathrm{h(elec)}} = 1$ is assumed. The equalizer gain of multi-carrier transmission with bit and power loading and single-tap ZF FFE is compared with the equalizer gain of single-carrier transmission with multi-tap ZF FFE and ZF DFE as the signal bandwidth grows larger than the channel coherence bandwidth. The result is presented in Fig. 6. It is shown that multi-carrier transmission incurs a lower SNR penalty in the equalization process.

When the DC bias power is added to the signal power, the systems incur an SNR penalty, because the DC bias reduces the useful AC signal power for a fixed total signal power. Based on the different signal statistics, the compared systems incur a different SNR penalty due to the DC bias. The DC bias gain is presented in Fig. 7 as the signal bandwidth exceeds the channel coherence bandwidth. For the considered dynamic range of the transmitter between $P_{\mathrm{Tx,min}} = 5$ mw and $P_{\mathrm{Tx,max}} = 50$ mW, the optimum signal clipping reduces the SNR penalty by up to 6.5 dB for DCO-OFDM and up to 1.4 dB for ACO-OFDM

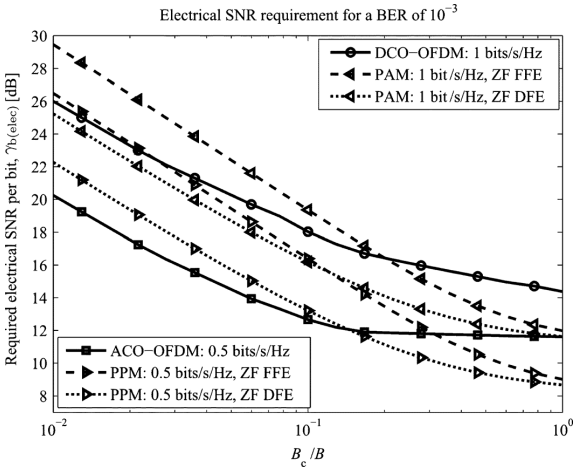


Fig. 8. Required electrical SNR per bit for signal bandwidth exceeding the channel coherence bandwidth. The target BER is $10^{-3}$ for a dynamic range of the transmitter between $P_{\mathrm{Tx,min}} = 5$ mw and $P_{\mathrm{Tx,max}} = 50$ mW.

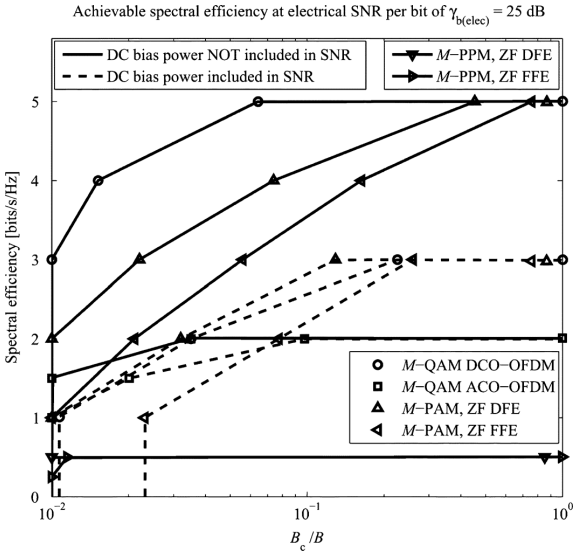


Fig. 9. Spectral efficiency for signal bandwidth exceeding the channel coherence bandwidth. The target BER is $10^{-3}$ with an available electrical SNR per bit of 25 dB.

as compared to minimum signal clipping. In addition, bit and power loading in combination with optimum signal clipping allow the DC bias gain to saturate above the DC bias gain in the minimum clipping case. Nevertheless, because of the close to Gaussian distribution of the signals, DCO-OFDM and ACO-OFDM still incur a larger SNR penalty as compared to PAM and PPM, respectively, which have distributions with finite support. Therefore, in order to obtain the electrical SNR requirement when the DC bias power is counted towards the signal power in a non-flat dispersive channel, the DC bias gain and the equalizer gain need to be subtracted from the electrical SNR requirement from Fig. 5. The result is presented in Fig. 8. It is shown that optimum signal clipping allows O-OFDM to close the gap to single-carrier transmission down to 2 dB in a flat fading channel when the DC bias power is included in the calculation of the SNR requirement. However, when the signal bandwidth exceeds the channel coherence bandwidth in a dispersive channel, ACO-OFDM shows a lower electrical SNR requirement as compared to PPM with both FFE and DFE. Equivalently, DCO-OFDM is shown to have a lower SNR requirement than PAM with FFE, and it approaches the SNR requirement of PAM with DFE.

By fixing the electrical SNR requirement, the relative performance of the systems can be obtained in terms of spectral efficiency. This is illustrated in Fig. 9 for $\gamma_{\mathrm{b(elec)}} = 25$ dB as the signal bandwidth exceeds the channel coherence bandwidth. When the DC power is not counted towards the electrical signal power, DCO-OFDM and ACO-OFDM show a superior spectral efficiency in the dispersive optical wireless channel as compared to PAM and PPM, respectively. When the DC power is included in the calculation of the electrical SNR, ACO-OFDM still outperforms PPM. DCO-OFDM outperforms PAM with FFE, and it approaches the performance of PAM with DFE. However, it has to be noted that the analysis of PAM with DFE represents an upper bound for the performance which is achieved when an infinite number of channel taps are considered in the equalizer. In a practical indoor optical wireless channel, where the impulse response only changes slowly, the channel taps and the required bit and power loading parameters with optimum signal shaping can be pre-computed and stored in look-up tables in memory. Therefore, the computational complexity at the receiver comes from the convolution operation of the DFE equalizer in single-carrier transmission and the FFT operation in multi-carrier transmission. It has been shown in [4] that the most efficient DFE implementation requires one FFT and one IFFT operation for $N$ channel taps. Therefore, for a fixed FFT size, O-OFDM is expected to require half of the computational complexity of single-carrier transmission with DFE.

## IV. Conclusion

In this paper, single-carrier transmission, e.g., $M$-PPM and $M$-PAM, and multi-carrier transmission, e.g., $M$-QAM DCO-OFDM and ACO-OFDM, are studied for OWC. A signal shaping framework is presented which through scaling and DC biasing conditions the transmitted signal within the optical power constraints of the transmitter front-end. The optimal signal shaping enables the Gaussian O-OFDM signals to minimize the electrical SNR requirement. The analytical expressions for the BER performance of the transmission schemes with equalization of the optical wireless channel in AWGN are obtained, excluding or including the DC bias power in the calculation of the electrical SNR. This enables a novel comparison of system performance in terms of SNR requirement and spectral efficiency. When the DC bias power is neglected, DCO-OFDM and ACO-OFDM show a superior spectral efficiency in the dispersive optical wireless channel as compared to PAM and PPM. DCO-OFDM is expected to deliver the highest throughput in applications, where the additional DC bias power required to create a non-negative signal can serve a complementary functionality, such as illumination

in VLC. In IR communication, where the DC power is generally constrained by eye-safety regulations, and it is included in the calculation of the electrical SNR, the optimum signal clipping enables O-OFDM to reduce the SNR requirement gap to single-carrier transmission down to 2 dB in the flat fading fading channel. However, when the signal bandwidth exceeds the channel coherence bandwidth, DCO-OFDM shows a higher spectral efficiency than PAM with FFE, and it approaches the performance of the more computationally intensive PAM with DFE.

## REFERENCES


[1] F. R. Gfeller and U. Bapst, "Wireless in-house data communication via diffuse infrared radiation," *Proc. IEEE*, vol. 67, no. 11, pp. 1474–1486, Nov. 1979.

[2] Y. Tanaka, T. Komine, S. Haruyama, and M. Nakagawa, "Indoor visible communication utilizing plural white LEDs as lighting," in *Proc. 12th IEEE Int. Symp. Personal, Indoor and Mobile Radio Communications*, San Diego, CA, Sep. 30-Oct. 3, 2001, vol. 2, pp. 81–85.

[3] J. M. Kahn and J. R. Barry, "Wireless infrared communications," *Proc. IEEE*, vol. 85, no. 2, pp. 265–298, Feb. 1997.

[4] J. G. Proakis, , S. W. Director, Ed., *Digital Communications*, ser. McGraw-Hill Series in Electrical and Computer Engineering, 4th ed. New York: McGraw-Hill Higher Education, Dec. 2000.

[5] H. Elgala, R. Mesleh, and H. Haas, "Practical considerations for indoor wireless optical system implementation using OFDM," in *Proc. IEEE 10th Int. Conf. Telecommunications (ConTel)*, Zagreb, Croatia, Jun. 8–10, 2009.

[6] J. Armstrong, "OFDM for optical communications," *J. Lightw. Technol.*, vol. 27, no. 3, pp. 189–204, Feb. 2009.

[7] J. Campello, "Practical bit loading for DMT," in *Proc. IEEE Int. Conf. Communications (IEEE ICC 1999)*, Vancouver, BC, Canada, Jun. 6–10, 1999, vol. 2, pp. 801–805.

[8] H. E. Levin, "A complete and optimal data allocation method for practical discrete multitone systems," in *Proc. IEEE Global Telecommunications Conf. (IEEE GLOBECOM 2001)*, San Antonio, TX, Nov. 25–29, 2001, vol. 1, pp. 369–374.

[9] J. B. Carruthers and J. M. Kahn, "Multiple-subcarrier modulation for nondirected wireless infrared communication," *IEEE J. Select. Areas Commun.*, vol. 14, no. 3, pp. 538–546, Apr. 1996.

[10] J. Armstrong and A. Lowery, "Power efficient optical OFDM," *Electron. Lett.*, vol. 42, no. 6, pp. 370–372, Mar. 16, 2006.

[11] Vishay Semiconductors, Datasheet: TSHG8200 High Speed Infrared Emitting Diode, 830 nm, GaAlAs Double Hetero, Jul. 2008. [Online]. Available: http://www.vishay.com/docs/84755/tshg8200.pdf.

[12] BS EN 62471:2008, Photobiological Safety of Lamps and Lamp Systems, BSI British Standards Std., Sep. 2008.

[13] S. Dimitrov, S. Sinanovic, and H. Haas, "Clipping noise in OFDM-based optical wireless communication systems," *IEEE Trans. Commun. (IEEE TCOM)*, to be published.

[14] R. J. Green, H. Joshi, M. D. Higgins, and M. S. Leeson, "Recent developments in indoor optical wireless," *IET Commun.*, vol. 2, no. 1, pp. 3–10, Jan. 2008.

[15] J. Armstrong and B. J. C. Schmidt, "Comparison of asymmetrically clipped optical OFDM and DC-biased optical OFDM in AWGN," *IEEE Commun. Lett.*, vol. 12, no. 5, pp. 343–345, May 2008.

[16] D. Tse and P. Viswanath, *Fundamentals of Wireless Communication*. Cambridge, U.K.: Cambridge Univ. Press, 2005.

[17] H. Elgala, R. Mesleh, and H. Haas, "Non-linearity effects and predistortion in optical OFDM wireless transmission using LEDs," *Inderscience Int. J. Ultra Wideband Commun. Syst. (IJUWBCS)*, vol. 1, no. 2, pp. 143–150, 2009.

[18] T. S. Rappaport, *Wireless Communications: Principles and Practice*, 2nd ed. Englewood Cliffs, NJ: Prentice Hall PTR, 2002.

[19] S. Dimitrov, R. Mesleh, H. Haas, M. Cappitelli, M. Olbert, and E. Bassow, "On the SIR of a cellular infrared optical wireless system for an aircraft," *IEEE J. Select. Areas Commun. (IEEE JSAC)*, vol. 27, no. 9, pp. 1623–1638, Dec. 2009.

[20] S. Dimitrov, H. Haas, M. Cappitelli, and M. Olbert, "On the throughput of an OFDM-based cellular optical wireless system for an aircraft cabin," in *Proc. Eur. Conf. Antennas and Propagation (EuCAP 2011)*, Rome, Italy, Apr. 11–15, 2011.

[21] D. Dardari, V. Tralli, and A. Vaccari, "A theoretical characterization of nonlinear distortion effects in OFDM systems," *IEEE Trans. Commun.*, vol. 48, no. 10, pp. 1755–1764, Oct. 2000.

[22] J. Li, X. Zhang, Q. Gao, Y. Luo, and D. Gu, "Exact BEP analysis for coherent M-arry PAM and QAM over AWGN and Rayleigh fading channels," in *Proc. IEEE Vehicular Technology Conf. (VTC 2008-Spring)*, Singapore, May 11–14, 2008, pp. 390–394.

[23] J. Bussgang, Cross Correlation Function of Amplitude-Distorted Gaussian Signals, Research Laboratory for Electronics, Massachusetts Institute of Technology, Cambridge, MA, Technical Report 216, Mar. 1952.

[24] J. Rice, *Mathematical Statistics and Data Analysis*, 2nd ed. Pacific Grove, CA: Duxbury, 1995.

[25] P. K. Vitthaladevuni, M.-S. Alouini, and J. C. Kieffer, "Exact BER computation for cross QAM constellations," *IEEE Trans. Wireless Commun.*, vol. 4, no. 6, pp. 3039–3050, Nov. 2005.

[26] J. Smith, "Odd-bit quadrature amplitude-shift keying," *IEEE Trans. Commun.*, vol. 23, no. 3, pp. 385–389, Mar. 1975.

[27] S. Boyd and L. Vandenberghe, *Convex Optimization*. Cambridge, U.K.: Cambridge Univ. Press, 2004.



**Svilen Dimitrov** (S'09) received the B.Sc. degree in electrical engineering and computer science in 2008, and the M.Sc. degree in communications, systems, and electronics in 2009 from Jacobs University, Bremen, Germany. Currently, he is working towards the Ph.D. degree in electrical engineering at the University of Edinburgh, Edinburgh, U.K.

He wrote his B.Sc. thesis (2007–2008) with the Department of Pre-Development of Cabin Electronic Systems of Airbus Germany on a simulation model for reproduction of infrared wireless path loss distribution in an aircraft cabin, using a Monte Carlo Ray-tracing algorithm. During his M.Sc. study (2008–2009), he extended the work on the characterization of the optical wireless channel with the department of Simulation and Graphical Technologies of EADS Innovation Works Germany. His main research interests are in the area of computer-aided system design, test, and optimization with emphasis on wireless communication systems.

**Sinan Sinanovic** (S'98–M'07) received the Ph.D. degree in electrical and computer engineering from Rice University, Houston, TX, in 2006.

In the same year, he joined Jacobs University, Bremen, Germany, as a post doctoral fellow. In 2007, he joined the University of Edinburgh, Edinburgh, U.K., where he currently works as a research fellow in the Institute for Digital Communications (IDCOM). While working with Halliburton Energy Services, he developed the acoustic telemetry receiver which was patented. He also worked for Texas Instruments.

Dr. Sinanovic is a member of the Tau Beta Pi engineering honor society and a member of the Eta Kappa Nu electrical engineering honor society. He won an honorable mention at the International Math Olympiad in 1994.

**Harald Haas** (S'98–A'00–M'03) holds the Chair of Mobile Communications in the Institute for Digital Communications (IDCOM) at the University of Edinburgh, Edinburgh, U.K., and he currently is the CTO of a university spin-out company VLC Ltd. His main research interests are in interference coordination in wireless networks, spatial modulation, and optical wireless communication. He holds more than 15 patents. He has published more than 50 journal papers including a *Science* article and more than 150 peer-reviewed conference papers. Nine of his papers are invited papers. He has co-authored a book entitled *Next Generation Mobile Access Technologies: Implementing TDD* (Cambridge, U.K.: Cambridge Univ. Press, 2008). Since 2007, he has been a Regular High Level Visiting Scientist supported by the Chinese "111 program" at Beijing University of Posts and Telecommunications (BUPT).

Prof. Haas was an invited speaker at the TED Global conference 2011, and his work on optical wireless communication was listed among the "50 best inventions in 2011" in *Time Magazine*.

This full text paper was peer reviewed at the direction of IEEE Communications Society subject matter experts for publication in the IEEE Globecom 2010 proceedings.

# On the Clipping Noise in an ACO-OFDM Optical Wireless Communication System

Svilen Dimitrov and Harald Haas
*Institute for Digital Communications, Joint Research Institute for Signal and Image Processing, The University of Edinburgh, Edinburgh EH9 3JL, UK, e-mail: {s.dimitrov, h.haas}@ed.ac.uk*

***Abstract*—In this paper, the clipping noise in an asymmetrically clipped optical orthogonal frequency division multiplexing (ACO-OFDM) wireless communication system is derived semi-analytically. Clipping noise in ACO-OFDM is introduced either because of insufficient forward biasing of the emitter, or a low power sensitivity of the detector. Following the Bussgang theorem, the non-linear distortion caused by the clipping of the time domain signal attenuates the frequency domain subcarriers at the receiver and adds zero-mean Gaussian noise. The attenuation factor and the clipping noise variance are determined and verified through simulation. Finally, bit-error ratio (BER) and goodput simulations compare the performance of ACO-OFDM with a direct-current-biased optical OFDM (DCO-OFDM) system for different clipping levels and multilevel quadrature amplitude modulation ($M$-QAM) schemes.**

***Index Terms*—Optical wireless communication, clipping noise, emitter biasing, detector sensitivity, ACO-OFDM, DCO-OFDM.**

## I. Introduction

With the advent of incoherent high-power light emitting diodes (LEDs) and highly sensitive photodiodes (PDs), optical wireless communication (OWC) has become a viable candidate for medium range indoor data transmission [1]. As opposed to a radio frequency (RF) system, where the data-carrying signal modulates the electric field radiated by an antenna, in an OWC system the signal modulates the intensity of the optical emitter. Pulsed modulation schemes such as pulse position modulation (PPM), pulse width modulation (PWM) or on-off keying (OOK) are often used in intensity modulated direct detection (IM/DD) OWC systems [2]. However, in an indoor environment the dispersive nature of the optical wireless channel is a major throughput limiting factor because of the resulting inter-symbol interference (ISI).

A well known technique with an inherent robustness to multipath fading is the OFDM transmission scheme [1, 3]. The time domain OFDM signal envelope is utilized to modulate the intensity of the LED [3]. For this purpose, the signal needs to be real and non-negative. A real-valued time domain signal is obtained when Hermitian symmetry is imposed on the frequency domain subcarriers. One approach to obtain a non-negative signal is the addition of a DC bias of at least two standard deviations, *i.e.* DCO-OFDM [4]. Another approach is proposed by Armstrong *et al.* [5, 6], the ACO-OFDM. Enabling only the odd subcarriers and setting the even ones to zero, the negative part of the time domain signal can be clipped. The data can be successfully retrieved from the odd subcarriers at the receiver. Since, however, the optical front-ends impose physical limitations on the signal, non-linear distortions such as non-linear transfer effects and signal clipping are a common issue. Because of the fact that the transmitted signal in an OFDM system has a Gaussian distribution over time [7], the Bussgang theorem applies. As a result, the non-linear distortion can be regarded as an attenuation and, possibly, a rotation of the intended subcarriers plus a zero-mean complex Gaussian noise component. There have been several studies which describe the non-linear transfer effects of high-power amplifiers (HPA) with a short dynamic range in OFDM RF systems [7, 8]. Signal clipping due to the large peak-to-average-power ratio (PAPR) in RF OFDM is studied in [9]. However, in an OWC system there are further sources of non-linear distortion. The non-linear transfer characteristic of the LED is compensated by pre-distortion [10]. In addition, the large path loss of the optical wireless channel [11, 12], along with insufficient forward biasing of the LEDs and low power sensitivity of PDs, can cause a clipping of the time domain data-carrying signal at a positive power level. However, instead of clipping a Rayleigh distributed amplitude as in RF OFDM systems, in OWC OFDM a real-valued Gaussian time domain signal is clipped single-sidedly. Thus, the existing derivation of clipping noise in RF OFDM has to be modified accordingly.

In this paper, a semi-analytical description of the positive-level clipping at the optical front-ends in an OWC system is presented. The attenuation factor and the variance of the complex Gaussian clipping noise are determined and verified through simulation. Next, the different clipping level BER and goodput performance of ACO-OFDM is compared with DCO-OFDM biased by two standard deviations. In addition, the impact of the clipping distortion on higher order modulation schemes and higher IFFT/FFT sizes is discussed.

The rest of the paper is organized as follows. Section II presents the ACO-OFDM system model. Section III explains the derivation of the clipping noise statistics. Simulation results are discussed in Section IV. Finally, Section V concludes the paper.

## II. ACO-OFDM system model

The ACO-OFDM system model considered in this study is illustrated in Fig. 1. First, the input bit stream at the transmitter is mapped onto complex symbols according to the chosen modulation scheme, *e.g.* $M$-QAM. According to the ACO-OFDM frame structure proposed in [5], for an IFFT/FFT size of $N$, the modulated symbols in $X(l)$, $l = 0, ..., N/4 - 1$, are mapped onto the odd subcarriers, whereas the even subcarriers are set to zero. In addition, Hermitian symmetry of the subcarriers is imposed to ensure a real-valued time

978-1-4244-5638-3/10/$26.00 ©2010 IEEE

This full text paper was peer reviewed at the direction of IEEE Communications Society subject matter experts for publication in the IEEE Globecom 2010 proceedings.

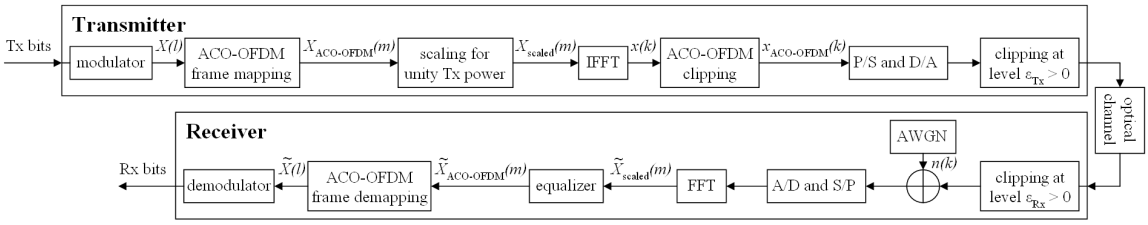


Fig. 1: ACO-OFDM system block diagram.

domain signal, $x(k)$, $k = 0, ..., N-1$. Thus, the ACO-OFDM subcarriers frame, $X_{\mathrm{ACO-OFDM}}(m)$, $m = 0, ..., N-1$, is formed. Further, in order to facilitate a certain average optical power, $P_x$, of the asymmetrically clipped time domain signal, $x_{\mathrm{ACO-OFDM}}(k)$, the subcarriers are pre-scaled by a factor, $\alpha$, to obtain $X_{\mathrm{scaled}}(m)$. Following the Parseval theorem and using an unbiased estimator for the variance of $x(k)$, the factor, $\alpha$, is derived as follows:

$$\alpha = P_x \sqrt{\frac{2\pi N(N-1)}{\sum_{m=0}^{N-1} |X_{\mathrm{ACO-OFDM}}(m)|^2}}, \quad (1)$$

which simplifies for 4-QAM or phase shift keying (PSK) symbols with unity amplitude to $\alpha = P_x\sqrt{4\pi(N-1)}$. Next, the scaled subcarriers are passed through an inverse fast Fourier transformer (IFFT) to form the bipolar real-valued time domain signal, $x(k)$. The negative samples of $x(k)$ are replaced by zeros to obtain $x_{\mathrm{ACO-OFDM}}(m)$. In general, a cyclic prefix (CP) is included in OFDM systems to combat ISI. However, in OWC the CP is shown to have a negligible impact on power and bandwidth efficiencies [13]. Therefore, in this study the CP is omitted for simplicity. After parallel-to-serial (P/S) and digital-to-analogue (D/A) conversion $x_{\mathrm{ACO-OFDM}}(m)$ is passed to the optical emitter, the LED. If the LED is insufficiently forward biased, the intensity-driving and data-carrying signal will be clipped at a level $\varepsilon_{\mathrm{Tx}} > 0$. Further, the signal is transmitted over the optical wireless channel and detected by a PD. The large path loss of the channel [11, 12] in combination with low power sensitivity of the PD can cause a further clipping at a level $\varepsilon_{\mathrm{Rx}} > 0$. Then, the signal is distorted by a real-valued bipolar additive white Gaussian noise (AWGN), $n(k)$ [6]. After serial-to-parallel (S/P) and analogue-to-digital (A/D) conversion it is passed through a fast Fourier transformer (FFT) back to the frequency domain, $\widetilde{X}_{\mathrm{scaled}}(m)$. According to [5], the asymmetrical clipping at the transmitter results in halving of the amplitude of the odd subcarriers at the receiver. In general, in the long term evolution (LTE) OFDM framework, pilot tones are used for channel estimation and equalization [14]. Thus, by the use of pilot tones within the ACO-OFDM frame, the following equalization block is able to compensate for the effect of the pre-scaling factor, $\alpha$, the optical wireless channel, the halving of the subcarrier amplitude and the further attenuation due to eventual clipping. As a last step, the data-carrying symbols in $\widetilde{X}_{\mathrm{ACO-OFDM}}(m)$ are identified according to the known ACO-OFDM frame structure and demodulated in a maximum likelihood (ML) fashion to produce the received bits.

## III. Assessment of the Clipping Noise Component

In general, the optical wireless channel has a short delay spread and can be mainly characterized by the path loss [12]. In addition, because of the linearity of the channel, the positive-level clipping effects at the transmitter and the receiver can be combined as follows:

$$\varepsilon = \varepsilon_{\mathrm{Tx}} + \frac{\varepsilon_{\mathrm{Rx}}}{h}, \quad (2)$$

where $\varepsilon$ is the combined clipping level, and $h$ is the channel path loss coefficient. In general, the optical power clipping ratio (OPCR), $\eta_{\mathrm{OPCR}}$, associated with clipping at a positive level $\varepsilon$ is defined as:

$$\eta_{\mathrm{OPCR}} = \frac{\varepsilon}{P_x}. \quad (3)$$

The positive-level clipping of an ACO-OFDM or DCO-OFDM time domain signal results in a reduction of its average optical power, $P_x$. The optical power reduction factor (OPRF),

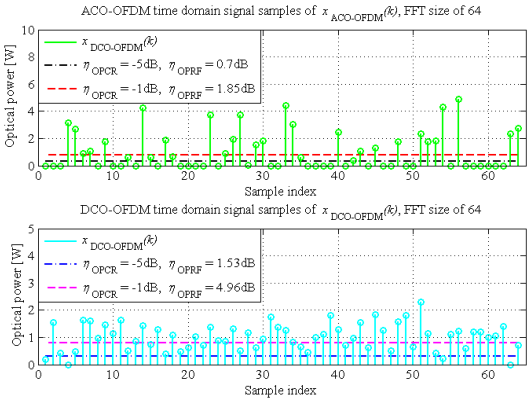


Fig. 2: Positive-level clipping of the time-domain signal in ACO-OFDM and DCO-OFDM for an IFFT/FFT size of 64.

978-1-4244-5638-3/10/$26.00 ©2010 IEEE

This full text paper was peer reviewed at the direction of IEEE Communications Society subject matter experts for publication in the IEEE Globecom 2010 proceedings.

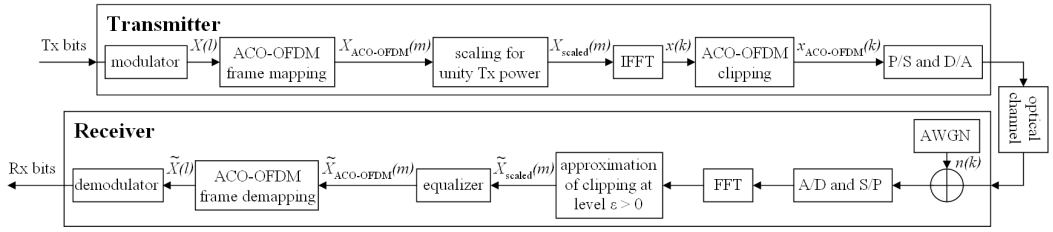


Fig. 3: Equivalent form of the ACO-OFDM system block diagram.

$\eta_{\mathrm{OPRF}}$, can be derived as follows:

$$\eta_{\mathrm{OPRF}} = \frac{P_x}{\sigma_{x(k)}\left(\phi(\lambda) - \lambda Q(\lambda)\right)}\,, \tag{4}$$

where

$$\lambda = \frac{\eta_{\mathrm{OPCR}} P_x - \kappa_{\mathrm{DC}}}{\sigma_{x(k)}}\,, \tag{5}$$

$$\phi(u) = \frac{1}{\sqrt{2\pi}} \exp\left(\frac{-u^2}{2}\right) \tag{6}$$

and

$$Q(u) = \frac{1}{\sqrt{2\pi}} \int_u^\infty \exp\left(-\frac{v^2}{2}\right)\, dv\,. \tag{7}$$

In general, in ACO-OFDM the DC bias, $\kappa_{\mathrm{DC}}$ equls 0, and the standard deviation of $x(k)$, $\sigma_{x(k)}$, is $P_x\sqrt{2\pi}$. It is a reasonable practical assumption to consider a DC bias of two standard deviations in DCO-OFDM, *i.e.* $\kappa_{\mathrm{DC}} = 2\sigma_{x(k)}$ where $\sigma_{x(k)}$ is $P_x/2$. The effect of power reduction due to clipping is illustrated in Fig. 2 for ACO-OFDM and DCO-OFDM signals with 64 samples and $P_x = 1$W. Two clipping ratios are applied, a lower ratio of $\eta_{\mathrm{OPCR}} = -5$dB and a higher ratio of $\eta_{\mathrm{OPCR}} = -1$dB. It is shown that the ACO-OFDM signal suffers a power reduction of 0.7dB and 1.85dB, whereas the DCO-OFDM signal power drops by 1.53dB and 4.96dB, respectively.

Following the Bussgang theorem, an equivalent ACO-OFDM system block diagram is proposed in Fig. 3. The distorted version of the scaled subcarriers after the clipping noise approximation block, $\widetilde{X}_{\mathrm{scaled}}(m)$, is given by:

$$\begin{aligned}\widetilde{X}_{\mathrm{scaled}}(m) = \alpha h K X_{\mathrm{ACO-OFDM}}(m) + \\ + \alpha h \sigma_{\mathrm{clip}} N_{\mathcal{CN}}(m) + \alpha\gamma N_{\mathcal{CN}}(m)\,,\end{aligned} \tag{8}$$

where $K$ is the attenuation factor introduced by the clipping and $\sigma_{\mathrm{clip}}$ is the standard deviation of the complex Gaussian clipping noise. Bellow we derive $K$ and $\sigma_{\mathrm{clip}}$ for this system. $N_{\mathcal{CN}}(m)$ is a sample of a complex Gaussian distribution with zero mean and unity variance. $\gamma$ represents a real-valued scaling factor for the AWGN needed to fix the target SNR. It also accounts for the optical-to-electrical SNR conversion [6].

According to the central limit theorem, an IFFT/FFT block yields a close to Gaussian signal for a large IFFT/FFT size. It has been shown in [7] that IFFT/FFT sizes as small as 64 are sufficient. Therefore, under the assumption that the non-zero-clipped signal, $x(k)$, is a Gaussian real-valued signal, the attenuation factor, $K$, is derived as follows:

$$K = Q\left(\frac{\eta_{\mathrm{OPCR}}}{\sqrt{2\pi}}\right). \tag{9}$$

Note that in this particular case $K$ is a real-valued function rather than a complex function as suggested by the Bussgang theorem. The variance of the clipping noise, $\sigma^2_{\mathrm{clip}}$, is estimated in a semi-analytical fashion. It is derived as follows:

$$\begin{aligned}\sigma^2_{\mathrm{clip}} = Q^2\left(\frac{\eta_{\mathrm{OPCR}}}{\sqrt{2\pi}}\right)\left(f_2\eta^2_{\mathrm{OPCR}}\frac{N}{4\pi(N-1)} - \right. \\ \left. - f_1\eta_{\mathrm{OPCR}}\sqrt{\frac{N}{4\pi(N-1)}} + \frac{f_0}{4} - 1\right).\end{aligned} \tag{10}$$

Because of intractable correlation within $f_0$, $f_1$ and $f_2$, these functions are approximated through a Monte Carlo simulation. They exhibit the following model, $f_i = \exp(p_i)$, where $p_i$ is a polynomial function of $\eta_{\mathrm{OPCR}}$. The simulation shows

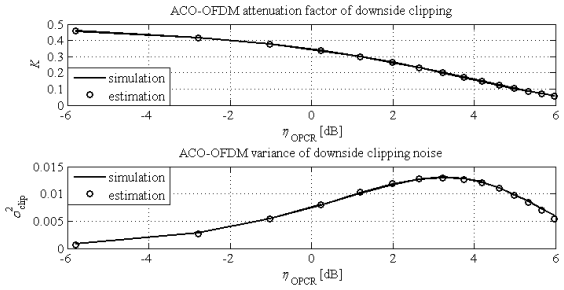


Fig. 4: Simulation vs. estimation of the attenuation factor and clipping noise variance as a function of the clipping ratio in an ACO-OFDM system.

| | $a_3$ | $a_2$ | $a_1$ | $a_0$ |
|---|---|---|---|---|
| $p_0$ | -0.0076 | 0.1027 | 0.5967 | 1.3873 |
| $p_1$ | -0.0030 | 0.0599 | 0.5701 | 0.7708 |
| $p_2$ | -0.0050 | 0.0896 | 0.2483 | 0.6174 |

TABLE I: Third order polynomial coefficients for the estimation of the clipping noise variance in ACO-OFDM.

978-1-4244-5638-3/10/$26.00 ©2010 IEEE

This full text paper was peer reviewed at the direction of IEEE Communications Society subject matter experts for publication in the IEEE Globecom 2010 proceedings.

that a third order polynomial is required to reduce the mean-squared-error (MSE) with respect to the simulation to less than $1\%$. The resulting graphs are presented in Fig. 4 for practical IFFT/FFT sizes, *i.e.* $N > 64$. The polynomial coefficients, $a_j, j = 0, 1, 2, 3$, are shown in TABLE I. Hence, $K$ and $\sigma^2_{\text{clip}}$ are independent of the modulation scheme and practical IFFT/FFT sizes, and they only depend on the clipping ratio.

## IV. BER/GOODPUT SIMULATION AND DISCUSSION

The performance of ACO-OFDM with positive-level clipping is assessed in terms of BER and goodput. The goodput is defined as the product of the spectral efficiency and the success rate, *i.e.* $(1 - \text{BER})$ [15]. As suggested in [6], BER and goodput are evaluated as a function of the electrical signal-to-noise ratio (SNR) per bit, $E_{\text{b(elec)}}/N_0$, and unity channel path loss, $h$, is assumed for simplicity. ACO-OFDM is compared with DCO-OFDM. In general, because of the structure of the OFDM frame, ACO-OFDM achieves half the spectral efficiency of DCO-OFDM for equal modulation orders. Therefore, in addition to 4-QAM ACO-OFDM, 16-QAM ACO-OFDM is simulated against a 4-QAM DCO-OFDM system to compare the BER performance at a similar spectral efficiency. IFFT/FFT size of $2048$ is chosen in accord with the LTE standard [14]. Three clipping scenarios are considered: no clipping noise, $\eta_{\text{OPCR}} = -5$dB and $\eta_{\text{OPCR}} = -1$dB. Furthermore, the equivalent ACO-OFDM system from Fig. 3 is also included in the comparison.

The BER performance of 4-QAM ACO-OFDM vs. 4-QAM DCO-OFDM is presented in Fig. 5. The proposed system depicted in Fig. 3 performs identically as its equivalent counterpart from Fig. 1. The results for the non-clipped ACO-OFDM and DCO-OFDM agree with the ones published in [6]. An important observation is that ACO-OFDM with a clipping of $\eta_{\text{OPCR}} = -1$dB outperformes the non-clipped DCO-OFDM in the SNR regime up to 14dB. This corresponds to better performance of the ACO-OFDM system under clipping of $1.85$dB of the optical power. However, the robustness and better performance of ACO-OFDM come at the expense of goodput. Fig. 6 presents the goodput of 4-QAM ACO-OFDM vs. 4-QAM DCO-OFDM. It is shown that for the same modulation order, DCO-OFDM outperforms ACO-OFDM over the entire SNR region. As expected, the goodput saturates at the spectral efficiency level dictated by the modulation scheme and the OFDM frame structure.

In order to achieve the same spectral efficiency as 4-QAM DCO-OFDM, 16-QAM ACO-OFDM is considered. The BER simulation is shown in Fig. 7. In agreement with the results in [6], the non-clipped 16-QAM ACO-OFDM outperformes 4-QAM DCO-OFDM. However, as the clipping ratio, $\eta_{\text{OPCR}}$, rises, the higher order modulation ACO-OFDM is impacted more dramatically and the SNR gap for similar $\eta_{\text{OPCR}}$ is closed. The goodput performance is given in Fig. 8. Non-clipped 16-QAM ACO-OFDM registers the highest goodput. In the low SNR region 16-QAM ACO-OFDM outperforms 4-QAM DCO-OFDM for similar clipping ratios. However, because of their similar BER performance in the high SNR region, their goodput performance saturates accordingly.

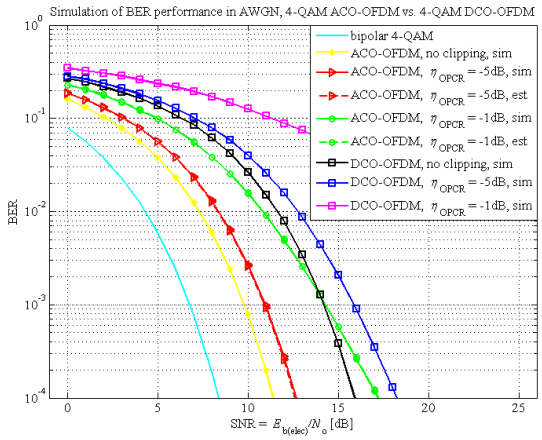


Fig. 5: BER simulation of 4-QAM ACO-OFDM vs. 4-QAM DCO-OFDM for clipping ratios of $-5$dB and $-1$dB.

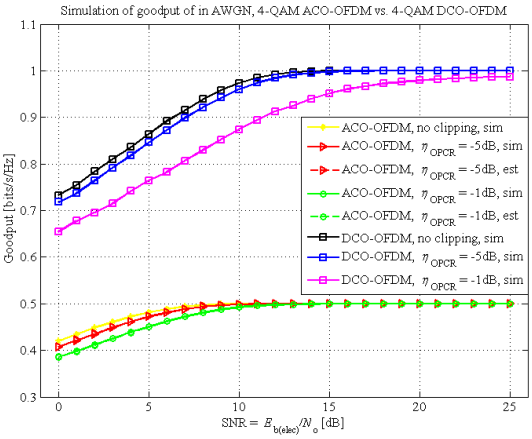


Fig. 6: Goodput simulation of 4-QAM ACO-OFDM vs. 4-QAM DCO-OFDM for clipping ratios of $-5$dB and $-1$dB.

As an important observation, higher order QAM modulation is more vulnerable to positive-level clipping. Achieving a similar spectral efficiency, $M^2$-QAM ACO-OFDM shows a worse BER performance than $M$-QAM DCO-OFDM for higher order of modulation when clipping noise is present. This is because, according to (8), (9) and (10), the clipping noise component is added regardless of the modulation scheme. Since shrinking the decision regions with higher order modulation degrades the performance of the ML detector, a worse BER performance is expected.

Another important observation concerns the performance of ACO-OFDM for different IFFT/FFT sizes. In general, in a Monte Carlo simulation with equal probability of 1's and 0's in the input bit stream, regardless of the modulation order,

978-1-4244-5638-3/10/$26.00 ©2010 IEEE

This full text paper was peer reviewed at the direction of IEEE Communications Society subject matter experts for publication in the IEEE Globecom 2010 proceedings.

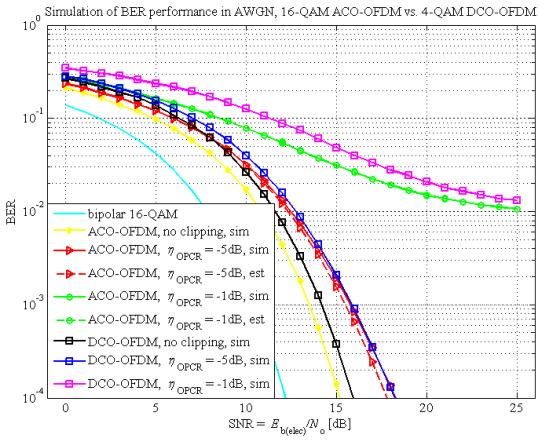


Fig. 7: BER simulation of 16-QAM ACO-OFDM vs. 4-QAM DCO-OFDM for clipping ratios of $-5$dB and $-1$dB.

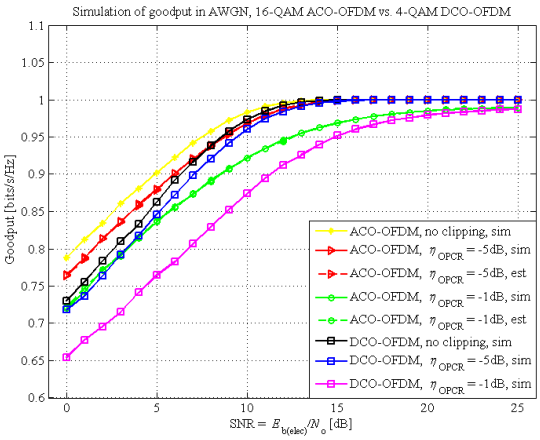


Fig. 8: Goodput simulation of 16-QAM ACO-OFDM vs. 4-QAM DCO-OFDM for clipping ratios of $-5$dB and $-1$dB.

the subcarrier pre-scaling factor, $\alpha$, averages to the expression in the 4-QAM case, $\alpha = P_x\sqrt{4\pi(N-1)}$. It is the only factor in (8) which is dependent on $N$. Since this scaling is compensated at the equalizer, the IFFT/FFT size will not influence the performance of the ACO-OFDM system.

## V. Conclusion

In this paper, positive-level clipping of an ACO-OFDM wireless signal due to insufficient forward biasing of the emitter or low power sensitivity of the detector is studied. In accord with the Bussgang theorem, the attenuation factor of the non-linear distortion is derived and it proves to be a real-valued function. In addition, the variance of the clipping noise is estimated in a semi-analytical fashion by means of a Monte Carlo simulation. Both the attenuation factor and the variance are only dependent on the clipping ratio for practical IFFT/FFT sizes greater than 64. ACO-OFDM and DCO-OFDM systems are studied for different clipping ratios. It is found that ACO-OFDM is more robust to the clipping effects than DCO-OFDM for similar modulation schemes at the expense of a reduction in spectral efficiency. Finally, higher order modulation is shown to be more vulnerable to positive-level clipping due to the shrinking of the ML decision region.

## Acknowledgement

We gratefully acknowledge EADS UK Ltd. for the support of this research. We would like to thank Professor Jean Armstrong for sharing with us detailed insights into ACO-OFDM. Professor Haas acknowledges the Scottish Funding Council support of his position within the Edinburgh Research Partnership in Engineering and Mathematics between the University of Edinburgh and Heriot Watt University.

## References

[1] Y. Tanaka, T. Komine, S. Haruyama, and M. Nakagawa, "Indoor Visible Communication Utilizing Plural White LEDs as Lighting," in *Proceedings of the* $12^{th}$ *IEEE International Symposium on Personal, Indoor and Mobile Radio Communications*, vol. 2, San Diego, CA, USA, Sep. 30–Oct. 3, 2001, pp. 81–85.

[2] J. Kahn, J. Barry, W. Krause, M. Audeh, J. Carruthers, G. Marsh, E. Lee, and D. Messerschmitt, "High–Speed Non–Directional Infrared Communication for Wireless Local-Area Networks," in *In the Proceeding of the* $26^{th}$ *Asilomar Conference on Signals, Systems and Computers*, vol. 1, California, USA, Oct. 26–28, 1992, pp. 83–87.

[3] H. Elgala, R. Mesleh, H. Haas, and B. Pricope, "OFDM Visible Light Wireless Communication Based on White LEDs," in *Proc. of the 64th IEEE Vehicular Technology Conference (VTC)*, Dublin, Ireland, Apr. 22–25, 2007.

[4] J. B. Carruthers and J. M. Kahn, "Multiple-subcarrier Modulation for Nondirected Wireless Infrared Communication," *IEEE Journal on Selected Areas in Communications*, vol. 14, no. 3, pp. 538–546, Apr. 1996.

[5] J. Armstrong and A. Lowery, "Power Efficient Optical OFDM," *Electronics Letters*, vol. 42, no. 6, pp. 370–372, Mar. 16, 2006.

[6] J. Armstrong and B. J. C. Schmidt, "Comparison of Asymmetrically Clipped Optical OFDM and DC-Biased Optical OFDM in AWGN," *IEEE Commun. Lett.*, vol. 12, no. 5, pp. 343–345, May 2008.

[7] D. Dardari, V. Tralli, and A. Vaccari, "A Theoretical Characterization of Nonlinear Distortion Effects in OFDM Systems," *IEEE Transactions on Communications*, vol. 48, no. 10, pp. 1755–1764, Oct. 2000.

[8] A. Frotzscher, P. Zillmann, and G. Fettweis, "A Detection Algorithm for Clipped OFDM Signals Using the IDFT-Matrix," in *Proc. of IEEE 64th Vehicular Technology Conference (IEEE VTC 2006)*, Montreal, Quebeck, Canada, Sep. 25–28 2006, pp. 1–5.

[9] H. Ochiai and H. Imai, "Performance analysis of deliberately clipped OFDM signals," *IEEE Transactions on Communications*, vol. 50, no. 1, pp. 89–101, Jan. 2002.

[10] H. Elgala, R. Mesleh, and H. Haas, "Non-linearity effects and predistortion in optical OFDM wireless transmission using LEDs," *Inderscience Intenational Journal of Ultra Wideband Communications and Systems (IJUWBCS)*, vol. 1, no. 2, pp. 143–150, 2009.

[11] S. Dimitrov, R. Mesleh, H. Haas, M. Cappitelli, M. Olbert, and E. Bassow, "Path Loss Simulation of an Infrared Optical Wireless System for Aircraft," in *IEEE Global Communications Conference (IEEE GLOBECOM 2009)*, Honolulu, HI, USA, Nov. 30 – Dec. 4 2009.

[12] ——, "On the SIR of a Cellular Infrared Optical Wireless System for an Aircraft," *IEEE Journal on Selected Areas in Communications (IEEE JSAC)*, vol. 27, no. 9, pp. 1623–1638, Dec. 2009.

[13] H. Elgala, R. Mesleh, and H. Haas, "Practical Considerations for Indoor Wireless Optical System Implementation using OFDM," in *Proc. of the IEEE 10th International Conference on Telecommunications (ConTel)*, Zagreb, Croatia, Jun. 8–10 2009.

[14] E. Dahlman, S. Parkvall, J. Sköld, and P. Beming, *3G Evolution: HSPA and LTE for Mobile Broadband*, 2nd ed. Academic Press, 2008.

[15] J. G. Proakis, *Digital Communications*, 4th ed., ser. McGraw-Hill Series in Electrical and Computer Engineering, S. W. Director, Ed. McGraw-Hill Higher Education, Dec. 2000.

978-1-4244-5638-3/10/$26.00 ©2010 IEEE

EuCAP 2011 - Convened Papers

# On the Throughput of an OFDM-based Cellular Optical Wireless System for an Aircraft Cabin

Svilen Dimitrov*, Harald Haas*, Mario Cappitelli‡ and Michael Olbert‡

*The University of Edinburgh, Institute for Digital Communications, Joint Research Institute for Signal and Image Processing, EH9 3JL Edinburgh, UK, e-mail: {s.dimitrov,h.haas}@ed.ac.uk

‡EADS Germany, D-21129 Hamburg, Germany, e-mail: {mario.cappitelli,michael.olbert}@eads.net

***Abstract*—In this paper, a cellular optical wireless communication system based on orthogonal frequency division multiplexing (OFDM) is simulated inside an aircraft cabin. Asymmetrically clipped optical OFDM (ACO-OFDM) and direct-current-biased optical OFDM (DCO-OFDM) transmission schemes are compared in terms of throughput and cell coverage. Cellular networks with wavelength reuse factors of $1$ (full reuse), $2$ and $3$ are modeled, and off-the-shelf optical front-end components are assumed. Signal-to-interference-and-noise ratio (SINR) maps are determined via a Monte Carlo ray-tracing (MCRT) global irradiation simulation in a computer-aided design (CAD) cabin model. Due to the use of OFDM, adaptive modulation and coding (AMC) can be applied to the SINR maps to arrive at the spatial throughput. It is shown that throughput within the range of $1.56 - 30$ Mbps is achievable with the considered ACO-OFDM system, whereas DCO-OFDM doubles the throughput to $3.13-60$ Mbps. In addition, wavelength reuse factors of $3$ or higher are needed to ensure full cell support for both transmission schemes.**

***Index Terms*—ACO-OFDM, DCO-OFDM, throughput, cellular optical wireless system, adaptive modulation and coding.**

## I. Introduction

Optical wireless communication (OWC) systems employing OFDM prove to be a robust candidate for communication over the dispersive optical wireless channel [1, 2]. Since there is no interference with radio frequency (RF) technology, an OWC system is very well suited for deployment in areas, where the interference with electromagnetic radiation is an issue, *i.e.* in hospitals or in an aircraft cabin. An additional advance in the aircraft cabin setup is that optical wireless communication can significantly reduce cabling, leading to a lighter aircraft, and consequently, to a reduction in $CO_2$ emissions. As a result, a variety of onboard applications are provided ranging from inter-system communication to flight entertainment. Several other studies have investigated optical wireless networks for aircrafts with the purpose of in-flight entertainment and intra-cabin passenger communication [3, 4]. The results from measurements reported in these studies demonstrate that data rates of several tens of Mbps are feasible within the cabin. Therefore, systems exhibiting high capacity and robustness are required in order to satisfy the increasing data rate demand, *e.g.* onboard high definition (HD) video streaming.

In this paper, a cellular deployment of an OFDM-based OWC system is investigated. A study conducted in [5] suggests that an optical wireless network with a hexagonal cell configuration and wavelength reuse of 3 is co-channel interference limited for small cell radii and noise limited for large cell radii, but it does not provide a comprehensive spatial SINR analysis. Gfeller [6] analyzed indoor peer-to-peer and client/server wireless infrared topologies, but he assumes a noise limited network only. However, the results obtained in a previous study [7] demonstrate that the optical wireless network in the aircraft cabin is interference limited. In particular, the optical signal-to-interference (SIR) maps over the network topology are obtained by means of a global MCRT simulation, assuming off-the-shelf optical components at the transmitter and the receiver. In the current study, the SIR maps are converted into throughput maps. After optical-to-electrical (O/E) conversion of the intended signal and the interfering signal at a receiver, also including the thermal and shot noise components at the receiver, the electrical SINR maps are obtained for wavelength reuse factors of 1, 2 and 3. Practical center wavelengths of $\lambda_1 = 830$ nm, $\lambda_2 = 870$ nm and $\lambda_3 = 940$ nm are assumed in combination with an optical bandpass filter at the intended receiver. In this way, the adjacent-channel interference is avoided, whereas only co-channel interference is present. Because of its inherent robustness to multipath fading and its capability of achieving high transmission rates, an OFDM-based system is considered. In the literature, two possible system realizations can be found: ACO-OFDM [8, 9] and DCO-OFDM [10]. It has been reported that ACO-OFDM achieves a higher power efficiency on the expense of $50\%$ reduction in spectral efficiency as compared to DCO-OFDM. In order to translate the electrical SINR maps into throughput, an AMC scheme [11] is employed. Finally, the throughput performance and the cell coverage of ACO-OFDM and DCO-OFDM are compared for the three wavelength reuse configurations.

The rest of the paper is organized as follows. Section II presents the SINR modeling in the OFDM-based OWC system. Section III explains the AMC scheme employed. Throughput simulation results are discussed in Section IV. Finally, Section V concludes the paper.

## II. SINR modeling

The same model of the aircraft cabin and MCRT simulation method as in [7] is used here, and the reader is kindly referred to [7] for more details. Omnidirectional transmitters and receivers are considered in the setup of the cellular network

| | $\lambda_1 = 830$ nm | $\lambda_2 = 870$ nm | $\lambda_3 = 940$ nm |
|---|---|---|---|
| Transmitter | 16× TSHG8200 | 16× TSFF5210 | 16× VSMB2020X01 |
| FOV of LED | $\pm 10^{\circ}$ | $\pm 10^{\circ}$ | $\pm 12^{\circ}$ |
| $P_{\mathrm{opt,ACO}}$ | 16× 100 mW | 16× 100 mW | 16× 100 mW |
| $P_{\mathrm{opt,DCO}}$ | 16× 250 mW | 16× 250 mW | 16× 250 mW |
| Receiver | 4× S6967 | 4× S6967 | 4× S6967 |
| FOV of PD | $\pm 70^{\circ}$ | $\pm 70^{\circ}$ | $\pm 70^{\circ}$ |
| Area | 4× 26.4 mm$^2$ | 4× 26.4 mm$^2$ | 4× 26.4 mm$^2$ |
| Sensitivity, $S$ | 0.6 A/W | 0.63 A/W | 0.65 A/W |
| Capacitance | 4× 50 pF | 4× 50 pF | 4× 50 pF |
| Bandwidth | 25 MHz | 25 MHz | 25 MHz |
| Optical filter | 4× FB830-10 | 4× FB870-10 | 4× FB940-10 |
| Transmittance | 0.8 | 0.8 | 0.8 |
| Bandwidth | ±10 nm | ±10 nm | ±10 nm |
| TIA | 1× AD8015 | 1× AD8015 | 1× AD8015 |
| Gain, $G$ | 10 KΩ | 10 KΩ | 10 KΩ |
| $R_{\mathrm{load}}$ | 50 Ω | 50 Ω | 50 Ω |
| $P_{\mathrm{N,elec}}$ | −30 dBm | −30 dBm | −30 dBm |
| BER | $10^{-5}$ | $10^{-5}$ | $10^{-5}$ |

TABLE I: Front-end setup [12–15].

based on off-the-shelf components. These include light emitting diodes (LEDs), photodiodes (PDs), optical bandpass filters and transimpedance amplifiers (TIAs) [12–15]. The front-end parameters used in the simulation are given in TABLE I. In addition, in accord with the characteristics of the components in the receiver, *i.e.* PD and TIA, −30 dBm of electrical power is considered for the additive white Gaussian noise (AWGN) component, representing the thermal and shot noise at the receiver. Furthermore, a practical bit-error ratio (BER) of less than $10^{-5}$ is targeted for video broadcast. The network configurations for the different wavelength reuse factors are presented in Fig. 1. The topologies of optical SIR distribution obtained in [7] are subjected to O/E conversion. Including the AWGN component, the electrical SINR per symbol at the receiver can be expressed as follows:

$$\frac{E_{\mathrm{s}}}{I + N_0} = \frac{\left(P_{\mathrm{S,opt}} h_{\mathrm{S}} S G\right)^2 F_{\mathrm{OE}}}{\left(\sum_i P_{\mathrm{I,opt}} h_{\mathrm{I},i} S G\right)^2 F_{\mathrm{OE}} + P_{\mathrm{N,elec}} R_{\mathrm{load}}}, \quad (1)$$

where the electrical symbol power, the total electrical interference power and and the electrical noise power are defined as $E_{\mathrm{s}}$, $I$ and $N_0$, respectively. Equal average optical power at the intended and interfering transmitters, $P_{\mathrm{S,opt}}$ and $P_{\mathrm{I,opt}}$, is considered. The radiated average optical power per transmitter in the ACO-OFDM and DCO-OFDM systems is given in TABLE I as $P_{\mathrm{opt,ACO}}$ and $P_{\mathrm{opt,DCO}}$, respectively. Accordingly, being more power efficient, the ACO-OFDM system radiates less optical energy than the DCO-OFDM system. Here, the factor $h_{\mathrm{S}}$ represents the path gain between the intended transmitter and the intended receiver, whereas $h_{\mathrm{I,i}}$ defines the path gain between the $i^{\mathrm{th}}$ interfering transmitter and the intended receiver. The sensitivity of the PD is denoted as $S$, $G$ is the gain of the TIA and $R_{\mathrm{load}}$ is the resistive load over which the electrical noise power, $P_{\mathrm{N,elec}}$, is measured. The O/E conversion factor in ACO-OFDM and DCO-OFDM, $F_{\mathrm{OE}}$, is given as $\pi$ and $(\kappa^2 + 1)/\kappa^2$, respectively, where $\kappa$ standard deviations are chosen to bias the DCO-OFDM signal [9]. In this study, $\kappa = 3$ is considered to minimize the time domain signal clipping distortion in DCO-OFDM [9].

## III. Adaptive modulation and coding

The obtained SINR maps are transformed into throughput maps by means of an AMC scheme. A combination of multilevel quadrature amplitude modulation ($M$-QAM), *i.e.* $M = \{4, 16, 64\}$, and variable convolutional coding rates, *i.e.* $R = \{4/5, 3/4, 2/3, 1/2, 1/3, 1/4, 1/5, 1/8\}$, is used. As a result, a wide operational SINR range is facilitated. The performance of an RF OFDM communication system for the chosen AMC scheme is given in [11]. In general, for a fixed combination of $M$ and $R$ the ACO-OFDM system requires 3

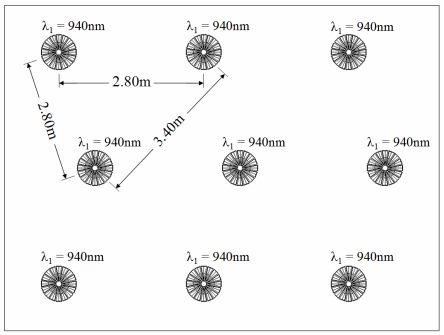


(a) Wavelength reuse of 1.

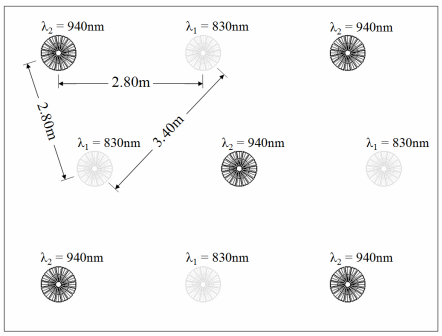


(b) Wavelength reuse of 2.

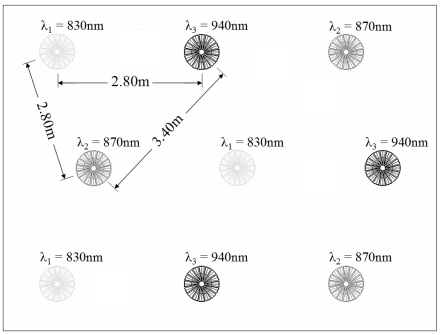


(c) Wavelength reuse of 3.

Fig. 1: Cell division and wavelength assignment for reuse factors of 1, 2 and 3.

dB higher SINR than the RF OFDM system in order to achieve a certain BER [9]. The DCO-OFDM system, in turn, requires $10\log_{10}(\kappa^2+1) = 10$ dB higher SINR for $\kappa = 3$ [9]. Accordingly, ACO-OFDM achieves a quarter of the throughput of the RF OFDM system, whereas DCO-OFDM delivers half the throughput. Therefore, the SINR requirements for a target BER of $10^{-5}$ and the corresponding throughput of RF OFDM with AMC from [11] can be used to obtain the SINR targets

| | SINR [dB] | | Throughput [Mbps] | |
|---|---|---|---|---|
| OFDM scheme | ACO-OFDM | DCO-OFDM | ACO-OFDM | DCO-OFDM |
| 4-QAM, $R$=1/8 | $-2.2$ | 4.8 | 1.56 | 3.13 |
| 4-QAM, $R$=1/5 | $-0.2$ | 6.8 | 2.5 | 5 |
| 4-QAM, $R$=1/4 | 0.8 | 7.8 | 3.13 | 6.25 |
| 4-QAM, $R$=1/3 | 2.4 | 9.4 | 4.17 | 8.33 |
| 4-QAM, $R$=1/2 | 4.6 | 11.6 | 6.25 | 12.5 |
| 4-QAM, $R$=2/3 | 6.6 | 13.6 | 8.33 | 16.67 |
| 4-QAM, $R$=4/5 | 8.6 | 15.6 | 10 | 20 |
| 16-QAM, $R$=1/2 | 10 | 17 | 12.5 | 25 |
| 16-QAM, $R$=2/3 | 13.6 | 20.6 | 16.67 | 33.33 |
| 16-QAM, $R$=4/5 | 14.8 | 21.8 | 20 | 40 |
| 64-QAM, $R$=2/3 | 17.2 | 24.2 | 25 | 50 |
| 64-QAM, $R$=3/4 | 19 | 26 | 28.13 | 56.25 |
| 64-QAM, $R$=4/5 | 20.2 | 27.2 | 30 | 60 |

TABLE II: SINR switching level and throughput of ACO-OFDM and DCO-OFDM for $M$-QAM and convolutional codes with a coding rate $R$.

and throughput of ACO-OFDM and DCO-OFDM given in TABLE II. As a result, the more power efficient ACO-OFDM system switches transmission rates between 1.56 Mbps and 30 Mbps over a range of SINR values between $-2.2$ dB and 20.2 dB. The more spectrally efficient DCO-OFDM system delivers double throughput, *i.e.* $3.13 - 60$ Mbps, over an SINR range between 4.8 dB and 27.2 dB. In TABLE II, it is important to notice that for an equal throughput in the lower throughput region, *e.g.* 3.13 Mbps, ACO-OFDM requires an SINR of 0.8 dB, whereas DCO-OFDM needs 4 dB more. The situation is the opposite for a throughput in the higher throughput region, *e.g.* 25 Mbps, where the ACO-OFDM system requires an SINR of 17.2 dB, while DCO-OFDM only requires 17 dB. This is a manifestation of the trade-off between power efficient and spectrally efficient systems. The throughput advantage of the power efficient ACO-OFDM system in the lower SINR region becomes inferior to the more spectrally efficient DCO-OFDM system in the higher SINR region. This can be explained by the the fact that ACO-OFDM requires an $M^2$-QAM modulation to achieve the same throughput as $M$-QAM DCO-OFDM. Therefore, the ACO-OFDM system using the squared order modulation requires a much higher SINR in order to achieve the BER target as compared to DCO-OFDM for the same high transmission rate.

## IV. Simulation Results and Discussion

The throughput distribution in the cabin is presented in Figs. 2 and 3 for ACO-OFDM and DCO-OFDM, respectively.

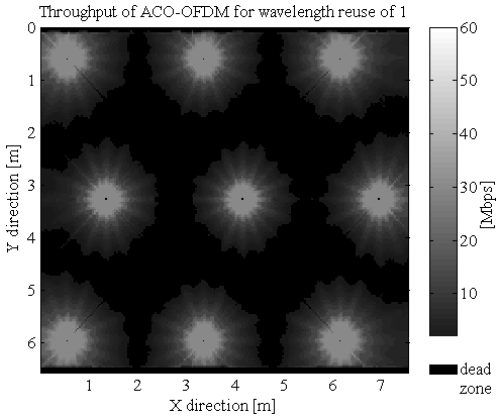


(a) Wavelength reuse of 1.

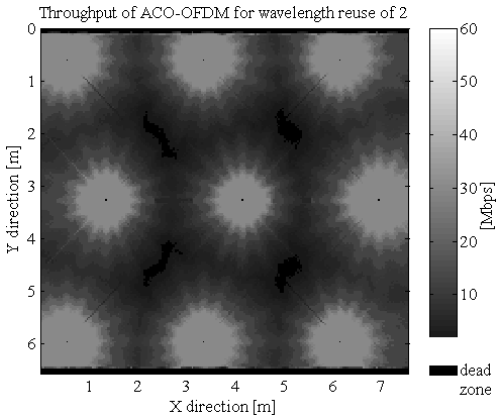


(b) Wavelength reuse of 2.

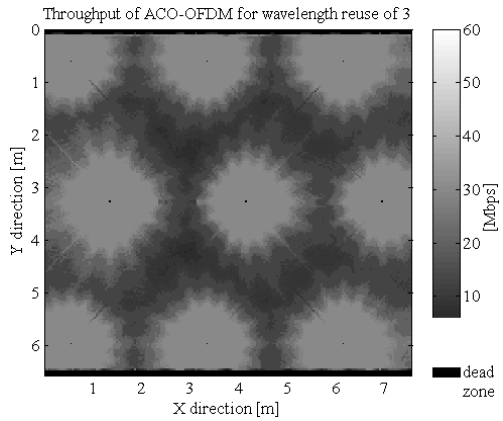


(c) Wavelength reuse of 3.

Fig. 2: Throughput of ACO-OFDM for wavelength reuse factors of 1, 2 and 3.

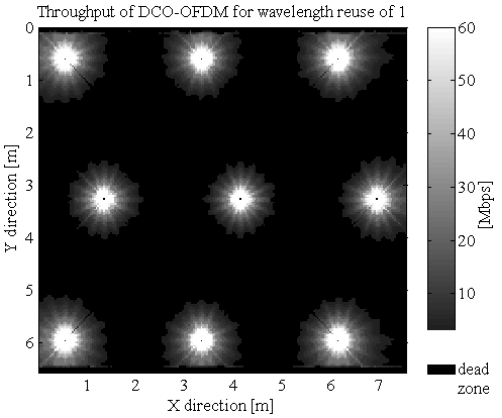


(a) Wavelength reuse of 1.

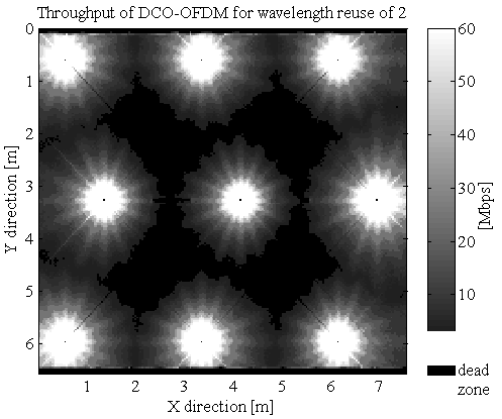


(b) Wavelength reuse of 2.

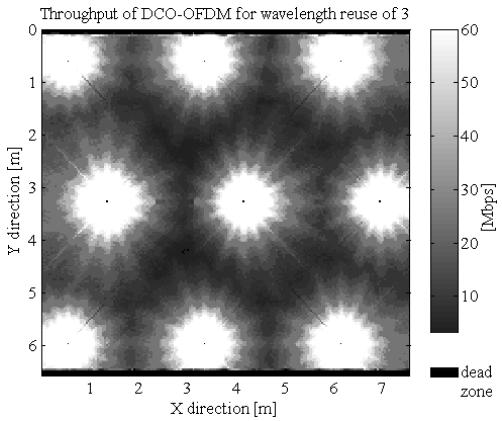


(c) Wavelength reuse of 3.

Fig. 3: Throughput of DCO-OFDM for wavelength reuse factors of 1, 2 and 3.

| | ACO-OFDM | | | DCO-OFDM | | |
|---|---|---|---|---|---|---|
| Wavelength reuse factor | 1 | 2 | 3 | 1 | 2 | 3 |
| Min. throughput [Mbps] | 1.56 | 1.56 | 6.25 | 3.13 | 3.13 | 3.13 |
| Min. throughput radius [m] | 1 | 1.4 | 1.7 | 0.7 | 1.2 | 1.7 |
| Max. throughput [Mbps] | 30 | 30 | 30 | 60 | 60 | 60 |
| Max. throughput radius [m] | 0.3 | 0.52 | 0.76 | 0.2 | 0.36 | 0.54 |

TABLE III: Throughput in the cell at (4.15 m, 3.25 m) in the cross-section through the transmitters.

The key results are summarized in TABLE III. The OWC systems are compared in terms of the delivered throughput range and the corresponding cell coverage. The ACO-OFDM system demonstrates transmission rates within $1.56-30$ Mbps, whereas DCO-OFDM doubles the rates to $3.13-60$ Mbps. For wavelength reuse factors of 1 and 2, ACO-OFDM supports a larger portion of the cell area as compared to DCO-OFDM. It is shown that both systems require wavelength reuse factors of 3 or higher in order to ensure a full cell coverage. In the latter case, the "dead zone" in the considered communication scenario only appears in the areas which lie beyond the boundaries of the cabin geometry or inside opaque objects. In addition, Figs. 2c and 3c exhibit the trade-off between power efficiency and spectral efficiency, discussed in the previous section. The more power efficient ACO-OFDM system delivers a higher throughput towards the cell edge, where the SINR is low. However, the more spectrally efficient DCO-OFDM doubles the throughput towards the cell center, where the SINR is high. In general, a multiuser access scheme other than frequency division multiple access (FDMA), *e.g.* OFDM time domain multiple access (OFDM-TDMA), may consider an adaptive switching between ACO-OFDM and DCO-OFDM. Such an approach enables the allocation of an optimal transmission rate according to the underlying SINR conditions in OFDM-based OWC systems.

## V. Conclusion

In this paper, the throughput of a cellular OFDM-based OWC system is simulated inside the cabin of an aircraft by means of a global MCRT irradiation simulation using a CAD cabin model and assuming off-the-shelf front-end components. After O/E conversion of the spatial irradiance distribution, electrical SINR maps are obtained for wavelength reuse factors of 1, 2 and 3. In addition, an AMC scheme is applied to the two possible system realizations, *i.e.* ACO-OFDM and DCO-OFDM, in order to translate the SINR maps into transmission rates for a BER of less than $10^{-5}$. The ACO-OFDM system supports higher data rates at the cell edge, whereas DCO-OFDM doubles the throughput towards the cell center, manifesting the trade-off between power efficiency and spectral efficiency. In the presented network configuration, both transmission schemes require wavelength reuse factors of 3 or higher in order to ensure full cell support.

## Acknowledgement

We gratefully acknowledge EADS UK Ltd. for the support of this research. Professor Haas acknowledges the Scottish Funding Council support of his position within the Edinburgh Research Partnership in Engineering and Mathematics between the University of Edinburgh and Heriot Watt University.

## References

[1] Y. Tanaka, T. Komine, S. Haruyama, and M. Nakagawa, "Indoor Visible Communication Utilizing Plural White LEDs as Lighting," in *Proceedings of the $12^{th}$ IEEE International Symposium on Personal, Indoor and Mobile Radio Communications*, vol. 2, San Diego, CA, USA, Sep. 30–Oct. 3, 2001, pp. 81–85.

[2] H. Elgala, R. Mesleh, H. Haas, and B. Pricope, "OFDM Visible Light Wireless Communication Based on White LEDs," in *Proc. of the 64th IEEE Vehicular Technology Conference (VTC)*, Dublin, Ireland, Apr. 22–25, 2007.

[3] N. Schmitt, "Wireless optical NLOS Communication in Aircraft Cabin for In-flight Entertainment," in *Proc. of ESA 1st Optical Wireless Onboard Communications Workshop*, Noordwijk, Netherlands, 29–30 Sep. 2004.

[4] N. Schmitt, T. Pistner, C. Vassilopoulos, D. Marinos, A. Boucouvalas, M. Nikolitsa, C. Aidinis, and G. Metaxas, "Diffuse Wireless Optical Link for Aircraft Intra-cabin Passenger Communication," in *Proc. of 5th International Symposium on Communication Systems, Networks and Digital Signal Processing CSNDSP 2006*, Patras, Greece, 19–21 Jul. 2006.

[5] G. W. Marsh and J. M. Kahn, "Channel Reuse Strategies for Indoor Infrared Wireless Communications," *IEEE Transactions on Communications*, vol. 45, no. 10, pp. 1280–1290, Oct. 1997.

[6] F. R. Gfeller, P. Bernasconi, W. Hirt, C. Elisii, and B. Weiss, *Mobile Communications Advanced Systems and Components*, ser. Lecture Notes in Computer Science. Springer Berlin/Heidelberg, 1994, vol. 783, ch. Dynamic Cell Planning for Wireless Infrared In-House Data Transmission, pp. 261–272, ISBN 978-3-540-57856-7.

[7] S. Dimitrov, R. Mesleh, H. Haas, M. Cappitelli, M. Olbert, and E. Bassow, "On the SIR of a Cellular Infrared Optical Wireless System for an Aircraft," *IEEE Journal on Selected Areas in Communications (IEEE JSAC)*, vol. 27, no. 9, pp. 1623–1638, Dec. 2009.

[8] J. Armstrong and A. Lowery, "Power Efficient Optical OFDM," *Electronics Letters*, vol. 42, no. 6, pp. 370–372, Mar. 16, 2006.

[9] J. Armstrong and B. J. C. Schmidt, "Comparison of Asymmetrically Clipped Optical OFDM and DC-Biased Optical OFDM in AWGN," *IEEE Commun. Lett.*, vol. 12, no. 5, pp. 343–345, May 2008.

[10] J. B. Carruthers and J. M. Kahn, "Multiple-subcarrier Modulation for Nondirected Wireless Infrared Communication," *IEEE Journal on Selected Areas in Communications*, vol. 14, no. 3, pp. 538–546, Apr. 1996.

[11] 3GPP, "Evolved Universal Terrestrial Radio Access (E-UTRA); Radio Frequency (RF) System Scenarios," 3GPP TR 36.942 V 8.2.0 (2009-05), May 2009. Retrieved Dec. 1, 2009 from www.3gpp.org/ftp/Specs/.

[12] Vishay Semiconductors, "Infrared Emitters," Retrieved Jan. 25, 2011 from http://www.vishay.com/ir-emitting-diodes/.

[13] Hamamatsu Photonics K.K., "Silicon PIN Photodiode," Retrieved Jan. 25, 2011 from http://sales.hamamatsu.com/en/products/solid-state-division/si-photodiode-series/si-pin-photodiode.php.

[14] Thorlabs, "Bandpass Filters," Retrieved Jan. 25, 2011 from http://www.thorlabs.com/NewGroupPage9.cfm?ObjectGroup_ID=1001.

[15] Analog Devices, "Transimpedance Amplifiers," Retrieved Jan. 25, 2011 from http://www.analog.com/en/fiberoptic/transimpedance-amplifiers/products/index.html.

This full text paper was peer reviewed at the direction of IEEE Communications Society subject matter experts for publication in the IEEE ICC 2011 proceedings

# Double-sided Signal Clipping in ACO-OFDM Wireless Communication Systems

Svilen Dimitrov, Sinan Sinanovic and Harald Haas

*Institute for Digital Communications, Joint Research Institute for Signal and Image Processing, The University of Edinburgh, EH9 3JL Edinburgh, UK, e-mail: {s.dimitrov, s.sinanovic, h.haas}@ed.ac.uk*

***Abstract*—In this paper, the impact of double-sided signal clipping on optical wireless communication (OWC) systems employing asymmetrically clipped optical orthogonal frequency division multiplexing (ACO-OFDM) is investigated. Time domain signal clipping generally results from direct current (DC) biasing and/or from physical limitations of the transmitter front-end. These include insufficient forward biasing and the maximum driving power limit of the emitter. The clipping noise can be modeled according to the Bussgang theorem and the central limit theorem (CLT) as attenuation of the subcarriers at the receiver and addition of zero-mean complex Gaussian noise. Analytical expressions for the attenuation factor and the clipping noise variance are determined in closed form and employed in the derivation of the electrical signal-to-noise ratio (SNR) at the receiver. Finally, the theoretical SNR is verified through a bit-error ratio (BER) simulation.**

***Index Terms*—ACO-OFDM, optical wireless communication, clipping noise, emitter biasing, detector noise.**

## I. Introduction

OFDM for indoor OWC systems is a robust transmission scheme which delivers high data rates over the dispersive optical wireless channel [1, 2]. Intensity modulation and direct detection (IM/DD) OWC systems employ a light emitting diode (LED) at the transmitter and a photodiode (PD) at the receiver. Since the time domain OFDM signal envelope modulates the intensity of the LED, the signal needs to be real and non-negative. A real-valued signal is obtained when Hermitian symmetry is imposed on the OFDM subcarriers. One approach to obtain a non-negative signal is the addition of a DC bias, *i.e.* DC-biased optical OFDM (DCO-OFDM) [3]. Another approach is proposed by Armstrong *et al.* [4, 5], ACO-OFDM. In comparison to DCO-OFDM, ACO-OFDM achieves a significant increase in the power efficiency on the expense of a $50\%$ reduction in spectral efficiency. Enabling the odd subcarriers for data transmission and setting the even ones to zero, the negative part of the time domain signal can be clipped at the transmitter without any information loss. The information can be still successfully decoded from the odd subcarriers at the receiver.

Imperfections of the optical front-ends due to the use of off-the-shelf components result in non-linear distortions of the transmitted signal such as non-linear transfer effects and signal clipping. Because of the fact that an OFDM system employs a unitary inverse fast Fourier transform (IFFT) as a multiplexing technique at the transmitter, according to the CLT the non-distorted signal follows a close to Gaussian distribution for large IFFT sizes greater than $64$ [6]. Therefore, the non-linear distortion can be modeled by means of the Bussgang theorem [7] as an attenuation of the transmitted signal plus a zero-mean non-Gaussian clipping noise component [6]. However, at the receiver, a unitary fast Fourier transform (FFT) is used for demultiplexing. Thus, the CLT can be applied again, and the clipping noise component can be modeled as a Gaussian process preserving the variance. This methodology is used in [6], where the non-linear transfer effects due to the short dynamic range of high-power amplifiers (HPA) in OFDM-based radio frequency (RF) systems are studied. In OWC, the non-linear transfer characteristic of the LED can be compensated by pre-distortion [8]. Symmetrical signal clipping due to the large peak-to-average-power ratio (PAPR) in RF OFDM is studied in [9]. Equivalently, symmetrical signal clipping in an optical OFDM transmission is investigated in [10]. In a previous study [11], bottom level single-sided time domain signal clipping in ACO-OFDM is investigated and the clipping noise statistics are derived in a semi-analytical fashion. However, in OWC the time domain signal is likely to be clipped double-sidedly, *i.e.* downside and upside clipping, because of insufficient forward biasing and the maximum power driving limit of the transmitter front-end. Since, in addition, the eye safety regulations [12] impose constrains on the level of transmitted average optical power, the real-valued Gaussian signal in OFDM-based OWC systems is likely to be clipped at independent bottom and top levels.

In this paper, double-sided time domain signal clipping at the transmitter front-end in an ACO-OFDM OWC system is studied. The attenuation factor and the variance of the complex Gaussian clipping noise at the received subcarriers are determined in closed form and included in the derivation of the electrical SNR at the receiver. The theoretical BER performance of clipped ACO-OFDM is verified through a Monte Carlo simulation. Finally, the impact of the clipping distortion on higher order modulation and higher IFFT/FFT sizes is discussed.

The rest of the paper is organized as follows. Section II presents the ACO-OFDM system model. Section III explains the derivation of the clipping noise statistics and the SNR at the receiver. Simulation results are presented in Section IV. Finally, Section V concludes the paper.

## II. System model

The ACO-OFDM system model considered in this study is illustrated in Fig. 1. First, the input bit stream at the transmitter

978-1-61284-233-2/11/$26.00 ©2011 IEEE

This full text paper was peer reviewed at the direction of IEEE Communications Society subject matter experts for publication in the IEEE ICC 2011 proceedings

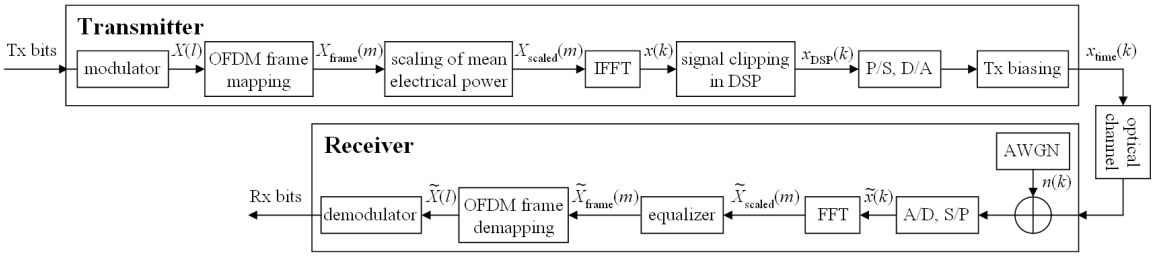


Fig. 1: ACO-OFDM system block diagram.

is mapped to complex symbols, $X(l)$, according to the chosen modulation scheme, *e.g.* multilevel quadrature amplitude modulation ($M$-QAM). For an IFFT/FFT size of $N$, $N$ subcarriers form the OFDM frame, $X_{\text{frame}}(m)$, $m = 0, ..., N-1$. In ACO-OFDM, $N/4$ symbols in $X(l)$, $l = 0, ..., N/4-1$, are mapped to half of the odd subcarriers in $X_{\text{frame}}(m)$, $m = 1, 3, 5, ..., N/2-1$, whereas the even subcarriers are set to zero. Hermitian symmetry of the subcarriers is imposed on the second half of $X_{\text{frame}}(m)$, $m = N/2, ..., N-1$, in order to ensure a real-valued time domain signal, $x(k)$, $k = 0, ..., N-1$, on the expense of $50\%$ reduction in spectral efficiency. In general, in the OFDM framework there exists the flexibility to employ QAM symbols from different modulation orders, $M$, across the OFDM frame. Square $M$-QAM constellations, *e.g.* $\{4\text{−QAM}, 16\text{−QAM}, 64\text{−QAM}, ...\}$, are considered. In addition, the $M$-QAM symbols are generally normalized for unity average electrical power, $\mathrm{E}\left[|X(l)|^2\right] = E_{\text{s(elec)}} = 1$. Here, $\mathrm{E}[\cdot]$ stands for the expectation operator. Since the clipping noise is added equally to each symbol in the OFDM frame, irrespectively of the modulation order [6], and for the sake of simplicity, in this study the same modulation order, $M$, is chosen across the symbols in the OFDM frame.

Conventionally, in OWC the average optical power of the signal is defined in the time domain as $\mathrm{E}\left[x_{\text{time}}(k)\right]$. The average electrical power of the signal, however, is defined in the frequency domain as $\mathrm{E}\left[|X_{\text{frame}}(m)|^2\right]$. According to [5], the mean electrical signal power is proportional to the variance of $x(k)$, $\sigma^2_{x(k)}$. Therefore, in order to fix a certain electrical SNR at the receiver, $\sigma^2_{x(k)}$ needs to be specified accordingly. For this purpose, the subcarriers at the transmitter require a pre-scaling by a factor, $\alpha$, to obtain $X_{\text{scaled}}(m)$. Applying the Parseval theorem and using an unbiased estimator for the variance of $x(k)$, the factor, $\alpha$, is expressed for ACO-OFDM as follows:

$$\alpha = \sigma_{x(k)} \sqrt{\frac{(N-1)}{\sum_{m=0}^{N-1} |X_{\text{frame}}(m)|^2}} \,. \tag{1}$$

Note that for practical IFFT/FFT sizes, *i.e.* $N > 64$, the average $\alpha$, $\bar{\alpha}$, can be simplified to $\bar{\alpha} = \sigma_{x(k)}\sqrt{2}$. Thus, the average electrical symbol power, $E_{\text{s(elec)}}$, can be related to the variance of $x(k)$, $\sigma^2_{x(k)}$, as $E_{\text{s(elec)}} = 2\sigma^2_{x(k)}$.

The scaled subcarriers are passed through an IFFT block. Without loss of generality, the unitary transform is employed:

$$x(k) = \frac{1}{\sqrt{N}} \sum_{m=0}^{N-1} X_{\text{scaled}}(m) \exp\left(\frac{j2\pi km}{N}\right) \,. \tag{2}$$

In order to efficiently utilize the dynamic range of the digital-to-analog (D/A) converter, any structure-specific signal clipping needs to be performed in the digital signal processor (DSP). Moreover, in order to facilitate a power efficient D/A conversion, further DC biasing is performed in the analog circuitry. Therefore, the constraints imposed by the limited dynamic range of the LED need to be preset in the DSP signal shaping block, which results in signal pre-clipping. In general, the LED is biased by a constant current source which supports the entire range of forward voltages across the LED. The bias current is added to the information carrying current yielding the forward current through the LED. Since the radiated optical power is directly proportional to the forward current, the signal and the constraints imposed by the transmitter front-end are described in terms of optical power in the rest of the paper. It is shown in [8] that the non-linear transfer characteristic of the LED can be compensated by pre-distortion. A linear characteristic is obtainable, however, only over a limited range. Therefore, in this paper a linear dynamic range of the LED is assumed between a point of minimum optical power, $P_{\text{Tx,min}}$, and a point of maximum optical power, $P_{\text{Tx,max}}$. The amount of optical power needed to bias the ACO-OFDM time domain signal is denoted as $P_{\text{Tx,bias}}$. In the case of insufficient forward biasing, *i.e.* $P_{\text{Tx,bias}} < P_{\text{Tx,min}}$, the signal is pre-clipped at a bottom level defined as $\varepsilon_{\text{bottom}} = P_{\text{Tx,min}} - P_{\text{Tx,bias}}$. In the opposite case, *i.e.* $P_{\text{Tx,bias}} \geq P_{\text{Tx,min}}$, $\varepsilon_{\text{bottom}}$ is kept at zero, in order to facilitate the structure-specific asymmetrical zero-level signal clipping of ACO-OFDM. Irrespectively of the bias, the signal is pre-clipped at a top level, $\varepsilon_{\text{top}} = P_{\text{Tx,max}} - P_{\text{Tx,bias}}$, to obtain $x_{\text{DSP}}(k)$. In general, a cyclic prefix (CP) is included in OFDM-based systems to combat inter-symbol interference (ISI). However, in OWC the CP is shown to have a negligible impact on power and bandwidth efficiencies [13]. Therefore, in this study the CP is omitted for simplicity. After parallel-to-serial (P/S) and D/A conversion and addition of the biasing power, $P_{\text{Tx,bias}}$, the signal is passed to the optical emitter.

This full text paper was peer reviewed at the direction of IEEE Communications Society subject matter experts for publication in the IEEE ICC 2011 proceedings

The biased time-domain signal, $x_{\text{time}}(k)$, is transmitted over the optical wireless channel and received by the optical detector, a combination of a PD and a transimpedance amplifier (TIA). In general, the channel is linear, it has a short delay spread and it can be primarily characterized by the path gain coefficient, $h$ [14]. Furthermore, it is unlikely that the signal is upside-clipped at the receiver. For instance, the linear range of a Vishay TEMD5110X01 PD reaches up to $0.5$ mW of incident optical power [15]. For a practical indoor path loss range between $50$ dB to $80$ dB [14], the transmitter needs to radiate more than $50$ W of optical power, in order to drive the PD to saturation. Since such an amount significantly exceeds the limits imposed by the eye safety regulations [12], it is assumed that the upside clipping occurs only at the transmitter. At the detector, the signal is distorted by a zero-mean real-valued bipolar additive white Gaussian noise (AWGN), $n_{\text{AWGN}}(k)$, with a two-sided power spectral density of $N_0$ [5].

After serial-to-parallel (S/P) and analog-to-digital (A/D) conversion the signal is passed through a unitary FFT block back to the frequency domain:

$$\widetilde{X}_{\text{scaled}}(m) = \frac{1}{\sqrt{N}} \sum_{k=0}^{N-1} \widetilde{x}(k) \exp\left(\frac{-j2\pi km}{N}\right) . \quad (3)$$

According to [4, 5], in ACO-OFDM the odd subcarriers arrive at the receiver with a halved amplitude. Therefore, further clipping at the front-ends will introduce further attenuation. In general, in the OFDM framework, pilot tones are used for channel estimation and equalization. Thus, by the use of pilot tones within the ACO-OFDM frame, the equalization block is able to compensate for the effect of the scaling factor, $\alpha$, the optical wireless channel, the halving of the received subcarriers and further attenuation due to front-end-induced signal clipping. Finally, the data-carrying symbols in $\widetilde{X}_{\text{frame}}(m)$ can be extracted due to the known frame structure and the symbols are demodulated using a maximum likelihood (ML) detector.

## III. Clipping noise statistics

The clipping of an OFDM time domain signal modifies its average optical power. Since the non-distorted signal follows a close to Gaussian distribution, the modified mean can be derived based on the statistics of a truncated Gaussian distribution [16]. Thus, the average optical power of the transmitted signal after front-end-induced clipping, $\mathrm{E}\left[x_{\text{time}}(k)\right]$, can be expressed as follows:

$$\begin{aligned}\mathrm{E}\left[x_{\text{time}}(k)\right] = \sigma_{x(k)}\Big(&\phi(\lambda_{\text{bottom}}) - \phi(\lambda_{\text{top}}) \\ &+\lambda_{\text{top}}Q(\lambda_{\text{top}}) - \lambda_{\text{bottom}}Q(\lambda_{\text{bottom}})\Big) \\ &+\max\Big(P_{\text{Tx,min}}, P_{\text{Tx,bias}}\Big) ,\end{aligned} \quad (4)$$

where

$$\lambda_{\text{bottom}} = \frac{\varepsilon_{\text{bottom}}}{\sigma_{x(k)}} , \quad (5)$$

$$\lambda_{\text{top}} = \frac{\varepsilon_{\text{top}}}{\sigma_{x(k)}} , \quad (6)$$

$$\phi(u) = \frac{1}{\sqrt{2\pi}} \exp\left(\frac{-u^2}{2}\right) \quad (7)$$

and

$$Q(u) = \frac{1}{\sqrt{2\pi}} \int_u^{\infty} \exp\left(-\frac{v^2}{2}\right) dv . \quad (8)$$

Here, $\lambda_{\text{bottom}}$ and $\lambda_{\text{top}}$ are the normalized downside and upside clipping levels relative to a standard normal distribution. In addition, $\phi(\cdot)$ and $Q(\cdot)$ are the respective probability mass function (PMF) and complementary cumulative distribution function (CCDF). For the sake of clarity, plausible clipping levels satisfy the inequality $\lambda_{\text{bottom}} < \lambda_{\text{top}}$. In addition, lower $\lambda_{\text{top}}$ results in larger signal clipping, whereas the opposite holds for $\lambda_{\text{bottom}}$. It can, therefore, be ascertained that for a given dynamic range of the transmitter, $P_{\text{Tx,min}}$ to $P_{\text{Tx,max}}$, the average optical power of the transmitted signal, $\mathrm{E}\left[x_{\text{time}}(k)\right]$, is a function of the front-end biasing parameters, $P_{\text{Tx,bias}}$ and $\sigma_{x(k)}$.

In addition to the modification of the average optical signal power, the front-end-induced signal clipping distorts the data-carrying symbols. An expression for the distorted scaled odd subcarriers at the receiver, $\widetilde{X}_{\text{scaled,odd}}(m)$, is derived by the use of the Bussgang theorem and the CLT. First, the Bussgang theorem is used to obtain $\widetilde{x}(k)$ as follows:

$$\begin{aligned}\widetilde{x}(k) = U\big(x(k)\big)hAx(k) + hn_{\text{clip}}(k) \\ +hP_{\text{Tx,bias}} + n_{\text{AWGN}}(k)/\sqrt{2} ,\end{aligned} \quad (9)$$

where $U(\cdot)$ is the unit step function. The theorem states that the signal after the non-linear clipping distortion is attenuated by a factor, $A$, and a zero-mean non-Gaussian clipping noise, $n_{\text{clip}}(k)$, is added. However, in ACO-OFDM the amplitude of the received odd subcarriers is reduced by $50\%$ in the absence of double-sided clipping because of the zero-level clipping and the symmetries discussed in [4]. Therefore, in the presence of double-sided clipping, the effective attenuation factor at the received odd subcarriers, $K$, is related to $A$ as $K = A/2$. Bellow $K$ is derived for the considered ACO-OFDM system. Note that the effective power of the AWGN on the odd subcarriers needs to be halved because of the $50\%$ power allocation to the even subcarriers. Further on, $\widetilde{x}(k)$ is passed through an FFT. Applying the CLT, the distorted scaled odd subcarriers, $\widetilde{X}_{\text{scaled,odd}}(m)$, can be expressed as a function of the transmitted odd subcarriers, $X_{\text{frame,odd}}(m)$, as follows:

$$\begin{aligned}\widetilde{X}_{\text{scaled,odd}}(m) = \alpha hKX_{\text{frame,odd}}(m) + \alpha h\sigma_{\text{clip}}N_{\mathcal{CN}}(m) \\ +\alpha\sigma_{\text{AWGN}}N_{\mathcal{CN}}(m)/\sqrt{2} ,\end{aligned} \quad (10)$$

where $\sigma_{\text{clip}}$ is the standard deviation of the complex Gaussian clipping noise. Bellow we also derive $\sigma_{\text{clip}}$ for the considered ACO-OFDM system. $N_{\mathcal{CN}}(m)$ is a sample of a complex Gaussian distribution with zero mean and unity variance.

Applying the assumption of Gaussianity of $x(k)$, the atten-

This full text paper was peer reviewed at the direction of IEEE Communications Society subject matter experts for publication in the IEEE ICC 2011 proceedings

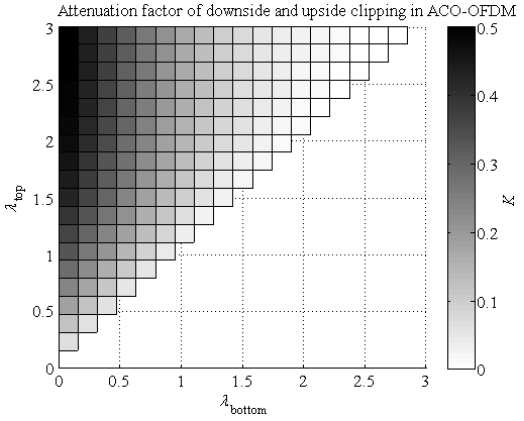


Fig. 2: Attenuation factor of the clipping noise as a function of the normalized clipping levels in ACO-OFDM.

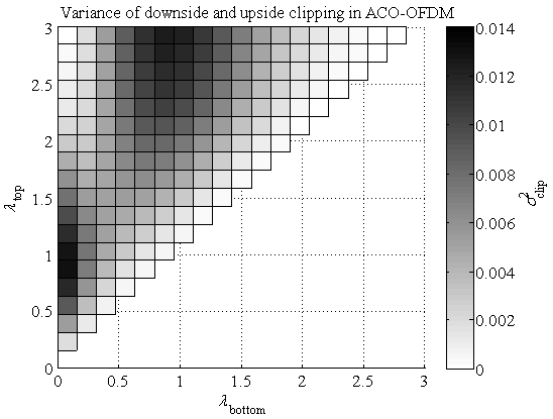


Fig. 3: Variance of the clipping noise as a function of the normalized clipping levels in ACO-OFDM.

uation factor, $K$, is expressed as follows:

$$K = Q(\lambda_{\text{bottom}}) - Q(\lambda_{\text{top}}) \; . \tag{11}$$

$K$ is illustrated in Fig. 2 as a function of the normalized downside and upside clipping levels. As suggested in [4, 5], $K$ approaches $0.5$ when the least double-sided clipping is present.

According to (9) the clipping noise, $n_{\text{clip}}(k)$, is an independent component and can be estimated separately. The ACO-OFDM time domain signal, subject only to double-sided clipping, $x_{\text{DSP}}(k)$, can be written as follows:

$$\begin{aligned} x_{\text{DSP}}(k) &= U\big(x(k)\big)\big(x(k) - \Delta_x(k)\big) \\ &= U\big(x(k)\big)Ax(k) + n_{\text{clip}}(k) \; , \end{aligned} \tag{12}$$

where $\Delta_x(k)$ is the clipped signal portion. Therefore, the clipping noise component, $n_{\text{clip}}(k)$, can be expressed as follows:

$$n_{\text{clip}}(k) = U\big(x(k)\big)\big((1-2K)x(k) - \Delta_x(k)\big) \; . \tag{13}$$

Applying the CLT on the unitary FFT, $n_{\text{clip}}(k)$ is transformed into a zero-mean Gaussian noise component at the received subcarriers preserving the variance, $\sigma^2_{\text{clip}}$. As a result, $\sigma^2_{\text{clip}}$ can be expressed as follows:

$$\begin{aligned} \sigma^2_{\text{clip}} = \frac{E_{\text{s(elec)}}}{2}\Big( & K\big(\lambda^2_{\text{bottom}} + 1\big) - 2K^2 \\ & - \lambda_{\text{bottom}}\big(\phi(\lambda_{\text{bottom}}) - \phi(\lambda_{\text{top}})\big) \\ & - \phi(\lambda_{\text{top}})\big(\lambda_{\text{top}} - \lambda_{\text{bottom}}\big) \\ & + Q(\lambda_{\text{top}})\big(\lambda_{\text{top}} - \lambda_{\text{bottom}}\big)^2\Big) \; . \end{aligned} \tag{14}$$

Note that $K$ and $\sigma^2_{\text{clip}}$ are independent of the modulation order, $M$, and the IFFT/FFT size, $N$. They only depend on the normalized downside and upside clipping levels. The clipping noise variance is presented in Fig. 3. As expected, when the least signal clipping is present, $\sigma^2_{\text{clip}}$ approaches zero. However, since $K$ and $\sigma^2_{\text{clip}}$ are coupled according to (10), as $K$ approaches zero, $\sigma^2_{\text{clip}}$ approaches zero, as well. In addition, Figs. 2 and 3 suggest that downside clipping introduces a larger ACO-OFDM symbol distortion than upside clipping.

Using (10), (11) and (14), an analytical expression for the electrical SNR per bit, $E_{\text{b(elec)}}/N_0$, can be expressed as follows:

$$\frac{E_{\text{b(elec)}}}{N_0} = \frac{K^2 E_{\text{s(elec)}}}{\log_2 M\Big(\sigma^2_{\text{clip}} + \dfrac{N_0}{2h^2}B_{\text{DC}}\Big)} \; , \tag{15}$$

The factor $B_{\text{DC}}$ is defined as follows:

$$B_{\text{DC}} = 2\frac{P^2_{\text{Tx,bias}}}{\sigma^2_{x(k)}} + \frac{4}{\sqrt{2\pi}}\frac{P_{\text{Tx,bias}}}{\sigma_{x(k)}} + 1 \; . \tag{16}$$

The $B_{\text{DC}}$ factor denotes the loss in the electrical signal power of $x_{\text{DSP}}(k)$ due to the biasing of the transmitter front-end by $P_{\text{Tx,bias}}$ in the best case clipping scenario, *i.e.* $\lambda_{\text{bottom}} = 0$ and $\lambda_{\text{top}} = +\infty$. In addition, zero forcing (ZF) is employed in the equalizer [2]. Even though ZF is an equalization technique widely used in OFDM-based systems, it results in AWGN amplification when the path gain decreases. Alternatively, minimum mean squared error (MMSE) equalization can be employed which alleviates this issue. In this context, because of the bias added to the ACO-OFDM signal, $P_{\text{Tx,bias}}$, the electrical-to-optical conversion factor for the bit power in [5] has to be modified as follows:

$$E_{\text{b(opt)}} = \sqrt{\frac{B_{\text{DC}} + 1/\pi - 1}{B_{\text{DC}}}E_{\text{b(elec)}}} \; . \tag{17}$$

## IV. BER SIMULATION RESULTS AND DISCUSSION

The performance of ACO-OFDM in the presence of double-sided signal clipping and AWGN is assessed in terms of BER. The accuracy of the derived expression for SNR in ACO-OFDM OWC systems from (15) is verified and compared with a Monte Carlo BER simulation. For this purpose, an IFFT/FFT size of 2048 is chosen. In addition, unity channel path gain, $h$, is assumed for simplicity. Two clipping scenarios are considered: zero-level clipping only and $\lambda_{\text{bottom}} = 0.1$,

This full text paper was peer reviewed at the direction of IEEE Communications Society subject matter experts for publication in the IEEE ICC 2011 proceedings

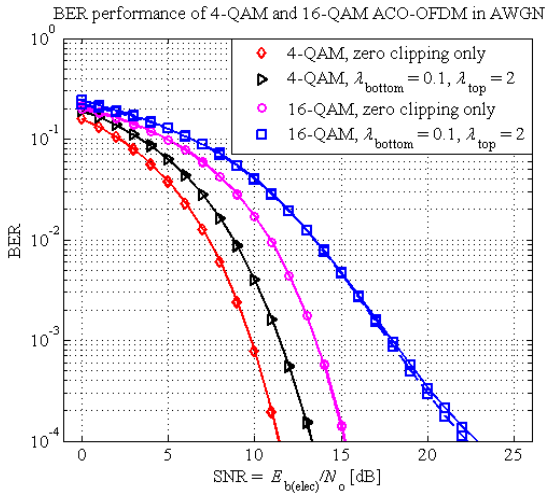


Fig. 4: BER performance of ACO-OFDM in AWGN, simulation (solid lines) vs. theory (dashed lines).

$\lambda_{\text{top}} = 2$. The latter scenario can be realized, if a Vishay TSFF5210 LED with a dynamic range between 50 mW and 500 mW of radiated optical power is driven by a signal $x(k)$ with $\sigma_{x(k)} = 236.8$ mW which is biased by $P_{\text{Tx,bias}} = 26.3$ mW [17]. Furthermore, 4-QAM and 16-QAM symbols are considered to show the effect of signal clipping on higher order modulation. The following analytical expression for the BER performance of $M$-QAM is employed [18]:

$$\text{BER} = \frac{4\left(\sqrt{M}-1\right)}{\log_2(M)\sqrt{M}} Q\left(\sqrt{\frac{3\log_2(M)}{M-1}\frac{E_{\text{b(elec)}}}{N_0}}\right) . \quad (18)$$

The theoretical and simulation results presented in Fig. 4 confirm a close match. Since the Gaussian clipping noise at the received subcarriers is added independently of the QAM modulation order in (10), higher order modulation is shown to be more vulnerable to signal clipping. In addition, since the factors in (10) are independent of $N$ for practical IFFT/FFT sizes, *i.e.* $N > 64$, the BER performance is independent of the total number of subcarriers.

## V. Conclusion

In this paper, double-sided signal clipping in an ACO-OFDM OWC system due to biasing issues and physical limitations of the front-ends is studied. In accord with the Bussgang theorem and the CLT, the statistics of the clipping noise as a function of the normalized downside and upside clipping levels are derived. An expression for the electrical SNR per bit at the receiver is presented and it proves to match the Monte Carlo BER simulation. The derived SNR shows that unlike in OFDM-based RF systems an SNR increase is not achievable simply by increasing the average electrical and/or optical power at the transmitter. In OWC, such a measure leads to a larger clipping distortion which is exactly quantified in (15). Finally, higher order modulation proves to be more vulnerable to signal clipping, whereas the IFFT/FFT size does not affect the BER performance.

## Acknowledgement

We gratefully acknowledge EADS UK Ltd. for the support of this research. Professor Haas acknowledges the Scottish Funding Council support of his position within the Edinburgh Research Partnership in Engineering and Mathematics between the University of Edinburgh and Heriot Watt University.

## References

[1] Y. Tanaka, T. Komine, S. Haruyama, and M. Nakagawa, "Indoor Visible Communication Utilizing Plural White LEDs as Lighting," in *Proceedings of the 12$^{th}$ IEEE International Symposium on Personal, Indoor and Mobile Radio Communications*, vol. 2, San Diego, CA, USA, Sep. 30–Oct. 3, 2001, pp. 81–85.

[2] H. Elgala, R. Mesleh, H. Haas, and B. Pricope, "OFDM Visible Light Wireless Communication Based on White LEDs," in *Proc. of the 64th IEEE Vehicular Technology Conference (VTC)*, Dublin, Ireland, Apr. 22–25, 2007.

[3] J. B. Carruthers and J. M. Kahn, "Multiple-subcarrier Modulation for Nondirected Wireless Infrared Communication," *IEEE Journal on Selected Areas in Communications*, vol. 14, no. 3, pp. 538–546, Apr. 1996.

[4] J. Armstrong and A. Lowery, "Power Efficient Optical OFDM," *Electronics Letters*, vol. 42, no. 6, pp. 370–372, Mar. 16, 2006.

[5] J. Armstrong and B. J. C. Schmidt, "Comparison of Asymmetrically Clipped Optical OFDM and DC-Biased Optical OFDM in AWGN," *IEEE Commun. Lett.*, vol. 12, no. 5, pp. 343–345, May 2008.

[6] D. Dardari, V. Tralli, and A. Vaccari, "A Theoretical Characterization of Nonlinear Distortion Effects in OFDM Systems," *IEEE Transactions on Communications*, vol. 48, no. 10, pp. 1755–1764, Oct. 2000.

[7] J. Bussgang, "Cross Correlation Function of Amplitude-Distorted Gaussian Signals," Research Laboratory for Electronics, Massachusetts Institute of Technology, Cambridge, MA, Technical Report 216, Mar. 1952.

[8] H. Elgala, R. Mesleh, and H. Haas, "Non-linearity effects and predistortion in optical OFDM wireless transmission using LEDs," *Inderscience Intenational Journal of Ultra Wideband Communications and Systems (IJUWBCS)*, vol. 1, no. 2, pp. 143–150, 2009.

[9] H. Ochiai and H. Imai, "Performance analysis of deliberately clipped OFDM signals," *IEEE Transactions on Communications*, vol. 50, no. 1, pp. 89–101, Jan. 2002.

[10] D. J. G. Mestdagh, P. Spruyt, and B. Biran, "Analysis of Clipping Effect in DMT-based ADSL Systems," in *Proc. IEEE International Conference on Communications ICC 1994*, vol. 1, New Orleans, LA, USA, 1–5 May 1994, pp. 293–300.

[11] S. Dimitrov and H. Haas, "On the Clipping Noise in an ACO-OFDM Optical Wireless Communication System," in *IEEE Global Communications Conference (IEEE GLOBECOM 2010)*, Miami, Florida, USA, 6–10 Dec. 2010.

[12] BS EN 62471:2008, *Photobiological Safety of Lamps and Lamp Systems*, BSI British Standards Std., Sep. 2008.

[13] H. Elgala, R. Mesleh, and H. Haas, "Practical Considerations for Indoor Wireless Optical System Implementation using OFDM," in *Proc. of the IEEE 10th International Conference on Telecommunications (ConTel)*, Zagreb, Croatia, Jun. 8–10 2009.

[14] S. Dimitrov, R. Mesleh, H. Haas, M. Cappitelli, M. Olbert, and E. Bassow, "On the SIR of a Cellular Infrared Optical Wireless System for an Aircraft," *IEEE Journal on Selected Areas in Communications (IEEE JSAC)*, vol. 27, no. 9, pp. 1623–1638, Dec. 2009.

[15] Vishay Semiconductors, "Datasheet: TEMD5110X01 Silicon PIN Photodiode," Retrieved Feb. 10, 2011 from http://www.vishay.com/docs/84658/temd5110.pdf, May 2009.

[16] N. Johnson, S. Kotz, and N. Balakrishnan, *Continuous Univariate Distributions*, 2nd ed. John Wiley & Sons Ltd., 1994, vol. 1.

[17] Vishay Semiconductors, "Datasheet: TSFF5210 High Speed Infrared Emitting Diode, 870 nm, GaAlAs Double Hetero," Retrieved Fec. 10, 2011 from http://www.vishay.com/docs/81090/tsff5210.pdf, Jun. 2009.

[18] I. A. Glover and P. M. Grant, *Digital Communications*, 2nd ed. Pearson Prentice Hall, 2004.

2nd IEEE Workshop on Optical Wireless Communications

# A Comparison of OFDM-based Modulation Schemes for OWC with Clipping Distortion

Svilen Dimitrov, Sinan Sinanovic and Harald Haas

*Institute for Digital Communications, Joint Research Institute for Signal and Image Processing, The University of Edinburgh, EH9 3JL Edinburgh, UK, e-mail: {s.dimitrov, s.sinanovic, h.haas}@ed.ac.uk*

***Abstract*—In this paper, the electrical power requirement and spectral efficiency of multi-carrier transmission schemes for optical wireless communications (OWC) are compared in the presence of front-end-induced double-sided signal clipping. The two existing multi-carrier modulation techniques based on orthogonal frequency division multiplexing (OFDM), direct-current-biased optical OFDM (DCO-OFDM) and asymmetrically clipped optical OFDM (ACO-OFDM), are studied. The clipping noise can be modeled according to the Bussgang theorem and the central limit theorem (CLT) as attenuation of the data-carrying subcarriers and addition of zero-mean complex-valued Gaussian noise. Presented closed-form expressions for the attenuation factor and the clipping noise variance are employed in the derivation of the effective electrical signal-to-noise ratio (SNR). Using multi-level quadrature amplitude modulation ($M$-QAM), the electrical power requirement of optical OFDM (O-OFDM) transmission is obtained from the bit-error ratio (BER) system performance. It is shown that in a practical front-end biasing setup DCO-OFDM has a lower electrical power requirement to achieve a target BER as compared to ACO-OFDM for modulation orders with equal spectral efficiencies above $1$ bit/s/Hz.**

***Index Terms*—DCO-OFDM, ACO-OFDM, optical wireless communication, clipping noise, emitter biasing, detector noise.**

## I. Introduction

OWC is a promising candidate for medium range high-speed data transmission. Both infrared [1] and visible light communication [2] have the potential to deliver several hundreds of Mbps throughput. In addition to being a complementary non-interfering solution alongside radio frequency (RF) technology, OWC has the advantage of license-free operation over a significantly wider spectrum.

The data transmission in OWC is achieved through intensity modulation and direct detection (IM/DD). A real-valued non-negative signal modulates the intensity of a light emitting diode (LED) at the transmitter, and it is detected by a photodiode (PD) at the receiver. Multi-carrier modulation such as $M$-QAM O-OFDM has inherent robustness to the multi-path dispersion of the optical wireless channel, and it promises to deliver very high data rates [2]. In the literature, two possible O-OFDM system realizations can be found: DCO-OFDM [3] and ACO-OFDM [4]. A real-valued signal is obtained, when Hermitian symmetry is imposed on the OFDM subcarriers. A non-negative signal is obtained in DCO-OFDM by the addition of a direct current (DC) bias. In ACO-OFDM, the odd subcarriers are enabled for data transmission, whereas the even ones are set to zero. Here, the negative part of the time domain signal can be clipped at the transmitter, and the information can be still successfully decoded from the odd subcarriers at the receiver. As a result, ACO-OFDM presents a greater optical power efficiency at the expense of a $50\%$ reduction in spectral efficiency as compared to DCO-OFDM. The two systems have been compared in terms of optical power requirement and spectral efficiency in [5] in an idealized front-end biasing setup, where a non-negative signal can turn on the LED, and the transmitter has an infinite dynamic range. Such conditions, however, are hardly achievable in practice. In addition, a comparison in terms of electrical power requirement, including both alternating current (AC) power and DC power, and spectral efficiency in a practical front-end biasing setup is considered an open issue.

The imperfections of the optical front-ends due to the use of off-the-shelf components result in a limited linear dynamic range of radiated optical power. In general, the transmitter LED is biased by a constant current source, which supports the entire range of forward voltages across the LED. The bias current is added to the information carrying current, yielding the forward current through the LED. Since the radiated optical power is directly proportional to the forward current, the signal and the transmitter constraints are described in terms of optical power in the rest of the paper. It is shown in [6] that the non-linear $I$-$V$ characteristic of the LED can be compensated by pre-distortion. A linear characteristic is obtainable, however, only over a limited range between $i_{\min}$ and $i_{\max}$, corresponding to a point of minimum optical power, $P_{\mathrm{Tx,min}}$, and a point of maximum optical power, $P_{\mathrm{Tx,max}}$. Furthermore, the eye safety regulations [7] and/or the design requirements constrain the level of radiated average optical power to $P_{\mathrm{Tx,avg}}$. In order to condition the signal in accord with these constraints, signal scaling in the digital signal processor (DSP) and DC-biasing in the analog circuitry is required. Because of the fact that an OFDM system employs the unitary inverse fast Fourier transform (IFFT) as a multiplexing technique at the transmitter, the non-clipped signal follows a close to Gaussian distribution for IFFT sizes greater than $64$ [8], according to the CLT. Therefore, signal shaping in DCO-OFDM and ACO-OFDM, in order to fit the front-end power constraints, results in a non-linear signal distortion. Using the fact that the unitary fast Fourier transform (FFT) is employed as a demultiplexing technique at the receiver, the non-linear distortion can be modeled by means of the Bussgang theorem and CLT as attenuation of the information carrying subcarriers plus zero-

978-1-4673-0040-7/11/$26.00 ©2011 IEEE

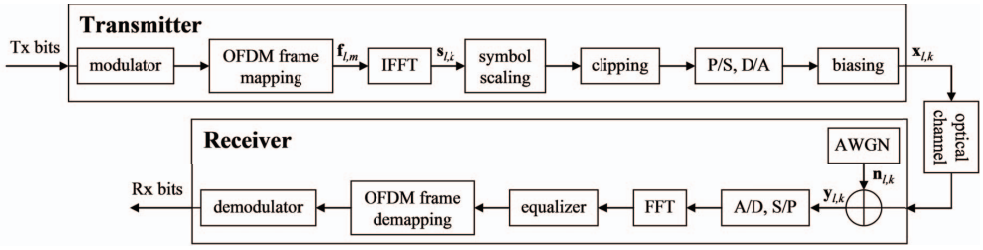


Fig. 1: Block diagram of O-OFDM transmission.

mean complex-valued Gaussian noise [9]. In the previous study, closed-form expressions for the attenuation factor and the clipping noise variance are determined for ACO-OFDM as a function of the independent bottom and top clipping levels. Symmetric signal clipping in DCO-OFDM has been analyzed in [10], whereas the signal clipping at independent bottom and top levels is still considered an open issue.

In this paper, double-sided signal clipping at the transmitter front-end is studied for DCO-OFDM and ACO-OFDM. The attenuation factor and the variance of the complex-valued Gaussian clipping noise at the received data-carrying subcarriers are determined in closed-form and included in the derivation of the effective electrical SNR. The O-OFDM systems are compared in a novel fashion in terms of electrical power requirement and spectral efficiency in a practical front-end biasing setup with several double-sided signal clipping scenarios. DCO-OFDM demonstrates a lower electrical power requirement to achieve a target BER for QAM modulation orders with spectral efficiencies above 1 bit/s/Hz. Equivalently, DCO-OFDM delivers higher throughput as compared to ACO-OFDM for SNR targets above 16 dB.

The rest of the paper is organized as follows. Section II presents the O-OFDM system model. DCO-OFDM and ACO-OFDM are compared in terms of electrical power requirement and spectral efficiency in Section III. Finally, Section IV concludes the paper.

## II. O-OFDM TRANSMISSION

The conventional discrete model for a noisy communication link is employed in this study:

$$\mathbf{y} = \mathbf{h} * \mathbf{x} + \mathbf{n}\,, \tag{1}$$

where $\mathbf{y}$ represents the received distorted replica of the transmitted signal $\mathbf{x}$, which is convolved with the channel impulse response, $\mathbf{h}$, and additive white Gaussian noise (AWGN), $\mathbf{n}$, is added at the receiver. In $M$-QAM O-OFDM, $\mathbf{n}$ represents a bipolar real-valued zero-mean Gaussian noise, which after optical-to-electrical (O/E) conversion is transformed into a complex-valued AWGN with an electrical power spectral density (PSD) of $N_0/2$ per complex dimension [11]. Here, $*$ stands for discrete linear convolution. The discrete signal vectors are obtained after sampling of the equivalent continuous-time signals with a sampling period of $T$. Here, $\mathbf{x}$ contains $Z_{\mathbf{x}}$ samples, $\mathbf{h}$ has $Z_{\mathbf{h}}$ samples, and as a result, $\mathbf{n}$ and $\mathbf{y}$ have $Z_{\mathbf{x}} + Z_{\mathbf{h}} - 1$ samples [11]. In multi-carrier systems, the optical wireless channel is transformed into a flat fading channel with an optical path gain, $g_{\mathrm{h(opt)}}$ [12], by the use of a large number of subcarriers and a cyclic prefix (CP). The CP transforms the linear convolution into a cyclic convolution. Therefore, single-tap zero forcing (ZF) or minimum mean-squared error (MMSE) equalization is sufficient to counter the channel effect. Since the CP has a negligible effect on the electrical power requirement or the spectral efficiency [13], it is omitted in the derivations in this study. The signal shaping framework for $\mathbf{x}$ is elaborated below.

The block diagram for multi-carrier O-OFDM transmission is presented in Fig. 1. Here, $\log_2(M)$ bits of the equiprobable input bits modulate the complex-valued information carrying frequency domain subcarrier in an $M$-QAM fashion. In general, $N$ subcarriers form the $l$-th OFDM frame, $\mathbf{f}_{l,m}$, $l = 0, 1, ..., L-1$, corresponding to the $l$-th OFDM symbol, where $m$, $m = 0, 1, ..., N-1$, is the subcarrier index. Each subcarrier occupies a bandwidth of $1/NT$ in a total OFDM frame bandwidth of $1/T$. Both systems have the Hermitian symmetry imposed on the OFDM frame, in order to ensure a real-valued time domain signal. Whereas in DCO-OFDM the information carrying subcarriers populate the first half of the frame, leaving the first one set to zero, in ACO-OFDM every even subcarrier is set to zero. The $l$-th OFDM symbol in the train of $L$ symbols, $\mathbf{s}_l$, is obtained by the IFFT of the $l$-th OFDM frame in the train of $L$ frames, $\mathbf{f}_l$. Here, the time domain sample index within the $l$-th OFDM symbol, $\mathbf{s}_{l,k}$, is denoted by $k$, $k = 0, 1, ..., N-1$. As a result, the time domain OFDM symbol with a bandwidth of $1/T$ has a duration of $NT$ [11]. The resulting spectral efficiency of DCO-OFDM is $\log_2(M)(N-2)/(2N)$ bits/s/Hz, whereas ACO-OFDM achieves $\log_2(M)/4$ bits/s/Hz. The train of OFDM symbols, $\mathbf{s}_{l,k}$, follows a close to Gaussian distribution for IFFT/FFT sizes greater than 64 [8]. In order to fit the signal within the limited linear dynamic range of the transmitter, $\mathbf{s}_{l,k}$ is scaled and clipped at normalized bottom and top clipping levels of $\lambda_{\mathrm{bottom}}$ and $\lambda_{\mathrm{top}}$ relative to a standard normal distribution [9]. In addition, because of the structure of the ACO-OFDM frame, the negative samples of the ACO-OFDM time domain signal can be clipped, and the information can still be successfully decoded from the odd subcarriers at the receiver. Next, the train of symbols is subjected to a parallel-to-

serial (P/S) conversion, and it is passed through the digital-to-analog (D/A) converter. Here, a pulse shaping filter is applied to obtain a continuous-time signal. In the analog circuitry the signal is DC-biased by $\beta_{\mathrm{DC}}$. Therefore, the transmitted signal vector, $\mathbf{x}$, with a length of $Z_{\mathbf{x}} = LN$ can be expressed as follows:

$$\mathbf{x}_{l,k} = \mathrm{CLIP}\left[\alpha_l \mathbf{s}_{l,k}\right] + \beta_{\mathrm{DC}} \ . \tag{2}$$

Here, $\alpha_l$ is given for a particular OFDM symbol as follows [9]:

$$\alpha_l = \sigma \sqrt{\frac{N-1}{\sum_{m=0}^{N-1} |\mathbf{f}_{l,m}|^2}} \ , \tag{3}$$

where $\sigma$ is the target standard deviation of the non-clipped time domain signal to be fit within the front-end optical power constraints. Note that $\mathrm{E}\left[\alpha_l^2\right]$ can be simplified to $\mathrm{E}\left[\alpha_l^2\right] = \sigma^2/b$. Here, $b$ is the utilization factor for a bandwidth of $B$, *i.e.* $b = (N-2)/N$ in DCO-OFDM and $b = 0.5$ in ACO-OFDM. Therefore, the information carrying subcarriers have an average electrical symbol power of $P_{\mathrm{s(elec)}} = P_{\mathrm{b(elec)}} \log_2(M) = \sigma^2/b$, where $P_{\mathrm{b(elec)}}$ is the average electrical bit power. The non-linear clipping distortion represented by the $\mathrm{CLIP}\left[\cdot\right]$ operator can be translated into an attenuation factor, $K$, on the information carrying subcarriers plus a zero-mean complex-valued Gaussian noise component with a variance of $\sigma^2_{\mathrm{clip}}$ [9]. In DCO-OFDM and ACO-OFDM, $K$ is given as follows [9]:

$$K = Q(\lambda_{\mathrm{bottom}}) - Q(\lambda_{\mathrm{top}}) \ . \tag{4}$$

Here, $Q(\cdot)$ stands for the complementary cumulative distribution function (CCDF) of a standard normal distribution with zero mean and unity variance. The variance of the clipping noise can be expressed in ACO-OFDM as follows [9]:

$$\begin{aligned} \sigma^2_{\mathrm{clip}} = \frac{P_{\mathrm{s(elec)}}}{2} \Big( & K\left(\lambda^2_{\mathrm{bottom}} + 1\right) - 2K^2 \\ & - \lambda_{\mathrm{bottom}}\left(\phi(\lambda_{\mathrm{bottom}}) - \phi(\lambda_{\mathrm{top}})\right) \\ & - \phi(\lambda_{\mathrm{top}})\left(\lambda_{\mathrm{top}} - \lambda_{\mathrm{bottom}}\right) \\ & + Q(\lambda_{\mathrm{top}})\left(\lambda_{\mathrm{top}} - \lambda_{\mathrm{bottom}}\right)^2 \Big) \ , \end{aligned} \tag{5}$$

where $\phi(\cdot)$ stands for the probability density function (PDF) of a standard normal distribution. Following the procedure elaborated in [9], the variance of the clipping noise in DCO-OFDM can be expressed as follows:

$$\begin{aligned} \sigma^2_{\mathrm{clip}} = P_{\mathrm{s(elec)}} \Big( & K - K^2 - \left(\phi(\lambda_{\mathrm{bottom}}) - \phi(\lambda_{\mathrm{top}})\right. \\ & \left. + (1 - Q(\lambda_{\mathrm{bottom}}))\lambda_{\mathrm{bottom}} + Q(\lambda_{\mathrm{top}})\lambda_{\mathrm{top}}\right)^2 \\ & + (1 - Q(\lambda_{\mathrm{bottom}}))\lambda^2_{\mathrm{bottom}} + Q(\lambda_{\mathrm{top}})\lambda^2_{\mathrm{top}} \\ & + \phi(\lambda_{\mathrm{bottom}})\lambda_{\mathrm{bottom}} - \phi(\lambda_{\mathrm{top}})\lambda_{\mathrm{top}} \Big) \ . \end{aligned} \tag{6}$$

The attenuation factor, $K$, as a function of the clipping levels is presented in Fig. 2 and Fig. 3 in DCO-OFDM and ACO-OFDM. The respective clipping noise variance, $\sigma^2_{\mathrm{clip}}$, is illustrated in Fig. 4 and Fig. 5. Here, a large symbol distortion is defined for a small $K$ and large $\sigma^2_{\mathrm{clip}}$. Therefore, Fig. 2 and Fig. 4 suggest that the symbol distortion in DCO-OFDM can be minimized with symmetric clipping levels. In addition, Fig. 3 and Fig. 5 show that downside clipping introduces a larger ACO-OFDM symbol distortion than upside clipping.

In addition to the distortion of the information carrying subcarriers, time domain signal clipping modifies the average optical power of the transmitted signal as follows:

$$\begin{aligned} \mathrm{E}\left[\mathbf{x}\right] = \sigma \Big( & \lambda_{\mathrm{top}} Q(\lambda_{\mathrm{top}}) - \lambda_{\mathrm{bottom}} Q(\lambda_{\mathrm{bottom}}) \\ & + \phi(\lambda_{\mathrm{bottom}}) - \phi(\lambda_{\mathrm{top}}) \Big) + P_{\mathrm{bottom}} \ . \end{aligned} \tag{7}$$

In DCO-OFDM, $P_{\mathrm{bottom}} = P_{\mathrm{Tx,min}}$. In ACO-OFDM, $P_{\mathrm{bottom}} = \max\left(P_{\mathrm{Tx,min}}, \beta_{\mathrm{DC}}\right)$ because of the default zero-level clipping. In general, the eye safety regulations [7] and/or the design requirements impose the constraint: $\mathrm{E}\left[\mathbf{x}\right] \leq P_{\mathrm{Tx,avg}}$. Since the signal is clipped, the resulting average optical signal power, $\mathrm{E}\left[\mathbf{x}\right]$, is not equal to the average optical

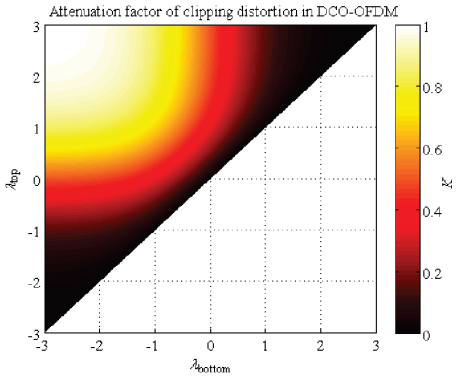


Fig. 2: Attenuation factor, $K$, in DCO-OFDM as a function of the normalized clipping levels.

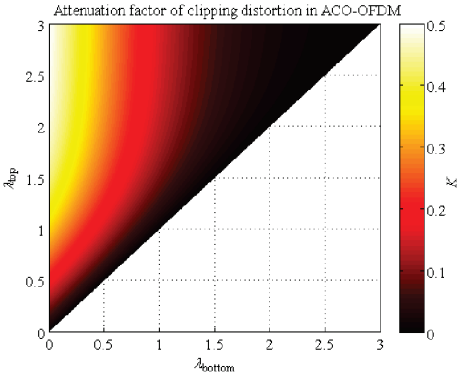


Fig. 3: Attenuation factor, $K$, in ACO-OFDM as a function of the normalized clipping levels.

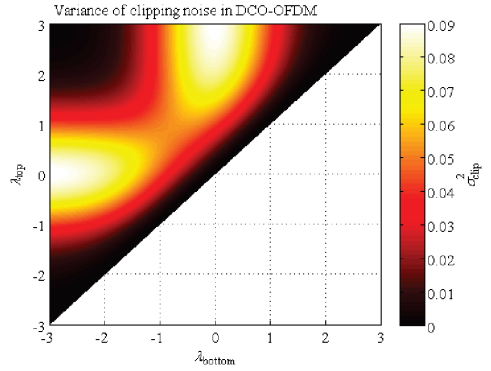


Fig. 4: Clipping noise variance, $\sigma^2_{\text{clip}}$, in DCO-OFDM as a function of the normalized clipping levels. Here, $P_{\text{s(elec)}} = 1$.

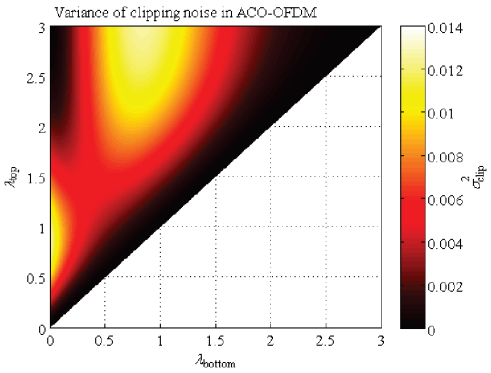


Fig. 5: Clipping noise variance, $\sigma^2_{\text{clip}}$, in ACO-OFDM as a function of the normalized clipping levels. Here, $P_{\text{s(elec)}} = 1$.

symbol power, $P_{\text{s(opt)}}$. In general, $P_{\text{s(opt)}}$, is defined for the scenario with the least signal clipping, which is given in DCO-OFDM as $\lambda_{\text{bottom}} = -\infty$ and $\lambda_{\text{top}} = +\infty$, and in ACO-OFDM as $\lambda_{\text{bottom}} = 0$ and $\lambda_{\text{top}} = +\infty$. Thus, in DCO-OFDM, $P_{\text{s(opt)}} = \beta_{\text{DC}}$, whereas in ACO-OFDM, $P_{\text{s(opt)}} = (\beta_{\text{DC}} + \sigma/\sqrt{2\pi})$. Combined with (7), these equations convey the relation between $\mathrm{E}[\mathbf{x}]$ and $P_{\text{s(opt)}}$.

The E/O conversion given in [5] can be generalized in DCO-OFDM and ACO-OFDM, respectively, as follows:

$$P_{\text{s(opt)}} = \sqrt{\frac{\mathrm{E}[\mathbf{x}]^2}{\mathrm{E}[\mathbf{x}^2]} P_{\text{s(elec)}}} = \sqrt{\frac{\beta^2_{\text{DC}}}{\sigma^2 + \beta^2_{\text{DC}}} P_{\text{s(elec)}}}\,, \tag{8}$$

$$P_{\text{s(opt)}} = \sqrt{\frac{2\pi\beta^2_{\text{DC}} + 2\sigma\beta_{\text{DC}}\sqrt{2\pi} + \sigma^2}{2\pi\beta^2_{\text{DC}} + 2\sigma\beta_{\text{DC}}\sqrt{2\pi} + \pi\sigma^2} P_{\text{s(elec)}}}\,. \tag{9}$$

Here, $\mathrm{E}[\mathbf{x}]$ and $\mathrm{E}[\mathbf{x}^2]$ are defined for the least signal clipping scenario, and these are used in every other clipping setup.

The signal $\mathbf{x}_{l,k}$ is transmitted over the optical wireless channel, and it picks up AWGN, $\mathbf{n}_{l,k}$, at the receiver to obtain $\mathbf{y}_{l,k}$. In the analog-to-digital (A/D) converter, the signal is passed through a matched filter, and it is sampled at a frequency of $1/T$ [11]. Using a serial-to-parallel (S/P) converter, the signal is passed through an FFT block back to the frequency domain. After ZF or MMSE equalization, a hard-decision decoder is employed on the known OFDM frame structure to obtain the received bits. Thus, the effective electrical SNR per bit in O-OFDM is given as follows [9]:

$$\Gamma_{\text{b(elec)}} = \frac{K^2 P_{\text{b(elec)}}}{\sigma^2_{\text{clip}} + \dfrac{bBN_0}{G_{\text{EQ}} G_{\text{DC}}}}\,, \tag{10}$$

where $G_{\text{EQ}}$ stands for the equalizer gain, and it is given for ZF and MMSE, respectively, as $g^2_{\text{h(opt)}}$ and $g^2_{\text{h(opt)}} + \left(P_{\text{b(elec)}}/N_0\right)^{-1}$. Here, $G_{\text{DC}}$ denotes the attenuation of the useful electrical signal power of $\mathbf{x}$ due to the DC component, and it can be expressed in DCO-OFDM and ACO-OFDM, respectively, as follows:

$$G_{\text{DC}} = \frac{\mathrm{E}\left[(\mathbf{x} - \beta_{\text{DC}})^2\right]}{\mathrm{E}[\mathbf{x}^2]} = \frac{\sigma^2}{\sigma^2 + \beta^2_{\text{DC}}}\,, \tag{11}$$

$$G_{\text{DC}} = \frac{\sqrt{2\pi}\sigma^2}{\sqrt{2\pi}\sigma^2 + 4\sigma\beta_{\text{DC}} + 2\sqrt{2\pi}\beta^2_{\text{DC}}}\,. \tag{12}$$

The factor $G_{\text{DC}}$ is defined for the least signal clipping scenario, and it is used in every other clipping setup.

The BER performance of $M$-QAM O-OFDM in AWGN can be obtained as follows [14]:

$$\text{BER} = \frac{4\left(\sqrt{M}-1\right)}{\log_2(M)\sqrt{M}} Q\left(\sqrt{\frac{3\log_2(M)}{M-1}\Gamma_{\text{b(elec)}}}\right)\,. \tag{13}$$

## III. Electrical power requirement *vs.* spectral efficiency in O-OFDM

DCO-OFDM and ACO-OFDM are compared in terms of electrical power requirement to achieve a target BER of $10^{-3}$ and the corresponding spectral efficiency. Here, the required electrical power is normalized by the noise power for unity bandwidth, *i.e.* the required electrical SNR per bit, $P_{\text{b(elec)}}/N_0$. The following modulation orders are chosen, $M = \{2, 4, 16, 64, 256, 1024\}$. Here, the case of $M = 2$ is realized in $M$-QAM through binary phase shift keying (BPSK) modulation, which requires the same $P_{\text{b(elec)}}/N_0$ as 4-QAM at the expense of 50% reduction in spectral efficiency. A practical linear dynamic range of a Vishay TSHG8200 LED between $P_{\text{Tx,min}} = 5$ mW and $P_{\text{Tx,max}} = 50$ mW at room temperature is considered at the transmitter [15]. Since this LED is eye-safe, even if operated at $P_{\text{Tx,max}} = 50$ mW [12], no constraint is imposed on the average optical power level. As suggested in Fig. 2 and Fig. 4, the non-linear clipping distortion in DCO-OFDM can be minimized, when symmetrical clipping levels are considered, *i.e.* $\lambda_{\text{bottom}} = -\lambda_{\text{top}}$. According to Fig. 3 and Fig. 5 the distortion in ACO-OFDM is minimum, when the bottom level clipping is kept at minimum, *i.e.* $\lambda_{\text{bottom}} = 0$. Therefore, the average optical power level in DCO-OFDM is set to $\mathrm{E}[\mathbf{x}] = \beta_{\text{DC}} = 27.5$ mW. In ACO-OFDM, $\mathrm{E}[\mathbf{x}]$ can be obtained from (7), where $\beta_{\text{DC}} = 5$ mW. The variance of

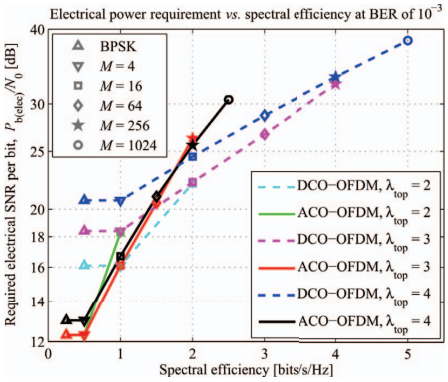


Fig. 6: Electrical power requirement *vs.* spectral efficiency at $10^{-3}$ BER of DCO-OFDM and ACO-OFDM.

the time domain signal, $\sigma^2$, results from the choice of the normalized top clipping level, $\lambda_{\text{top}}$. Here, $\lambda_{\text{top}} = \{2, 3, 4\}$ is considered, in order to illustrate the influence of the biasing setup on the electrical power requirement and the spectral efficiency of the O-OFDM systems. In addition, since the optical path gain coefficient, $g_{\text{h(opt)}}$, directly translates into an SNR penalty in (10), $g_{\text{h(opt)}} = 1$ is assumed for simplicity. An MMSE equalizer is used.

The power requirement *vs.* spectral efficiency plot of DCO-OFDM and ACO-OFDM is presented in Fig. 6. It is shown that ACO-OFDM requires an SNR of 12.3 dB, in order to enable BPSK and 4-QAM transmission. In order to enable BPSK and 4-QAM transmission in DCO-OFDM, an SNR of 16 dB is required. However, it is shown that for modulation orders with spectral efficiencies greater than 1 bit/s/Hz DCO-OFDM has a lower electrical power requirement as compared to ACO-OFDM to achieve the target BER of $10^{-3}$. Equivalently, DCO-OFDM delivers higher throughput for SNR targets above 16 dB. In addition, it is shown that the electrical power requirement and the spectral efficiency of the O-OFDM systems greatly depend on the choice of the biasing setup. A lower $\lambda_{\text{top}}$ value corresponds to a higher signal variance and a lower SNR target. However, such a scenario is unable to realize higher order modulation because of the increased nonlinear clipping distortion. A higher $\lambda_{\text{top}}$ value corresponds to a lower signal variance, which requires a higher SNR target, but it enables higher order modulation, *e.g.* 1024-QAM.

## IV. Conclusion

In this paper, double-sided signal clipping in DCO-OFDM and ACO-OFDM is studied. In accord with the Bussgang theorem and the CLT, the statistics of the clipping noise at the received data-carrying subcarriers are presented in closed-form as a function of the normalized bottom and top clipping levels. The derived expression for the effective electrical SNR in optical OFDM is employed to obtain the electrical power requirement to achieve a target BER of $10^{-3}$. As a result, DCO-OFDM and ACO-OFDM are compared in a novel fashion in terms of electrical power requirement and spectral efficiency in a practical front-end biasing setup for several clipping scenarios. DCO-OFDM demonstrates a lower electrical power requirement for modulation orders with spectral efficiency above 1 bit/s/Hz. Equivalently, DCO-OFDM shows a greater spectral efficiency for SNR targets above 16 dB. While a higher signal variance reduces the SNR target, it introduces a larger clipping distortion, which prevents the realization of higher order QAM. Even though a lower signal variance increases the SNR target, it reduces the clipping distortion, which enables higher order QAM and the highest system throughput.

## Acknowledgement

We gratefully acknowledge EADS UK Ltd. for the support of this research. Professor Haas acknowledges the Scottish Funding Council support of his position within the Edinburgh Research Partnership in Engineering and Mathematics between the University of Edinburgh and Heriot Watt University.

## References

[1] F. R. Gfeller and U. Bapst, "Wireless In-House Data Communication Via Diffuse Infrared Radiation," *Proceedings of the IEEE*, vol. 67, no. 11, pp. 1474–1486, Nov. 1979.

[2] Y. Tanaka, T. Komine, S. Haruyama, and M. Nakagawa, "Indoor Visible Communication Utilizing Plural White LEDs as Lighting," in *Proceedings of the 12$^{th}$ IEEE International Symposium on Personal, Indoor and Mobile Radio Communications*, vol. 2, San Diego, CA, USA, Sep. 30–Oct. 3, 2001, pp. 81–85.

[3] J. B. Carruthers and J. M. Kahn, "Multiple-subcarrier Modulation for Nondirected Wireless Infrared Communication," *IEEE Journal on Selected Areas in Communications*, vol. 14, no. 3, pp. 538–546, Apr. 1996.

[4] J. Armstrong and A. Lowery, "Power Efficient Optical OFDM," *Electronics Letters*, vol. 42, no. 6, pp. 370–372, Mar. 16, 2006.

[5] J. Armstrong and B. J. C. Schmidt, "Comparison of Asymmetrically Clipped Optical OFDM and DC-Biased Optical OFDM in AWGN," *IEEE Commun. Lett.*, vol. 12, no. 5, pp. 343–345, May 2008.

[6] H. Elgala, R. Mesleh, and H. Haas, "Non-linearity effects and predistortion in optical OFDM wireless transmission using LEDs," *Inderscience Intenational Journal of Ultra Wideband Communications and Systems (IJUWBCS)*, vol. 1, no. 2, pp. 143–150, 2009.

[7] BS EN 62471:2008, *Photobiological Safety of Lamps and Lamp Systems*, BSI British Standards Std., Sep. 2008.

[8] D. Dardari, V. Tralli, and A. Vaccari, "A Theoretical Characterization of Nonlinear Distortion Effects in OFDM Systems," *IEEE Transactions on Communications*, vol. 48, no. 10, pp. 1755–1764, Oct. 2000.

[9] S. Dimitrov, S. Sinanovic, and H. Haas, "Double-sided Signal Clipping in ACO-OFDM Wireless Communication Systems," in *Proc. of IEEE International Conference on Communications (IEEE ICC 2011)*, Kyoto, Japan, 5–9 Jun. 2011.

[10] S. Randel, F. Breyer, S. C. J. Lee, and J. W. Walewski, "Advanced Modulation Schemes for Short-Range Optical Communications," *IEEE Journal of Selected Topics in Quantum Electronics*, vol. PP, no. 99, pp. 1 –10, 2010.

[11] D. Tse and P. Viswanath, *Fundamentals of Wireless Communication*. Cambridge University Press, 2005.

[12] S. Dimitrov, R. Mesleh, H. Haas, M. Cappitelli, M. Olbert, and E. Bassow, "On the SIR of a Cellular Infrared Optical Wireless System for an Aircraft," *IEEE Journal on Selected Areas in Communications (IEEE JSAC)*, vol. 27, no. 9, pp. 1623–1638, Dec. 2009.

[13] H. Elgala, R. Mesleh, and H. Haas, "Practical Considerations for Indoor Wireless Optical System Implementation using OFDM," in *Proc. of the IEEE 10th International Conference on Telecommunications (ConTel)*, Zagreb, Croatia, Jun. 8–10 2009.

[14] I. A. Glover and P. M. Grant, *Digital Communications*, 2nd ed. Pearson Prentice Hall, 2004.

[15] Vishay Semiconductors, "Datasheet: TSHG8200 High Speed Infrared Emitting Diode, 830 nm, GaAlAs Double Hetero," Retrieved Jul. 26, 2011 from http://www.vishay.com/docs/84755/tshg8200.pdf, Jul. 2008.

# Optimum Signal Shaping in OFDM-based Optical Wireless Communication Systems

Svilen Dimitrov and Harald Haas

*Institute for Digital Communications, Joint Research Institute for Signal and Image Processing, The University of Edinburgh, EH9 3JL Edinburgh, UK, e-mail: {s.dimitrov, h.haas}@ed.ac.uk*

***Abstract*—In this paper, a framework for optimum signal shaping in multi-carrier modulation is presented for optical wireless communications (OWC). The two fundamental multi-carrier transmission schemes based on orthogonal frequency division multiplexing (OFDM), direct-current-biased optical OFDM (DCO-OFDM) and asymmetrically clipped optical OFDM (ACO-OFDM), are studied. The optimum signal shaping is defined as optimum biasing and optimum scaling of the time domain signal within the optical power constraints of the transmitter front-end. These include the boundaries of the limited linear dynamic range, such as minimum and maximum radiated optical power, and the desired average optical power level. As a result, the minimum required electrical signal-to-noise ratio (SNR) to maintain a target bit-error ratio (BER) is obtained for a desired multi-level quadrature amplitude modulation ($M$-QAM) scheme and a given combination of optical power constraints. The average optical power is varied over dynamic ranges of $10$ dB, $20$ dB and $30$ dB. With the increase of the dynamic range and for a major portion of the average optical power levels, DCO-OFDM demonstrates a lower minimum electrical SNR requirement for a target BER as compared to ACO-OFDM for modulation orders with similar spectral efficiencies.**

***Index Terms*—Signal shaping, optimization, DCO-OFDM, ACO-OFDM, optical wireless communication.**

## I. Introduction

Optical OFDM (O-OFDM) transmission has proven to be a robust candidate for high-speed data communication over the dispersive optical wireless channel [1]. The data transmission in OWC is achieved through intensity modulation and direct detection (IM/DD). A real-valued non-negative signal modulates the intensity of a light emitting diode (LED) at the transmitter, and it is detected by a photodiode (PD) at the receiver. In the literature, two possible O-OFDM system realizations can be found: DCO-OFDM [2] and ACO-OFDM [3]. A real-valued signal is obtained when Hermitian symmetry is imposed on the OFDM subcarriers. A non-negative signal is obtained in DCO-OFDM by the addition of a direct current (DC) bias. In ACO-OFDM, the odd subcarriers are enabled for data transmission, whereas the even ones are set to zero. Here, the negative part of the time domain signal can be clipped at the transmitter, and the information can be still successfully decoded from the odd subcarriers at the receiver.

Imperfections of the optical front-ends due to the use of off-the-shelf components result in a limited linear dynamic range of radiated optical power [4]. It is shown in [5] that the non-linear transfer characteristic of the LED can be compensated by pre-distortion. A linear characteristic is obtainable, however, only over a limited range. Therefore, the transmitted signal is constrained between levels of minimum and maximum optical power. Furthermore, the average optical power level is constrained by the eye safety regulations [6] and/or design requirements such as signal dimming. An example of the latter is OWC in an aircraft cabin [7] where the cabin illumination serves the dual purpose of visible light communication (VLC). In order to condition the signal in accordance with these constraints, signal scaling in the digital signal processor (DSP) and DC-biasing in the analog circuitry is required. For a large number of subcarriers, *e.g.* greater than $64$ [8], the time domain signals in DCO-OFDM and ACO-OFDM closely follow Gaussian and half-Gaussian distributions, respectively. Therefore, scaling and DC-biasing in DCO-OFDM and ACO-OFDM result in a non-linear signal distortion.

In this paper, the analysis of the clipping distortion from [9] is employed in the demonstration of the minimum electrical SNR requirement to achieve a target BER for a given combination of optical power constraints and a desired QAM order, $M$. Both alternating current (AC) power and DC power are included in the calculation of the electrical SNR requirement for average optical power levels varied over dynamic ranges of $10$ dB, $20$ dB and $30$ dB. For the majority of average optical power levels, DCO-OFDM demonstrates a lower minimum electrical SNR requirement for a target BER as compared to ACO-OFDM for modulation orders with similar spectral efficiencies as the dynamic range increases. Therefore, DCO-OFDM proves to be the more flexible transmission scheme for OWC with an ability to sweep over more than $50\%$ of the dynamic range within a 3 dB SNR margin.

The rest of the paper is organized as follows. Section II presents the O-OFDM system model and the formulation of the optimization problem. Results are discussed in Section III. Finally, Section IV concludes the paper.

## II. O-OFDM transmission

The conventional discrete model for a noisy communication link is employed in this study:

$$\mathbf{y} = \mathbf{h} * \mathbf{x} + \mathbf{n} \,, \tag{1}$$

where $\mathbf{y}$ represents the received distorted replica of the transmitted signal, $\mathbf{x}$, which is convolved with the channel impulse response, $\mathbf{h}$, and it is distorted by additive white Gaussian noise (AWGN), $\mathbf{n}$, at the receiver. In $M$-QAM O-OFDM, $\mathbf{n}$ has a zero-mean real-valued Gaussian distribution which after optical-to-electrical (O/E) conversion is transformed into

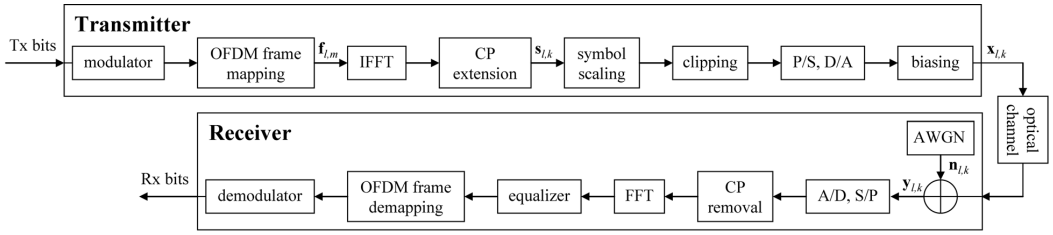


Fig. 1: Block diagram of O-OFDM transmission.

a complex-valued AWGN with an electrical power spectral density (PSD) of $N_0/2$ per complex dimension [10]. Here, $*$ stands for discrete linear convolution. The discrete signal vectors are obtained by sampling of the equivalent continuous-time signals with a sampling period of $T$. Here, $\mathbf{x}$ contains $Z_{\mathbf{x}}$ samples, $\mathbf{h}$ has $Z_{\mathbf{h}}$ samples, and as a result, $\mathbf{n}$ and $\mathbf{y}$ have $Z_{\mathbf{x}} + Z_{\mathbf{h}} - 1$ samples [10]. In multi-carrier systems, a large number of subcarriers and a cyclic prefix (CP) transform the dispersive optical wireless channel into a flat fading channel over the subcarrier bandwidth [10]. In OWC, the flatness of the channel can be extended over all subcarriers for bandwidths up to 20 MHz [11], and it can be primarily characterized by the optical path gain coefficient, $g_{\mathrm{h(opt)}}$ [7]. Single-tap zero forcing (ZF) or minimum mean-squared error (MMSE) equalization are employed to counter the channel effect [10].

The block diagram for multi-carrier O-OFDM transmission is presented in Fig. 1. Here, $\log_2(M)$ bits of the equiprobable input bits modulate the complex-valued information carrying frequency domain subcarrier in an $M$-QAM fashion. In general, $N$ subcarriers form the $l$-th OFDM frame, $\mathbf{f}_{l,m}$, $l = 0, 1, ..., L-1$, corresponding to the $l$-th OFDM symbol, where $m$, $m = 0, 1, ..., N-1$, is the subcarrier index. Each subcarrier occupies a bandwidth of $1/NT$ in a total OFDM frame double-sided bandwidth of $B = 1/T$. Here, the bandwidth utilization factor is denoted by $G_{\mathrm{B}}$, where $G_{\mathrm{B}} = (N-2)/N$ in DCO-OFDM and $G_{\mathrm{B}} = 0.5$ in ACO-OFDM. Both systems have the Hermitian symmetry imposed on the OFDM frame, in order to ensure a real-valued time domain signal. Whereas in DCO-OFDM the information carrying subcarriers populate the first half of the frame, leaving the first one set to zero, in ACO-OFDM every even subcarrier is set to zero. Here, the $l$-th OFDM symbol in the train of $L$ symbols, $\mathbf{s}_l$, is obtained by the inverse fast Fourier transformation (IFFT) of the $l$-th OFDM frame in the train of $L$ frames, $\mathbf{f}_l$. Next, $N_{\mathrm{CP}}$ samples from the end of each OFDM symbol are appended at the beginning of the symbol, creating the CP extension. Here, the time domain sample index within the $l$-th OFDM symbol with CP, $\mathbf{s}_{l,k}$, is denoted by $k$, $k = 0, 1, ..., N + N_{\mathrm{CP}} - 1$. As a result, the time domain OFDM symbol with CP occupies a double-sided bandwidth of $B = 1/T$, and it has a duration of $(N + N_{\mathrm{CP}})T$. Because of the Hermitian symmetry, the spectral efficiency of optical OFDM with $M$-QAM amounts to $\log_2(M)G_{\mathrm{T}}G_{\mathrm{B}}/2$ bits/s/Hz, where $G_{\mathrm{T}} = N/(N + N_{\mathrm{CP}})$ is the utilization factor for the information carrying time. The train of OFDM symbols, $\mathbf{s}_{l,k}$, follows a close to Gaussian distribution for IFFT sizes greater than 64 [8]. In order to fit the signal within the limited linear dynamic range of the transmitter, $\mathbf{s}_{l,k}$ is scaled and clipped at normalized bottom and top clipping levels of $\lambda_{\mathrm{bottom}}$ and $\lambda_{\mathrm{top}}$ relative to a standard normal distribution [9]. In DCO-OFDM, $\lambda_{\mathrm{bottom}} = \big(P_{\mathrm{Tx,min}} - \beta_{\mathrm{DC}}\big)/\sigma$, whereas in ACO-OFDM, $\lambda_{\mathrm{bottom}} = \max\Big(\big(P_{\mathrm{Tx,min}} - \beta_{\mathrm{DC}}\big)/\sigma, 0\Big)$. Here, $\sigma$ is the target standard deviation of the non-clipped time domain signal to be fit within the minimum and maximum level of radiated optical power, $P_{\mathrm{Tx,min}}$ and $P_{\mathrm{Tx,max}}$, and $\beta_{\mathrm{DC}}$ is the DC bias. In both systems, $\lambda_{\mathrm{top}} = \big(P_{\mathrm{Tx,max}} - \beta_{\mathrm{DC}}\big)/\sigma$. Next, the train of symbols with CPs is subjected to a parallel-to-serial (P/S) conversion, and it is passed through the digital-to-analog (D/A) converter. Here, a pulse shaping filter is applied to obtain the continuous-time signal. In the analog circuitry the signal is DC-biased by $\beta_{\mathrm{DC}}$. Therefore, the transmitted signal vector, $\mathbf{x}$, with a length of $Z_{\mathbf{x}} = L(N + N_{\mathrm{CP}})$ can be expressed as follows:

$$\mathbf{x}_{l,k} = \mathrm{CLIP}\left[\alpha \mathbf{s}_{l,k}\right] + \beta_{\mathrm{DC}} \,, \tag{2}$$

where

$$\alpha = \sigma \sqrt{\frac{N-1}{\sum_{m=0}^{N-1} |\mathbf{f}_{l,m}|^2}} \,. \tag{3}$$

Before the scaling clock, the average electrical power of the $G_{\mathrm{B}}N$ QAM symbols on the enabled subcarriers amounts to $P_{\mathrm{s(elec)}} = 1$. In order to maintain the signal variance of $\sigma^2$, the power of the enabled subcarriers is scaled through $\alpha$ to $P_{\mathrm{s(elec)}}/G_{\mathrm{B}}$, where $P_{\mathrm{s(elec)}} = \sigma^2$. Thus, the average bit energy can be expressed as follows: $E_{\mathrm{b(elec)}} = \sigma^2/(\log_2(M)G_{\mathrm{T}}G_{\mathrm{B}}B)$. The non-linear clipping distortion represented by the CLIP $[\cdot]$ operator can be translated into an attenuation factor, $K$, on the information carrying subcarriers plus a zero-mean complex-valued Gaussian noise component with a variance of $\sigma^2_{\mathrm{clip}}$. In DCO-OFDM and ACO-OFDM, $K$ is given as follows [9]:

$$K = Q(\lambda_{\mathrm{bottom}}) - Q(\lambda_{\mathrm{top}}) \,. \tag{4}$$

Here, $Q(\cdot)$ stands for the complementary cumulative distribution function (CCDF) of a standard normal distribution with zero mean and unity variance. The variance of the clipping noise in DCO-OFDM and ACO-OFDM, respectively, can be

expressed as follows [9]:

$$\begin{aligned}\sigma^2_{\text{clip}} = P_{\text{s(elec)}}\Big(&K - K^2 - \big(\phi(\lambda_{\text{bottom}}) - \phi(\lambda_{\text{top}})\\ &+(1-Q(\lambda_{\text{bottom}}))\lambda_{\text{bottom}} + Q(\lambda_{\text{top}})\lambda_{\text{top}}\big)^2\\ &+(1-Q(\lambda_{\text{bottom}}))\lambda^2_{\text{bottom}} + Q(\lambda_{\text{top}})\lambda^2_{\text{top}}\\ &+\phi(\lambda_{\text{bottom}})\lambda_{\text{bottom}} - \phi(\lambda_{\text{top}})\lambda_{\text{top}}\Big)\,,\end{aligned} \tag{5}$$

$$\begin{aligned}\sigma^2_{\text{clip}} = P_{\text{s(elec)}}\Big(&K\big(\lambda^2_{\text{bottom}}+1\big) - 2K^2\\ &-\lambda_{\text{bottom}}\big(\phi(\lambda_{\text{bottom}}) - \phi(\lambda_{\text{top}})\big)\\ &-\phi(\lambda_{\text{top}})\big(\lambda_{\text{top}} - \lambda_{\text{bottom}}\big)\\ &+Q(\lambda_{\text{top}})\big(\lambda_{\text{top}} - \lambda_{\text{bottom}}\big)^2\Big)\,,\end{aligned} \tag{6}$$

where $\phi(\cdot)$ stands for the probability density function (PDF) of a standard normal distribution. In addition to the distortion of the information carrying subcarriers, time domain signal clipping modifies the average optical power of the transmitted signal as follows:

$$\begin{aligned}\mathrm{E}\left[\mathbf{x}_l\right] = \sigma\Big(&\lambda_{\text{top}}Q(\lambda_{\text{top}}) - \lambda_{\text{bottom}}Q(\lambda_{\text{bottom}})\\ &+\phi(\lambda_{\text{bottom}}) - \phi(\lambda_{\text{top}})\Big) + P_{\text{bottom}}\,.\end{aligned} \tag{7}$$

In DCO-OFDM, $P_{\text{bottom}} = P_{\text{Tx,min}}$, while in ACO-OFDM, $P_{\text{bottom}} = \max\Big(P_{\text{Tx,min}}, \beta_{\text{DC}}\Big)$ because of the default zero-level clipping. The eye safety regulations [6] and/or the design requirements such as signal dimming impose the average optical power constraint, $P_{\text{Tx,avg}}$, *i.e.* $\mathrm{E}\left[\mathbf{x}_l\right] \leq P_{\text{Tx,avg}}$.

The signal $\mathbf{x}_{l,k}$ is transmitted over the optical wireless channel. At the receiver, it is distorted by AWGN, $\mathbf{n}_{l,k}$, to obtain $\mathbf{y}_{l,k}$. A matched filter is employed, and at the analog-to-digital (A/D) converter the signal is sampled at a frequency of $1/T$ [10]. Next, the CP extension of each OFDM symbol is removed, and after serial-to-parallel (S/P) conversion the signal is passed through a fast Fourier transformation (FFT) block back to the frequency domain. A single-tap ZF or MMSE equalizer and a hard-decision decoder are employed to obtain the received bits. Thus, the effective electrical SNR per bit in $M$-QAM O-OFDM is given as follows:

$$\Gamma_{\text{b(elec)}} = \frac{K^2}{\dfrac{G_{\text{B}}\log_2(M)\sigma^2_{\text{clip}}}{P_{\text{s(elec)}}} + \dfrac{G_{\text{B}}\gamma^{-1}_{\text{b(elec)}}}{G_{\text{T}}G_{\text{EQ}}G_{\text{DC}}}}\,, \tag{8}$$

where $\gamma_{\text{b(elec)}} = E_{\text{b(elec)}}/N_0$ is the undistorted electrical SNR per bit. Here, $G_{\text{EQ}}$ stands for the equalizer gain, and it is given for ZF and MMSE, respectively, as $g^2_{\text{h(opt)}}$ and $g^2_{\text{h(opt)}} + \gamma^{-1}_{\text{b(elec)}}$. The gain factor $G_{\text{DC}}$ denotes the attenuation of the useful electrical signal power of $\mathbf{x}$ due to the DC component, and it can be expressed in DCO-OFDM and ACO-OFDM, respectively, as follows [9]:

$$G_{\text{DC}} = \frac{\sigma^2}{\sigma^2 + \beta^2_{\text{DC}}}\,, \tag{9}$$

$$G_{\text{DC}} = \frac{\sqrt{2\pi}\sigma^2}{\sqrt{2\pi}\sigma^2 + 4\sigma\beta_{\text{DC}} + 2\sqrt{2\pi}\beta^2_{\text{DC}}}\,. \tag{10}$$

The BER performance of $M$-QAM O-OFDM in AWGN can be obtained as follows [12]:

$$\text{BER} = \frac{4\big(\sqrt{M}-1\big)}{\log_2(M)\sqrt{M}}Q\left(\sqrt{\frac{3\log_2(M)}{M-1}\Gamma_{\text{b(elec)}}}\right)\,. \tag{11}$$

The choice of the biasing parameters, such as the signal variance, $\sigma^2$, and the DC bias, $\beta_{\text{DC}}$, in consideration of the front-end optical power constraints, $P_{\text{Tx,min}}$, $P_{\text{Tx,max}}$ and $P_{\text{Tx,avg}}$, for a given QAM modulation order, $M$, can be formulated as an optimization problem. The objective of the optimization is the minimization of the electrical SNR requirement to achieve a target BER which is summarized in TABLE I. Here, the electrical SNR requirement is represented by the electrical SNR per bit, $\gamma_{\text{b(elec)}}$. The analytical approach to solve the minimization problem leads to a system of non-linear transcendental equations which does not have a closed-form solution. Therefore, a numerical optimization procedure

Given:

BER, $M$, $P_{\text{Tx,min}}$, $P_{\text{Tx,max}}$ and $P_{\text{Tx,avg}}$

Find:

$$\underset{\substack{\sigma \geq 0\\ \beta_{\text{DC}} \geq 0}}{\text{argmin}}\ \ f(\sigma, \beta_{\text{DC}}) = \gamma_{\text{b(elec)}} \geq 0$$

where

ZF equalizer

$$\gamma_{\text{b(elec)}} = \frac{G_{\text{B}}}{g^2_{\text{h(opt)}}G_{\text{T}}G_{\text{DC}}}\left(qK^2 - \frac{G_{\text{B}}\log_2(M)\sigma^2_{\text{clip}}}{P_{\text{s(elec)}}}\right)^{-1}$$

MMSE equalizer

$$\gamma_{\text{b(elec)}} = \frac{\dfrac{G_{\text{B}}}{G_{\text{T}}G_{\text{DC}}} - \left(qK^2 - \dfrac{G_{\text{B}}\log_2(M)\sigma^2_{\text{clip}}}{P_{\text{s(elec)}}}\right)}{g^2_{\text{h(opt)}}\left(qK^2 - \dfrac{G_{\text{B}}\log_2(M)\sigma^2_{\text{clip}}}{P_{\text{s(elec)}}}\right)}$$

$$q = \frac{3\log_2(M)}{M-1}\left(Q^{-1}\left(\frac{\text{BER}\sqrt{M}\log_2(M)}{4(\sqrt{M}-1)}\right)\right)^{-2}$$

Constraints:

$$\begin{aligned}\mathrm{E}\left[\mathbf{x}_l\right] = \sigma\Big(&\phi(\lambda_{\text{bottom}}) - \phi(\lambda_{\text{top}}) + \lambda_{\text{top}}Q(\lambda_{\text{top}})\\ &-\lambda_{\text{bottom}}Q(\lambda_{\text{bottom}})\Big) + P_{\text{bottom}} \leq P_{\text{Tx,avg}}\end{aligned}$$

DCO-OFDM: $\lambda_{\text{top}} > \lambda_{\text{bottom}}$

ACO-OFDM: $\lambda_{\text{top}} > \lambda_{\text{bottom}} \geq 0$

TABLE I: Minimization of $\gamma_{\text{b(elec)}}$ over $\sigma$ and $\beta_{\text{DC}}$ for given target BER, $M$, $P_{\text{Tx,min}}$, $P_{\text{Tx,max}}$ and $P_{\text{Tx,avg}}$.

is required, and the minimization can be carried out through a computer simulation for a particular choice of front-end optical power constraints.

## III. Results and Discussion

In this paper, the optimum signal scaling and DC-biasing are obtained as a minimization of the electrical SNR requirement of DCO-OFDM and ACO-OFDM for a set of optical power constraints. The following QAM orders are chosen: $M = \{4, 16, 64, 256, 1024\}$. In order to facilitate forward error correction (FEC) coding, a target BER of $10^{-3}$ is considered. In addition, the average optical power constraint in TABLE I is met with equality, *i.e.* $\mathrm{E}[\mathbf{x}_l] = P_{\mathrm{Tx,avg}}$, in order to illustrate the influence of signal dimming on the electrical SNR requirement. For the sake of generality, the optical power constraints are normalized to $P_{\mathrm{Tx,max}}$ as follows: $P_{\mathrm{Tx,min,norm}} = P_{\mathrm{Tx,min}}/P_{\mathrm{Tx,max}}$, $P_{\mathrm{Tx,avg,norm}} = P_{\mathrm{Tx,avg}}/P_{\mathrm{Tx,max}}$ and $P_{\mathrm{Tx,max,norm}} = 1$. Linear dynamic ranges of 10 dB, 20 dB and 30 dB are considered, and therefore the normalized minimum optical power is set to $P_{\mathrm{Tx,min,norm}} = \{0.1, 0.01, 0.001\}$. For a large number of subcarriers, the inter-symbol interference (ISI) from maximum delay spreads up to 100 ns can be compensated by a CP of 2 samples at a sampling rate of 20 MHz with a negligible reduction of the electrical SNR requirement and the spectral efficiency [13]. In addition, since the optical path gain coefficient, $g_{\mathrm{h(opt)}}$, is merely a factor in the equalization process which equally scales every $\gamma_{\mathrm{b(elec)}}$ minimum from TABLE I, $g_{\mathrm{h(opt)}}$ does not influence the optimum biasing parameters, such as $\sigma^2$ and $\beta_{\mathrm{DC}}$. Therefore, $g_{\mathrm{h(opt)}} = 1$ is assumed for simplicity. An MMSE equalizer is used.

The electrical SNR requirement for a target BER of $10^{-3}$ is presented in DCO-OFDM and ACO-OFDM for linear dynamic ranges of 10 dB, 20 dB and 30 dB in Fig. 2, Fig. 3 and Fig. 4, respectively. The small slopes of the graphs in the middle of the dynamic range suggest that average optical powers over more than 50% and 25% of the dynamic range

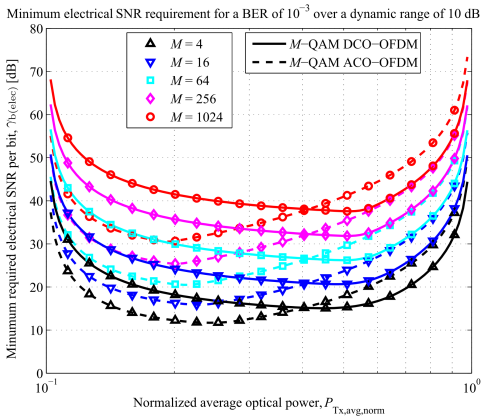


Fig. 2: Minimum electrical SNR requirement for a BER of $10^{-3}$ *vs.* average optical power over a 10 dB dynamic range.

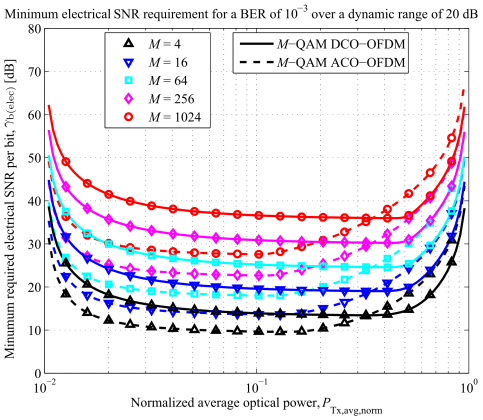


Fig. 3: Minimum electrical SNR requirement for a BER of $10^{-3}$ *vs.* average optical power over a 20 dB dynamic range.

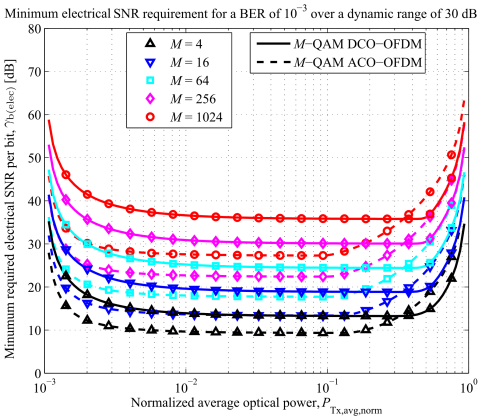


Fig. 4: Minimum electrical SNR requirement for a BER of $10^{-3}$ *vs.* average optical power over a 30 dB dynamic range.

can be supported by an SNR margin as low as 3 dB in DCO-OFDM and ACO-OFDM, respectively. It is shown that for an equal modulation order, $M$, DCO-OFDM outperforms ACO-OFDM in terms of minimum electrical SNR requirement in the upper part of the dynamic range, whereas ACO-OFDM prevails for lower average optical power levels because of the respective Gaussian and half-Gaussian distributions of the signals. In addition, the minimum electrical SNR requirement graphs exhibit an absolute minimum. This suggests that there is an average optical power level which allows for the best joint maximization of the signal variance, minimization of the clipping distortion and minimization of the DC-bias penalty from TABLE I. For both systems, the absolute minimum electrical SNR requirement and the corresponding average optical power level are presented in Fig. 5. They decrease with the increase of the dynamic range because of the relaxed $P_{\mathrm{Tx,min}}$ and $P_{\mathrm{Tx,max}}$ constraints in the optimization. In order to find out which system delivers the higher throughput for a given

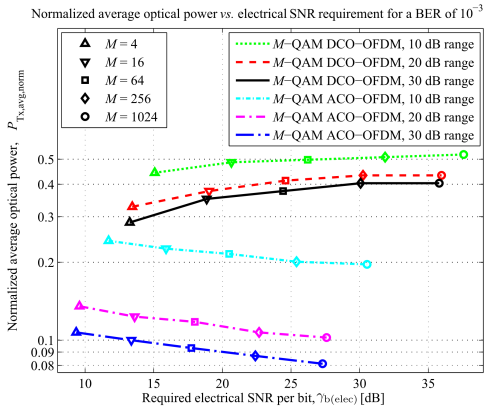


Fig. 5: Normalized average optical power *vs.* absolute minimum electrical SNR requirement for a target BER of $10^{-3}$.

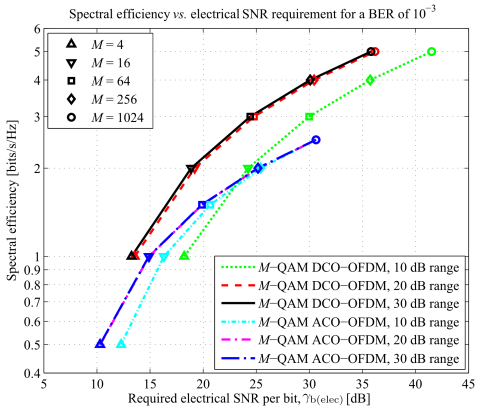


Fig. 6: Spectral efficiency *vs.* minimum electrical SNR requirement for a target BER of $10^{-3}$. The average optical power level is set to $20\%$ of the maximum of the dynamic range.

average optical power level, the spectral efficiency and the minimum electrical SNR requirement are shown in Fig. 6 for an average optical power level dimmed down to $20\%$. DCO-OFDM is expected to have a lower electrical SNR requirement and a superior spectral efficiency as compared to ACO-OFDM for average optical power levels in the upper part of the dynamic range. However, this is shown to be the case also for low average optical power levels, *i.e.* $P_{\text{Tx,avg,norm}} = 0.2$, as the dynamic range increases. Here, LEDs with wider linear dynamic ranges are proven to be the enabling factor for OWC with low optical power radiation. In addition, DCO-OFDM demonstrates a lower minimum electrical SNR requirement for a target BER as compared to ACO-OFDM for modulation orders with similar spectral efficiencies for average optical power levels over more than $85\%$, $90\%$ and $95\%$ of the dynamic ranges of $10$ dB, $20$ dB and $30$ dB, respectively.

## IV. Conclusion

In this paper, a framework for optimum signal scaling and biasing is presented for OFDM-based OWC with minimum, average and maximum optical power constraints. The minimum electrical SNR requirement is obtained in DCO-OFDM and ACO-OFDM for a target BER, $M$-QAM scheme, and an average optical power constraint varied over dynamic ranges of $10$ dB, $20$ dB and $30$ dB. It is shown that a transmitter front-end with a wide linear dynamic range of $20$ dB or higher provides sufficient electrical power for OWC with optical power output close to the boundaries of the dynamic range, where the LED appears to be off or driven close to its maximum. In addition, an SNR margin of $3$ dB is sufficient to support an average optical power sweep over $50\%$ and $25\%$ of the dynamic range in DCO-OFDM and ACO-OFDM, respectively. Finally, DCO-OFDM is expected to deliver the higher throughput as compared to ACO-OFDM for average optical power levels over a major portion of the dynamic range.

## Acknowledgement

We gratefully acknowledge EADS UK Ltd. for the support of this research. Professor Haas acknowledges the Scottish Funding Council support of his position within the Edinburgh Research Partnership in Engineering and Mathematics between the University of Edinburgh and Heriot Watt University.

## References

[1] Y. Tanaka, T. Komine, S. Haruyama, and M. Nakagawa, "Indoor Visible Communication Utilizing Plural White LEDs as Lighting," in *Proc. of the* $12^{th}$ *IEEE International Symposium on Personal, Indoor and Mobile Radio Communications*, vol. 2, San Diego, CA, USA, Sep. 30–Oct. 3, 2001, pp. 81–85.

[2] J. B. Carruthers and J. M. Kahn, "Multiple-subcarrier Modulation for Nondirected Wireless Infrared Communication," *IEEE Journal on Selected Areas in Communications*, vol. 14, no. 3, pp. 538–546, Apr. 1996.

[3] J. Armstrong and A. Lowery, "Power Efficient Optical OFDM," *Electronics Letters*, vol. 42, no. 6, pp. 370–372, Mar. 16, 2006.

[4] Vishay Semiconductors, "Datasheet: TSHG8200 High Speed Infrared Emitting Diode, 830 nm, GaAlAs Double Hetero," Retrieved Jul. 26, 2011 from http://www.vishay.com/docs/84755/tshg8200.pdf, Jul. 2008.

[5] H. Elgala, R. Mesleh, and H. Haas, "Non-linearity Effects and Predistortion in Optical OFDM Wireless Transmission Using LEDs," *Inderscience International Journal of Ultra Wideband Communications and Systems (IJUWBCS)*, vol. 1, no. 2, pp. 143–150, 2009.

[6] BS EN 62471:2008, *Photobiological Safety of Lamps and Lamp Systems*, BSI British Standards Std., Sep. 2008.

[7] S. Dimitrov, R. Mesleh, H. Haas, M. Cappitelli, M. Olbert, and E. Bassow, "On the SIR of a Cellular Infrared Optical Wireless System for an Aircraft," *IEEE Journal on Selected Areas in Communications (IEEE JSAC)*, vol. 27, no. 9, pp. 1623–1638, Dec. 2009.

[8] D. Dardari, V. Tralli, and A. Vaccari, "A Theoretical Characterization of Nonlinear Distortion Effects in OFDM Systems," *IEEE Transactions on Communications*, vol. 48, no. 10, pp. 1755–1764, Oct. 2000.

[9] S. Dimitrov, S. Sinanovic, and H. Haas, "Clipping Noise in OFDM-based Optical Wireless Communication Systems," *IEEE Transactions on Communications (IEEE TCOM)*, vol. 60, no. 4, pp. 1072–1081, Apr. 2012.

[10] D. Tse and P. Viswanath, *Fundamentals of Wireless Communication*. Cambridge University Press, 2005.

[11] J. M. Kahn and J. R. Barry, "Wireless Infrared Communications," *Proceedings of the IEEE*, vol. 85, no. 2, pp. 265–298, Feb. 1997.

[12] I. A. Glover and P. M. Grant, *Digital Communications*, 2nd ed. Pearson Prentice Hall, 2004.

[13] H. Elgala, R. Mesleh, and H. Haas, "Practical Considerations for Indoor Wireless Optical System Implementation using OFDM," in *Proc. of the IEEE 10th International Conference on Telecommunications (ConTel)*, Zagreb, Croatia, Jun. 8–10 2009.

# Bibliography


[1] BS EN 62471:2008, *Photobiological Safety of Lamps and Lamp Systems*, BSI British Standards Std., Sep. 2008.

[2] "Visible Light Communication (VLC) - A Potential Solution to the Global Wireless Spectrum Shortage," GBI Research, Tech. Rep., 2011. [Online]. Available: http://www.gbiresearch.com/

[3] Wireless Gigabit Aliance, "Specifications," Retrieved Nov. 19, 2012 from http://wirelessgigabitalliance.org/specifications/.

[4] IEEE P802.11 - Task Group AD, "Very High Throughput in 60 GHz," Retrieved Nov. 19, 2012 from http://www.ieee802.org/11/Reports/tgad_update.htm.

[5] Z. Ghassemlooy, W. Popoola, and S. Rajbhandari, *Optical Wireless Communications: System and Channel Modeling with MATLAB(R)*, 1st ed. CRC Press, 2012.

[6] F. R. Gfeller and U. Bapst, "Wireless In-House Data Communication Via Diffuse Infrared Radiation," *Proceedings of the IEEE*, vol. 67, no. 11, pp. 1474–1486, Nov. 1979.

[7] G. W. Marsh and J. M. Kahn, "Performance Evaluation of Experimental 50-Mb/s Diffuse Infrared Wireless Link using on-off Keying with Decision-Feedback Equalization," *IEEE Transactions on Communications*, vol. 44, no. 11, pp. 1496–1504, Nov. 1996.

[8] J. B. Carruthers and J. M. Kahn, "Angle Diversity for Nondirected Wireless Infrared Communication," *IEEE Transactions on Communications*, vol. 48, no. 6, pp. 960–969, Jun. 2000.

[9] Y. Tanaka, T. Komine, S. Haruyama, and M. Nakagawa, "Indoor Visible Light Data Transmission System Utilizing White LED Lights," *IEICE Transactions on Communications*, vol. E86-B, no. 8, pp. 2440–2454, Aug. 2003.

[10] J. Vucic, C. Kottke, S. Nerreter, K. D. Langer, and J. W. Walewski, "513 Mbit/s Visible Light Communications Link Based on DMT-Modulation of a White LED," *Journal of Lightwave Technology*, vol. 28, no. 24, pp. 3512–3518, Dec. 2010.

[11] J. R. Barry, *Wireless Infrared Communications*. Springer, 1994, vol. 280.

[12] J. M. Kahn and J. R. Barry, "Wireless Infrared Communications," *Proceedings of the IEEE*, vol. 85, no. 2, pp. 265–298, Feb. 1997.

[13] J. G. Proakis, *Digital Communications*, 4th ed. McGraw–Hill, 2000.

[14] H. Haas and P. Valtink, *100 Produkte der Zukunft - Wegweisende Ideen, die unser Leben verändern werden*. Econ Verlag, 2007, ch. Sprechendes Licht - Leuchtdioden übermitteln Daten.

[15] M. Afgani, H. Haas, H. Elgala, and D. Knipp, "Visible Light Communication Using OFDM," in *Proc. of the 2nd International Conference on Testbeds and Research Infrastructures for the Development of Networks and Communities (TRIDENTCOM)*, Barcelona, Spain, Mar. 1–3 2006, pp. 129–134.

[16] H. Elgala, R. Mesleh, H. Haas, and B. Pricope, "OFDM Visible Light Wireless Communication Based on White LEDs," in *Proc. of the 64th IEEE Vehicular Technology Conference (VTC)*, Dublin, Ireland, Apr. 22–25, 2007.

[17] Q. Pan and R. J. Green, "Bit-Error-Rate Performance of Lightwave Hybrid AM/OFDM Systems with Comparison with AM/QAM Systems in the Presence of Clipping Impulse Noise," *IEEE Photonics Technology Letters*, vol. 8, no. 2, pp. 278–280, Feb. 1996.

[18] D. Dardari, V. Tralli, and A. Vaccari, "A Theoretical Characterization of Nonlinear Distortion Effects in OFDM Systems," *IEEE Transactions on Communications*, vol. 48, no. 10, pp. 1755–1764, Oct. 2000.

[19] S. Randel, F. Breyer, S. C. J. Lee, and J. W. Walewski, "Advanced Modulation Schemes for Short-Range Optical Communications," *IEEE Journal of Selected Topics in Quantum Electronics*, vol. PP, no. 99, pp. 1 –10, 2010.

[20] H. Elgala, R. Mesleh, and H. Haas, "Non-linearity Effects and Predistortion in Optical OFDM Wireless Transmission Using LEDs," *Inderscience International Journal of Ultra Wideband Communications and Systems (IJUWBCS)*, vol. 1, no. 2, pp. 143–150, 2009.

[21] S. Dimitrov and H. Haas, "On the Clipping Noise in an ACO-OFDM Optical Wireless Communication System," in *Proc. of IEEE Global Communications Conference (IEEE GLOBECOM 2010)*, Miami, Florida, USA, 6–10 Dec. 2010.

[22] S. Dimitrov, S. Sinanovic, and H. Haas, "Double-sided Signal Clipping in ACO-OFDM Wireless Communication Systems," in *Proc. of IEEE International Conference on Communications (IEEE ICC 2011)*, Kyoto, Japan, 5–9 Jun. 2011.

[23] ——, "A Comparison of OFDM-based Modulation Schemes for OWC with Clipping Distortion," in *Proc. of the 2nd Optical Wireless Communications (OWC) Workshop in conjunction with IEEE Global Telecommunications Conference (IEEE GLOBECOM 2011)*, Houston, Texas, USA, 5–9 Dec. 2011.

[24] ——, "Clipping Noise in OFDM-based Optical Wireless Communication Systems," *IEEE Transactions on Communications (IEEE TCOM)*, vol. 60, no. 4, pp. 1072–1081, Apr. 2012.

[25] ——, "Signal Shaping and Modulation for Optical Wireless Communication," *IEEE/OSA Journal on Lightwave Technology (IEEE/OSA JLT)*, vol. 30, no. 9, pp. 1319–1328, May 2012.

[26] S. Dimitrov and H. Haas, "Optimum Signal Shaping in OFDM-based Optical Wireless Communication Systems," in *Proc. of the IEEE Vehicular Technology Conference (IEEE VTC Fall)*, Quebec City, Canada, Sep. 3–6 2012.

[27] J. Bussgang, "Cross Correlation Function of Amplitude-Distorted Gaussian Signals," Research Laboratory for Electronics, Massachusetts Institute of Technology, Cambridge, MA, Technical Report 216, Mar. 1952.

[28] J. Rice, *Mathematical Statistics and Data Analysis*, 2nd ed. Duxbury Press, 1995.

[29] The Flag Press, "History Behind Semaphore Flags," Retrieved Nov. 17, 2012 from http://flagexpressions.wordpress.com/2010/03/23/history-behind-semaphore-flags/.

[30] A. G. Bell, "Selenium and the Photophone," *Nature*, vol. 22, no. 569, pp. 500–503, 1880.

[31] C. Singh, J. John, Y. N. Singh, and K. K. Tripathi, "A Review of Indoor Optical Wireless Systems," *IETE Technical Review*, vol. 19, pp. 3–17, Jan.–Apr. 2002.

[32] P. Barker and A. C. Boucouvalas, "Performance modeling of the IrDA protocol for infrared wireless communications," *IEEE Commun. Mag.*, vol. 36, no. 12, pp. 113–117, 1998.

[33] European Commission, "Technical briefing: Phasing out Incandescent Bulbs in the EU," Retrieved from http://ec.europa.eu, Sep. 2008.

[34] T. Komine and M. Nakagawa, "Fundamental Analysis for Visible–Light Communication System using LED Lights," *IEEE Transactions on Consumer Electronics*, vol. 50, no. 1, pp. 100–107, Feb. 2004.

[35] ——, "Performance Evaluation of Visible-Light Wireless Communication System using White LED Lightings," in *Proc. ISCC 2004. Ninth International Symposium on Computers and Communications*, vol. 1, 28 June-1 July 2004, pp. 258– 263.

[36] M. Miki, E. Asayama, and T. Hiroyasu, "Visible-Light Communication using Visible–Light Communication Technology," in *In the Proceeding of the IEEE Conference on Cybernetics and Intelligence Systems (CIS 06)*, Bangkok, Thailand, Jun. 7–9, 2006, pp. 1–6.

[37] J. Grubor, S. Randel, K. Langer, and J. W. Walewski, "Broadband Information Broadcasting Using LED-Based Interior Lighting," *Journal of Lightwave Technology*, vol. 26, pp. 3883–3892, 2008.

[38] D. C. O'Brien, L. Zeng, H. Le-Minh, G. Faulkner, J. W. Walewski, and S. Randel, "Visible light communications: challenges and possibilities," in *IEEE International Symposium on Personal, Indoor and Mobile Radio Communications*, ser. ISBN: 978-1-4244-2644-7/08, Cannes, France, Sept. 2008.

[39] H. Elgala, R. Mesleh, and H. Haas, "Indoor Broadcasting via White LEDs and OFDM," *IEEE Transactions on Consumer Electronics*, vol. 55, no. 3, pp. 1127–1134, Aug. 2009.

[40] ——, "Indoor Optical Wireless Communication: Potential and State-of-the-Art," *IEEE Commun. Mag.*, vol. 49, no. 9, pp. 56–62, Sep. 2011, ISSN: 0163-6804.

[41] D. O'Brien, "Visible light communications: challenges and potential," in *IEEE Photonics Conference (PHO)*, Virginia, USA, Oct. 2011, pp. 365–366.

[42] L. Hanzo, H. Haas, S. Imre, D. O'Brien, M. Rupp, and L. Gyongyosi, "Wireless Myths, Realities and Futures: From 3G/4G to Optical and Quantum Wireless," *Proc. IEEE*, vol. 100, pp. 1853–1888, May 2012.

[43] Visible Light Communications Consortium (VLCC), Retrieved from http://www.vlcc.net, Feb. 2007.

[44] IEEE Std. 802.15.7-2011, *IEEE Standard for Local and Metropolitan Area Networks, Part 15.7: Short-Range Wireless Optical Communication Using Visible Light*, IEEE Std., 2011.

[45] F. R. Gfeller, P. Bernasconi, W. Hirt, C. Elisii, and B. Weiss, *Mobile Communications Advanced Systems and Components*, ser. Lecture Notes in Computer Science. Springer Berlin/Heidelberg, 1994, vol. 783, ch. Dynamic Cell Planning for Wireless Infrared In-House Data Transmission, pp. 261–272, ISBN 978-3-540-57856-7.

[46] G. W. Marsh and J. M. Kahn, "Channel Reuse Strategies for Indoor Infrared Wireless Communications," *IEEE Transactions on Communications*, vol. 45, no. 10, pp. 1280–1290, Oct. 1997.

[47] S. Dimitrov, R. Mesleh, H. Haas, M. Cappitelli, M. Olbert, and E. Bassow, "On the SIR of a Cellular Infrared Optical Wireless System for an Aircraft," *IEEE Journal on Selected Areas in Communications (IEEE JSAC)*, vol. 27, no. 9, pp. 1623–1638, Dec. 2009.

[48] S. B. Alexander, *Optical Communication Receiver Design*, 1st ed. SPIE Press Book, Jan. 1997.

[49] D. C. O'Brien, G. E. Faulkner, S. Zikic, and N. P. Schmitt, "High Data-Rate Optical Wireless Communications in Passenger Aircraft: Measurements and Simulations," in *6th International Symposium on Communication Systems, Networks and Digital Signal Processing (CSNDSP'08)*, Graz, Austria, 23–25 Jul. 2008, pp. 68–71.

[50] Vishay Semiconductors, "Datasheet: TSHG8200 High Speed Infrared Emitting Diode, 830 nm, GaAlAs Double Hetero," Retrieved Jul. 26, 2011 from http://www.vishay.com/docs/84755/tshg8200.pdf, Jul. 2008.

[51] Osram Opto Semiconductors, "Datasheet: LCW W5SM Golden Dragon white LED," Retrieved from http://www.osram.de, Apr. 2011.

[52] S. Dimitrov, H. Haas, M. Cappitelli, and M. Olbert, "On the Throughput of an OFDM-based Cellular Optical Wireless System for an Aircraft Cabin," in *Proc. of European Conference on Antennas and Propagation (EuCAP 2011)*, Rome, Italy, 11–15 Apr. 2011, invited Paper.

[53] Hamamatsu Photonics K.K., "Silicon PIN Photodiode," Retrieved Jan. 25, 2011 from http://sales.hamamatsu.com/en/products/solid-state-division/si-photodiode-series/si-pin-photodiode.php.

[54] Thorlabs, "Bandpass Filters," Retrieved Jan. 25, 2011 from http://www.thorlabs.com/NewGroupPage9.cfm?ObjectGroup_ID=1001.

[55] Analog Devices, "Transimpedance Amplifiers," Retrieved Jan. 25, 2011 from http://www.analog.com/en/fiberoptic/transimpedance-amplifiers/products/index.html.

[56] G. Yun and M. Kavehrad, "Indoor Infrared Wireless Communications Using Spot Diffusing and Fly-Eye Receivers," in *The Canadian Journal of Electrical and Computer Engineering*, vol. 18, no. 4, Oct. 1993.

[57] M. Kavehrad and S. Jivkova, "Indoor Broadband Optical Wireless Communications: Optical Subsystems Designs and their Impact on Channel Characteristics," *IEEE Wireless Communications Magazine*, vol. 10, no. 2, pp. 30–35, 2003.

[58] F. E. Alsaadi and J. M. H. Elmirghani, "Spot Diffusing Angle Diversity MC-CDMA Optical Wireless System," *In the Proceeding of the IET Optoelectronics*, vol. 3, no. 3, pp. 131–141, Jun. 2009.

[59] T. Borogovac, M. Rahaim, and J. B. Carruthers, "Spotlighting for visible light communications and illumination," in *IEEE Global Communications Conference (GLOBECOM 2010) Workshops*, 6-10 Dec 2010, pp. 1077–1081.

[60] J. Kahn, J. Barry, W. Krause, M. Audeh, J. Carruthers, G. Marsh, E. Lee, and D. Messerschmitt, "High–Speed Non–Directional Infrared Communication for Wireless Local-Area Networks," in *In the Proceeding of the* $26^{th}$ *Asilomar Conference on Signals, Systems and Computers*, vol. 1, California, USA, Oct. 26–28, 1992, pp. 83–87.

[61] J. M. Kahn, W. J. Krause, and J. B. Carruthers, "Experimental Characterization of Non-Directed Indoor Infrared Channels," *IEEE Transactions on Communications*, vol. 43, no. 234, pp. 1613–1623, Feb.–Mar.–Apr. 1995.

[62] J. B. Carruthers and J. M. Kahn, "Modeling of Nondirected Wireless Infrared Channels," in *In the Proceeding of the IEEE Conference on Communications.: Converging Technologies for Tomorrow's Applications*, vol. 2, Dallas, TX, USA, Jun. 23–27, 1996, pp. 1227–1231.

[63] M. R. Pakravan, M. Kavehrad, and H. Hashemi, "Indoor Wireless Infrared Channel Characterization by Measurements," *IEEE Transactions on Vehicular Technology*, vol. 50, no. 4, pp. 1053–1073, Jul. 2001.

[64] D. C. O'Brien, S. H. Khoo, W. Zhang, G. E. Faulkner, and D. J. Edwards, "High-speed Optical Channel Measurement System," in *Proc. SPIE, Optical Wireless Communications IV*, vol. 4530, Denver, CO, USA, Aug. 21–22, 2001, pp. 135–144.

[65] K. Smitha and J. John, "Propagation Measurements of Indoor Infrared Channels," retreived Dec. 29, 2008 http://ee.iust.ac.ir/profs/Sadr/Papers/ltwp20.pdf, Dec. 2004.

[66] J. Barry, J. Kahn, W. Krause, E. Lee, and D. Messerschmitt, "Simulation of multipath impulse response for indoor wireless optical channels," *IEEE J. Select. Areas Commun.*, vol. 11, no. 3, pp. 367–379, Apr. 1993.

[67] A. Muller, "Monte-Carlo Multipath Simulation of Ray Tracing Channel Models," in *Proc. IEEE Global Telecommunications Conference GLOBECOM '94. 'Communications: The Global Bridge'*, vol. 3, Nov. 28 – Dec. 2 1994, pp. 1446–1450.

[68] F. Lopez-Hernandez, R. Perez-Jimenez, and A. Santamaria, "Ray-tracing Algorithms for Fast Calculation of the Impulse Response on Diffuse IR-wireless Indoor Channels," *Optical Engineering*, vol. 39, no. 10, pp. 2775–2780, Oct. 2000.

[69] V. Pohl, V. Jungnickel, and C. von Helmolt, "A Channel Model for Wireless Infrared Communication," in *Proc. 11th IEEE International Symposium on Personal, Indoor and Mobile Radio Communications PIMRC 2000*, vol. 1, London, UK, Sep. 18–21, 2000, pp. 297–303.

[70] V. Jungnickel, V. Pohl, S. Nonnig, and C. von Helmolt, "A Physical Model of the Wireless Infrared Communication Channel," *IEEE Journal on Selected Areas in Communications*, vol. 20, no. 3, pp. 631–640, Apr. 2002.

[71] S. Rodriguez, R. Perez-Jimenez, F. Lopez-Hernandez, O. Gonzalez, and A. Ayala, "Reflection Model for Calculation of the Impulse Response on IR-wireless Indoor Channels Using Ray-tracing Algorithm," *Microwave Optical Technology Letter*, vol. 32, no. 4, pp. 296–300, Jan. 2002.

[72] O. Gonzalez, S. Rodriguez, R. Perez-Jimenez, B. R. Mendoza, and A. Ayala, "Error Analysis of the Simulated Impulse Response on Indoor Wireless Optical Channels Using

a Monte Carlo-based Ray-tracing Algorithm," *IEEE Transactions on Communications*, vol. 53, no. 1, pp. 124–130, Jan. 2005.

[73] H. Naoki and I. Takeshi, "Channel Modeling of Non-Directed Wireless Infrared Indoor Diffise Link," *Electronics and Communications in Japan (Part I: Communications)*, vol. 90, no. 6, pp. 9–19, Feb. 2007.

[74] G. Ntogari, T. Kamalakis, and T. Sphicopoulos, "Performance Analysis of Non-directed Equalized Indoor Optical Wireless Systems," in *Proc. 6th International Symposium on Communication Systems, Networks and Digital Signal Processing CSNDSP 2008*, Graz, Austria, 23–25 Jul. 2008, pp. 156–160.

[75] M. Bertrand, O. Bouchet, and P. Besnard, "Personal Optical Wireless Communications: LOS/WLOS/DIF Propagation Model and QOFI," in *Proc. 6th International Symposium on Communication Systems, Networks and Digital Signal Processing CSNDSP 2008*, Graz, Austria, 23–25 Jul. 2008, pp. 179–182.

[76] T. S. Rappaport, *Wireless Communications: Principles and Practice*, 2nd ed. Prentice Hall PTR, 2002.

[77] N. Schmitt, "Wireless optical NLOS Communication in Aircraft Cabin for In-flight Entertainment," in *Proc. of ESA 1st Optical Wireless Onboard Communications Workshop*, Noordwijk, Netherlands, 29–30 Sep. 2004.

[78] N. Schmitt, T. Pistner, C. Vassilopoulos, D. Marinos, A. Boucouvalas, M. Nikolitsa, C. Aidinis, and G. Metaxas, "Diffuse Wireless Optical Link for Aircraft Intra-cabin Passenger Communication," in *Proc. of 5th International Symposium on Communication Systems, Networks and Digital Signal Processing CSNDSP 2006*, Patras, Greece, 19–21 Jul. 2006.

[79] ATENAA Project, "Advanced Technologies for Networking of Avionic Applications," Retrieved May 8, 2009, from http://www.atenaa.org/.

[80] S. Dimitrov, R. Mesleh, H. Haas, M. Cappitelli, M. Olbert, and E. Bassow, "Path Loss Simulation of an Infrared Optical Wireless System for Aircraft," in *Proc. of IEEE Global Communications Conference (IEEE GLOBECOM 2009)*, Honolulu, HI, USA, Nov. 30 – Dec. 4 2009.

[81] P. Djahani and J. M. Kahn, "Analysis of Infrared Wireless Links Employing Multibeam Transmitters and Imaging Diversity Receivers," *IEEE Transactions on Communications*, vol. 48, no. 12, pp. 2077–2088, Dec. 2000.

[82] F. E. Alsaadi and J. M. H. Elmirghani, "Mobile MC-CDMA Optical wireless System Employing an Adaptive Multibeam Transmitter and Diversity Receivers in a Real Indoor Environment," in *In the Proceeding of the IEEE International Conference on Communications (ICC 08)*, May 19–23, 2008, pp. 5196–5203.

[83] D. Wu, Z. Ghassemlooy, H. Le-Minh, S. Rajbhandari, and Y. Kavian, "Power Distribution and Q-factor Analysis of Diffuse Cellular Indoor Visible Light Communication Systems," in *16th European Conference on Networks and Optical Communications (NOC 2011)*, Newcastle upon Tyne, UK, 20–22 Jul. 2011, pp. 28–31.

[84] D. Wu, Z. Ghassemlooy, H. Le-Minh, S. Rajbhandari, and L. Chao, "Channel Characteristics Analysis of Diffuse Indoor Cellular Optical Wireless Communication Systems," in *Proc. of OSA Asia Communications and Photonics Conference and Exhibition (OSA ACP 2011)*, Shanghai, China, 13–16 Nov. 2011, pp. 1–6.

[85] S. Dimitrov, R. Mesleh, H. Haas, M. Cappitelli, M. Olbert, and E. Bassow, "Line-of-sight Infrared Wireless Path Loss Simulation in an Aircraft Cabin," in *Proc. of European Workshop for Photonic Solutions for Wireless, Access, and In-House Networks (IPHOBAC'09)*, Duisburg, Germany, May 18–20 2009. [Online]. Available: http://www.ist-iphobac.org/workshop/program.asp

[86] C. Shannon, "A Mathematical Theory of Communication," *Bell System Technical Journal*, vol. 27, pp. 379–423 & 623–656, Jul. & Oct. 1948.

[87] B. Wilson and Z. Ghassemlooy, "Pulse Time Modulation Techniques for Optical Communications: A Review," in *In the Proceeding of the IEE on Optoelectronics*, vol. 140, no. 6, Dec. 1993, pp. 347–357.

[88] M. D. Audeh, J. M. Kahn, and J. R. Barry, "Performance of Pulse-position Modulation on Measured Non-directed Indoor Infrared Channels," *IEEE Transactions on Communications*, vol. 44, no. 6, pp. 654–659, Jun. 1996.

[89] D. Lee, J. Kahn, and M. Audeh, "Trellis–Coded Pulse–Position Modulation for Indoor Wireless Infrared Communications," *IEEE Transactions on Communications*, vol. 45, no. 9, pp. 1080–1087, Sep. 1997.

[90] Y. Zeng, R. Green, and M. Leeson, "Multiple Pulse Amplitude and Position Modulation for the Optical Wireless Channel," in *Proc. 10th Anniversary International Conference on Transparent Optical Networks (ICTON'08)*, vol. 4, Athens, Greece,, Jun. 22–26 2008, pp. 193–196.

[91] S. Rajbhandari, Z. Ghassemlooy, and M. Angelova, "Optimising the Performance of Digital Pulse Interval Modulation With Guard Slots for Diffuse Indoor Optical Wireless Links ," *IET Microwaves, Antennas and Propagation*, vol. 5, no. 9, pp. 1025–1030, Jun. 2011.

[92] H. Elgala, R. Mesleh, and H. Haas, "Practical Considerations for Indoor Wireless Optical System Implementation using OFDM," in *Proc. of the IEEE 10th International Conference on Telecommunications (ConTel)*, Zagreb, Croatia, Jun. 8–10 2009.

[93] J. Armstrong, "OFDM for Optical Communications," *Journal of Lightwave Technology*, vol. 27, no. 3, pp. 189–204, Feb. 2009.

[94] J. Campello, "Practical Bit Loading for DMT," in *Proc. of IEEE International Conference on Communications (IEEE ICC 1999)*, vol. 2, Vancouver, BC, Canada, 6–10 Jun. 1999, pp. 801–805.

[95] H. E. Levin, "A Complete and Optimal Data Allocation Method for Practical Discrete Multitone Systems," in *Proc. of IEEE Global Telecommunications Conference (IEEE GLOBECOM 2001)*, vol. 1, San Antonio, TX , USA, 25–29 Nov. 2001, pp. 369–374.

[96] J. B. Carruthers and J. M. Kahn, "Multiple-subcarrier Modulation for Nondirected Wireless Infrared Communication," *IEEE Journal on Selected Areas in Communications*, vol. 14, no. 3, pp. 538–546, Apr. 1996.

[97] T. Ohtsuki, "Multiple–Subcarrier Modulation in Optical Wireless Communications," *IEEE Communications Magazine*, vol. 41, no. 3, pp. 74–79, Mar. 2003.

[98] P. Golden, H. Dedieu, and K. Jacobsen, *Fundamentals of DSL Technology*. Auerbach Publications, 2006.

[99] J. Armstrong and A. Lowery, "Power Efficient Optical OFDM," *Electronics Letters*, vol. 42, no. 6, pp. 370–372, Mar. 16, 2006.

[100] J. Armstrong and B. J. C. Schmidt, "Comparison of Asymmetrically Clipped Optical OFDM and DC-Biased Optical OFDM in AWGN," *IEEE Commun. Lett.*, vol. 12, no. 5, pp. 343–345, May 2008.

[101] B. Inan, S.C.J. Lee, S. Randel, I. Neokosmidis, A.M.J. Koonen and J.W. Walewski, "Impact of LED Nonlinearity on Discrete Multitone Modulation," *IEEE/OSA Journal of Optical Communications and Networking*, vol. 1, no. 5, pp. 439 –451, oct 2009.

[102] H. Elgala, R. Mesleh, and H. Haas, "Impact of LED nonlinearities on optical wireless OFDM systems," in *2010 IEEE 21st International Symposium on Personal Indoor and Mobile Radio Communications (PIMRC)*, sept 2010, pp. 634 – 638.

[103] S. C. J. Lee, S. Randel, F. Breyer, and A. M. J. Koonen, "PAM-DMT for Intensity-Modulated and Direct-Detection Optical Communication Systems," *IEEE Photonics Technology Letters*, vol. 21, no. 23, pp. 1749–1751, Dec. 2009.

[104] N. Fernando, Y. Hong, and E. Viterbo, "Flip-OFDM for Optical Wireless Communications," in *Information Theory Workshop (ITW)*, IEEE. Paraty, Brazil: IEEE, Oct., 16–20 2011, pp. 5–9.

[105] K. Asadzadeh, A. Dabbo, and S. Hranilovic, "Receiver Design for Asymmetrically Clipped Optical OFDM," in *GLOBECOM Workshops (GC Wkshps)*, IEEE. Houston, TX, USA: IEEE, Dec., 5–9 2011, pp. 777–781.

[106] D. Tsonev, S. Sinanović, and H. Haas, "Novel Unipolar Orthogonal Frequency Division Multiplexing (U-OFDM) for Optical Wireless," in *Proc. of the Vehicular Technology Conference (VTC Spring)*, IEEE. Yokohama, Japan: IEEE, May 6–9 2012.

[107] H. Ochiai and H. Imai, "Performance analysis of deliberately clipped OFDM signals," *IEEE Transactions on Communications*, vol. 50, no. 1, pp. 89–101, Jan. 2002.

[108] A. Bahai, M. Singh, A. Goldsmith, and B. Saltzberg, "A New Approach for Evaluating Clipping Distortion in Multicarrier Systems," *IEEE Journal on Selected Areas in Communications*, vol. 20, no. 5, pp. 1037–1046, Jun. 2002.

[109] D. J. G. Mestdagh, P. Spruyt, and B. Biran, "Analysis of Clipping Effect in DMT-based ADSL Systems," in *Proc. IEEE International Conference on Communications ICC 1994*, vol. 1, New Orleans, LA, USA, 1–5 May 1994, pp. 293–300.

[110] E. Vanin, "Signal Restoration in Intensity-modulated Optical OFDM Access Systems," *OSA Optics Letters*, vol. 36, no. 22, pp. 4338–4340, 2011.

[111] S. C. J. Lee, F. Breyer, S. Randel, H. P. A. van der Boom, and A. M. J. Koonen, "High-speed Transmission over Multimode Fiber Using Discrete Multitone Modulation," *Journal of Optical Networking*, vol. 7, no. 2, pp. 183–196, Feb. 2008.

[112] R. J. Green, H. Joshi, M. D. Higgins, and M. S. Leeson, "Recent Developments in Indoor Optical Wireless," *IET Communications*, vol. 2, no. 1, pp. 3–10, Jan. 2008.

[113] R.-J. Essiambre, G. Kramer, P. Winzer, G. Foschini, and B. Goebel, "Capacity Limits of Optical Fibre Networks," *IEEE/OSA Journal on Lightwave Technology (IEEE/OSA JLT)*, vol. 28, no. 4, pp. 662–701, Feb. 15 2010.

[114] S. Hranilovic and F. Kschischang, "Capacity Bounds for Power- and Band-limited Optical Intensity Channels Corrupted by Gaussian Noise," *IEEE Transactions on Information Theory*, vol. 50, no. 5, pp. 784–795, May 2004.

[115] C. Shannon, "Communication in the Presence of Noise," in *Proc. of the IRE*, vol. 37, no. 1, Jan. 1949, pp. 10–21.

[116] A. Farid and S. Hranilovic, "Capacity of Optical Intensity Channels with Peak and Average Power Constraints," in *Proc. of IEEE International Conference on Communications (IEEE ICC 2009)*, Dresden, Germany, 14–18 Jun. 2009, pp. 1–5.

[117] ——, "Capacity Bounds for Wireless Optical Intensity Channels With Gaussian Noise," *IEEE Transactions on Information Theory*, vol. 56, no. 12, pp. 6066–6077, Dec. 2010.

[118] R. You and J. Kahn, "Upper-bounding the Capacity of Optical IM/DD Channels With Multiple-subcarrier Modulation and Fixed Bias Using Trigonometric Moment Space Method," *IEEE Transactions on Information Theory*, vol. 48, no. 2, pp. 514–523, Feb. 2002.

[119] X. Li, R. Mardling, and J. Armstrong, "Channel Capacity of IM/DD Optical Communication Systems and of ACO-OFDM," in *Proc. of IEEE International Conference on Communications (IEEE ICC 2007)*, Glasgow, UK, Jun. 24–28 2007, pp. 2128–2133.

[120] X. Li, J. Vucic, V. Jungnickel, and J. Armstrong, "On the Capacity of Intensity-Modulated Direct-Detection Systems and the Information Rate of ACO-OFDM for In-

door Optical Wireless Applications," *IEEE Transactions on Communications (IEEE TCOM)*, vol. 60, no. 3, pp. 799–809, Mar. 2012.

[121] J. Tellado, L. M. C. Hoo, and J. M. Cioffi, "Maximum-Likelihood Detection of Nonlinearly Distorted Multicarrier Symbols by Iterative Decoding," *IEEE Transactions on Communications*, vol. 51, no. 2, pp. 218–228, Feb. 2003.

[122] I. Gutman and D. Wulich, "On Achievable Rate of Multicarrier with Practical High Power Amplifier," in *Proc. of European Wireless Conference (EW 2012)*, Poznan, Poland, 18–20 Apr. 2012, pp. 1–5.

[123] D. Kim and G. L. Stueber, "Clipping Noise Mitigation for OFDM by Decision-Aided Reconstruction," *IEEE Communications Letters*, vol. 3, no. 1, pp. 4–6, Jan. 1999.

[124] H. Chen and A. M. Haimovich, "On Achievable Rate of Multicarrier with Practical High Power Amplifier," *IEEE Communications Letters*, vol. 7, no. 7, pp. 305–307, Jul. 2003.

[125] D. Tse and P. Viswanath, *Fundamentals of Wireless Communication*. Cambridge University Press, 2005.

[126] Vishay Semiconductors, "Datasheet: TEMD5110X01 Silicon PIN Photodiode," Retrieved Jul. 26, 2011 from http://www.vishay.com/docs/84658/temd5110.pdf, May 2009.

[127] J. Li, X. Zhang, Q. Gao, Y. Luo, and D. Gu, "Exact BEP Analysis for Coherent M-arry PAM and QAM over AWGN and Rayleigh Fading Channels," in *Proc. of the IEEE Vehicular Technology Conference (VTC 2008-Spring)*, Singapore, 11-14 May 2008, pp. 390–394.

[128] N. Johnson, S. Kotz, and N. Balakrishnan, *Continuous Univariate Distributions*, 2nd ed. John Wiley & Sons Ltd., 1994, vol. 1.

[129] P. K. Vitthaladevuni, M.-S. Alouini, and J. C. Kieffer, "Exact BER Computation for Cross QAM Constellations," *IEEE Transactions on Wireless Communications*, vol. 4, no. 6, pp. 3039–3050, Nov. 2005.

[130] J. Smith, "Odd-Bit Quadrature Amplitude-Shift Keying," *IEEE Transactions on Communications*, vol. 23, no. 3, pp. 385–389, Mar. 1975.

[131] S. Boyd and L. Vandenberghe, *Convex Optimization*. Cambridge University Press, 2004.

[132] MathWorks, "Matlab Documentation Center," Retrieved Nov. 17, 2012 from http://www.mathworks.co.uk/help/matlab/index.html.

[133] G. D. Forney and G. Ungerboeck, "Modulation and Coding for Linear Gaussian Channels," *IEEE Transactions on Information Theory*, vol. 44, no. 6, pp. 2384–2415, Oct. 1998.